University of Southampton

The Geochemistry and Geomicrobiology of Relict Hydrothermal Sulphide Deposits

by Silke Severmann

A dissertation submitted for the Degree of Doctor of Philosophy

School of Ocean and Earth Science

May 2000

Declaration

This dissertation describes my own original work except where acknowledgement is made in the text. To the best of my knowledge it is not substantially the same as any work that has been, or is being submitted to any other university for any degree, diploma or other qualification.

May, 2000

Silke Severmann

UNIVERSITY OF SOUTHAMPTON

ABSTRACT

FACULTY OF SCIENCE, SCHOOL OF OCEAN AND EARTH SCIENCE

Doctor of Philosophy

The geochemistry and geomicrobiology of relict hydrothermal sulphide deposits

by Silke Severmann

The diagenetic re-mineralisation of seafloor-sulphide deposits and the role of microbes in the metal-exchange processes were investigated in metalliferous sediments from the *Alvin* relict hydrothermal zone in the TAG area at 26°08'N (Mid-Atlantic Ridge). The solid-phase and concomitant pore water concentrations of Al, Si, Ca, C_{tot}, C_{org}, S, Fe, Mn, Cu, Zn, P, V, Co, U, Mo, Au, Ag and REE's were measured in a 230 cm long gravity core from the southern periphery of the relict vent field. These measurements were complemented by detailed analysis of bacterial abundance and specific activity. The altered sulphidic sediments are capped with a ~30cm thick layer of carbonate-rich (~60% $CaCO_3$), Fe-stained sediments. Two distinct sulphide layers, interbedded with Fe-oxysilicates, and overlain by a thin layer of Fe/Mn oxyhydroxides, were found in this core. The dominant mineral-phase in both sulphide layers, which originate from mass-wasting of mound sediments, is pyrite with some goethite. Reaction of the exposed metal-sulphides in the upper sulphide layer with seawater has produced a thin layer of secondary atacamite, which is enriched in Au. Primary sphalerite is dissolved in the upper sulphide layer and re-precipitation as secondary sphalerite directly above and below. U continues to be scavenged from the porewater, producing marked enrichments on oxidised sulphide rims. The re-mineralisation processes identified in this core are in close analogy to the large-scale zone-refining that has been described for the active TAG mound and ancient ore-deposits.

REE/Fe ratios clearly distinguish between plume derived sediments in the carbonate cap and slumped material from the hydrothermal mound. The REE signature of bulk sediments and clay phases imply multiple stages of alteration by diffuse fluids in the upper sulphide layer and intermediate layer, whereas the lower sulphide layer is not affected. Alteration by reactive low-temperature hydrothermal fluids is also inferred to be responsible for the observed diagenetic overprinting of trace-metal distributions in the upper sulphide layer. The intermediate layer is rich in nontronite, which has been precipitated *in situ* from diffuse fluids.

The presence of Mn- and Fe-reducing bacteria coincide with elevated porewater concentrations of Mn and Fe, indicating direct involvement of bacteria in the cycling of these metals. Total counts of viable cells and general activity measurements show that although bacterial populations are relatively small, they are healthy and well adapted to this potentially toxic environment. The existence of active microbial communities in metalliferous sediments may therefore provide a continuum of bacterial populations between high and low temperature hydrothermal systems, thus representing an important transitional stage in the hydrothermal ecosystem. Microbial reduction and oxidation of S was observed throughout the core, indicating that microorganisms are particularly active in terms of S-cycling. For deep-sea sediments extremely high sulphate reduction rates (67 nmol/cm^3/d) were measured in the iron-stained carbonate cap. In the absence of significant organic carbon (~0.2 %) this strongly suggests the synthesis of alternative electron-donors by chemolithotrophic bacteria to support the observed high rates of heterothrophic activity in these sediments.

Contents

List of Figures

List of Tables

Acknowledgements

First of all thanks to Rachel for taking me on despite me being foreign, penniless and not even having a proper first degree (oops, should I have mentioned this here?). I was only lucky that I managed to slip through before proper graduate screening was introduced. Thanks for looking after me over the past years, entertaining me, distracting me, feeding me, superdupervising me and trusting me with your first-born son. I hope you got your moneys worth, I certainly did, and sometimes more than I could have hoped for.
The microbiological analysis was performed in Bristol by Barry Cragg, John Parkes, Jo Rhodes (now at the OU), Jon Telling and Kim Goodman (who helped with the sampling), many thanks for that. The geomicrobiology part has been the most challenging but also the most inspiring part of this PhD for me, I hope I didn't let you down. Thanks also to Martin Palmer who wrote the initial grant proposal, and who has been extremely patient waiting for me to finish this off.
A big hand for the basement boys: Ian Croudace and Phil Warwick for invaluable expertise, and for letting me borrow the odd bit of lab-equipment, which I promise I will return as soon as I can locate it. Aren't you glad that I won't leave town just yet? Bob Jones and John Ford have prepared many fine SEM slides for me, which provided endless entertainment on those long winter-nights. Who needs a telly anyway? And when I had run out of slides, there were always Andy Milton's ICP-MS data to keep me out of trouble.
And as for the ladies-team, Posy Boella has been a great help in the lab, and Barbara Cressey instructed me on the SEM, thanks to both of them.
Going back to the beginning, there are many glorious moment to remember and pictures to show from that fateful CD102. Most of all thanks to Sid Sykes for finding me that multicoloured green mud, without which this thesis would not have been half as exciting, and to Mark Rudnicki for squeezing the hell out of it – remember those long summer nights, you and me at 2°C, going down on Mr Blobby?
Many more people at SOC have been very helpful over the years. Peter Statham was often the first port of call when I needed advice on the analysis of anything that needed analysing, Alan Tappin, who is now in Plymouth, trained me in the clean lab, Brian Dickie made sure that everything was safe and sound, Shir Akbari introduced me to the joys of origami and CNS analysis, Trevor Clayton help with the XRD, Darryl Green provided me with some ICP-AES data, the IT team - who somehow seemed very relieved when my German laptop finally broke down for good - has been very patient with me, the chocolate machine, my friend and foe, and the security guys, who always have an open(ing) mind. And for all the people I didn't name here, the SOC phone directory is probably a pretty comprehensive list.
And in case you were wondering what's happened to that chapter entitled 'Comparison of hydrothermal systems with a sewage outfall in Southampton Water – the global picture', I know you've all been looking forward to that, but it somehow didn't quite work out. Thanks anyway to the DoE and Dave Hydes for a years worth of funding, and to David Burden for some very enjoyable times on the old Bill Conway.
But most importantly, it's good to know that once you've asked the audience and tried 50:50, you can always phone a friend. There've been quite a few office-mates over the years, most memorably Andreas, Lisa, and Clare.
And where would I be without the girls (not down the pub quite that often, I hear you shout). Sharon, how could you desert me, now that I'll be stuck here for at least another two years? And you didn't even tell me the code for the Challenger division

chemical store before you left. Comes summer and half past five I'll be lost without you. Sacha, you're sure you don't want to come back? Liebe Liebste Lisa and Rachel, who now think that picking up a baby from nursery is more important than staying for another swift half.
Jonathan, I've counted all my data-points: 2284. I know it would only take you well under five minutes to collect that many with any of you fancy gadgets, but you'll have to admit it's not bad for a geochemist. They are far to many for a decent regression anyway. Thanks for nutritional and spiritual guidance, and putting up with me over the last few months. Justin, I know I haven't seen much of you recently, but you are still my friend, don't worry. And Damon, thanks a lot for all the encouragement and moral support during my times of need. You're absolutely right: think positive!
Und zu guter Letzt, meine Familie, die mich aus der Ferne über Wasser gehalten haben. Vielen Dank für die moralische und finanzielle Unterstützung, und wenn Ihr mal wieder 'nen Doktor braucht, sagt doch einfach bescheid.

It's been quite an experience, thanks to all of you.

Chapter 1

Introduction

The ridge crest environment, which spans the globe over a distance of ~50,000 km, is the largest continuous volcanic feature on our planet. The circulation of seawater through the crust near the ridge axis is one of the principal processes by which energy and mass is exchanged between the ocean and the Earth interior. The discovery of hydrothermal vents has not only fundamentally changed our understanding of global geochemical cycling, but it has also changed our understanding of deep-sea biology. Whilst the hydrothermal circulation of seawater through the crust had long been predicted from heat balances and chemical signatures in the sedimentary record, the discovery of hydrothermal communities came as a complete surprise (Corliss *et al.*, 1979; Edmond *et al.*, 1979a).

1.1 The global heat balance

The large scale convective circulation of seawater through the global ridge crests and flanks was predicted by Lister (1972), who noted that the conductive heat flow measured through the ocean crust could not account for the predicted heat losses. The total hydrothermal heat flux as it is has been estimated from geophysical methods is $9 \pm 2 \times 10^{12}$ W (Morton and Sleep, 1985; Stein and Stein,

10^6 to 10^7 years, and the high-temperature fluids that are discharging near the axis are thought to have a major impact on the oceans chemistry and biology (Jannasch and Wirsen, 1979; Edmond *et al.*, 1979a; Alt and Honnorez, 1984; Wolery and Sleep, 1988). Only 10 to 20 % of the total heat loss, however, occurs through axial heat flux, and the volume of seawater flowing through the ridge flanks is substantially greater than at the axis (Wolery and Sleep, 1976; Stein and Stein, 1994; Kadko *et al.*, 1995). Hydrothermal heat loss decreases with distance from the ridge axis until a sealing age is reached. This is defined as the crustal age at which observed and predicted conductive heat flows coincide, and it is estimated that heat anomalies extend to crustal ages of 65 ±10 Myr (Stein *et al.*, 1995), which is equivalent to half of the total area of the oceans. Recently low-temperature flow has been observed on the eastern flank of the Juan de Fuca Ridge (JdFR) on crust that is 3.5 Myr in age (Mottl *et al.*, 1998). At this site clear, shimmering, altered seawater is issued along a fault near an isolated basement outcrop. Theoretical considerations suggest that off-axis venting similar to that observed on the JdFR flank is relatively common, and that most of the total global hydrothermal heat loss occurs on crust older than 1 Myr (Schultz and Elderfield, 1997). Detailed quantification of the diffuse heat flux and chemical composition of the fluids is therefore essential for the understanding of the impact of hydrothermal circulation on the oceans chemistry (Elderfield and Schultz, 1996).

1.2 Surface and subsurface morphology of ridge crest hydrothermal systems

According to their geological setting, high-temperature hydrothermal systems are commonly subdivided into slow *versus* fast spreading ridges and sedimented *versus* unsedimented systems, but hydrothermal activity also occurs near seamounts, fracture zones and back-arc spreading centres (German *et al.*, 1995).

Whilst 42% of all currently known vent sites have been found on fast spreading ridges (Fouquet, 1997) frequent disruption of the hydrothermal system by dike injection and volcanic eruption produces only relatively small and ephemeral vent fields (Haymon *et al.*, 1993). The geometry of a fast spreading ridge such as the East Pacific Rise (EPR) is characterised by an axial summit caldera sitting on top of the axial high, which marks the volcanic ridge. A magma chamber is present beneath much of the volcanic ridge at a depth of 1.6 to 2.4 km (Detrick *et al.*, 1987). The focused hydrothermal discharge from black smoker type vents is commonly confined to the only few hundreds of metres wide zone of the summit caldera.

Earlier predictions that hydrothermal activity would be restricted to fast-spreading ridges because of the insufficient heat flow on slow-spreading ridges were proven wrong when in 1985 black smokers and massive sulphides were discovered in the Trans-Atlantic Geotraverse (TAG) hydrothermal field on the Mid-Atlantic Ridge (MAR) at 26°N (Rona *et al.*, 1986). Slow-spreading ridges are characterised by a much lower magma supply, and although volcanic events are less frequent, they are more localised and larger (Sinton and Detrick, 1992). Deeply penetrating faults provide long-term conduits for hydrothermal flow, producing bigger and more mature deposits (Hannington *et al.*, 1995).

It has been postulated that the frequency of vents along spreading ridges increases linearly with spreading rate (Baker *et al.*, 1996). A recent survey of hydrothermal activity along the southwest Indian ridge, however, has identified a surprisingly high abundance of potential vent sites along this ultra-slow spreading-centre (German *et al.*, 1998). The overriding control on the frequency of hydrothermal venting at this site is therefore interpreted to be tectonic processes rather than spreading alone.

The cross-sectional morphology of a slow-spreading ridge exhibits considerable differences to that of a fast-spreading ridge. The spreading plate boundaries located in a 5-10km wide axial rift valley which is enclosed by steep fault-

bounded valley walls rising 1000-2000m up on either side. No continuous magma chamber has been identified below the MAR, instead the broad volcanic ridge is underlain by a relatively deep and predominantly solid, crystalline mush zone (Sinton and Detrick, 1992). The abundance of discrete seamounts on the valley floor and off-axis is indicative of point-source volcanism fed by isolated magma pockets (Smith and Cann, 1990). As the injection of magma into the upper crust subsides, the development of a downward penetrating cracking front cause increased crustal permeability and facilitate the deep penetration of fluids towards large volumes of hot rock (Eberhart *et al.*, 1989; Wilcock and Delaney, 1996). In the absence of frequent volcanic eruption convective hydrothermal circulation may be stable over long periods of time, thus producing favourable conditions for the formation of large deposits (Hannington *et al.*, 1995; Wilcock and Delaney, 1996).

1.3 Controls on the growth of sulphide deposits

The TAG deposit is amongst the largest known sea floor massive sulphide deposits on mid-oceanic spreading axis, comparable in size and grade to many land-based ore deposits. Massive sulphide deposits on the sea floor and on land have been estimated to contain few tens of thousands up to several hundred millions of tonnes of sulphide (Hannington *et al.*, 1995). This range in size over three orders of magnitude reflects the variety of tectonic systems in which hydrothermal systems occur as well as their long-term stability.

After initial venting is established, the growth of the sulphide deposit depends greatly on the development of an efficient subsurface trapping mechanism for the metals and sulphur. As much as 97% of metals from black smokers may be lost into the ambient seawater (Converse *et al.*, 1984). A portion of the metals are precipitated below the seafloor due to convective cooling of the ascending fluid and mixing with seawater within the mound. This is often helped by the presence of impermeable caps, such as the siliceous cap rock that has been

described for the TAG mound (Humphris *et al.*, 1995) and the Lau Basin (Fouquet *et al.*, 1993). Thick sedimentary cover of terrestrial origin, as they occur in the Guaymas Basin and the Middle Valley are also very effective trapping mechanisms (Bowers *et al.*, 1985; Mottl *et al.*, 1994).

The large sulphide deposits of the Galapagos ridge have formed through coalescence of adjacent chimneys to form a composite body that has evolved from several smaller hydrothermal mounds (Embley *et al.*, 1988). In this case the mound itself on which the chimneys grow acts as a cap on the hydrothermal system. At TAG the sulphide mound has been constructed through the repeat collapse of chimneys and accumulation of sulphide debris, which is continuously overgrown and cemented during episodic re-occurrence of high-temperature venting (Humphris and Kleinrock, 1996; Hannington *et al.*, 1998).

Another factor that influences the growth of the deposit is the contrasting permeability of the lava morphologies (Hammond, 1990) and the stability of the hydrothermal system (Lalou *et al.*, 1995). Focusing of hydrothermal fluids along deeply penetrating faults on slow spreading ridges and the relative stability of the convective cell are more favourable to the formation of sizeable deposits such as TAG (Kleinrock and Humphris, 1996). The largest mid-ocean ridge deposits, including Galapagos, Explorer and TAG, are characterised by a broad subseafloor alteration zone, branching stockwork mineralisation, extensive seawater entrainment, a wide range of venting styles over the entire surface, and development of large mounds (Hannington *et al.*, 1995). This is in stark contrast to the Endeavour vent fields, where numerous freestanding structures are distributed along major fissure zones (Delaney *et al.*, 1992). The tall chimneys grow above well-sealed, pipe-like stockwork with only little or no mixing with seawater in the subsurface (Butterfield *et al.*, 1994).

development of large mounds (Hannington *et al.*, 1995). This is in stark contrast to the Endeavour vent fields, where numerous freestanding structures are distributed along major fissure zones (Delaney *et al.*, 1992). The tall chimneys grow above well-sealed, pipe-like stockwork with only little or no mixing with seawater in the subsurface (Butterfield *et al.*, 1994).

1.4 Hydrothermal plumes

When hydrothermal fluids exit the vents, they are rapidly diluted by background seawater with mixing ratios of 1:100 to 1:1000 in the first 5 to 10 m of the plume rise (Lupton, 1995). The initial phase of plume buoyancy refers to the stage during which the dilute hydrothermal fluid has positive buoyancy and is thus ascending from the seafloor. Once the plume reaches density equilibrium with the ambient seawater and attains neutral buoyancy it begins to spread out laterally. At this point the dilution will have increased further by another order of magnitude (Lupton, 1995). Kadko (1993) calculated an oceanic circulation time of the entire ocean through the global plume system to be of the order of 2.4 $x10^3$ years, which is significantly faster than the circulation of seawater through the crust.

Because the average depth of the caldera at fast spreading ridges is only 10-20m, the hot fluids can easily escape from the restricting topography as they mix with the ambient seawater and rise 100-300m above the seafloor. Despite the extreme dilution the chemical signature and anomalous physical properties of the plume can be detected over distances of up to 2000 km from the source (Lupton and Craig, 1981). Chemical tracer of hydrothermal plumes include Mn, Fe, Al, Si, ^3He, CH_4, H_2 and ^{222}Rn, and these are introduced into the deep-sea at concentrations many orders of magnitude above ambient seawater. The reaction of dissolved constituents with oxygenated seawater produces suspended particles, which will eventually be removed to the sediments. Significant

In contrast to this more familiar chronic style of venting, large event plumes or megaplumes were first observed over the southern Juan de Fuca Ridge (JdFR) in 1986 (Baker *et al.*, 1987). These are detached and transient hydrothermal plumes that are generated during an episodic and sudden release of massive volumes of buoyant fluid over a period of days, rising up to 1000m above the sea floor. The chemical composition of these event plumes is distinctly different from chronic plumes with Fe/heat, Mn/Heat and ^{3}He/heat ratios all being markedly lower in the event plumes (Lupton *et al.*, 1989; Massoth *et al.*, 1994). The close spatial and temporal association with recent volcanic eruptions and lava flows strongly implies that megaplumes are directly related to seafloor spreading events (Chadwick *et al.*, 1991). Following the close monitoring of seismic activity near spreading ridges, several similar megaplumes have since been observed and sampled above the JdFR (Baker *et al.*, 1994; Embley *et al.*, 1995) and the EPR (Haymon *et al.*, 1993). A number of models have subsequently been proposed for the generation of these event plumes, including the rapid release of large volumes of hydrothermal fluids from a sub-surface reservoir (Baker *et al.*, 1987; Cann and Strens, 1989; Wilcock, 1997; Lupton *et al.*, 1999), rapid heat extraction from a recently emplaced dyke (Lowell and Germanovich, 1995) or from erupted lava flows on the seafloor (Palmer and Ernst, 1989; Butterfield *et al.*, 1997). Continuous monitoring of these sites has shown that high temperature hydrothermal vents and their associated fauna are established within a year after the eruption of lava (Lutz *et al.*, 1994; Tunnicliffe *et al.*, 1997). The thus proposed sequence of events for each phase of hydrothermal activity on fast-spreading ridges begins with a dike injection, which will potentially trigger a large-scale event plume if the crustal activity is sufficiently shallow (Butterfield *et al.*, 1997). The early phase of the continuous hydrothermal discharge is dominated by diffuse flow, until eventually a more mature vent field with more focused chronic high-temperature discharge is established (Haymon *et al.*, 1993; Koski *et al.*, 1994). Depending on the local spreading rate, this cycle may repeat itself on a less than decadal scale (Chadwick *et al.*, 1991; Haymon *et al.*, 1993).

1.5 Microbes in hydrothermal systems

Unique geothermally-driven microbial communities are the primary producers of the hydrothermal ecosystem (Jannasch, 1995). Microbial chemosynthetic interaction with hydrothermal fluids is conducted by free-living bacteria and prokaryotic symbionts. Abundant redox- and temperature gradients, as they occur in chimney walls, in worms tubes, at vent orifices, in the hydrothermal plume, on surficial sulphide deposits and below the seafloor, provide suitable habitats for microbial colonisation (Jannasch, 1985; Jørgensen *et al.*, 1992; Eberhard *et al.*, 1995; Karl, 1995b; Cowen *et al.*, 1998; Juniper *et al.*, 1998; Naganuma, 1998). Electron donors such as H_2, H_2S, CH_4, Fe^{2+} and Mn^{2+} are generated from the reaction of seawater with basalt. Mixing of these hydrothermal fluids with surface water provides electron donors such as O_2, SO_4^{2-} and NO_3^-, and it is under these conditions that bacteria can most successfully utilise the available energy that is generated deep in the oceanic crust (Jannasch, 1995; Karl, 1995a).

The primary and most important electron donor for microbial reactions in the hydrothermal system is H_2S. In the absence of light energy from the sun, free energy is produced from oxidation of H_2S with O_2. This reaction can then be coupled to the reduction of CO_2 to produce organic carbon, and this endogenic reaction is termed 'bacterial photosynthesis' in analogy to green plant photosynthesis (Jannasch, 1995). Sulphide oxidation provides about 99 % of the energy that is available for primary productivity.

The nature of the microbial interactions depends greatly on the chemistry of the hydrothermal fluid (McCollom and Shock, 1997). For example, the alteration of the fluids during the passage through organic-rich sediments at the Guaymas basin results in marked modification of the vent emissions. This is also reflected in the distinctly different microbial populations at the Guaymas site compared to

unsedimented hydrothermal systems of the Galapagos Rift (Jannasch and Wirsen, 1981; Jannasch *et al.*, 1989).

A more detailed discussion of the interaction between microbes and minerals is provided in Chapter 6.

1.6 Aims of the present study and dissertation outline

The subject of this study are metalliferous sediments from the *Mir* and *Alvin* zone, two relict hydrothermal deposit in the TAG hydrothermal field on the Mid-Atlantic Ridge (MAR), where active venting has ceased several thousand years ago (Lalou *et al.*, 1993; Rona *et al.*, 1993b). Investigation of hydrothermalism in this area until now has focused primarily on the active TAG mound. Relict hydrothermal deposits form an integral part in the development of an active high-temperature deposit to massive sulphides on land (Constantinou and Govett, 1972; Robertson and Fleet, 1986).

The aim of this study is

- to investigate the formation of metalliferous sediments in this area and the origin of the different hydrothermal mineral phases,
- to assess the nature and timing of the post-depositional diagenetic alteration of a seafloor deposit following cessation of active venting and mass wasting of sulphides from the steep talus slopes,
- to establish the role of microbes in the mineral transformation and metal mobilisation.

Chapter 2 provides an introduction to the geological settings of the study area. Chapter 3 describes the general mineralogy and bulk chemical composition of core 43, which was recovered from the southern periphery of the *Alvin* zone. The extent of metal transformation, re-mineralisation and the zonation of

hydrothermally enriched trace metals are investigated in Chapter 4. In Chapter 5 rare earth elements are used as a geochemical proxy to establish the origin of the hydrothermal minerals and study the post-depositional alteration of the deposit. In contrast to most previous studies of metal-diagenesis in shallow and deep-sea marine environments (Colley *et al.*, 1989; Shaw *et al.*, 1990; Thamdrup *et al.*, 1994; Thomson *et al.*, 1995; Thomson *et al.*, 1998), metalliferous sediments in the TAG hydrothermal field are poor in organic carbon yet naturally enriched in a wide variety of metals. In the absence of significant organic carbon, microbes are required to adapt to alternative sources of energy. The abundance of active microbial populations and the role of sulphur and reduced metals are examined in Chapter 6.

Chapter 2

Geological Setting: The TAG Hydrothermal Field

2.1 The TAG hydrothermal field

The TAG hydrothermal field was first discovered in 1972 during the Trans-Atlantic Geotraverse (TAG) programme (Rona *et al.*, 1975), when unusually Mn-rich crusts were dredged from the median valley of the MAR. These deposits provided the first strong evidence for localised hydrothermal discharge on a slow spreading mid-oceanic ridge (MOR). It was not until 1985, however, that the active sulphide mound with high-temperature hydrothermal activity was discovered (Rona *et al.*, 1986). The TAG hydrothermal field is located at 26° N on the MAR at the centre of a 40 km long segment bounded by non-transform discontinuities (Purdy *et al.*, 1990; Rona *et al.*, 1993b). The spreading rates on this segment have been asymmetric over the past 10 million years with half-spreading rates of 1.1 cm /year to the west and 1.3 cm/year to the east (McGregor *et al.*, 1977). This is reflected in the asymmetric structural morphology of the rift valley, where the eastern valley wall is markedly higher, steeper and smoother than its western counterpart (Zonenshain *et al.*, 1989; Karson and Rona, 1990).

The TAG field is situated between 2 and 8 km east of the axial high, near the lower eastern wall of the rift valley (Figure 2.1). A wide range of presently active and fossil hydrothermal deposits, which may be related to small volcanic centres (Rona *et al.*, 1996), can be found here in an area of 5 km x 5 km between 2400 and 3650 m water depth. The rift valley is confined by

walls up to 1800 m high, which effectively prevents dispersal of the hydrothermal plume away from the ridge.

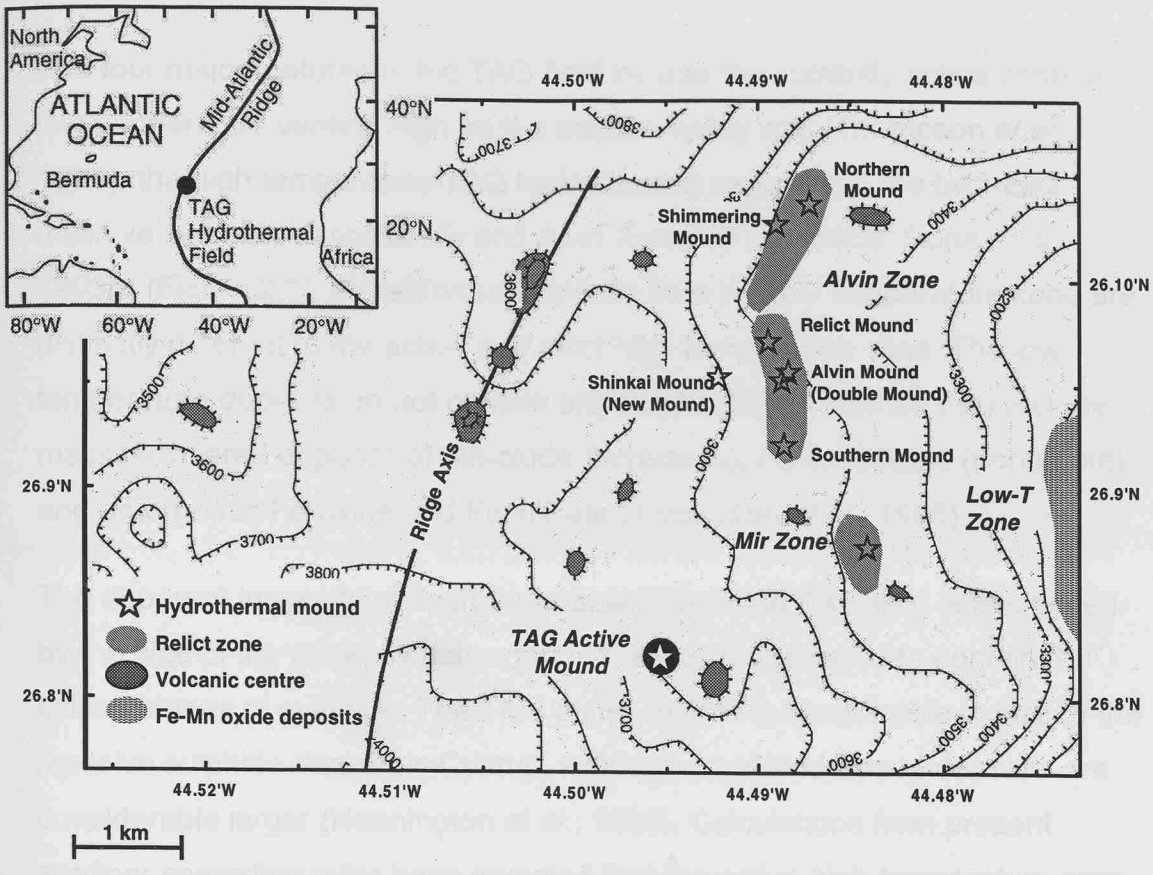

Figure 2.1: Bathymetric map of the TAG vent field showing the locations of the active TAG mound, the *Alvin* and *Mir* relict hydrothermal zones and the low temperature field on the eastern median valley wall (adapted from Tivey *et al.*, 1995).

A micro-earthquake and seismic refraction survey indicated that the central part of the segment is underlain by a mid-crustal low-velocity zone at relatively shallow depth of 3 km (Kong *et al.*, 1992). This suggests the presence of a largely solid but still hot magmatic intrusion. Deep penetrating high-angle normal faulting beneath the axis (ENE) are intersected by actively developing axis-parallel faults and fissures (NNE) with intermediate angle (Kong *et al.*, 1992). It appears that these faults have provided permeable pathways through the fault breccia and thus contributed to the highly focused discharge

evident in this area (Kleinrock and Humphris, 1996). No seismicity was observed beneath the area of the active sulphide mound. The alignment of a recent depression on the active mound with ridge-parallel faults does, however, suggest that extension is still ongoing (Humphris and Kleinrock, 1996; Kleinrock and Humphris, 1996).

The four major features of the TAG field include the currently active zone of low temperature venting high on the median valley wall (Thompson *et al.*, 1985), the high temperature TAG hydrothermal mound and the two relict massive sulphide deposits *Mir* and *Alvin* (Rona *et al.*, 1993a; Rona *et al.*, 1993b) (Figure 2.1). Metalliferous deposits from the low temperature zone are distinctly different to the active and relict high temperature sites. The low temperature deposits do not contain any sulphides, but instead they include massive layered deposits of Mn-oxide (birnessite), Fe-oxysilicate (nontronite) and amorphous Fe-oxide and Fe-silicate (Thompson *et al.*, 1985).

The apparent longevity of hydrothermal activity in the TAG field is evidenced by the size of the currently active mound, which is estimated to contain 3.9 million tonnes of sulphide. The TAG active mound is comparable in size to the massive sulphide deposit in Cyprus, although most land-based deposits are considerable larger (Hannington *et al.*, 1998). Calculations from present seafloor spreading rates have revealed that the active high temperature zone is located on oceanic crust at least 100 ka old, and U-series radiogenic dating on sulphide samples indicate the venting at this site started at least 50,000 years ago with pulsed high temperature activity every 5,000 to 6,000 years during the past 20,000 years (Lalou *et al.*, 1993; Lalou *et al.*, 1998; You and Bickle, 1998). Precipitation of sulphides in the *Alvin* zone started at a similar time, whereas the oldest sulphide sample in the TAG field was recovered from the *Mir* zone and has been dated as 100,000 year old (Lalou *et al.*, 1993).

Hosting one of the largest currently known hydrothermal deposits on the modern seafloor, the TAG field has been the subject of intensive investigation over the past 25 years, including dredging, photographic imagery, high resolution side-scan sonar and submersible observations (Rona *et al.*, 1984;

Thompson *et al.*, 1985; Thompson *et al.*, 1988; Rona *et al.*, 1993a; Rona *et al.*, 1993b; BRAVEX Scientific team, 1994; Tivey *et al.*, 1995; Humphris and Kleinrock, 1996; Kleinrock *et al.*, 1996; Rona *et al.*, 1998; White *et al.*, 1998). Most recently, drilling of the active TAG mound by the Ocean Drilling Program (ODP) during Leg 158 has revealed the internal structure of the deposit (Humphris and Kleinrock, 1996).

2.2 Low-temperature deposits

The chemistry and mineralogy of precipitates in the low temperature zone differs greatly from high-temperature deposits. A range of deposits including massive nontronite, Fe-oxides and Mn-oxides have been identified in an area of 2 km x 3 km on the east rift valley wall (Rona *et al.*, 1984; Thompson *et al.*, 1985). The bulk of this deposit was dated radiometrically at ages between 4,000 and 16,000 years B.P., and an earlier episode of hydrothermal activity is indicated by two samples with dates of up to 125,000 years B.P. (Lalou *et al.*, 1986). Although similar in composition, these deposits form at much faster rates (100 to 200 mm/Myr) than average hydrogenous ferromanganese nodules (Scott *et al.*, 1974). No hydrothermal venting has been observed directly in this area, but chemical and physical parameters indicate that low-temperature diffuse flow is occurring (Scott *et al.*, 1974; Rona *et al.*, 1975; Jenkins *et al.*, 1980; Thompson *et al.*, 1985; Ravizza *et al.*, 1996). Formation of Mn-oxide crusts is inferred to be by a combination of sedimentation of Mn-rich plume particles and direct precipitation from diffuse hydrothermal fluids (Scott *et al.*, 1974; Klinkhammer and Hudson, 1986; Wells, 1998). The implication is that fractionation of Mn from other hydrothermally-derived metals occurs through plume processes as well as spatial distribution of diffuse flow within the vent field (Wells, 1998).

2.3 The TAG mound

The currently active TAG hydrothermal mound is located on the floor of the rift valley at 3670-3680 m depth, 2.4 km east of the ridge axis. It has a diameter of ~250 m, and rises ~50 m above the seafloor. It is constructed of altered

and unaltered blocky sulphides and anhydrite, and is surrounded by an apron of carbonate and metalliferous sediments up to 100 m wide (Tivey *et al.*, 1995). The mound is a large circular feature of two discrete platforms, indicating at least two phases of growth, and both with strongly focused flow. The asymmetric superposition of the two platforms indicates that the focus of the hydrothermal discharge must have moved following sealing of previous fluid-flow pathways and redirection of fluids (Humphris and Kleinrock, 1996).

Black smoker fluids are currently venting from a cluster of chimneys, which form the Black Smoker Complex (BSC). This is located on the upper platform atop a conical structure slightly northwest of the centre of the mound (Figure 2.2). The clustering of the black smoker chimneys in one large complex reflects the focusing of the fluid flow as a result of the structural control (Tivey *et al.*, 1995). The presence of fault scarps immediately to the NE and SW of the mound, as well as the slight change in seafloor depth indicates faulting beneath the mound (Humphris and Kleinrock, 1996).

The lower platform has an irregular surface with sulphide debris, talus, standing and toppled chimneys and Fe-oxide crusts. A group of 10 bulbous, 1-2 m high white smoker chimneys, known as the Kremlin area (Thompson *et al.*, 1988), is situated near the southeastern periphery of the mound. In addition, the emission of diffuse hydrothermal fluids with temperatures of <50°C occurs over the entire surface of the mound and through isolated pockets of metalliferous sediments. The importance of diffuse flow in the heat budget of a hydrothermal system has long been underestimated and recent estimates of the heat flux from diffuse flow are as high as 2000 MW (Schultz *et al.*, 1996), thus exceeding the chemical and mass transfer from high temperature venting, which is up to 940 MW (Rudnicki and Elderfield, 1992).

The fluids emanating from the black and white smokers are characterised by their distinct difference in temperature and chemistry (Edmond *et al.*, 1995; Edmonds *et al.*, 1996; Gamo *et al.*, 1996). Chimneys up to 15 m high are currently issuing black smoker fluids at 363°C. These are rich in Fe, Cu and H_2S, and the major element composition is similar to high-temperature fluids

H_2S, and the major element composition is similar to high-temperature fluids from vents in the Pacific (Campbell *et al.*, 1988). White smoker fluids, in contrast, have a more variable temperature range of 260° to 300° C and are more acidic than black smoker fluids with a pH of 3. They are poor in Fe and H_2S but rich in Zn. The contrasting fluid chemistry is also reflected in the mineralogy of the chimneys. Black smoker chimneys are composed of chalcopyrite ($FeCuS_2$)–pyrite (FeS_2) with anhydrite ($CaSO_4$) in the outer layer, whereas white smokers chimneys are dominated by sphalerite (ZnS) with minor amorphous silica, marcasite (FeS_2) or pyrite but no anhydrite (Tivey *et al.*, 1995).

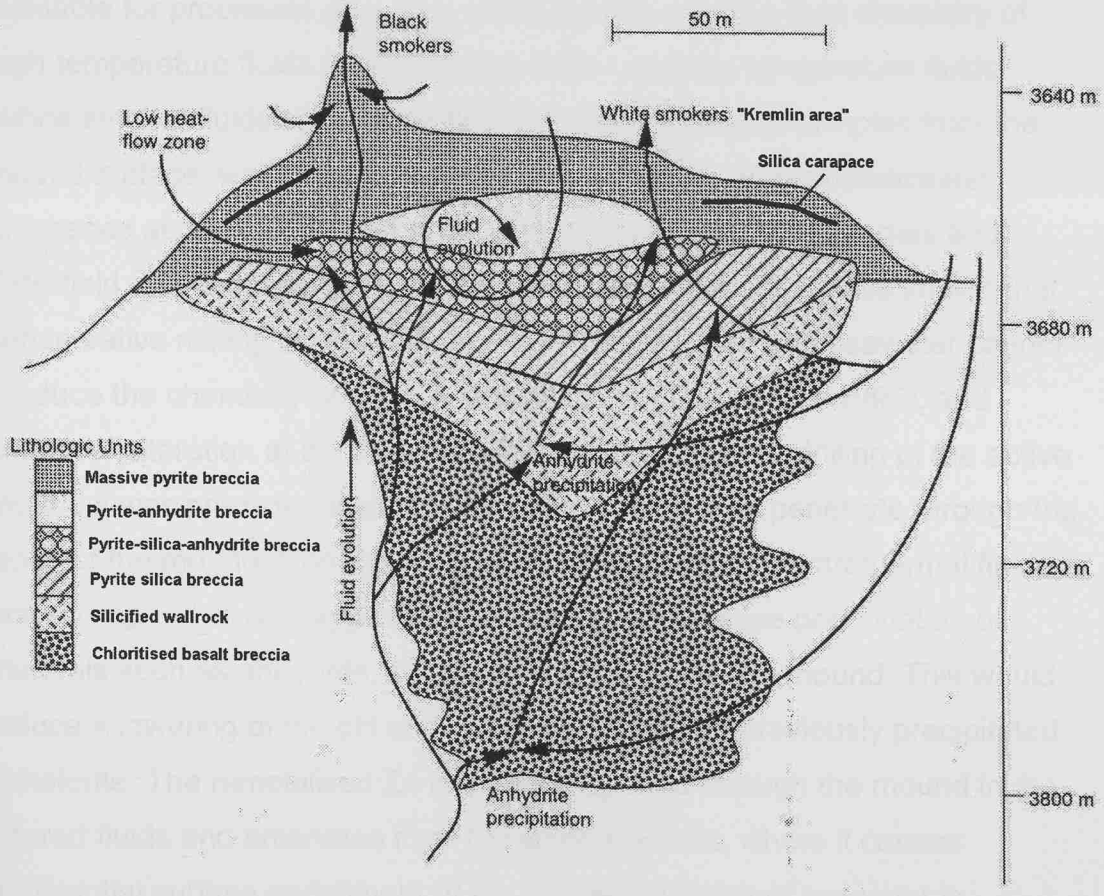

Figure 2.2: Cross-section of the TAG hydrothermal mound, showing the two platforms, the circulation and mixing of seawater and hydrothermal fluid within the mound and the different styles of venting (adapted from Mills *et al.*, 1998).

The chemistry of diffuse fluids indicates that they are produced by mixing of high-temperature black smoker fluid with seawater within the hydrothermal mound (Figure 2.2). Deviation from an ideal mixing line between these two components for a number of elements is explained by simultaneous precipitation and dissolution of silica, Fe-sulphides and anhydrite in different parts of the mound (James and Elderfield, 1996b; Mills *et al.*, 1996). These evolved fluids play an important role in the low-temperature alteration of sulphide and basalt and the supergene formation of secondary mineral phases near the mound surface (Mills *et al.*, 1996).

Prior to ODP drilling of the active mound in 1994, only indirect evidence was available for processes occurring within the mound. The fluid chemistry of high temperature fluids (black-smoker fluids) and low temperature fluids (white-smoker fluids and diffuse flow), as well as mineral samples from the mound surface, was used to constrain the alteration and mineralisation processes at depth (Edmond *et al.*, 1995; Tivey *et al.*, 1995; James and Elderfield, 1996a; Mills *et al.*, 1996). Simple mixing models have shown that conservative mixing of end-member hydrothermal fluid and seawater cannot produce the chemistry of low temperature fluid (Tivey *et al.*, 1995), and chemical alteration at depth is therefore required. Before drilling of the active mound it was predicted that large volumes of seawater penetrate through the sides of the mound. Conductive cooling of end-member hydrothermal fluids and mixing with cold, oxygenated seawater would cause precipitation of minerals such as anhydrite, silicate and pyrite within the mound. This would induce a lowering of the pH and hence dissolution of previously precipitated sphalerite. The remobilised Zn is thus transported through the mound in the altered fluids and emanates from the white smokers, where it causes substantial surface enrichment of Zn. The entrainment of seawater is promoted by the permeability of the mound and the high velocity discharge of the focused flow at the centre (Schultz *et al.*, 1992). An area of low heat flow on the western section of the upper platform within a few tens of metres of the BSC indicates local recharge of bottom seawater (Becker and von Herzen, 1996).

2.3.1 The internal structure of the TAG mound: ODP drilling results

The presence of massive anhydrite in the central core of the deposit was indeed confirmed by the findings of the ODP Leg 158 (Humphris *et al.*, 1995). The mound was drilled in five target areas (Figure 2.3), with the longest core (125 m) recovered from just east of the BSC. Four major lithological zones were distinguished (Figure 2.4):

(1) 0-20 mbsf; massive pyrite and pyrite breccia with sulphide cement.

(2) 20-45 mbsf; pyrite-anhydrite breccia and pyrite-silica-anhydrite breccia with extensive anhydrite veining (up to 45 cm thick).

(3) 45-100 mbsf; pyrite-silica breccia overlying silicified basalt breccia.

(4) 100-125 mbsf; lower quartz-chlorite stockwork zone of altered basalt.

A hardened carapace of pyrite breccia cemented by cherty silica (Figure 2.2) has been found in the upper few metres to a depth of ~15 mbsf in the TAG-2, TAG-3 and TAG-4 areas (Fouquet *et al.*, 1998). Precipitation of silica at this depth may contribute to the focusing of the uprising fluids and is most likely to be the result of conductive cooling of hydrothermal fluids at the surface of the mound (Hannington *et al.*, 1998).

2.3.2 Mound growth and fluid evolution

Combining the three dimensional drilling observations with earlier studies of hydrothermal fluids and precipitates sampled from the mound surface has led to the development of a new model for mound growth and fluid evolution (Tivey *et al.*, 1995; Mills and Elderfield, 1995b; Gamo *et al.*, 1996; James and Elderfield, 1996a; Chiba *et al.*, 1998; Gemmell and Sharpe, 1998; Herzig *et al.*, 1998; Knott *et al.*, 1998; Mills *et al.*, 1998; Teagle *et al.*, 1998). The precipitation of anhydrite within the mound is crucial for the growth of the sulphide deposit. The total amount of anhydrite in the TAG mound has been estimated as ~$2x10^5$ t (Humphris, 1998). Massive anhydrite appears to be concentrated below the BSC in areas TAG-1 and TAG-5, with only minor

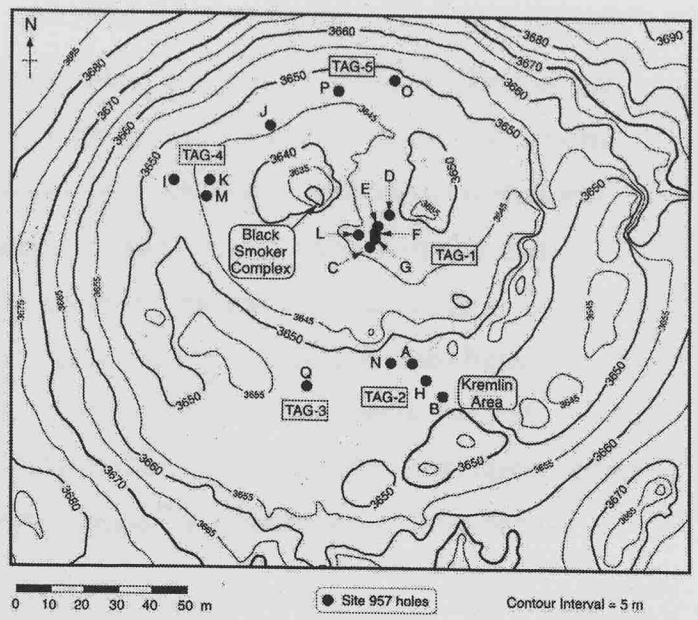

Figure 2.3: Detailed bathymetry of the active TAG mound and location of the 5 areas targeted during drilling, ODP Leg 158 (from Humphris *et al.*, 1998)

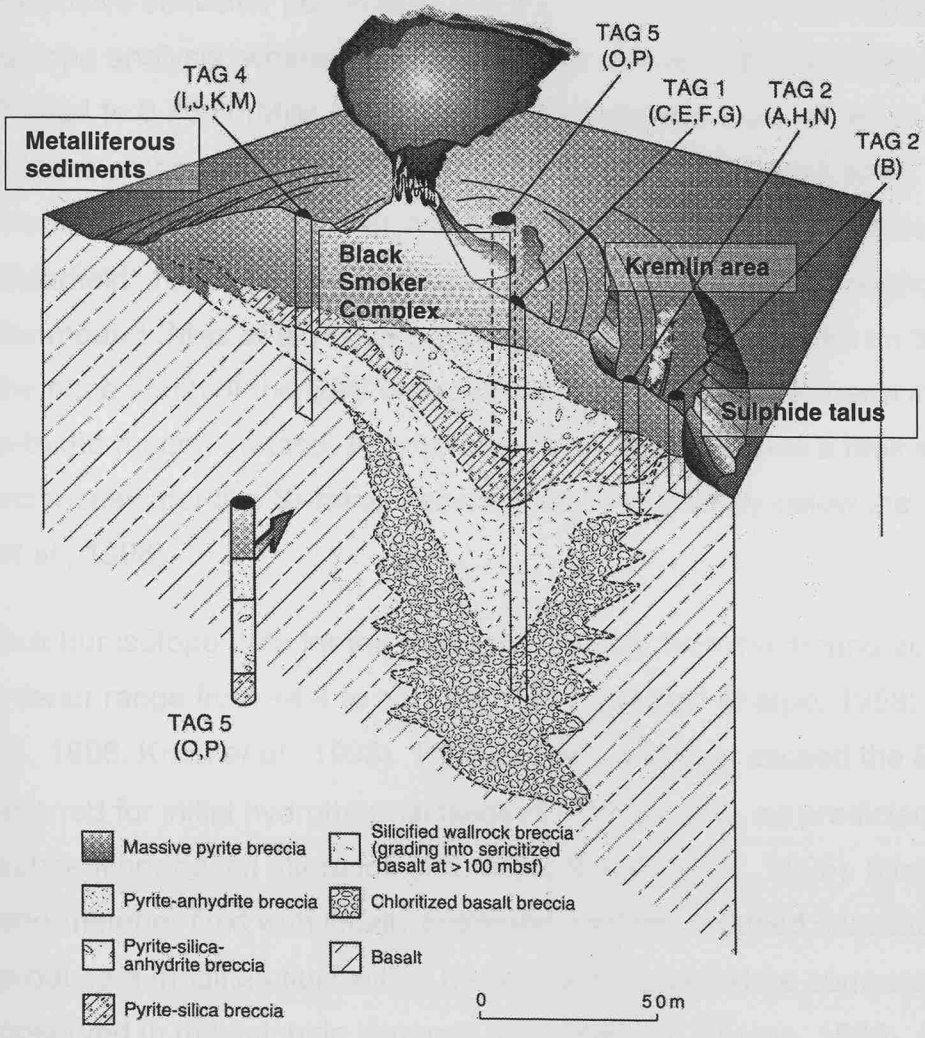

Figure 2.4: Morphology and internal structure of the active TAG mound with the major lithological zones, based on the drilling results of ODP Leg 158 (adapted from Humphris *et al.*, 1998).

anhydrite in the TAG-2 area (Kremlin area) and none in TAG-4. The narrow range in $\delta^{34}S$ of +19.2 to +23.0 ‰ of the anhydrite compared to +20.9 ‰ for seawater and +0.3 ‰ for mid-ocean ridge basalt (MORB) confirms that the source of sulphate must be seawater (Chiba *et al.*, 1998; Gemmell and Sharpe, 1998). Anhydrite precipitates when seawater is heated to temperatures of >150°C. The close association of anhydrite with high-temperature sulphides, especially chalcopyrite, in veins below the BSC indicates that mixing of seawater with end-member hydrothermal fluids rather than conductive heating of seawater causes the formation of anhydrite (Fouquet *et al.*, 1998).

Extensive seawater penetration into the mound is further confirmed by Sr-isotope analysis, where $^{87}Sr/^{86}Sr$ ratios for mound anhydrites range from 0.7064 to 0.7091 (Mills *et al.*, 1998). This indicates a broad range in the relative proportions of seawater ($^{87}Sr/^{86}Sr$= 0.70918; Hodell *et al.*, 1991) and black-smoker fluid ($^{87}Sr/^{86}Sr$ = 0.70348; Gamo *et al.*, 1996; James and Elderfield, 1996b), with a seawater-dominated circulation throughout most of the mound (Mills *et al.*, 1998). Outcrops of massive anhydrite on the flanks of the cone south of the BSC delineate where the 150° C-isotherm intersects with the mound surface. Alternatively the exposure marks a fault surface. The most seawater-like Sr-ratios occur at 120 mbsf directly below the BSC (Mills *et al.*, 1998).

Sulphur isotope data for the sulphide minerals from the mound-surface and interior range from +4.4 to +10.3 ‰ (Gemmell and Sharpe, 1998; Herzig *et al.*, 1998; Knott *et al.*, 1998). These values markedly exceed the $\delta^{34}S$ values inferred for initial hydrothermal fluids of +0‰ to +1‰, as predicted from deep subseafloor basalt alteration (Alt, 1995; Shanks *et al.*, 1995). Mixing of the end-member fluid with locally entrained, partially reduced seawater would produce a modified fluid with a heavier isotope signature comparable to that observed in the sulphide minerals (Gemmell and Sharpe, 1998). Alternatively, Knott *et al.* (1998) suggest that a deep hydrothermal source with elevated $\delta^{34}S$ is required in order to explain the isotopically heavier $\delta^{34}S$ of sulphides

disseminating in altered basalt. This would generate an end-member fluid with an estimated $\delta^{34}S$ of +5.5.

The interior of the mound is characterised by intensive and complex brecciation, with silicified and chloritised basalt breccia, and pyrite breccia cemented by anhydrite (Humphris *et al.*, 1995). This is interpreted to reflect multiple stages of high-temperature venting where hydrothermal mineralisation during periods of high-temperature venting is followed by mound collapse during periods of hydrothermal quiescence (Humphris and Kleinrock, 1996). The episodic nature of high-temperature venting has been inferred from close association of hydrothermal precipitates (sulphide and anhydrite) with widely differing U-series ages throughout the mound (You and Bickle, 1998). During the initial stages of mound growth, clusters of chimneys are formed where fluid flow through the permeable basement is well focused. As the sulphides accumulate, seawater is drawn into the structure and heated to temperatures where precipitation of anhydrite occurs. The result is the cementation of pyrite breccia by anhydrite and vein filling. Thus the mound is effectively inflated. During periods of inactivity, the continuous penetration of seawater into the mound causes the temperature to drop below 150°C, at which point the supportive anhydrite starts dissolving. Consequently, the chimneys and breccia in the central part of the mound collapse. During renewed periods of high-temperature venting the fluids are channelled through the collapsed breccia. This results in the repeated cementation of the pyrites, which were originally formed near the surface of the mound during an earlier stage of activity, but which are now found at the base of the mound (Hannington *et al.*, 1998; You and Bickle, 1998). The cementation of the breccias at the base of the mound with quartz is cumulative and will eventually replace the anhydrite matrix in the overlying breccias (Hannington *et al.*, 1998). Figure 2.5 is a schematic overview of the inferred stages for the evolution of the stockwork complex of the active TAG mound based on drilling results.

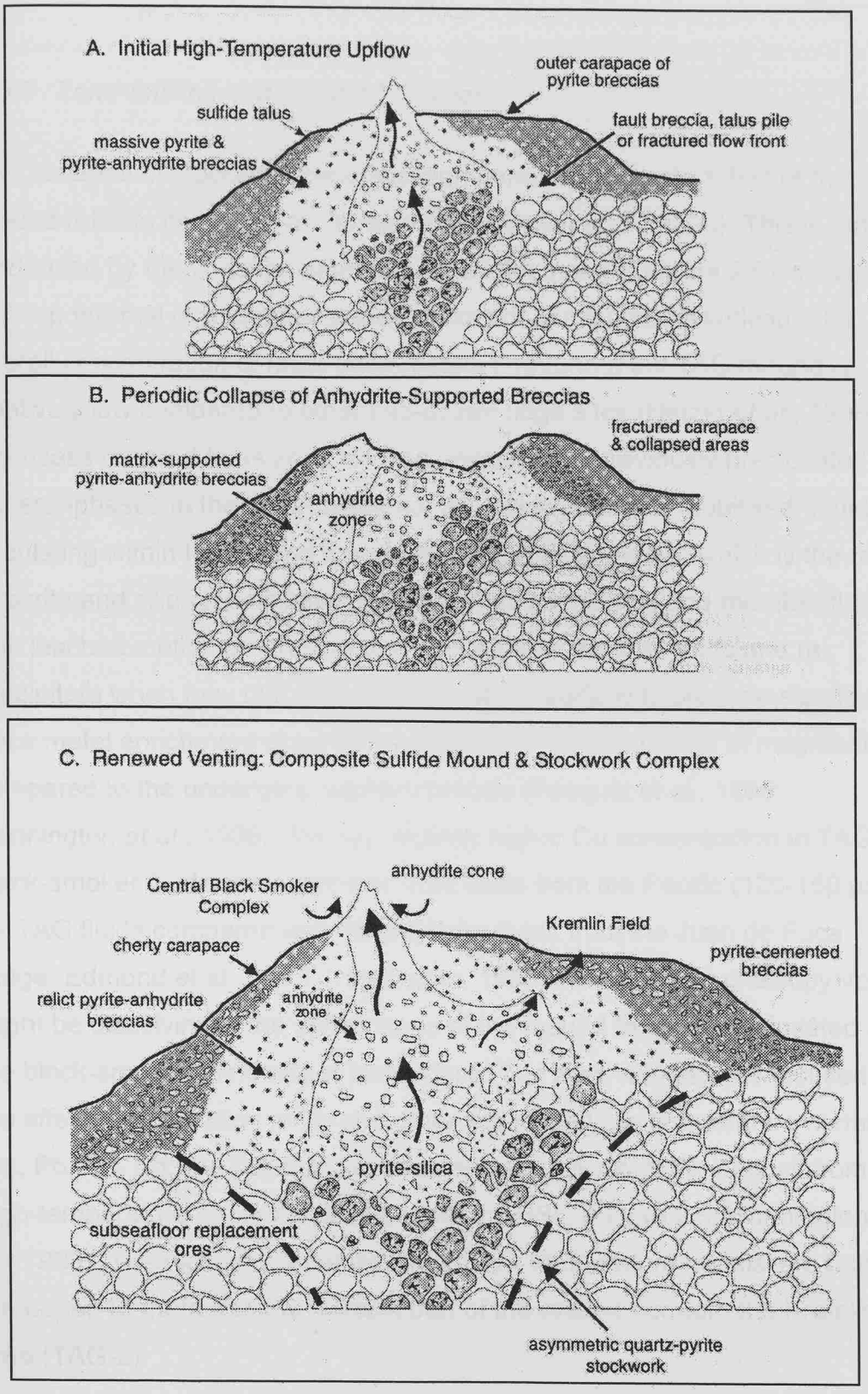

Figure 2.5: Model for the growth of the TAG mound and the development of a subseafloor stockwork. (A) Initial period of mound growth during episode of high-temperature venting and accumulation of sulphide and anhydrite in the mounds interior. (B) Dissolution of anhydrite during hydrothermal quiescence and collapse of the anhydrite-supported breccia. (C) Renewed hydrothermal activity through the collapsed breccia and development of new fluid pathways (adapted from Hannington *et al.*, 1998).

2.3.3 Zone-refining and gossan formation

The absence of stockwork mineralisation beneath the eastern half of the mound reflects its overall asymmetry (Hannington *et al.*, 1998). This is further evidenced by the zonation of metals within the mound (Figure 2.6), indicating a steep thermal gradient and a long history of continuous reworking. The overall concentration of most trace-metals throughout the TAG mound is relatively low compared to other mid-ocean ridge sites (Herzig *et al.*, 1998). In a process referred to as zone refining, metals from previously precipitated mineral-phases in the mounds interior are leached and re-mobilised. Fluids circulating within the mound are characterised by a low pH, which is the result of pyrite and silica precipitation from conductively cooled end-member fluids. The leached metals are transported within these reactive fluids and re-precipitate when they mix with seawater at the surface to produce significant trace metal enrichment of surficial sulphides of up to an order of magnitude compared to the underlying sulphide breccia (Fouquet *et al.*, 1998; Hannington *et al.*, 1998). The significantly higher Cu concentration in TAG black-smoker fluids compared with vent fluids from the Pacific (120-150 µmol/l for TAG fluids compared with 35 µmol/l for fluids from the Juan de Fuca Ridge; Edmond *et al.*, 1995; Von Damm, 1995) indicates that chalcopyrite might be dissolving in the upflow zone of the mound to be re-precipitated in the black-smoker chimneys at the surface. The zone refining has resulted in the effective separation of Zn and other associated low temperature metals (As, Pb, Cd, Ag, Au) towards the southeastern margin of the deposit from high-temperature assemblages beneath the BSC (Figure 2.6; Hannington *et al.*, 1998). The highest concentrations of 'low temperature metals' are found in the upper 10 metres of the eastern part of the mound beneath the Kremlin area (TAG-2).

A carapace of Fe-oxides and gossanous sulphide talus, overlying the cherty units and pyrite breccia is developed over much of the mound surface (Hannington *et al.*, 1998). On the flanks of the deposit the massive sulphides are exposed to seawater, causing extensive seafloor oxidation and metal-

mobilisation from primary phases. The metals are re-precipitated as crusts of secondary minerals including heamatite, goethite, jarosite, covellite and atacamite (Hannington *et al.*, 1988; Hannington *et al.*, 1995). Hydrothermal fluids undergo conductive cooling in the mound to precipitate a siliceous Fe-oxide cap before they are vented as diffuse fluids through the upper mound surface (Tivey *et al.*, 1995).

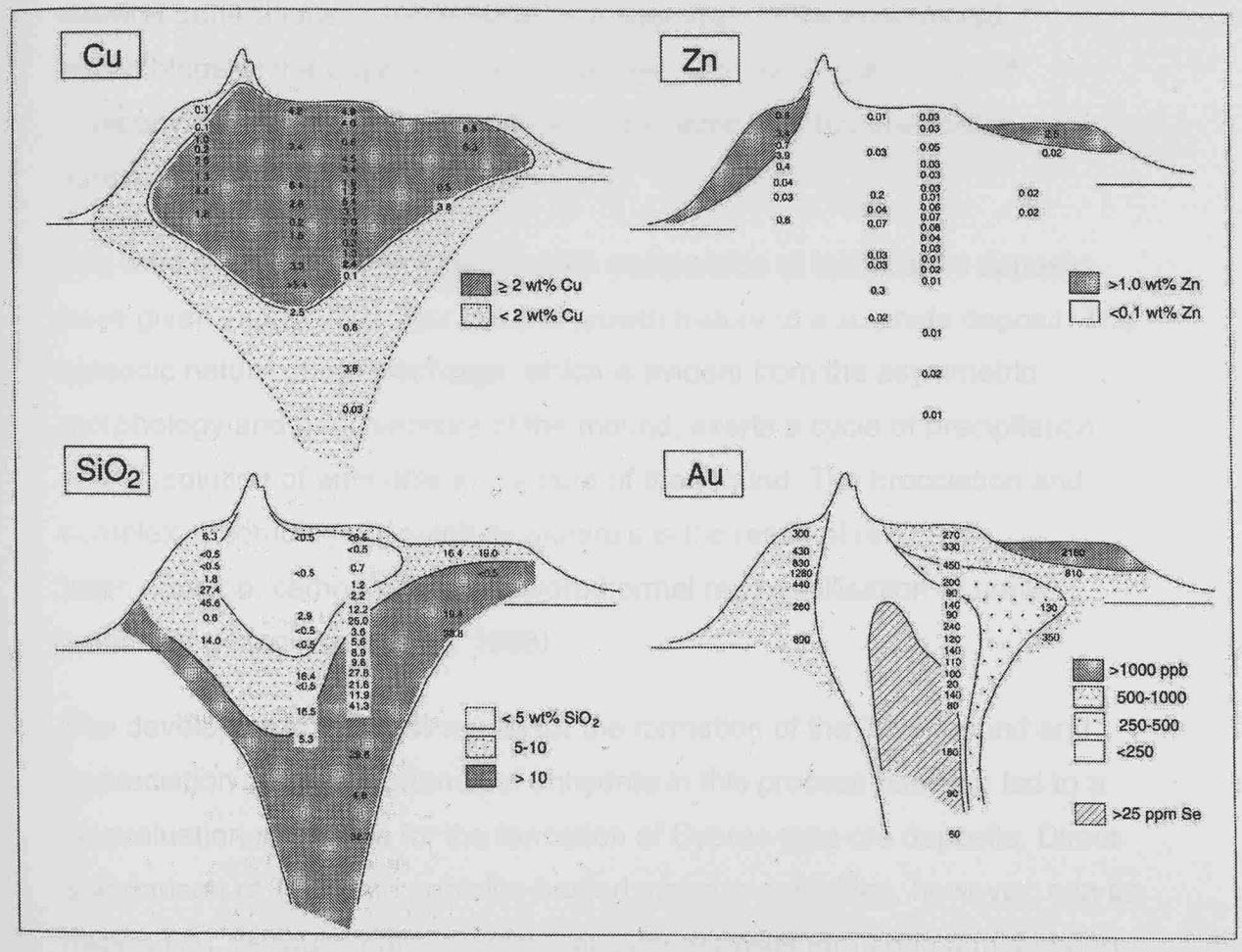

Figure 2.6: Zonation of metals in the TAG mound-stockwork complex (from Hannington *et al.*, 1998). Numbers projected onto the figures indicate bulk chemical analysis for the different drill holes. Zn and Au are concentrated near the surface and especially near the zone of low-temperature venting. Cu, in contrast, is present throughout the mound (adapted from Hannington *et al.*, 1998).

2.3.4 Ancient analogues

The morphology, size and bulk geochemistry of the TAG mound bears striking resemblance to ancient massive sulphide deposits in Cyprus (Constantinou and Govett, 1972; Boyle, 1987) and Oman (Robertson and Fleet, 1986; Karpoff *et al.*, 1988). A similar separation of metals into distinct zones and the occurrence of a funnel-shaped quartz-pyrite stockwork zone beneath the highest portions of the deposit makes the Troodos ophiolite in Cyprus the closest known ancient analogue to the TAG mound (Hannington *et al.*, 1998). Several generations of pyrite have been identified in the mineralised assemblage of the Cyprus mound sulphides, with varying amounts of chalcopyrite but virtually no sphalerite in the interior of the ore bodies (Constantinou and Govett, 1972).

The results of the drilling, together with comparison of land-based deposits, have given important insight into the growth history of a sulphide deposit. The episodic nature of the discharge, which is evident from the asymmetric morphology and geochemistry of the mound, exerts a cycle of precipitation and dissolution of anhydrite in the core of the mound. The brecciation and complex assemblage of sulphide minerals is the result of repeated fragmentation, cementation and hydrothermal re-crystallisation of earlier sulphides (Hannington *et al.*, 1998).

The development of a new model for the formation of the TAG mound and appreciation of the importance of anhydrite in this process has also led to a re-evaluation of models for the formation of Cyprus-type ore deposits. Direct comparison of TAG with ophiolite-hosted massive sulphides, however, can be misleading, because only few of the ancient deposits formed in a mid-ocean ridge setting, and more frequently they were formed in sedimented rifts (Hannington *et al.*, 1995).

A number of weathering features, such as the surficial metal enrichment and formation of gossan, have previously been thought to be the product of alteration by meteoric groundwater (Lydon, 1984). Drilling results and other

studies however, indicate that the majority of these features have formed while the deposit was still submerged beneath the sea. The presence of a siliceous carapace in the uppermost part of the mound may have inhibited deep weathering of the sulphides after cessation of active venting, by inhibiting fluid exchange between the mound and the surrounding seawater (Fouquet *et al.*, 1998; Hannington *et al.*, 1998). This silica-cemented layer is similar to the red cherts that are found in Cyprus-type massive sulphides (Richards and Boyle, 1986).

2.4 Relict hydrothermal deposits

2.4.1 The Mir zone

The *Mir* zone lies ~1.5 km northeast of the active mound (Figure 2.1) at a depth between 3430 and 3575 m. Its maximum diameter is 1 km and it comprises of diverse hydrothermal precipitates, including coarse-grained massive sulphide, Fe-oxides, silicate and other low-temperature deposits (Rona *et al.*, 1993a; Rona *et al.*, 1993b). A small mound, ~100 m in diameter and ~10 m high, has been identified and discrete groups of tens of massive sulphide chimneys in the central area were imaged during a deep-tow camera deployment (Rona *et al.*, 1993b), suggesting that high-temperature venting at this site may have stopped only recently. The youngest samples from these chimneys were dated radiometrically as 870±200 years (Lalou *et al.*, 1995). Rona *et al.* (1996) have detected heat flow values of 9-13 W/m^2 in several areas across the *Mir* zone, which are significantly higher than background values from the same area (0.3-1.9 W/m^2). The similarity in dimension and shape to the currently active TAG mound is striking and suggests that the *Mir* zone represents a later stage in the development of a high-temperature deposit, when venting has ceased and the sulphide mound is destroyed by mass wasting and submarine weathering.

2.4.2 The Alvin zone

The *Alvin* zone is situated 2-4 km northnortheast of the TAG mound (Figure 2.1) on the lower east wall between 3400 and 3600 m depth. A set of axis

parallel faults extends from the TAG mound into the *Alvin* zone. This may suggest that these faults exert control on the location of the hydrothermal activity by producing pathways for fluid flow from a heat source below the ridge axis (White *et al.*, 1998). The 2 km long discontinuous exposure of sulphide deposits consists of several circular or semi-circular mound-like features, each about 200 m in diameter (Rona *et al.*, 1996). Samples from the flanks and top of the mounds consist of pyrite with minor chalcopyrite and sphalerite, and with only a thin layer of Fe-oxide. Atacamite coating on some of the samples indicates leaching of Cu from the sulphide (Rona *et al.*, 1996). A gravity core recovered from the southern periphery of this zone revealed a succession of distinct layers of sulphide debris intercalated with carbonate-rich deposits (Metz and Trefry, 1988; Mills *et al.*, 1993). These record hydrothermal events at 8,500 and 6,000 years B.P., whereas no significant sulphidic hydrothermal input is evident over the past 4,000 years (Metz and Trefry, 1988).

Following a high-resolution side scan sonar and video survey in the TAG field, Rona *et al.* (1998) and White *et al.* (1998) reported the discovery of three previously unidentified mounds in the *Alvin* zone. The Southern mound extends the known length of the *Alvin* zone by ~500 m towards the southwest. It is covered with weathered and sedimented sulphide blocks and it appears that this mound has been inactive for quite some time (White *et al.*, 1998). A newly described mound near the southwestern margin of the *Alvin* zone was identified by White *et al.* (1998), who named it the New mound, and by Rona *et al.* (1998), who proposed to call it the Shinkai mound. This mound rises ~70 m from the seafloor, which is markedly higher than the active TAG mound (~50 m). This relict mound is currently undergoing dissection by mass wasting, and a central low might indicate that previously present massive anhydrite below the mounds surface has been dissolved after high-temperature venting at this site ceased (Rona *et al.*, 1998).

The most significant finding however, is the discovery of the Shimmering mound at the northern end of the *Alvin* zone. It owes its name to the venting of clear, low-temperature solutions (22.5°C), which has been observed across

the southwestern half of the mound. The diffuse fluids are seeping through layers of Mn- and Fe-oxyhydroxides, and some anemones and bacterial mats have also been observed (Rona *et al.*, 1998). The occurrence of nearby high-temperature venting is indicated by significant transmissometer anomalies, although no direct evidence has been found to date (Rona *et al.*, 1998).

2.5 Summary

The drilling results from the active mound confirm the predictions from earlier models of mound growth and mineralisation-processes within the mound as they were derived from comparison of vent fluid chemistry and analysis surface mineral phases. The implication is that the TAG hydrothermal system is episodic and highly dynamic in nature (Edmond *et al.*, 1995; Humphris *et al.*, 1995; Mills and Elderfield, 1995a; Edmonds *et al.*, 1996; James and Elderfield, 1996a; Honnorez *et al.*, 1998; Knott *et al.*, 1998; You and Bickle, 1998). The penetration of seawater into the deep subsurface zone and also at shallower depth appears to be an important feature of the active mound. It causes not only precipitation of massive anhydrite, but also significant fluid alteration and hence re-working of the mound sulphides. The ongoing sulphide precipitation beneath the surface cap of Si- and Fe-oxides reduces the loss of sulphide and metals to the hydrothermal plume, thus facilitating the growth of a sulphide deposit of significant size (Edmond *et al.*, 1995; Tivey *et al.*, 1995). The fate of a massive sulphide deposit following cessation of high-temperature venting is demonstrated in the two relict hydrothermal zones, where the inferred dissolution of massive anhydrite in the deposits interior and continuous mass-wasting and erosion enhances the weathering of the deposit.

The extreme longevity of venting at TAG is attributed to a deep-seated semi-continuous heat source (Kong *et al.*, 1992) that is tapped by structural and permeability controls manifest on the seafloor (Kleinrock and Humphris, 1996). The active mound is only a minor part of the overall hydrothermal field, maybe <5 % by volume. Understanding the fate of hydrothermal deposits after cessation of venting is crucial to our understanding of their impact on the ocean system and preservation in the geological record.

Chapter 3

Sampling and General Sediment Geochemistry

As part of the BRIDGE (British Mid-Atlantic Ridge Initiative) programme, a large number of sediment cores were recovered from the *Mir* and *Alvin* relict zone in the TAG hydrothermal area during RV Charles Darwin cruise CD102 in September '96 (Palmer and scientific party, 1996). A box-corer, gravity-corer and a multi-corer were successfully deployed. Twelve of the cores recovered were processed directly on board and a further 13 cores plus a number of small samples were archived for later experiments. The locations of the cores are listed in Table 3.1 and plotted in Figure 3.1. After preliminary porewater and solid phase analysis on several cores, it was decided to concentrate on core 43, since this proved to contain significant sulphide enrichment. Core 43 was collected from the southern periphery of the *Alvin* zone at 26°09.26'N 44°48.90'W and 3595 m water depth. Detailed measurements from this core were compared with a number of other cores from the *Mir* and *Alvin* zones, including published data for a metalliferous sediments core that was recovered <500 m northwest of core 43 (Metz and Trefry, 1988; Mills *et al.*, 1993). Also described is the background core 10, which was recovered at 29°23.55'N 43°25.00'W about 50 km west of the Broken Spur hydrothermal vent site.

Station No.	Latitude	Logitude	Core Type	Recovery (cm)	Action*	Comments
10	29°23.55'N	43°25.00'W	Gravity	221	P	carbonate ooze
11	29°23.44'N	43°24.92'W	Multi	30	P	carbonate ooze
13	29°23.64'N	43°24.92'W	Box	36	P	carbonate ooze
17	26°08.65'N	44°48.39'W	Gravity	77	A	Fe-stained carbonate ooze
18	26°08.53'N	44°48.38'W	Gravity	221	P	carbonate ooze grading into Fe-oxide rubble
19	26°08.59'N	44°48.22'W	Box	33	P	Fe-stained carbonate ooze, some Mn-oxide staining, filamentous organism on surface
24	26°08.63'N	44°48.32'W	Gravity	40	A	Fe-stained carbonate ooze
25	26°08.61'N	44°48.42'W	Multi	15	P	carbonate ooze grading into Fe-oxide rubble, Mn-oxide crusts on surface
27	26°08.51'N	44°48.45'W	Gravity	120	A	Fe-oxide rubble, some chimney fragments
31	26°08.47'N	44°48.47'W	Gravity	20	A	sulphide debris
32	26°08.49'N	44°48.49'W	Gravity	152	A	Fe-oxide rubble
37	26°08.56'N	44°48.42'W	Gravity	205	P	carbonate ooze grading into Fe-oxide rubble
41	26°09.20'N	44°48.93'W	Gravity	139	A	carbonate ooze grading into Fe-oxide rubble
42	26°09.26'N	44°48.95'W	Gravity	182	A	carbonate ooze grading into Fe-oxide rubble, some sulphide layers?
43	26°09.26'N	44°48.90'W	Gravity	228	P	carbonate ooze grading into Fe-oxide rubble, two sulphide layers
47	26°09.30'N	44°48.89'W	Box	40	P	carbonate ooze grading into Fe-oxide rubble
50	26°09.26'N	44°48.88'W	Gravity	52	A	Fe-stained carbonate ooze
52	26°09.28'N	44°48.92'W	Gravity	257	A	carbonate ooze grading into Fe-oxide rubble
53	26°09.26'N	44°48.93'W	Multi	25	P	Fe-stained carbonate ooze, nontronite (?) layer, some Fe-oxide rubble
55	26°08.48'N	44°48.48'W	Gravity	79	A	Fe-oxide rubble
56	26°08.59'N	44°48.39'W	Box	35	P	carbonate ooze grading into Fe-oxide rubble, weathered chimney fragments with filamentous organism on surface, some atacamite
57	26°08.54'N	44°48.44'W	Gravity	140	A	carbonate ooze grading into Fe-oxide rubble and nontronite (?) at base
58	26°09.26'N	44°48.90'W	Gravity	200	A	carbonate ooze grading into Fe-oxide rubble
60	26°08.48'N	44°48.50'W	Gravity	112	A	carbonate ooze grading into Fe-oxide rubble
66	26°08.51'N	44°48.47'W	Multi	4	P	Fe-oxide rubble

* P = processed on board, A = archived

Table 3.1: Core locations and brief description for cores recovered during cruise CD102.

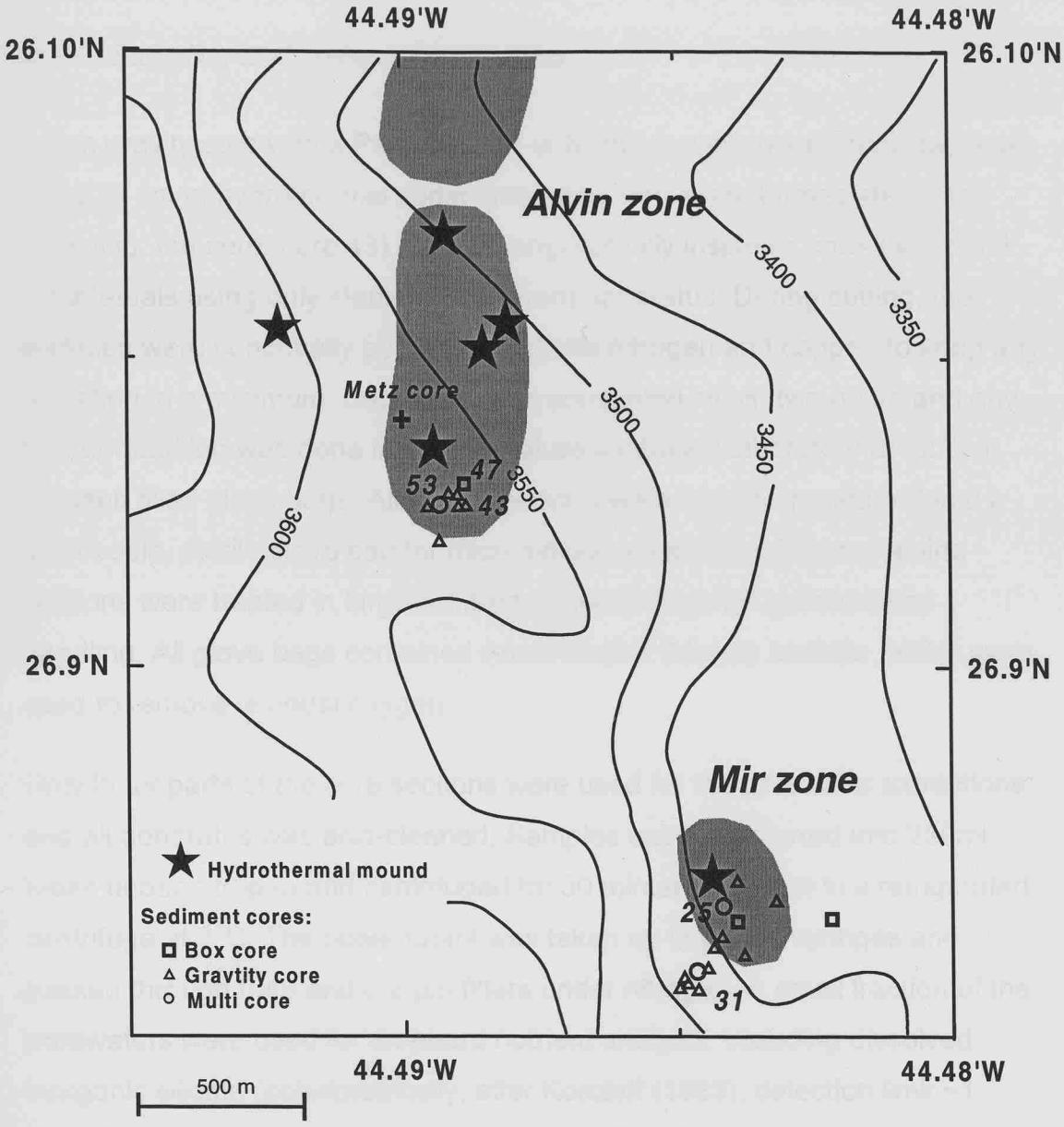

Figure 3.1: Core location of metalliferous sediments recovered during cruise CD102 from the *Alvin* and *Mir* relict hydrothermal deposits in the TAG vent field. Numbers indicate locations of cores that are discussed in this thesis, including core 43 and the 'Metz core', which was described in detail by Metz *et al.* (1988) and Mills *et al.* (1993).

3.1 Methods

3.1.1 Sampling and on-board processing

A 3 m gravity core with a Perspex liner of 6 cm i.d. was successfully deployed, and 228 cm of hydrothermal sediments were recovered. Immediately after sampling, the core (core 43) was cut longitudinally inside its core-liner into 5 cm intervals using only sterile (autoclaved) apparatus. During cutting, the surfaces were continually purged with sterile nitrogen and capped to keep any oxidation to a minimum. Sectioning was completed within two hours and any further handling was done in a temperature controlled laboratory at ~2°C in nitrogen filled glove bags. Alternate sections were directly transferred into a disposable, sterile glove bag for microbiological handling. The remaining sections were treated in large solid-frame glove bags for geochemical handling. All glove bags contained Anaerocult-A (Merck) sachets, which were used to remove residual oxygen.

Only inner parts of the core sections were used for the porewater extractions and all apparatus was acid-cleaned. Samples were transferred into 250ml tubes under nitrogen and centrifuged for 30 min at 3000 rpm in a refrigerated centrifuge at 2°C. The supernatant was taken up in plastic syringes and passed through 0.45 and 0.2 µm filters under nitrogen. A small fraction of the porewaters were used for on-board nutrient analysis, including dissolved inorganic silicate (colorimetrically, after Koroleff (1983), detection limit ~1 µmol/l) and hydrogen-sulphide (colorimetrically, after Cline (1969), detection limit ~1 µmol/l). Aliquots of sample were added to zinc acetate (10 % w/v) and stored for subsequent sulphate analysis by ion exchange chromatography. The remaining samples were acidified with 100 µl 6 M sub-boiling distilled (SBD) HCl and stored in 15 ml acid washed LDPE bottles for later metal analysis. The solid phase in the centrifuge bottles were sealed airtight under nitrogen and stored in anaerobic bags.

For the bacterial analysis, up to 10 mini-subcores were taken from whole round sections using autoclaved 5 cm^3 plastic-syringes from which the luer

ends had been removed. These were sealed with rubber seals and dealt with immediately, or temporarily stored in anaerobic bags for later experiments.

3.1.2 Shore-based geochemical analysis

Only the analytical techniques for major elements, mineralogy and carbon and sulphur analysis are described in this chapter. All further analyses are described in the relevant chapters, except for the microbiological processing, which is described in Appendix A.

For the solid phase analysis, sediments from the porewater squeeze cakes as well as left-over samples from the microbiological analysis were used. All samples were oven-dried at 110°C over night and crushed using an agate pestle and mortar

3.1.2.1 Major elements

Major elements (Si, Al, Fe, Mn, Ca, P, Cu and Zn) were determined on a Philips PW 1400 X-ray Fluorescence Spectrometer. Before preparation of a fused bead, the samples were ignited at 980°C to remove any sulphides, carbonates or organic matter. A lithium tetraborate flux (Spectroflux 100) was used and samples were fused in platinum crucibles at a dilution of 1:5 (for carbonate samples) to 1:40 (for samples rich in Cu). The final concentrations were corrected for loss on ignition. Inter-batch precision was 1-5% for Si, Fe, Ca, and P, and 5-10 % for Al, Mn, Cu, Zn (both 2σ). Accuracy for the analysis was monitored by simultaneous analysis of standard reference materials of known concentrations (BEN: international basalt standard, Zn and Cu standards are in-house reference material). Accuracy was better than 3% except for Cu and Zn, where it was better than 6% (Table 3.2).

3.1.2.2 Mineralogy

An overview of the bulk mineralogy was obtained from X-ray diffraction (XRD) patterns for selected samples for each sedimentary layer. Analysis was done

on a Philips EW 1730 automated powder diffractometer using Co-K_α radiation. Dry powder mounts were scanned between 0° and 60° at 1.2° 2θ/min.

3.1.2.3 Carbon and sulphur analysis

Total carbon, organic carbon and total sulphur were analysed using a Carlo Erba EA 1108 elemental analyser. The dry, ground sediments were weighed directly into tin pressed capsules. Pure calcite and acetanilide were used to calibrate for C and S respectively, and the same materials were used to monitor the signal drift. The calibration was only repeated if instrument parameters, such as gas flow rate, were adjusted, or if the signal drift exceeded ±5 % of the original value for the reference material. The detection limit for C was 0.07 % for ~3 mg of sample (3 times the standard deviation of the blank tin capsule). The detection limit for S is not determined by the blank, but by the sensitivity of the detector, and is quoted by the manufacturer as 0.1%. The within-run precision was typically better than 4% for C and 10 % for S (2σ). The calcium carbonate content was calculated from the bulk Ca content assuming that all Ca is held as $CaCO_3$, an assumption that is justified by a molar ratio of Ca to C_{tot} of ~1.

	SiO_2	Al_2O_3	Fe_2O_3	MnO	CaO	P_2O_5	Cu	Zn
	%	%	%	%	%	%	%	%
BEN	38.48	10.04	12.67	0.20	14.02	1.08	-	-
BEN	38.60	10.08	13.03	0.19	13.70	1.06	-	-
BEN	38.36	10.22	13.15	0.19	13.89	1.09	-	-
BEN	38.19	10.38	13.18	0.20	14.25	1.12	-	-
BEN	37.45	10.73	13.35	0.20	14.32	1.05	-	-
Mean	38.22	10.29	13.08	0.20	14.04	1.08	-	-
RSD (2σ)	2.4	5.5	3.9	6.0	3.7	4.9	-	-
BEN reference value*	38.20	10.07	12.84	0.20	13.87	1.05	-	-
Accuracy (%)	0.0	2.2	1.9	1.8	1.2	3.1	-	-
Zn std.	50.12	12.00	15.91	0.20	7.62	0.48	-	0.91
Zn std.	50.64	12.45	15.53	0.21	7.38	0.45	-	0.95
Zn std.	49.87	12.12	15.62	0.21	7.69	0.50	-	0.97
Mean	50.21	12.19	15.69	0.21	7.87	0.48		0.94
RSD (2σ)	1.6	3.8	2.5	5.6	4.1	10.6		6.5
Zn std. predicted conc.**								1.00
Accuracy (%)								5.7
Cu std.	76.17	-	21.20	-	-	-	1.09	-
Cu std.	75.51	-	21.54	-	-	-	1.07	-
Cu std.	76.64	-	21.07	-	-	-	1.03	-
Mean	76.11		21.27				1.06	
RSD (2σ)	1.5		2.3				5.4	
Cu std. predicted conc.**							1.00	
Accuracy (%)							6.2	

* Recommended values from Govindaraju (1996)
** Predicted concentrations (I.W. Croudace, pers. comm.)
Dash indicates element not reported.

Table 3.2: Repeat analysis of standard reference material by XRF.

3.2 General features of cores from the Alvin and Mir zones

Almost all cores that were recovered from the two relict hydrothermal vent sites had a carbonate cap ranging from only few centimetres up to 75 cm in thickness. The carbonate typically showed increasing iron-staining with depth (Figure 3.2). Another common feature is a surficial Mn enrichment, which was visible as a dark band in the carbonate cap. The Mn enrichment was usually of the order of 1-10 %. Extreme Mn enrichment of 18% was found in core 25 from the *Mir* zone, which had a surface crust of 2-4 mm Mn-oxide. Mn-rich deposits are commonly found at greater distances from the sites of high temperature venting, such as the low-temperature deposits on the eastern valley wall (Thompson *et al.*, 1985). Mn enrichments of similar magnitude have however, been described for a core from the southern periphery of the active TAG mound (Goulding *et al.*, 1998).

The carbonate caps were usually underlain by Fe-rich sediment of hydrothermal origin. Some cores contained chimney fragments in the surface sedimentary layer that were up to 5 cm across. The Fe-rich deposits graded from bright red, indicative of Fe-oxide, to greenish colour, which is indicative of nontronite. Sulphides were less common, but this is probably explained by the difficulties encountered during sampling rather than reflecting their true abundance. For example, when core 31 was recovered it appeared that the core barrel was filled with sulphidic sediments. However, as soon as the core came out of the water, due to the weight of the sulphides the core catcher was not able to hold the sediments inside the core barrel and almost the entire content slumped out before the corer could be brought back on deck.

Atacamite ($Cu_2Cl(OH)_3$) is a common sulphide weathering product that was frequently found in layers up to few centimetres thick. Atacamite is a secondary hydrothermal mineral, which is intimately associated with weathering of chalcopyrite (Hannington, 1993). Figure 3.3 shows a sediment sample from a core-catcher that contains bright green crusts of atacamite.

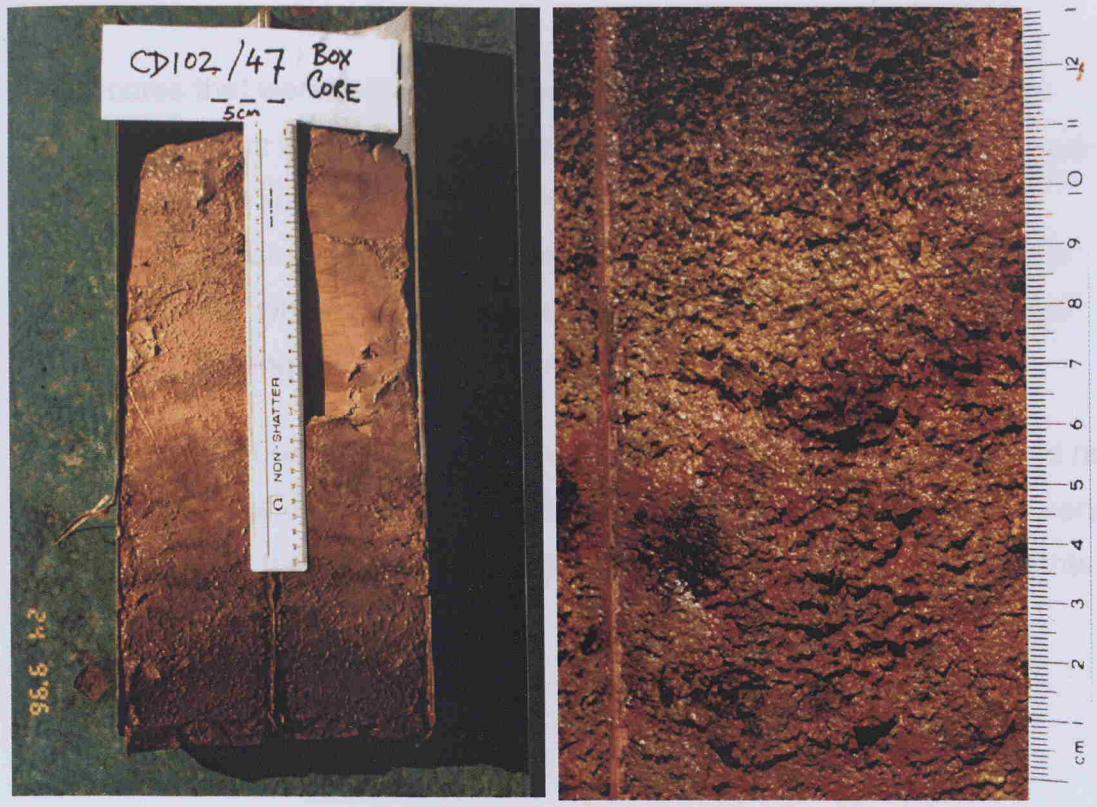

Figure 3.2: Carbonate cap of core 47, which was recovered in close proximity to core 43. The image shows the increasing iron-staining towards the base of the carbonate cap. The right hand panel is a detail from the carbonate cap from about 35 cm depth, showing the heterogeneous nature of the sediments (note that ruler on right hand panel is for scale only).

Figure 3.3: Oxidised sulphide sediments with bright green atacamite crust.

Many cores that were recovered by box- or multi-core showed hair-like organisms of less than 1 mm diameter and ~1 cm length, which were growing on the sediment surface or on chimney fragments. These are tentatively interpreted as filamentous bacteria, as they are commonly observed in the vicinity of vents, where they grow as dense mats and are often associated with diffuse venting (Jannasch and Wirsen, 1981).

Frequently the corer came up empty with only a few basalt fragments and no indication that the corer had penetrated the sediments. This reflects the very patchy nature of the sediment cover in this rugged terrain, where sediments often occur in isolated ponds.

3.3 Results

Major element data for core 43 are listed in Table 3.3, and these are plotted in Figure 3.4. Missing sample ID's in Table 3.3 (e.g. samples 2 and 4) indicate that no analysis was performed for these core sections, because high sample resolution at that depth was considered less important. From the initial visual inspection, and as subsequently confirmed by the solid phase data, core 43 was subdivided into four stratigraphic layers. At the surface, the sediments are capped by a ~50 cm thick layer of carbonate–rich sediments of dominantly pelagic origin, which grades into Fe-oxides towards the base. The carbonate content in this layer ranges between 2 and 66 %, whereas below 50 cm depth the carbonate content is generally less than 1 %. A visibly darker layer at 30 cm is marked by an increase in solid phase Mn, which increases from 0.1 to a maximum of 0.75 %.

An upper sulphide layer is located between 50 and 70 cm, and a second sulphide layer extends from 170 cm to the base of the core (228 cm). Both layers are marked by a sharp increase in S_{tot} to concentrations of up to 27 %, whereas for the remainder of the core, levels are mostly below detection limit. The two layers are interbedded with a 100 cm thick zone of Fe-oxysilicates.

The dominant mineral phases in both sulphide layers are pyrite (FeS_2) and goethite (FeOOH) with some chalcopyrite ($CuFeS_2$), sphalerite ([Zn,Fe]S), and the upper sulphide layer also contains some atacamite. Silica concentrations are low in the lower sulphide layer, but markedly elevated in the upper sulphide layer.

The background core consists of dominantly calcium carbonate ranging from 85 to 92 %. Si concentrations range between 1 and 3 % and Fe content is below 1 % throughout the core.

Sample ID	Depth cm	Si %	Al %	Fe %	Mn %	Ca %	Ctot %	Stot %
Core 43								
1	2.5	4.6	0.8	16.8	0.43	22.1	6.6	0.1
3	12.5	3.8	0.8	10.3	0.13	26.4	8.1	0.2
5	22.5	4.8	0.8	12.1	0.41	25.2	7.8	bdl
6	27.5	8.3	1.7	17.9	0.46	15.8	3.7	bdl
7	32.5	7.6	1.4	18.7	0.74	16.5	5.0	bdl
8	37.5	8.5	1.0	29.7	0.41	7.5	3.1	0.1
9	42.5	11.1	1.3	33.7	0.25	1.8	0.6	0.2
10	47.5	9.4	0.5	39.4	0.06	0.7	0.4	0.1
11	52.5	4.3	bdl	38.9	0.02	0.2	0.3	25.7
12	57.5	11.9	bdl	37.2	0.03	0.4	0.6	6.4
13	62.5	8.7	bdl	37.9	0.02	0.2	0.1	19.7
14	67.5	11.6	0.1	35.4	0.03	0.4	0.2	10.9
15	72.5	13.9	0.6	31.3	0.02	0.3	0.5	0.4
16	77.5	14.3	0.1	37.3	0.03	0.4	0.2	0.6
17	82.5	12.7	0.1	34.1	0.01	0.3	0.3	0.4
19	92.5	14.3	bdl	34.2	0.02	0.3	0.2	0.6
21	102.5	15.7	bdl	30.8	0.01	0.3	0.1	0.3
23	112.5	13.6	bdl	33.9	0.03	0.2	0.2	0.2
25	122.5	13.8	bdl	38.2	0.03	0.3	0.2	0.7
27	132.5	12.3	bdl	37.9	0.09	0.6	0.2	0.2
28	137.5	14.4	0.1	34.1	0.10	0.7	0.3	0.3
29	142.5	16.3	bdl	32.7	0.07	0.6	0.2	0.2
30	147.5	15.2	bdl	32.9	0.10	0.6	0.2	0.1
31	152.5	15.6	bdl	32.6	0.06	0.4	0.2	0.2
32	157.5	16.5	0.3	30.1	0.07	0.3	0.3	0.1
33	162.5	10.4	0.5	37.0	0.04	0.3	0.3	0.2
34	167.5	5.7	bdl	46.2	0.05	0.5	0.4	1.8
35	172.5	2.4	bdl	44.4	0.01	0.2	0.3	20.3
36	177.5	5.0	bdl	46.6	0.05	0.3	0.4	7.2
37	182.5	4.0	bdl	46.8	0.03	0.3	0.4	10.6
38	187.5	3.7	bdl	45.6	0.01	0.2	0.3	13.7
39	192.5	3.2	bdl	44.7	0.01	0.2	0.2	21.3
40	197.5	3.2	bdl	45.2	0.01	0.2	0.4	17.9
41	202.5	2.6	bdl	45.3	0.00	0.1	0.2	27.3
42	207.5	3.6	bdl	43.2	0.01	0.1	0.2	24.2
43	212.5	5.6	bdl	42.9	0.00	0.3	0.3	11.2
44	217.5	5.4	bdl	41.2	0.02	0.2	0.3	13.9
45	222.5	4.5	bdl	44.9	0.01	0.3	0.4	6.9
46	227	4.2	0.3	44.8	0.02	0.3	0.3	11.8
Core 10								
minimum		1.1	0.5	0.5	bdl	33.9	10.3	bdl
maximum		2.8	1.1	0.8	0.1	36.9	11.1	bdl

bdl = below detection limit

Table 3.3: Major element concentrations for core 43, and minimum and maximum concentrations for the background core 10.

3.4 Discussion

3.4.1 Core 43

A distinct peak in Mn at 30 cm marks the locus of the Mn^{2+}/Mn^{4+} transition (Figure 3.4), where upwards diffusing dissolved Mn is precipitated as Mn-oxide on encounter of oxidised bottom water. Towards the base of the carbonate cap, the sediments are increasingly admixed with Fe-oxyhydroxides. This is evident from the bright red staining, the increase in Fe content and the coupled decrease in $CaCO_3$. In order to sample the pore-waters anoxically it was not possible to split the core, but Figure 3.2 shows the carbonate cap from a box core that was recovered in close proximity to core 43. The most likely source of the Fe-staining is fall-out from the hydrothermal plume, which produces a continuous rain of Fe-oxyhydroxides. Some of the staining however, occurs as dark red spots up to several millimetres across. These have the appearance of weathered sulphide

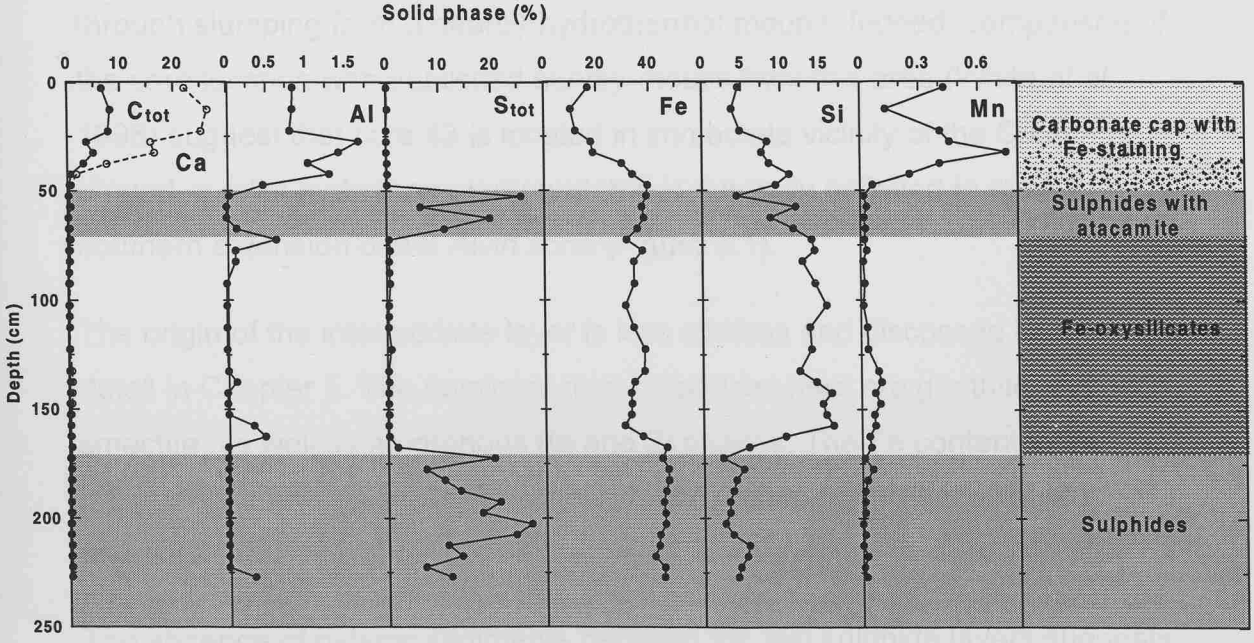

Figure 3.4: Profiles for major elements and stratigraphy for core 43. The grey shading marks the location of the two sulphide layers.

fragments, which have been mixed into the sediments through mass-gravitational transport in addition to the fine-grained plume-derived particles. Apart from the top 30 cm, solid phase Fe is very high throughout the core (30 to 47 %), and levels are comparable to published data for metalliferous sediments (Metz and Trefry, 1988; German *et al.*, 1993; Mills *et al.*, 1993).

The occurrence of sulphides in distinct layers is interpreted as the result of episodic transport of debris from sulphide sources higher up on the *Alvin* mound. The two sulphide layers are composed of dominantly medium- to coarse-grained sulphides. Similar sulphide layers have been described for sediments from this area, where X-radiography clearly identified them as mass-flow events (Metz and Trefry, 1988). Slumping is a commonly observed process in the rugged terrain of the median valley. Once the high temperature venting ceases, chimneys on top of the mound collapse and disintegrate, and a blanket of sulphide debris accumulates across the surface of the mound. Mass-gravitational sediment transport from the mound and the steep talus slope is promoted by frequent fault activation and micro-earthquakes near the ridge-axis. It is assumed that the two sulphide layers in core 43 formed through slumping from a nearby hydrothermal mound. Indeed, comparison of the core location with published survey-results from this area (White *et al.*, 1998) suggest that core 43 is located in immediate vicinity of the Southern Mound, a relict hydrothermal mound that is currently believed to mark the southern extension of the *Alvin* zone (Figure 3.1).

The origin of the intermediate layer is less obvious and discussed in more detail in Chapter 5. The dominant mineral phases here are goethite and smectite, as well as amorphous Fe and Si phases. The Fe content in the intermediate layer is similar to concentrations measured in the sulphide layers.

The absence of pelagic sediments between the two sulphide layers suggests that they were deposited in close succession, probably during the same phase of high-temperature venting in this zone. The Fe oxysilicate in the intermediate layer could have been deposited by a similar mass-wasting

event from the steep talus slope of the active mound. The lack of any significant Ca or Al in the intermediate layer indicates that these sediments were deposited rapidly without dilution by pelagic sedimentation.

3.4.2 Core 10

The background core 10 was recovered from ~50 km west of the MAR at the latitude of the Broken Spur vent field, outside the median valley on crust ~5 Ma old. The water depth at this site was 3350 m, which is well above the lysocline at ~4400 m in the North Atlantic. The core liner contained 221 cm of homogenous, relatively indurated carbonate ooze. These sediments are of dominantly pelagic origin with no indication of hydrothermal plume input.

3.5 Summary

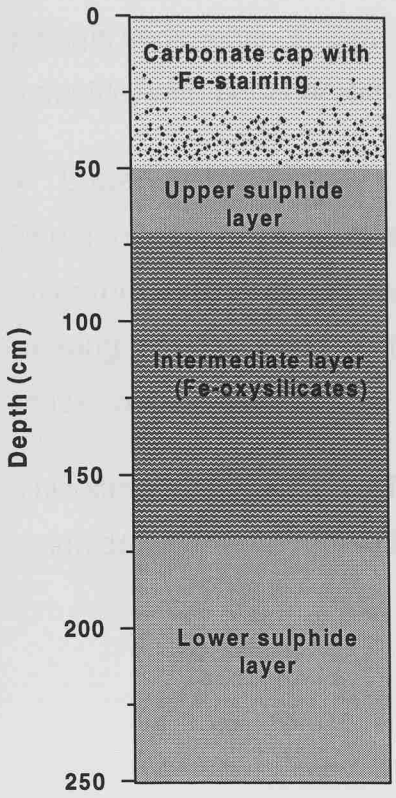

Figure 3.5: The major lithologies of core 43.

According to the major element chemistry and the mineralogy, core 43 can be subdivided into four distinct stratigraphic units (Figure 3.5):

- Carbonate cap, 0-50 cm:

Sediments at the surface grade from carbonate ooze into Fe-oxyhydroxides with only minor carbonate. The Fe enrichment in this layer is derived primarily from plume-fallout. A layer of Mn-oxide at 30 cm marks the redox-boundary.

- Upper sulphide layer, 50-70 cm:

This layer is composed of mostly pyrite with some Fe-oxide and traces of other sulphide minerals. It has been emplaced through mass-wasting from a high-temperature sulphide mound. Atacamite is the principle Cu-bearing mineral phase in this layer.

- Intermediate layer, 70-170 cm:

This layer of Fe-oxysilicates contains only trace amounts of sulphide and pelagic sediments. The most abundant mineral phases are goethite and smectite, with some amorphous Fe-oxide and silica.

- Lower sulphide layer, 170-228 cm (base):

The dominant mineral phase is pyrite, but in contrast to the upper sulphide layer this layer does not contain any atacamite. Instead, the dominant Cu-bearing mineral phase is chalcopyrite. Again, deposition occurred through a mass-wasting event.

This stratigraphy will be referred to throughout the thesis, and the two sulphide layers are marked in all elemental profiles as shaded areas.

Chapter 4

The Diagenesis of Metalliferous Sediments

4.1 Introduction

4.1.1 The origin of sedimentary metal enrichments in the deep sea

Over a decade before the first active vents were discovered on the TAG mound (Rona *et al.*, 1986), metal-rich deposits composed predominantly of Mn-oxide (39% Mn) were described from the TAG hydrothermal field (Scott *et al.*, 1974). The sediments occur as a discontinuous veneer up to several metres thick directly on terraces that were formed by faulting on the valley wall, or in isolated ponds on the valley floor (Shearme *et al.*, 1983). They are easily identified by their striking colours, ranging from orange, brown, buff, black, green to bright red (Bischoff, 1969).

The link between active ocean ridges and high Mn and Fe content in deep-sea sediments was established in the mid to late 1960's (Arrhenius and Bonatti, 1965; Boström and Peterson, 1966; Boström *et al.*, 1969; Boström and Peterson, 1969; Bender *et al.*, 1971). To examine the geographic distribution of sedimentary metal enrichment, Boström et al. (1969) produced a map of Al/(Al+Fe+Mn) ratios from core top samples throughout the Pacific, Atlantic and Indian Ocean. This map clearly shows that metalliferous sediments, which are characterised by ratios markedly below 0.6 and hence

markedly lower than average detrital material of continental origin, delineate the spreading centres. Boström *et al.* (1969) invoked the source of these anomalies to be "juvenile contributions from the deeper zones of the earth". At the same time Corliss (1971) noted that freshly extruded basalts have a reduced metal content, and concluded that the metals are leached from the rocks during reaction with cold seawater. The origin of these metal enrichments in the sediments, however, could only be hypothesized before the first direct evidence of hydrothermal venting was found in the Pacific (Corliss *et al.*, 1979).

Metal enriched deposits were also observed in basal sediments to either side of the spreading centres (von der Borch and Rex, 1970; Cronan *et al.*, 1972; Barrett *et al.*, 1987). Compositional and mineralogical similarities strongly implied that these deposits formed under similar conditions and hence are quite uniform in time and space. These sediments also show striking similarities with the umbrous hydrothermal deposits that are overlying the Troodos ophiolite (Constantinou and Govett, 1972; Robertson and Hudson, 1973; Robertson and Boyle, 1983).

A more detailed geochemical analysis of the sediments has shown that whilst some components have a distinct volcanigenic signature, others are clearly derived from seawater (Bender *et al.*, 1971; Dymond *et al.*, 1973). Oxygen isotope ratios indicate that metalliferous sediments are in equilibrium with seawater and their formation is not significantly influenced by magmatic water. Similarly, Sr and U isotopic ratios demonstrate that most of the Sr and U are derived from seawater. Fully oxidised, goethite-rich sediments show a narrow range of S-isotopic values which are similar to marine sulphates and do not correlate with either magmatic or biogenic sulphides (Dymond *et al.*, 1973). Pb isotopes, in contrast, all exhibit fairly uniform values typical of mixing of local basalts with detrital material (Bender *et al.*, 1971; Dymond *et al.*, 1973; Barrett *et al.*, 1987; German *et al.*, 1993).

Two different end-members of metalliferous sediments can be distinguished: (1) deposits that are very rich in Mn and are composed essentially of Mn-

oxide, and (2) deposits that are relatively Mn-poor but have high concentrations of Fe, Cu and Zn, and often contain Fe-sulphide phases in addition to Fe-oxides (Shearme *et al.*, 1983). It was not until the direct observation of low-temperature metal-enriched hydrothermal fluids at the Galapagos Spreading Centre (Corliss *et al.*, 1979) and high-temperature venting at 21°N EPR (Edmond *et al.*, 1979a) that a common origin of these apparently different sediment types could be demonstrated (Edmond *et al.*, 1979b). Sulphide phases indicate rapid precipitation at high temperatures (>150°C) when the acidic, metal-laden end-member hydrothermal fluids debouch on the seafloor. Post-depositional oxidation of these primary minerals produces the commonly observed ochres. In contrast, the formation of pure Mn-oxide deposits from a hydrothermal fluid requires that the fluid is oxidising and hence has been greatly diluted by seawater (Edmond *et al.*, 1979b).

4.1.2 Metalliferous sediments as a temporal record of hydrothermal activity

Shearme *et al.* (1983) attribute variations in the degree of metal enrichment between sediments from the EPR and TAG to differences in spreading rates between the two ridge-systems, and hence the extent of seawater circulation through the oceanic crust. The implication is that a link exists between spreading rate, crustal permeability and metal accumulation, and that metalliferous sediments preserve a historical record of the heat flux at mid-ocean ridges. Examination of metalliferous sediments from the FAMOUS area, 37°N on the MAR, however, indicate that the observed metal enrichments are produced not only from direct precipitation from enriched hydrothermal fluids, but are also affected by diagenetic re-mobilisation and post-depositional injection of hydrothermal fluids at the base of the sediment column (Scott *et al.*, 1979).

Metz *et al.* (1988) studied a metalliferous sediment core from the southern part of the *Alvin* zone, and applied a three-component model to distinguish between hydrothermal, biogenic and detrital material in the core. Dark reddish-brown sediments with a high hydrothermal component of >90 % was

present in distinct layers. These appeared to have been deposited rapidly by mass-flow events from one of the relict mounds in the *Alvin* zone. These layers alternate with brown to yellow, carbonate-rich sediments of predominantly pelagic origin. By determining of the sediment ages using ^{14}C geochronology, Metz *et al.* (1988) demonstrated that this core provides a record of 14,000 years of episodic hydrothermal input.

It appears that the highly variable geochemistry of Cu, Zn, and Mn in metalliferous sediments is controlled by direct deposition of sulphides and oxides from hydrothermal fluids, scavenging of metals from seawater and the oxidation of sulphide minerals. Mills *et al.* (1993) presented a further distinction of the different hydrothermal components in metalliferous sediments from $^{230}Th/Fe$, REE/Fe and U/Fe ratios, which define two different modes of deposition. Low $^{230}Th/Fe$ and REE/Fe but high U/Fe ratios indicate mass-wasting of sulphide material, whereas fall-out of particles from the hydrothermal plume have much higher, plume-like $^{230}Th/Fe$ and REE/Fe ratios and low U/Fe ratios. The study by Mills *et al.* (1993) confirmed earlier results that the source of metals in metalliferous sediments is not only from seawater-basalt interaction, but also from scavenging of seawater constituents by Fe-oxyhydroxides in the dispersive plume (Bender *et al.*, 1971; Bonatti, 1975; Ruhlin and Owen, 1986; Trefry and Metz, 1989).

4.1.2.1 Plume derived metalliferous sediments

Feely *et al.* (1994) estimated that about 99 % of the Fe that was injected into the bottom water from the North Cleft segment is transported in the hydrothermal plume along the ridge axis and thus dispersed in the deep ocean. About 50% of the Fe^{2+} in the hydrothermal fluid is precipitated immediately within the first 8 m of plume rise as sulphides (Feely *et al.*, 1990; Mottl and McConachy, 1990; Rudnicki and Elderfield, 1993). The remaining Fe^{2+} is oxidised and precipitated as Fe-oxyhydroxide particles (Campbell, 1991). Trace metals are incorporated into the Fe-oxyhydroxide particles by co-precipitation in the buoyant plume, and scavenging in the buoyant and neutrally buoyant plume (Rudnicki and Elderfield, 1993). The source of the

metals is dissolved input from the vent fluid, but also adsorption of trace elements from seawater (Klinkhammer *et al.*, 1983; Trocine and Trefry, 1988; Feely *et al.*, 1991; German *et al.*, 1991b; Rudnicki and Elderfield, 1993).

The scavenging behaviour in the plume is highly variable for different elements. Fe precipitation strongly predominates over Mn precipitation and Mn remains in solution as the plume disperses over the first 100-1000 m away from the source (German *et al.*, 1991a). This is also reflected in the low Mn content of near-field plume derived sediments (Metz and Trefry, 1988). The chalcophyle elements Cu, Zn, Cd, Co and Pb are incorporated into sulphide phases during the early phase of plume rise and these phases will settle out within a 1500 m radius of the source (Feely *et al.*, 1994). A negative departure of the trace metals from a linear correlation with Fe in the particulate phase indicates oxidative dissolution of these elements from the plume particles (German *et al.*, 1991a). U, V, Cr and As are incorporated predominantly during the buoyant phase of the plume, whereas the rare earth elements (REEs) and Th exhibit further scavenging from seawater in the neutrally buoyant plume (Trocine and Trefry, 1988; Trefry and Metz, 1989; Feely *et al.*, 1991; German *et al.*, 1991a; German *et al.*, 1991b; Rudnicki and Elderfield, 1993).

Plume particles that are produced during the initial mixing of vent fluids with cold seawater consist of mainly pyrite and Fe-monosulphide that are similar to primary mineral phases in the walls of chimneys (Koski *et al.*, 1984). As the hydrothermal plume is dispersed by bottom currents, the Fe-oxyhydroxides in the neutrally buoyant plume will eventually settle out onto the seafloor and imprint their distinct geochemical signature into the underlying sediments (German *et al.*, 1993; Mills *et al.*, 1993). If the sediments become reducing, Fe-oxyhydroxide particles may undergo dissolution and release metals and P back into the porewater. In the Pacific, where the dispersal of the plume is not hindered by the ridge-crest walls, plumes are dispersed over several tens to hundreds of kilometres away from the ridge axis (Klinkhammer and Hudson, 1986; Feely *et al.*, 1992). Plume derived particles are commonly intermixed with carbonate ooze (German *et al.*, 1993; Mills *et al.*, 1993).

4.1.2.2 Near-vent sulphide and oxide debris

The concentration of trace metals in mound sulphides is highly variable, and depends on the mineral assemblage and the conditions under which they were formed. The marked compositional difference in the black and white smoker fluids, which is a function of mineralisation processes occurring in the mound, are also reflected in the mineralogy and chemistry of the hydrothermal precipitates (Edmond *et al.*, 1995; Tivey *et al.*, 1995). This is most pronounced for Zn, which is present only in trace amounts of usually <1 % in minerals from black smoker chimneys, whereas in samples from white smoker chimneys concentrations as high as 60 % have been observed (Tivey *et al.*, 1995). Other metals that are typically associated with low temperature precipitates are Cd, Pb and Ag, while Co and Se are indicative of high temperature deposition (Fouquet *et al.*, 1988; Hannington *et al.*, 1991; Tivey *et al.*, 1995). Consequently, the composition of sulphide-rich samples from the surface of the mound depends on the relative proportions of sphalerite, chalcopyrite and pyrite. It is, however, not only the mineralogy that determines the composition, but also the source of the respective sulphide mineral. So for example the Ag concentration in sphalerite from a white smoker chimney is markedly higher compared to sphalerite from the sulphide crust on the black smoker complex (Tivey *et al.*, 1995).

Seafloor weathering of the original sulphide assemblage produces a blanket of Fe-oxide deposits that cover parts of the active mound. These deposits often contain abundant secondary mineral phases such as Fe-oxides and –silicates, and Cu-chlorides (Alt *et al.*, 1987; Herzig *et al.*, 1991; Hannington, 1993). Mass wasting of this ocherous material from the mound surface has produced an apron of bright red sediments around the active TAG mound, which is extending over several tens of metres (German *et al.*, 1993; Mills *et al.*, 1993).

4.1.3 Chapter outline

This chapter identifies the type and extent of diagenetic alteration that has occurred in core 43, a sulphide-rich sediment core from the southern periphery of the Alvin zone. This is accomplished by examining the relationship between mineralogy, solid and porewater geochemistry of the sediments and comparison with primary mineral phases from the active TAG mound. The mechanism of alteration is discussed only briefly in this chapter, but is investigated in more detail in chapters 5 and 6.

4.2 Methods

The sampling and on-board processing of the sediment cores was described in Chapter 3. The geochemical analyses were performed within the School of Ocean and Earth Science, Southampton Oceanography Centre except porewater sulphate, which was analysed in the Department of Earth Sciences, University of Bristol, and hydrogen sulphide, which was analysed on-board the ship.

4.2.1 Porewaters analysis

4.2.1.1 Metals

Fe, Mn, Cu, Zn, Cd and Mo were determined using a graphite furnace atomic absorption spectrometer (GF-AAS; Perkin Elmer 1100B, and Varian Spectra AA 300 Zeeman). Fe and Mn were analysed directly on acidified samples at a dilution of at least 1:10, using a platinum matrix modifier (Sachsenberg *et al.*, 1993) and standard addition to minimise any matrix effect. The detection limits for both metals were 100 nmol/l (Table 4.1).

For the remaining elements, the porewaters were extracted employing a modified version of the micro-extraction technique after Rivera-Duarte (1996). In summary, this technique uses ammonium pyrrolidine dithiocarbamate (APDC) and diethylammonium diethyldithiocarbamate (DDDC) as organic chelators and chloroform as solvent. All laboratory ware was sequentially cleaned in a series of baths with laboratory detergent (MICRO, 2 %v/v), 50%v/v HCl and 50%v/v HNO_3, and rinsed with sub-boiling distilled (SBD) high purity water. $CHCl_3$ was cleaned with successive extractions (>5 times) with SBD water, and the chelator (3%w/w APDC/DDDC in 3.5% NaCl-solution) was purified with four blank extractions with the cleaned $CHCl_3$. High purity water and mineral acids (both SBD) were used throughout the extraction and during later analysis.

A known exact volume of acidified sample in the order of 1-2 ml was made up to 50ml with SBD water in a 125 ml Teflon separatory funnel. Before adding the chelator (1ml per sample) and the $CHCl_3$ (2ml per extraction), the pH of the samples was adjusted to between 5 and 8 using a 1.5 M acetic acid ammonia buffer. Adjusting the pH to >5 minimises any loss of Mn during the extraction. Extractions were repeated >3 times per sample until any brown discoloration in the extract had disappeared. After a further oxidation step with concentrated HNO_3 and drying down of the extract, the residue was taken up in 4% HNO_3. The recovery of each batch of samples was monitored by simultaneously extracting a series of spiked standards, which were made up in seawater that had been stripped of its metals by passing it through an ion-exchange column. The extraction efficiency was better than 90% for all metals. The extracted samples were analysed by GF-AAS. Following the extraction, it was no longer necessary to use standard additions. The detection limits for extracted samples for Cu, Zn, Cd, Mo, V, and Co are shown in Table 4.1, and generally do not exceed 25 nmol/l. Repeat analysis of the samples has shown that the intra-batch precision was usually better than 10% (2σ).

Element	n	Mean nmol/l	St. dev. nmol/l	LOD* nmol/l
Fe	5	142	28	84
Mn	5	91	16	48
Cu	5	32	4	12
Zn	3	47	7	21
Cd	3	0.4	0.5	1.5
Mo	3	2.1	1.8	5.4
V	3	17	5	15
Co	3	12	8	23

*LOD = 3x standard deviation of blank

Table 4.1: Procedural blank concentrations and limits of detection (LOD) for porewater analysis by GF-AAS

U in porewater was determined on an Inductively Coupled Plasma - Mass Spectrometer (ICP-MS: VG Elemental PlasmaQuad PQ2+). Aliquots of acidified porewater were dried down in a Teflon beaker and taken up in 2%

HNO_3 spiked with known concentrations of In and Re for internal correction. The instrument was calibrated using appropriate dilutions of a U standard solution (spectroscopic grade) made up in the same acid as the samples. Depending on the amount of porewater available, samples were made up at 20-50 fold dilutions. The external precision was usually better than 6% (2σ).

4.2.1.2 Sulphate and hydrogen sulphide

Sulphate and hydrogen sulphide analysis was performed by Jo Rhodes in Bristol and on board the ship respectively.

Sulphate was analysed on frozen samples using a Dionex 4000I ion chromatograph equipped with an Ion Pack AG4A 4mm guard column and an Ion Pack AC4A 4mm anion separator column. Sodium sulphate was used to make up standards of appropriate concentration. Precision was typically better than 1% (2σ).

Hydrogen-sulphide was analysed colorimetrically on board the ship after the methylene blue method of Cline (1969). The detection limit for this method using a 1 cm cell is ~1 μmol/l.

Samples were also taken for nitrate and ammonia analysis, but due to some contamination during analysis the data are not included here. Oxygen measurements were not obtained.

4.2.2 Solid phase analysis

4.2.2.1 Major elements

Major elements (Mn, P, Cu and Zn) for bulk sediments were determined by X-ray fluorescence spectrometry using the analytical method described in Chapter 3, Section 3.1.2. External precision was 1-5% for P, and 5-10 % for Mn, Cu and Zn (both 2σ). Accuracy was better than 3% for P and better than 6% for Cu and Zn.

4.2.2.2 Sample dissolution

Complete sample dissolution is required for mass-spectrometric analysis. Prior to acid digestion, all samples except carbonate rich core-top samples were roasted at 650°C for 6 hrs to remove the sulphide present. About 250 mg of the dry ground sediment was transferred into Teflon pressure digestion vessels and digested over night after addition of 3ml concentrated HF and 5 drops of concentrated $HClO_4$. After further digestion for 1 hr in 3ml of concentrated HCl, samples were transferred into 8M HNO_3 for storage. In order to avoid the formation of insoluble CaF, carbonate-rich samples were dissolved in a two-step digestion. Initially, the $CaCO_3$ was dissolved with 5ml 6M HCl, and after completion of the reaction, the supernatant, which contains all Ca^{2+} as dissolved $CaCl_2$, was centrifuged off and transferred into a separate digestion vessel. After repeat rinses with de-ionised water, the residue was digested with 3ml of concentrated HF and 15 drops concentrated HNO_3 overnight. Supernatant and dissolved residue were re-combined and transferred into 8M HNO_3. Only high purity acids (Aristar grade) were used during the digestion.

4.2.2.3 ICP-MS analysis of minor elements

Minor elements, including rare earth elements (REEs), Mo, Cd, Au, Ag, Pb, Th and U were determined using Inductively Coupled Plasma Mass Spectrometry (VG Elemental PlasmaQuad PQ2+). The dissolved samples were transferred into 2% HNO_3 and spiked with known concentrations of In and Re for internal correction. The instrument was calibrated using a multi-element solution of appropriate dilutions of metal standards (spectroscopic grade) and an in-house chondrite reference material for REE. Standards were run at the beginning and end of each batch. The effect of ^{135}BaO interference on ^{151}Eu was assessed by running a series of Ba standard solutions with concentrations similar to those measured in the bulk samples by XRF analysis. The interference was found to be negligible and no correction was applied. External precision was judged by repeat analysis of a sulphidic sediment sample from the TAG mound. This is the first analysis of this

sample, but it is envisaged that in future it can be used as an in-house reference material for metalliferous sediments. Accuracy of the analyses was monitored by simultaneous analysis of adequate standard reference materials with known concentrations (BEN: international basalt standard; NOD-P1: international manganese nodule standard; BRR: in-house REE standard). The external precision was better than 5% (2σ) and accuracy was better than 4% for REE (Tables 4.2 and 4.3). Precision and accuracy for trace elements (except U) was markedly poorer, but this is believed to be due to the lack of reliable reference data for these elements rather than a true reflection of the analysis. A selection of samples from core 43 were also run as standard additions on the GF-AAS, and these data are shown together with the ICP results in Table 4.6. The general agreement between the two methods was usually better than 10%.

4.2.2.4 ICP-AES analysis of transition metals

The transition metals V and Co were determined using an Inductively Coupled Plasma – Atomic Emission Spectrometer. For the analysis the dissolved samples were transferred into 5% HCl. The instrument was calibrated using a multi-element solution of appropriate dilutions of metal standards (spectroscopic grade). A mixed standard solution was analysed at regular intervals (after every five samples) to monitor the instrument drift, and a correction was applied. Analytical precision was generally in the range of 3-5% (2σ).

4.2.3 Electron microscopy and elemental mapping

The scanning electron microscope (SEM) proved to be a very useful tool for comparison of bulk geochemical data with fine-scale compositional variability. Polished slides were prepared from splits of wet sediments, which were dried in an oven at about 60° C. The dry sediments were broken up into smaller lumps before impregnating them with resin. Thin sections of the resin-impregnated blocks were prepared by standard techniques and glued to a glass microscope slide. For qualitative and quantitative X-ray microanalysis

on the SEM it is important to polish the thin sections thoroughly before carbon coating. The analysis was undertaken on a JSM 6400 SEM, which is fitted with an EDS (Energy Dispersive Spectrometry) X-ray detector, backscatter electron detector, and interfaced with a PGT IMIX image processing system. Imaging and X-ray microanalysis was done pre-dominantly in backscattered electron imaging (BSEI) mode. In this mode, mineral grains with relatively high average atomic number (e.g. sulphides) have a higher backscatter coefficient and hence produce a brighter image. This makes them easily distinguishable from mineral phases with low backscatter coefficients, such as silica or iron-oxide, and from the carbon-based resin. The SEM was operated at an acceleration voltage of 15 to 20 kV and a probe current of $3x10^{-9}$ to $6x10^{-9}$ A. X-ray single-point analysis, where each point was scanned for 30 to 60 seconds, was used for preliminary assessment of the various phases and detailed quantitative analysis of mineral composition. Elemental maps were used to examine subtle compositional changes on a small spatial scale (100μm to 1mm). Maps were acquired for selected elements only and each image was scanned for 2 to 3 hours until a satisfactory resolution was achieved.

	1 (ppm)	2 (ppm)	3 (ppm)	4 (ppm)	5 (ppm)	6 (ppm)	Mean (ppm)	External precision St.dev. (2σ) (ppm)	RSD (2σ) (%)
La	3.4	3.4	3.6	3.5	3.6	3.6	3.5	0.2	5.8
Ce	4.3	4.3	4.6	4.4	4.7	4.5	4.5	0.3	6.9
Pr	0.8	0.8	0.9	0.8	0.9	0.9	0.8	0.04	4.9
Nd	3.5	3.6	3.7	3.7	3.7	3.7	3.6	0.2	5.5
Sm	0.8	0.8	0.8	0.8	0.8	0.8	0.8	0.04	5.0
Eu	0.7	0.7	0.8	0.8	0.7	0.8	0.7	0.02	2.8
Gd	0.9	0.9	1.0	1.0	1.0	1.0	0.9	0.1	5.9
Tb	0.1	0.1	0.1	0.1	0.1	0.1	0.1	0.01	7.0
Dy	0.8	0.8	0.9	0.8	0.9	0.9	0.9	0.03	3.9
Ho	0.2	0.2	0.2	0.2	0.2	0.2	0.2	0.01	4.7
Er	0.5	0.5	0.5	0.5	0.5	0.5	0.5	0.03	5.1
Tm	0.1	0.1	0.1	0.1	0.1	0.1	0.1	0.00	5.0
Yb	0.5	0.5	0.5	0.5	0.5	0.5	0.5	0.03	6.7
Lu	0.1	0.1	0.1	0.1	0.1	0.1	0.1	0.00	5.1
								Average:	5.3
Mo	73	76	82	80	81	79	79	6.8	8.7
Cd	8.7	9.1	9.2	8.5	9.1	8.1	8.8	0.9	10.3
Au	0.8	0.7	0.8	0.9	0.8	0.7	0.8	0.1	13.2
Ag	5.3	4.9	5.7	5.1	5.0	5.4	5.2	0.6	11.3
Pb	141	151	155	141	163	151	150	16.9	11.2
U	4.2	4.3	4.5	4.5	4.4	4.5	4.4	0.3	5.8
								Average:	10.1

Table 4.2: Repeat analysis of in-house reference material (sulphidic sediments from the TAG mound surface) by ICP-MS.

Standard ID	BRR*		NOD-P1**		BEN**	
	this study (ppm)	ref. value (ppm)	this study (ppm)	ref. value (ppm)	this study (ppm)	ref. value (ppm)
La	2.3	1.6	107	104	84	82
Ce	6.7	5.4	309	294	156	152
Pr	1.0	1.1	31	-	18	17.5
Nd	5.6	5.6	129	119	66	67
Sm	2.0	2.1	32	29.5	12.1	12.2
Eu	0.8	0.8	7.9	7.5	3.8	3.6
Gd	2.6	3.1	33	28.2	12.2	9.7
Tb	0.5	0.6	4.7	-	1.3	1.3
Dy	3.5	4.1	27	26.8	6.6	6.4
Ho	0.8	0.9	5.2	-	1.1	1.1
Er	2.2	2.8	13.3	12.5	2.5	2.5
Tm	0.3	-	2.0	-	0.3	0.34
Yb	2.2	2.7	12.9	12.7	1.9	1.8
Lu	0.34	0.43	2.02	1.78	0.26	0.24
Mo	1.4	-	590	762	5.1	2.8
Cd	2.5	-	22.7	-	0.4	0.12
Pb	2.8	-	417	555	2.1	4
U	2.6	-	3.9	-	2.3	2.4

* In-house basalt reference material, recommended concentrations are from R.Taylor (pers. comm.)
** International standard reference material, recommended concentrations are from Govindaraju (1996)
dashed indicate element was not reported

Table 4.3: Analysis of trace elements in standard reference materials by ICP-MS.

4.3 Results

4.3.1 Porewater geochemistry

The results of the porewater analysis are presented in Table 4.4. The mean sulphate concentration in core 43 is 29.0 mmol/l, which is only slightly higher than average seawater concentrations of 28 mmol/l. Maximum sulphate concentrations were measured in the carbonate cap at ~30 cm and in the lower sulphide layer at about 180 cm, were concentrations reached 33.3 mmol/l and 32.1 mmol/l respectively. The mean sulphate concentration in the background core 10 is 27.8 mmol/l. Hydrogen sulphide was below detection limit (<1 µmol/l) throughout the core.

Dissolved Fe and Mn concentrations in core 43 were negligible in the carbonate cap and increase within the upper sulphide layer to remain high throughout the rest of the core. Mn shows a sharp increase at 52.5 cm from levels below detection limit to concentrations of 2-4 µmol/l at depth. Fe increases more gradually and the highest concentrations of 93 µmol/l were measured in the lower sulphide layer compared to 33 µmol/l at the base of the upper sulphide layer. In the background core concentrations of Mn were <0.1 µmol/l, and Fe concentrations were <1µmol/l.

Porewater profiles for core 43 show distinct maxima for Cu, Zn, Cd and Mo within the upper sulphide layer or in the intermediate layer, whilst concentrations in the lower sulphide layer are low or below detection limit. In the background core all porewater trace metals are below detection limit. U concentrations in core 43 range between 5 and 13 nmol/l, but no distinct peaks were observed. Maximum concentrations in the intermediate layer are still lower than typical seawater concentration of 14 nmol/l. Attempts were also made to measure V, Co and Pb but these were below detection limit for all three metals.

Sample ID	Depth (cm)	Mn (µmol/l)	Fe (µmol/l)	Cu (µmol/l)	Zn (µmol/l)	Cd (µmol/l)	Mo (nmol/l)	U (nmol/l)	SO_4^{2-} (mmol/l)
2	7.5	bdl	0.8	bdl	0.7	bdl	13.1	10.4	27.6
4	17.2	bdl	1.3	bdl	1.9	bdl	17.5	9.2	-
6	27.5	bdl	1.4	bdl	1.9	bdl	38.3	-	33.3
10	47.5	0.2	0.6	1.0	9.7	bdl	27.3	11.1	-
12	57.5	3.4	7.8	12.1	9.2	bdl	21.4	10.3	27.6
14	67.5	3.6	33.3	1.1	12.4	1.0	6.9	10.2	26.9
16	77.5	2.3	32.3	1.9	14.9	0.1	162.1	12.9	27.8
18	87.5	3.8	29.0	4.6	9.2	0.1	114.7	12.1	27.2
20	97.5	3.7	24.7	0.3	6.0	0.1	27.0	12.3	26.9
22	107.5	2.9	18.9	0.7	5.4	bdl	5.3	8.8	29.2
24	117.5	2.7	41.4	0.8	3.2	bdl	25.5	10.2	28.8
26	127.5	3.5	39.9	0.7	1.7	bdl	14.9	7.9	29.3
34	167.5	3.7	84.3	bdl	16.3	bdl	114.5	-	31.2
36	177.5	3.3	93.3	bdl	1.0	bdl	75.0	6.0	32.1
44	217.5	2.0	82.6	bdl	0.8	bdl	4.8	5.0	29.6
Average seawater		0.005	0.001	0.004	0.006	0.0007	110	14	28

bdl = below detection limit; dashes indicate element was not reported

Table 4.4: Porewater concentrations for metals and sulphate for core 43 and average seawater.

4.3.2 Solid phase geochemistry

The trace metal concentrations for bulk sediments are presented in Table 4.6. V and P both show enrichment in the carbonate cap, and a sharp peak is also observed in Mn at ~30 cm depth. In the upper sulphide layer U, Cu and Au show a distinct enrichment in the uppermost sample from this layer, whilst Cd is enriched at the base off the upper sulphide layer. Other metals that are enriched in the upper sulphide layer and show peaks that mirror the concentration of total S are Mo, Pb and Ag. For Co concentrations in the upper sulphide layer are only slightly higher than in the carbonate cap or the intermediate layer. Zn shows enrichment at the top and the base of the upper sulphide layer with broad peaks that level out into the adjacent carbonate cap and intermediate layer. Pb shows similar elevated concentrations in the intermediate layer that gradually decease to a minimum at ~140 cm. Similar to the upper sulphide layer, P is markedly enriched directly above the lower

sulphide layer. All of the trace metals analysed here show high concentrations in the lower sulphide layer. The high V concentrations in the lower sulphide layer extend into the intermediate layer to a depth of ~160 cm.

Table 4.5 compares the trace metal content of core 43 with typical values for sulphide and Fe-oxide samples from the surface of the active TAG mound. With the exception of V concentrations of trace metals in core 43 fall within the range reported for mound samples.

		core 43[1]	Black smoker chimney[2]	White smoker chimney[2]	Sulphide-rich mound samples[2]	Ocherous Fe-oxides[2]	Atacamite-bearing Fe-oxides[3]
Mn	(%)	0.0-0.7	<0.01-0.02	<0.01-0.02	<0.01-1.36	0.08-0.20	0.01-0.05
Cu	(%)	0.0-6.0	4.0-12.1	0.4-0.6	0.4-17.6	0.09-0.99	18.4-43.8
Zn	(%)	0.0-0.7	0.01-0.25	53.6-62.3	0.39-59.9	0.22-0.85	0.01-0.31
Mo	(ppm)	11.0-71.9	9-160	<1-70	35-100	12-28	-
Ag	(ppm)	0.0-36.2	1-7	190-1200	28-1920	<2-4	<5-125
Cd	(ppm)	0.0-40.0	<10	950-2260	18-2190	<10	<10
Au	(ppm)	0.0-4.8	0.05-0.38	0.28-15.3	0.07-20.8	<0.01-0.03	4.7-23.0
Pb	(ppm)	5.6-510.0	<20-34	440-1000	150-480	35-440	<100
V	(ppm)	45.2-297	<5	<5-36	<5-140	<10	-
Co	(ppm)	7.4-445.7	47-910	<2	<2-154	<2-17	3-5

[1] Minimum and maximum concentrations from core 43
[2] Data from Tivey *et al.* (1995)
[3] Data from Herzig *et al.* (1991)
dashes indicate element was not reported

Table 4.5: Comparison of trace metal concentrations for core 43 with sulphidic and ocherous samples from the surface of the active TAG mound.

Sample ID	Depth (cm)	Cu (%)	Zn (%)	Mo (ppm)	Mo (ppm)	Ag (ppm)	Cd (ppm)	Au (ppm)	Pb (ppm)	U (ppm)	V (ppm)	V (ppm)	Co (ppm)	Co (ppm)
	Method:	*XRF*	*XRF*	*ICP-MS*	*GF-AAS*	*ICP-MS*	*ICP-MS*	*ICP-MS*	*ICP-MS*	*ICP-MS*	*ICP-AES*	*GF-AAS*	*ICP-AES*	*GF-AAS*
1	2.5	0.3	0.03	40	47	bdl	0.1	0.3	63	4.3	292	275	30	27
3	12.5	0.2	0.03	18	15	0.2	0.2	0.2	39	2.8	175	-	21	-
5	22.5	0.1	0.03	19	17	bdl	0.5	0.2	38	3.1	122	110	21	19
6	27.5	0.1	0.1	22	20	0.8	0.8	bdl	62	4.2	139	-	32	-
7	32.5	0.5	0.1	32	30	0.1	2.0	0.5	184	8.4	189	182	35	29
8	37.5	0.6	0.2	25	30	0.1	1.2	bdl	86	5.1	225	-	39	-
9	42.5	1.1	0.3	29	29	0.1	2.0	1.1	181	8.5	243	220	35	28
10	47.5	1.5	0.7	25	29	0.3	2.8	1.6	321	9.2	229	-	14.9	-
11	52.5	4.9	0.3	72	69	26.9	4.2	4.8	510	27.9	149	-	48	-
12	57.5	0.4	0.4	34	29	19.4	2.6	0.7	278	13.6	69	65	17.0	12.0
13	62.5	0.7	0.7	53	64	36.2	40	0.8	328	15.7	58	-	31	-
14	67.5	0.4	0.7	41	34	3.9	29	1.1	310	12.0	85	83	20	-
15	72.5	0.1	0.7	16	16	1.2	3.4	0.1	198	9.0	136	-	8.8	5.8
16	77.5	0.03	0.4	14	14	3.5	0.9	0.2	140	10.2	87	77	7.4	-
17	82.5	0.1	0.5	16	16	0.7	0.5	0.4	200	9.8	113	-	7.4	5.0
19	92.5	0.1	0.4	14	13	2.8	2.2	0.2	155	9.9	55	49	7.8	-
21	102.5	0.1	0.3	12	12	2.7	1.1	0.1	120	7.1	72	-	7.4	-
22	107.5	-	-	19	19	0.8	0.1	0.2	218	8.6	131	116	8.7	-
23	112.5	0.1	0.2	-	-	-	-	-	-	-	-	-	-	-
24	117.5	-	-	14	14	1.0	0.2	0.4	165	8.7	66	-	10.4	8.3
25	122.5	0.1	0.2	15	14	0.8	bdl	0.3	94	10.2	48	44	14.5	-
26	127.5	-	-	14	14	0.5	bdl	0.1	122	8.9	57	-	13.2	109
27	132.5	0.1	0.1	19	21	bdl	bdl	0.1	27	11.9	92	86	13.7	-
28	137.5	0.1	0.1	17	17	2.6	bdl	0.0	22	8.7	82	-	12.8	-
29	142.5	0.1	0.03	11	11	bdl	bdl	0.3	6	11.7	45	-	9.8	-
30	147.5	0.1	0.03	18	18	bdl	bdl	0.2	27	7.3	91	-	12.7	9.3
31	152.5	0.1	0.03	12	10	6.2	bdl	0.2	24	6.6	95	81	14.9	-
32	157.5	0.1	0.04	13	13	1.9	bdl	0.2	24	6.1	82	-	14.7	11.9
33	162.5	0.1	0.04	24	26	bdl	bdl	0.5	95	7.7	205	203	19.4	15.9
34	167.5	1.6	0.1	42	47	0.4	bdl	0.0	161	9.7	228	-	36	34.8
35	172.5	4.6	0.2	67	67	12.7	6.7	1.9	194	16.4	212	187	144	145
36	177.5	1.5	0.1	60	56	3.7	0.6	1.4	163	14.6	214	-	82	83
37	182.5	2.8	0.2	61	55	6.5	2.0	1.1	124	16.3	192	-	165	181
38	187.5	3.8	0.3	53	57	10.4	7.3	2.1	190	17.4	194	-	161	152
39	192.5	4.2	0.2	57	57	16.6	22.7	1.4	200	16.4	149	143	250	255
40	197.5	4.4	0.6	54	49	9.5	4.1	0.9	221	15.2	189	-	246	-
41	202.5	3.1	0.35	65	60	11.7	12.7	1.2	217	18.0	149	-	132	119
42	207.5	4.0	0.3	56	-	10.9	9.6	0.9	130	18.0	-	-	-	-
43	212.5	3.6	0.1	40	35	5.4	2.1	0.7	113	15.1	183	-	295	275
44	217.5	6.0	0.2	44	42	8.6	2.9	1.0	116	15.8	173	-	446	471
45	222.5	4.3	0.1	46	42	4.7	1.3	1.4	155	14.2	263	-	202	-
46	227	2.6	0.1	57	53	5.3	7.0	1.3	156	13.8	297	260	104	-

bdl = below detection limit; dashes indicate element was not reported

Table 4.6: Solid phase trace metal data for core 43.

4.4 Discussion

4.4.1 General redox conditions and Mn cycling

Markedly elevated concentrations of dissolved Mn at depth below 47.5 cm and dissolved Fe below 57.5 cm show that the sediments become suboxic below the carbonate cap (Figure 4.1). Porewater sulphate concentrations are close to seawater throughout the core, and the absence of detectable hydrogen sulphide, indicate that conditions are not reducing. The zonation of Fe and Mn in core 43 follows the general model of standard energy potential, where Mn reduction precedes Fe reduction (Froelich *et al.*, 1979). Porewater profiles for both Fe and Mn indicate upward diffusion and re-precipitation above the upper sulphide layer in the oxic carbonate cap. In the case of Fe the diagenetic peak in solid phase Fe is masked by the generally high Fe content of the sediments, whereas for Mn a marked peak in Mn-oxides was observed at ~30 cm depth.

Mn is strongly decoupled from Fe in seafloor hydrothermal systems, because the kinetics of Mn oxidation in the water column are slow compared with those of Fe (Krauskopf, 1957). As a result, Mn concentrations in plume-derived sediments tend to be low in the near vent field and only increase to values above >0.1 % at distances >1 km from the source (Trocine and Trefry, 1988). Cowen *et al.* (1986) and Mandernack and Tebo (1993) have demonstrated that Mn-binding bacteria mediate the removal of Mn from the plume.

Surficial Mn enrichments have been attributed to fractionation of this element from Fe into distal plume fall-out (Shearme *et al.*, 1983). In addition, crust-like accumulations of Mn-oxide are formed by effective scavenging of Mn from diffuse hydrothermal fluids (Edmond *et al.*, 1979b; Mills *et al.*, 1996). In the sediments the oxidation of Mn is autocatalytic, whereby newly formed Mn-oxides provide reaction sites for further Mn oxidation (Krauskopf, 1957). Goulding *et al.* (1998) reported significant Mn enrichment of up to 15 % in the upper part of a sediment core from the south eastern flank of the active TAG mound. Ferromanganese crusts are also present in the relict *Mir* and *Alvin*

zones (Lalou *et al.*, 1993; Rona *et al.*, 1993a; Rona *et al.*, 1993b; Wells, 1998). Mn concentrations of similar magnitude (19 %) were further observed in this study in core 25, which was recovered from the centre of the *Mir* zone. The Fe-stained carbonate cap in core 25 was overlain by fragments of Mn-oxide crust and covered by hair-like organism, suggesting that they were located at the sediment-water interface. These organisms were not further analysed, but they may represent filamentous bacteria as they are commonly observed in association with diffuse hydrothermal venting (Jannasch and Wirsen, 1981).

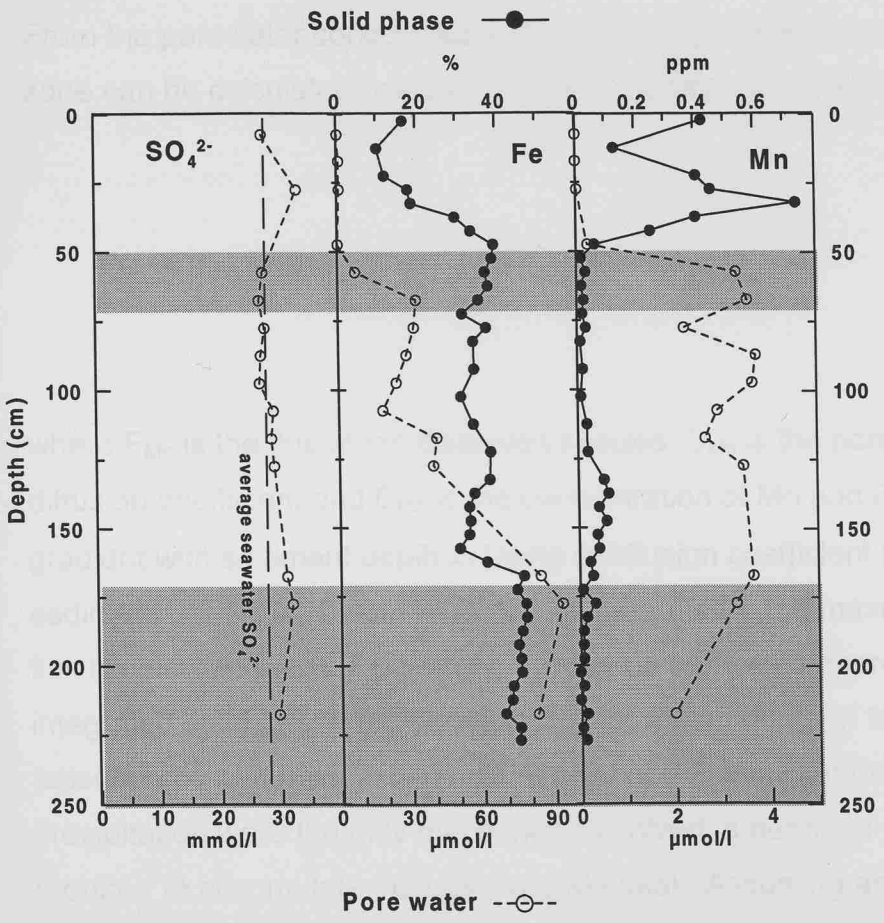

Figure 4.1: Vertical profiles of dissolved sulphate, and porewater and solid phase Fe and Mn for core 43. Also marked is the typical seawater sulphate concentration.

Comparison of Mn porewater and solid phase data for core 43 clearly show that the solid phase peak at ~30 cm is of diagenetic origin, marking the redox-boundary for the transition of Mn^{2+} to Mn^{4+} (Figure 4.1). Dark bands of Mn-oxide have been observed in the surface sediments of many cores from this study (Palmer and scientific party, 1996), and similar Mn enrichments have been reported previously for sediments from this area (Scott *et al.*, 1978; Metz and Trefry, 1988; Mills *et al.*, 1993). The source of the Mn could be from reductive mobilisation of sedimentary Mn at depth, or from diffuse fluids enriched in Mn that are percolating through the sediment pile.

From the porewater concentration, the diffusional transport of Mn into the oxic zone can be calculated using the general equation for Fickian diffusion

$$F_{Mn} = D_{Mn} (\partial C_{Mn}/\partial x) \qquad (4.1)$$

where F_{Mn} is the flux of the dissolved species, D_{Mn} is the porosity corrected diffusion coefficient and C_{Mn} is the concentration of Mn and $\partial C_{Mn}/\partial x$ is the Mn-gradient with sediment depth *x*. Using a diffusion coefficient for Mn in sediments of 1.3×10^{-6} cm^2/s (Klinkhammer, 1980), the maximum diffusive flux is calculated as 0.7 $\mu g/cm^2/y$. This value can be compared with the integrated solid phase Mn between 20 and 45 cm depth of 83.5 mg/cm^2 (assuming a sediment *in situ* bulk density of 0.8 g/cm^3). If diffusive flux and re-precipitation were the only mechanism involved, a period of 120 kyr would be required to accumulate the observed Mn peak. Assuming an average carbonate accumulation rate of 0.6 $g/cm^2/1000$ yr for pelagic sediments in the Mid-Atlantic (Broecker and Peng, 1982), the base of the carbonate cap is only 23 kyr, and hence about one order of magnitude lower than the required age. This discrepancy suggests that the porewater gradient for Mn has been higher in the past and/or that the accumulation of Mn in the oxic zone may have been microbially enhanced.

4.4.2 Secondary mineral replacement

When sulphide deposits become exposed on the seafloor a range of weathering reactions take place, which in the most extreme case can cause complete oxidation of the sulphides to Fe-oxides. Sediment material at the periphery of a hydrothermal mound may get into contact with low temperature fluids that have evolved within the mound (Mills *et al.*, 1996). In core 43 remineralisation of the original mineral assemblage is clearly indicated by the presence of atacamite in the upper sulphide layer. Atacamite is a common secondary mineral in marine deposits that has been observed in the oxidising sulphide talus of active and fossil hydrothermal sites (Embley *et al.*, 1988; Alt, 1988a; Herzig *et al.*, 1991; Hannington, 1993). Atacamite is a supergene weathering product of primary chalcopyrite, the latter is abundant especially in high temperature deposits. The dissolution of chalcopyrite under acidic conditions in seawater releases Cu^{2+} into the porewater, which form cuprous chloride complexes. These are re-precipitated as basic copper salts where the oxidising solution comes into contact with ambient seawater. Consequently, atacamite veinlets in gossans delineate the extent to which seawater was able to penetrate the deposit (Hannington, 1993). The occurrence of atacamite in the upper sulphide layer is therefore interpreted to mark the extent to which oxygenated seawater has diffused into the sediments.

Cu is released from chalcopyrite through dissolution of the mineral, but also during re-crystallisation of chalcopyrite to pyrite. Figure 4.2(a) is an SEM image of a mineral grain from the intermediate layer where the darker pyrite in the centre of the mineral is gradually replacing the much brighter chalcopyrite on the outside. This process is inferred to have occurred throughout the core.

Poorly structured iron sulphide phases often accommodate trace amounts of Cu and Zn, and chalcopyrite has been observed as discrete inclusions in the pyrite mineral (Figure 4.2(b)). Re-crystallisation of the primary sulphide phase to pyrite will release Cu and Zn into solution, since these are largely incompatible with a true pyrite lattice (Vaughan and Craig, 1978). Figure 4.2(c) is such an example where secondary euhedral pyrite is overgrowing

and replacing a core of impure primary Fe sulphide from which the Cu and Zn (bright areas) are exsolving.

The replacement of chalcopyrite by covellite is another remineralisation process that is typical of supergene alteration of massive Cu sulphides (Sillitoe and Clark, 1969). It involves the removal of Fe from chalcopyrite minerals and formation of bornite along grain boundaries. As the re-crystallisation progresses, bornite is replaced by digenite, then chalcocite and finally covellite (Oudin, 1983). Figure 4.2(d) shows a chalcopyrite grain with a coating of a brighter, more Cu-rich covellite precursor along its grain boundary.

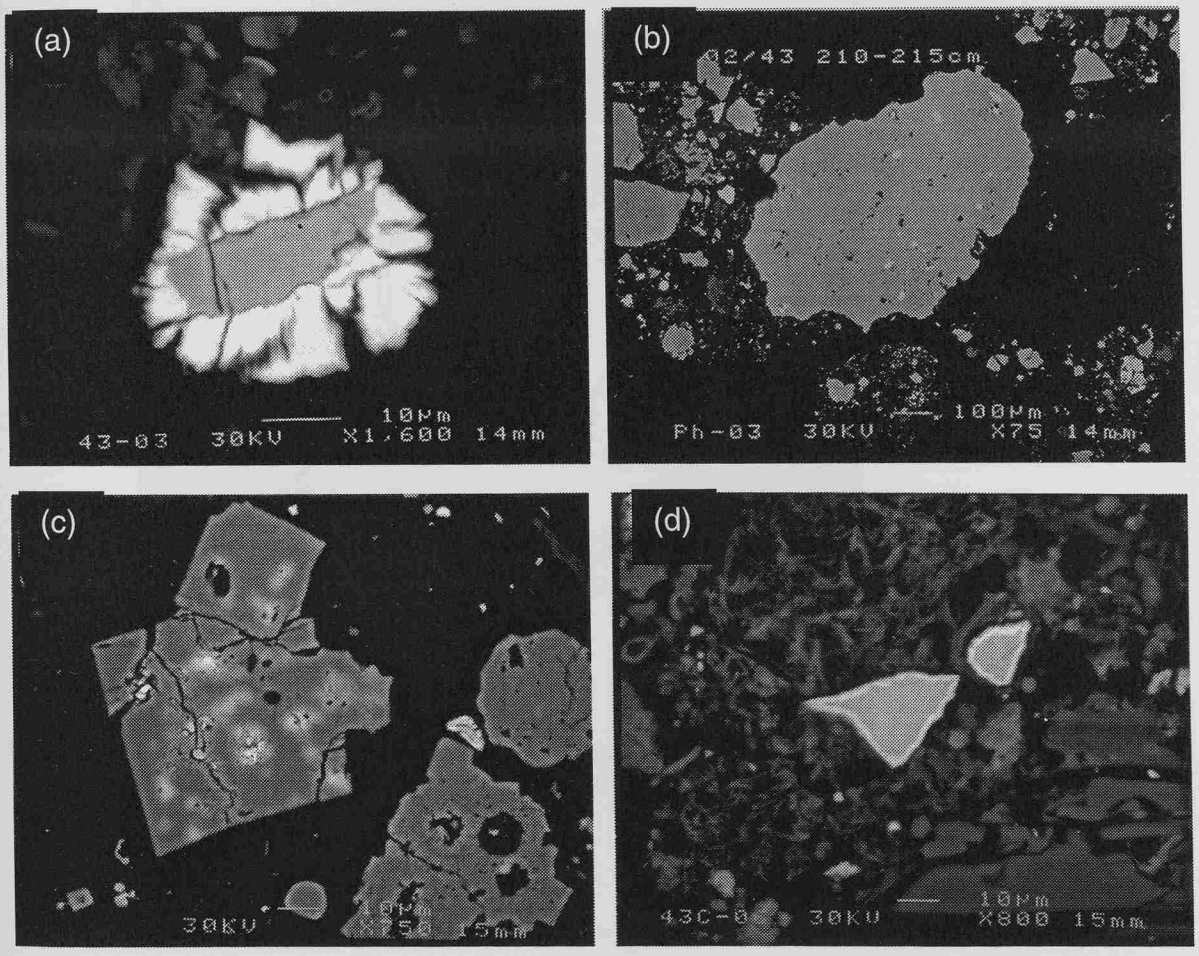

Figure 4.2: SEM images of sulphide minerals with typical examples of secondary mineral replacement: (a) replacement of chalcopyrite (bright outer zone) with pyrite (darker centre), (b) chalcopyrite inclusions in pyrite, (c) secondary pyrite with Cu and Zn staining (light areas) and (d) chalcopyrite with covellite coating.

4.4.3 The effect of re-mineralisation on trace metal distributions

4.4.3.1 Copper, Gold and Cadmium distributions

Cu, Au and Cd all show distinct and sharp solid phase peaks in the upper sulphide layer. In the case of Cu and Au the enrichment is in the topmost sample of the upper sulphide layer, whereas the Cd peak is slightly broader and towards the base of this layer (Figure 4.3).

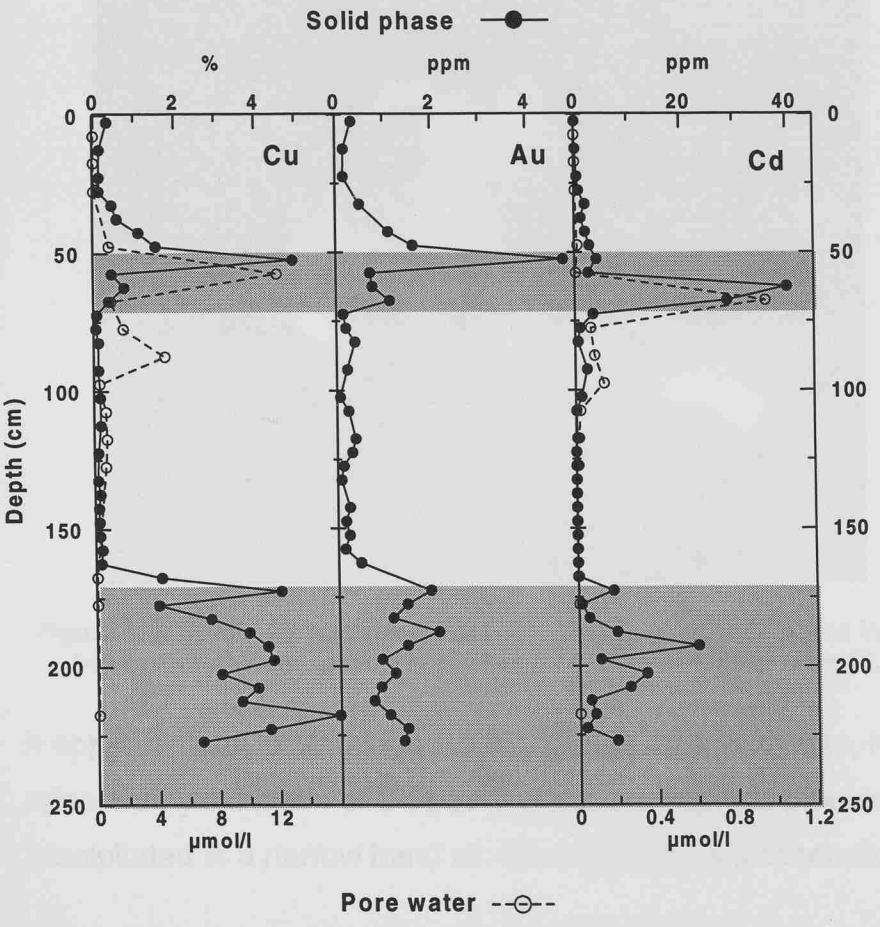

Figure 4.3: Vertical profiles of porewater and solid phase Cu, Au (no porewater data available for Au) and Cd for core 43.

A close association between Cu-bearing atacamite and Au, as it is evident from the solid phase data in core 43 has been described previously at TAG (Herzig *et al.*, 1991). Figure 4.4 shows an SEM image of a native Au grain surrounded by atacamite. Au concentrations in pristine sulphides from TAG

black and white smoker chimneys rarely exceed 1 ppm, but concentrations as high as 20 ppm have been measure in atacamite bearing Fe oxides from the TAG mound (Tivey *et al.*, 1995). Both Cu and Au are released into the porewater when primary sulphides are oxidised by reactive pore fluids. They are transported as chloride complexes, and the cuprous chloride precipitates as Au-rich atacamite when the pH increases on mixing of the pore fluid with oxygenated seawater (Herzig *et al.*, 1991; Hannington, 1993).

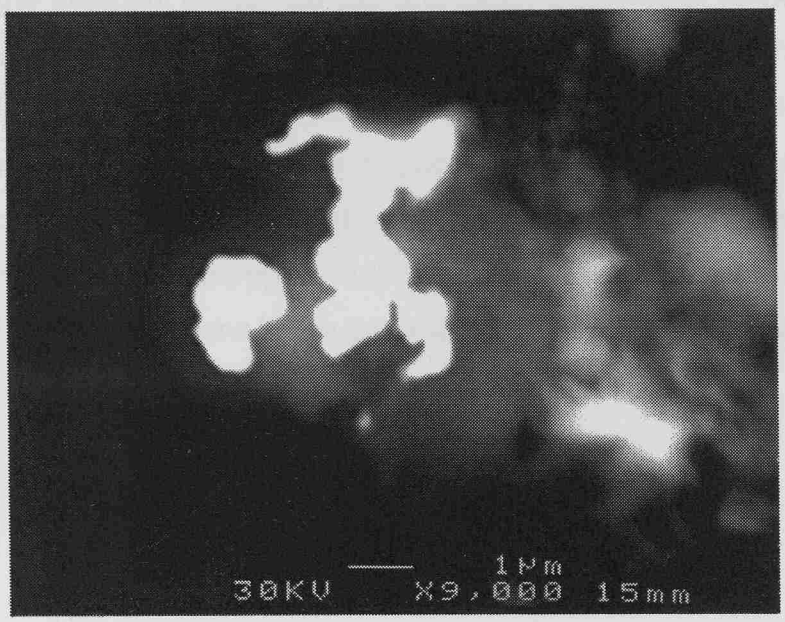

Figure 4.4: Native Au surrounded by atacamite (fuzzy bight areas in the background) from the top of the upper sulphide layer of core 43.

It appears that Cd, although not associated with atacamite, has also been released by oxidation of Cd-bearing primary sulphide phases and re-precipitated in a narrow band at ~65 cm depth as a secondary mineral phase.

Cu and Cd both show elevated porewater concentrations that closely match the solid phase peaks (no data are available for Au), indicating that mobilisation of these metals is still ongoing. The zonation of these two metals with Cu mobilisation occurring at shallower depth and higher inferred E_h values than Cd follows the model of standard energy potential, and is in agreement with previous observations for metal-enrichments in organic-rich deep-sea sediments (Thomson *et al.*, 1998).

4.4.3.2 Zinc and Lead distributions

Of all the elements analysed in this study, Zn shows the most pronounced effect of diagenetic mobilisation. The highest Zn concentrations were measured at 47.5 cm, in the sample that marks the base of the carbonate cap. A minimum in Zn concentration in the upper sulphide layer on the other hand coincides with the maximum S_{tot} content. A second Zn peak is evident at the base of the upper sulphide layer, and both peaks decrease only gradually into the adjacent carbonate cap and intermediate layer respectively. The fact that the Zn peak in the upper sulphide layer at ~70 cm depth is penetrating into the intermediate layer, where it reaches a minimum at 140 cm depth, clearly indicates that this is a diagenetic feature rather than an expression of the original mineralogy. Pb shows a similar gradual decrease from maximum concentrations in the upper sulphide layer to a minimum at ~140 cm, although the Pb concentrations in the intermediate layer are more variable compared with Zn (Figure 4.5).

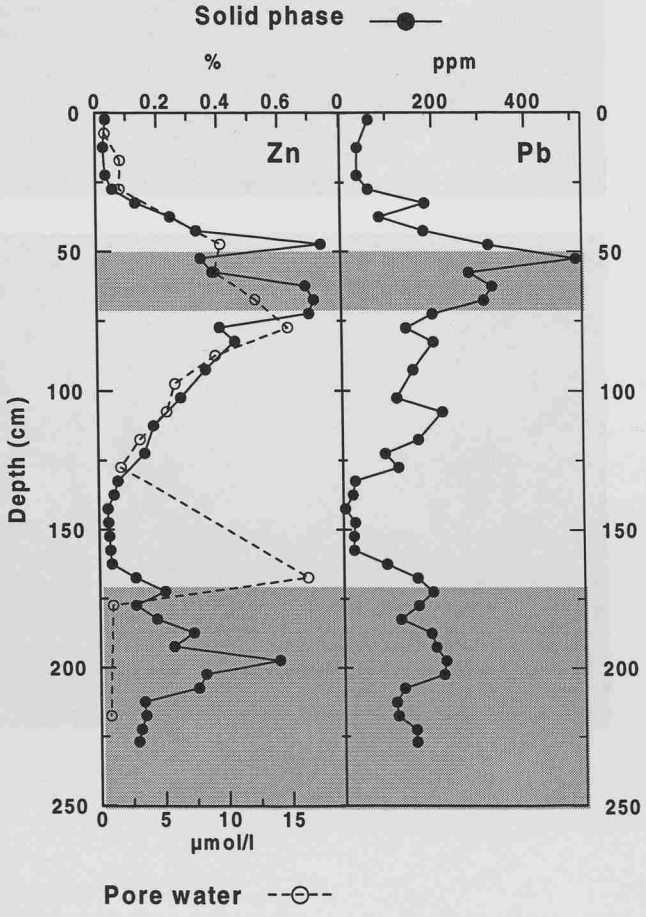

Figure 4.5: Vertical profiles for porewater and solid phase Zn, and solid phase Pb for core 43 (porewater Pb was below detection limit throughout).

It appears that Zn and Pb are being released from primary sulphides minerals in the upper sulphide layer to be re-precipitated above and below this layer. This has been confirmed for Zn from SEM images, where primary sphalerite from the upper sulphide layer shows clear sign of marginal corrosion, whereas sphalerite minerals from directly below this layer are angular in appearance indicating re-precipitation of sphalerite as secondary mineral phase (Figure 4.6). The inferred sphalerite levels are below the detection limit for S_{tot} in the intermediate layer, but SEM X-ray microanalysis of minerals from this layer have confirmed the presence of sphalerite.

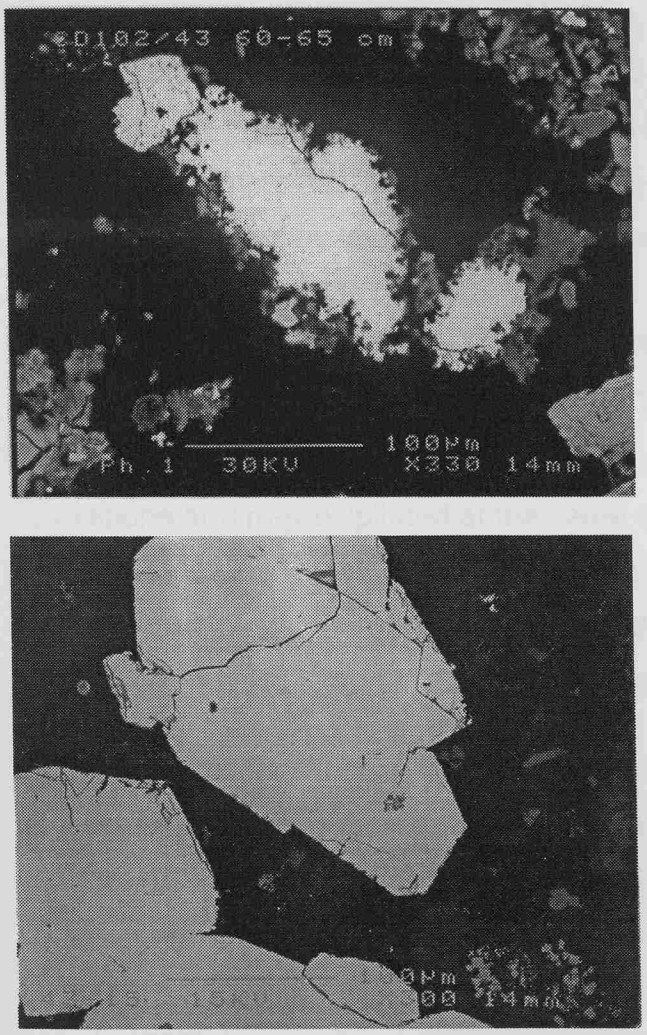

Figure 4.6: SEM images of sphalerite from the upper sulphide layer (top panel), showing marginal corrosion, and from just below the upper sulphide layer (lower panel), where it has been re-precipitated as secondary, euhedral sphalerite.

Porewater concentrations show that mobilisation of Zn is still active. The porewater profile closely follows the solid phase profile, suggesting that the release of Zn is no longer restricted to the upper sulphide layer but is now also affecting sphalerite in the intermediate layer. A sharp peak at the base of the intermediate layer, however, indicates that Zn is diffusing into the lower sulphide layer where it is removed from solution.

4.4.3.3 Cobalt and Silver distributions

Co concentrations are markedly elevated in the lower sulphide layer in similar fashion to other trace metals analysed. Concentrations in the upper sulphide layer, in contrast, are indistinguishable from concentrations in the carbonate cap and intermediate layer (figure 4.7). This may suggest that any Co that was originally present in the upper sulphide layer has been removed by diagenetic re-mineralisation. In the absence of any Co enrichment in the adjacent sedimentary layers this would, however, require that all of the Co from the upper sulphide layer has been lost to the overlying bottom water. Diagenetic relocation of Co has been described for coastal and deep-sea organic-rich sediments (Shaw *et al.*, 1990; Thomson *et al.*, 1998). These studies have shown that, similar to Mn, Co is released under reducing conditions and re-precipitated at the same depth where the Mn^{2+}/Mn^{4+} redox-transition occurs. No such Co enrichment is evident in the carbonate cap of core 43 and it must therefore be assumed that sulphides in the upper sulphide layer were relatively poor in Co compared to the lower sulphide layer.

Ag, in contrast, is enriched in both sulphide layers and Ag concentrations in the upper sulphide layer markedly exceed those in the lower sulphide layer (Figure 4.7). The double peak in the upper sulphide layer mirrors that of the S_{tot} content. Concentrations in the carbonate cap and the intermediate layer reflect background levels. It appears that Ag, which usually follows Zn (Tivey *et al.*, 1995), has not been affected by significant diagenetic mobilisation.

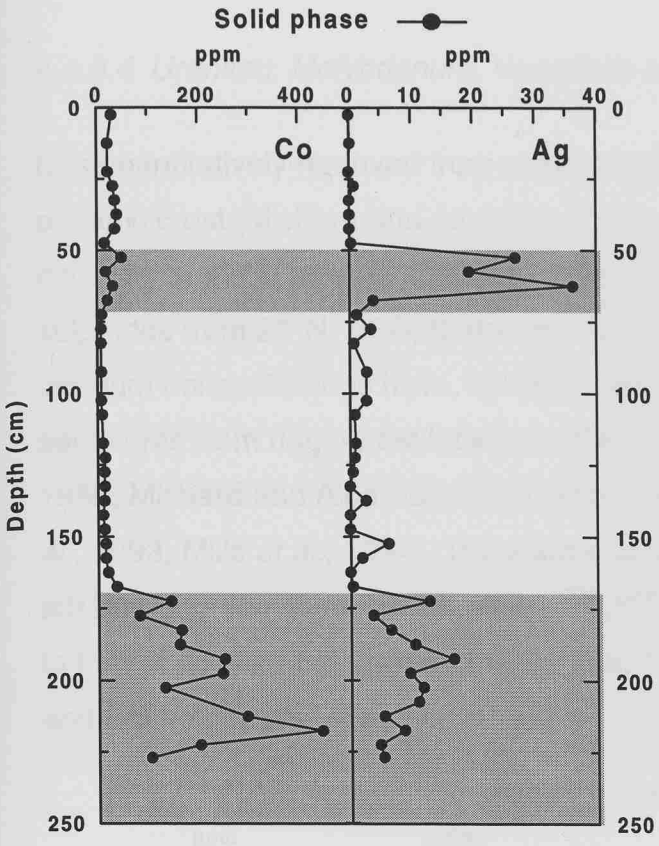

Figure 4.7: Vertical profiles for solid phase Co and Ag for core 43.

The observed pattern of high Ag content and low Co content in the upper sulphide layer, and *visa versa* for the lower sulphide layer indicates that the sulphides from the two layers were formed under different temperature regimes. In sulphides from the surface of the active TAG mound Co displays a positive temperature-concentration relationship, and enrichments of Co are typically associated with sulphides from high temperature chimneys. Elevated Ag concentrations on the other hand are more typical for lower temperature fluids and mineral precipitates (Trefry *et al.*, 1994; Tivey *et al.*, 1995). This implies that the upper sulphide layer has a higher proportion of low temperature sulphides, whereas the lower sulphide layer appears to be composed primarily of black smoker chimney-sulphides. This is consistent with the high Zn content of the upper sulphide layer.

4.4.3.4 Uranium, Molybdenum, Vanadium and Phosphorus distributions

U is quantitatively removed from seawater during circulation through the oceanic crust (Michard and Albarède, 1985). This is reflected in the low U concentrations in pristine sulphides from active vents (0.6-2.8 ppm for sulphides from 21°N, EPR; (Lalou and Brichet, 1980). Anomalously high uranium concentrations have, however, been observed in metalliferous sediments from ridge-crest locations (Bender *et al.*, 1971; Lalou and Brichet, 1980; Michard and Albarède, 1985; Shimmield and Price, 1988; German *et al.*, 1993; Mills *et al.*, 1994). The source of this enrichment is generally attributed to seawater, based on the $^{234}U/^{238}U$ ratio, which is typically similar to that of seawater (Turekian and Bertine, 1971; Dymond *et al.*, 1973; Lalou and Brichet, 1980; Mills *et al.*, 1993).

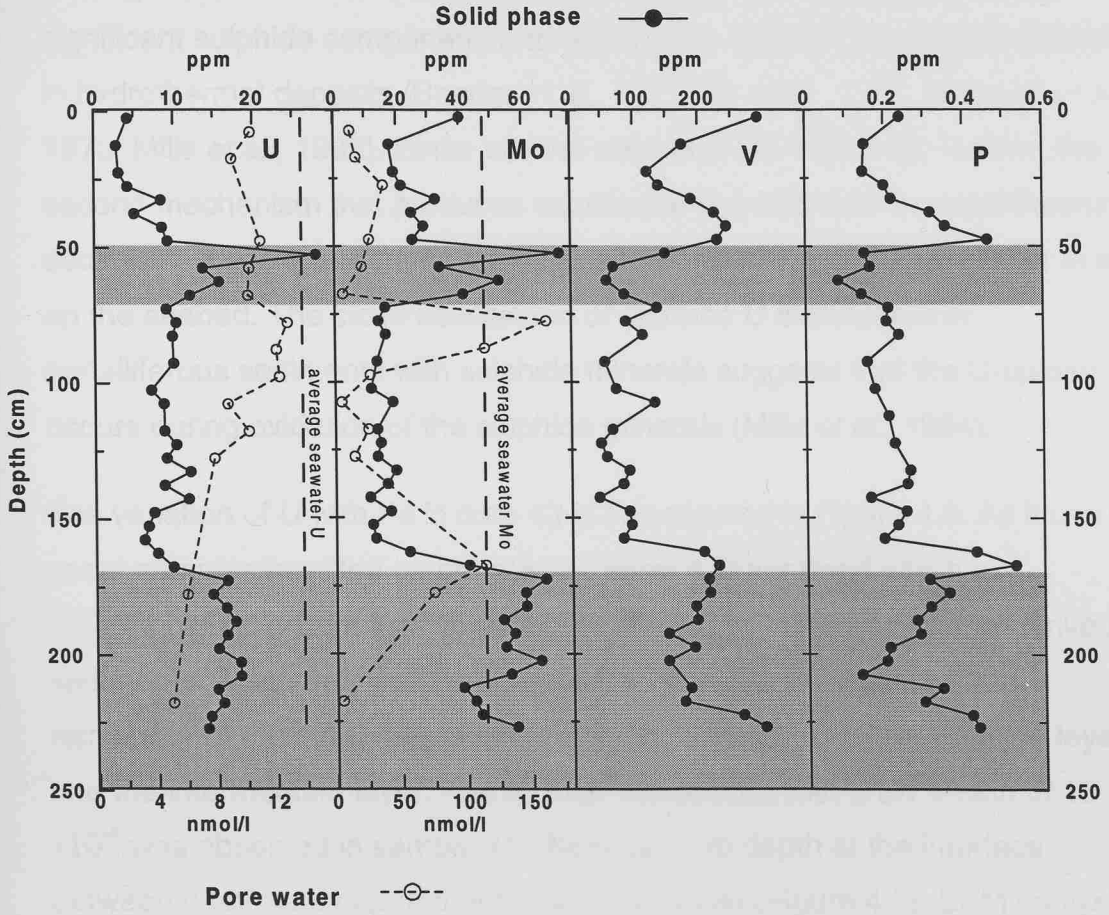

Figure 4.8: Vertical profiles for porewater and solid phase U and Mo, and solid phase V and P. Also marked are average seawater concentrations for U and Mo.

The mechanism by which U enters the sediment is twofold. Firstly, it has been demonstrated that U, and the other oxyanions V, Mo and P, are co-precipitated with Fe when Fe-oxyhydroxides are formed during buoyant plume rise (Feely *et al.*, 1990; German *et al.*, 1991b; Feely *et al.*, 1994). Comparison of particles from the buoyant and neutrally buoyant plume have shown that the U/Fe ratio, which is established during the early phase of the plume rise, remains unaltered over the lifetime of the particle in the hydrothermal plume, indicating that no continuous scavenging from seawater occurs. A linear relationship between U and Fe has also been observed for plume-derived sediments, although the U/Fe ratio in the sediments of 1-5 $x10^{-6}$ is approximately one order of magnitude higher compared with ratios of 0.5-1 $x10^{-6}$ observed in plume particulates (German *et al.*, 1993; Mills *et al.*, 1993). Still higher U/Fe ratios are found in metalliferous sediments that have a significant sulphide component, and ratios up to 15 $x10^{-6}$ have been observed in hydrothermal deposits (Bender *et al.*, 1971; Ku *et al.*, 1972; Dymond *et al.*, 1973; Mills *et al.*, 1993). Since pristine sulphides are extremely U-poor, the second mechanism that produces substantial U enrichment in metalliferous sediments therefore requires that U is incorporated into the solid phase *in situ* on the seabed. The close association of extreme U enrichment in metalliferous sediments with sulphide minerals suggests that the U-uptake occurs during oxidation of the sulphide minerals (Mills *et al.*, 1994).

The variation of U with Fe in core 43 is investigated in Figure 4.9. As it can be seen, samples from the carbonate cap show a linear trend which is indistinguishable from that observed by Mills *et al.* (1993) for plume-derived sediments. A second, less well-defined relationship is evident for the remainder of the core, representing an enrichment of U in the sulphide layers and the intermediate layer. The highest enrichment with a U/Fe ratio of 15 $x10^{-6}$ was observed in sample #11 from 52.5 cm depth at the interface between carbonate cap and upper sulphide layer (Figure 4.8). SEM analysis of sulphide minerals from this section have shown that the U enrichment is extremely localised in a zone <1 µm across (Figure 4.10). Similar U enrichments have been described by Mills *et al.* (1994), who measured

concentrations of up to 1000 ppm in discrete zones only ~100 nm across. Based on the lack of any other oxyanion enrichment in these zones and the close association with P, Mills *et al.* (1994) attributed the selective U accumulation in the oxidised rims of sulphides to microbial fixation, possibly by Fe(III) reducing bacteria that utilise U(VI) as an alternative electron donor (Lovley *et al.*, 1991).

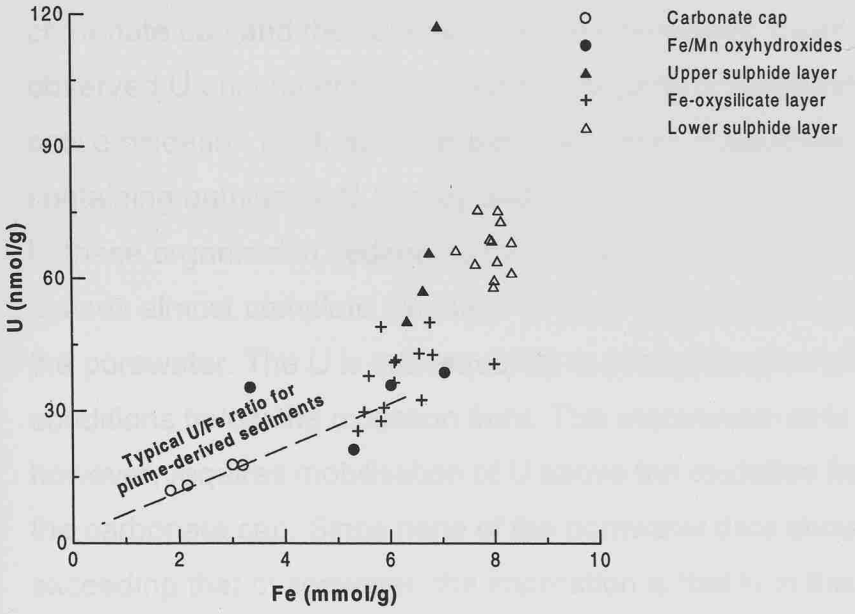

Figure 4.9: Relationship of U and Fe in core 43. The dashed line shows the typically observed trend for plume-derived sediments (from Mills *et al.*, 1993), which matched well with samples from the carbonate cap.

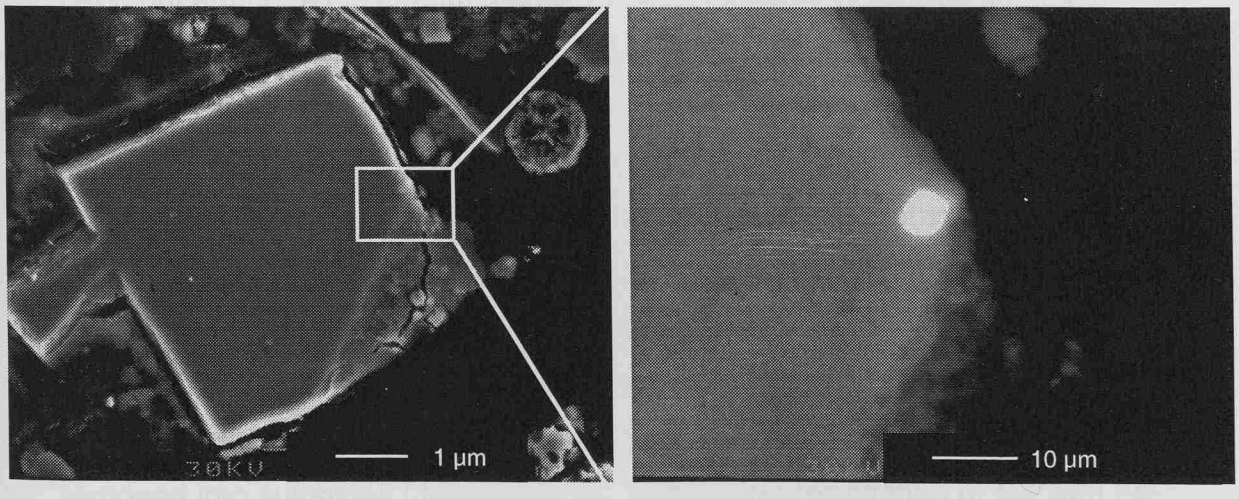

Figure 4.10: SEM images of localised U enrichment on the surface of a pyrite grain. Upper panel shows an overview of pyrite grain in SEI mode, lower panel shows detail in BSI mode.

The porewater U concentrations are markedly below seawater U concentration for all samples analysed, which is consistent with reduction of U and removal from the porewater into the solid phase throughout the core. The lowest U concentrations were measured in the lower sulphide layer, where there is consistent solid phase U enrichment (Figure 4.8). The upper sulphide layer also shows slightly reduced concentrations compared to adjacent samples from the carbonate cap and the intermediate layer. The location of the highest U enrichment in sample #11 at the interface between the oxidised carbonate cap and the suboxic upper sulphide layer might suggest that the observed U enrichment is the result of diagenetic mobilisation of U along an active oxidation front, as it has been observed in turbidites and sapropels containing authigenic U (Colley and Thomson, 1985; Thomson *et al.*, 1995). In these organic-rich sediments the penetration of an active oxidation front causes almost complete oxidation of the organic carbon and release of U into the porewater. The U is subsequently re-precipitated on encounter of reducing conditions below the oxidation front. This mechanism of U enrichment, however, requires mobilisation of U above the oxidation front, in this case in the carbonate cap. Since none of the porewater data show U concentrations exceeding that of seawater, the implication is that U in this core is not affected by diagenetic mobilisation but only by uptake from porewater.

No concentration data are available for V and Mo in black smoker fluids from TAG, but enrichments in both metals have been found in surface samples from the active TAG mound (Tivey *et al.*, 1995). Mo concentrations of up to 160 ppm were measured in samples from black smoker chimneys, whilst the highest V concentrations of up to 170 ppm were measured in sulphide-poor ocherous Fe-oxides. Recent data from trace metals in hydrothermal fluids from the Juan de Fuca Ridge indicate that Mo is removed from seawater during basalt alteration (Trefry *et al.*, 1994). Significant enrichment of Mo in mound deposits and chimney walls suggests that relatively Mo-rich seawater is entrained into the near-surface hydrothermal circulation and subsequently removed into sulphides (Janecky *et al.*, 1989). Co-precipitation of Mo with Fe-oxyhydroxides in the rising plume has also been suggested (Rudnicki and

Elderfield, 1993), although no well-defined linear relationship with Fe has been found in plume particles (German *et al.*, 1991a). The similarity in Mo/Fe ratios in plume particles and vent fluids implies that no further scavenging uptake from seawater occurs (Feely *et al.*, 1994).

In core 43 Mo is enriched in both sulphide layers (Figure 4.8). In contrast to U, Mo does not exhibit a linear relationship with Fe in the carbonate cap (Figure 4.11). The shape of the Mo profile in core 43 mirrors that of S_{tot}, which implies that Mo is dominantly associated with primary sulphides. Porewater concentrations are markedly elevated in the intermediate layer and locally exceeding average seawater concentrations. This implies that some mobilisation is taking place, and some of the mobilised Mo is diffusing into the lower sulphide layer where it is precipitated.

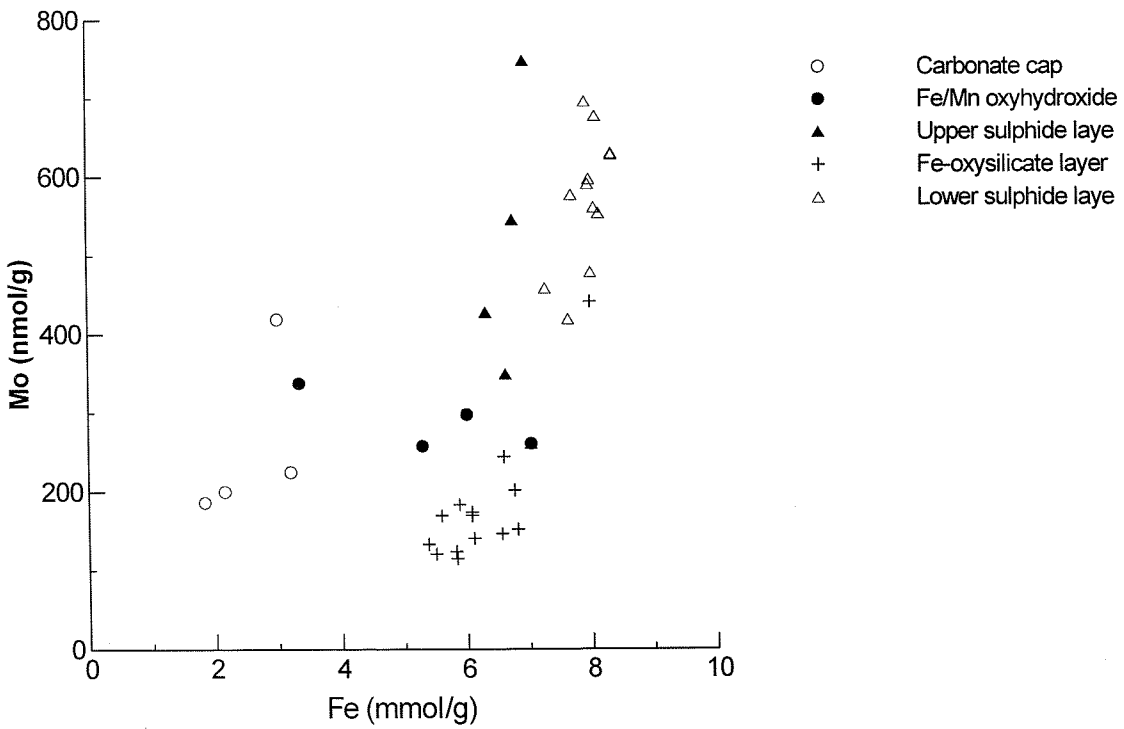

Figure 4.11: Relationship of Mo with Fe in core 43. In contrast to U, Mo does not show any close correlation with Fe.

The good correlation of both V and P with Fe in plume particles, indicating co-precipitation with Fe-oxyhydroxides, is well documented (Trefry and Metz, 1989; Feely *et al.*, 1990; German *et al.*, 1991a; Metz and Trefry, 1993; Feely *et al.*, 1994). Ratios of V/Fe and P/Fe in neutrally buoyant plume particles are significantly enriched compared with vent fluids, which is consistent with scavenging uptake of both elements from seawater (Feely *et al.*, 1994). In fact, P is the most efficiently scavenged element in seawater and in hydrothermal plumes, and it has been estimated that its removal by plume particles may represent as much as 5% of the total P removal from the ocean (Kadko *et al.*, 1994).

In core 43 elevated concentrations of V were found in the lower sulphide layer, and enrichments in V and P are evident above both sulphide layers (Figure 4.8). The lack of correlation between V or P and Fe in the carbonate cap or any other part of the core (Figure 4.12(a and b)) indicates that the source of at least some of the enrichment above the sulphide layers must be from a process other than plume fall-out. The greater particle affinity of P and V compared to U means that V and P are continuously precipitated from seawater during secondary mineralisation whereas U-fixation only occurs under reducing conditions below the Fe^{2+}/Fe^{3+} boundary (Thomson *et al.*, 1993). This is also demonstrated by the much improved correlation between V and P ($r^2 = 0.51$) compared to the lack of correlation of either element with Fe ($r^2 = 0.02$ and 0.17 for V/Fe and P/Fe respectively) (Figure 4.12). The low concentration of V in the upper sulphide layer and enrichment directly above might suggest that V was originally present in the upper sulphide layer, but has been lost to the carbonate cap through diagenetic mobilisation. The absence of V in the porewater, however, argues against significant diagenetic mobilisation of V. It is therefore assumed that, similar to Co, V was not enriched in the upper sulphide layer, and the source for the V in the carbonate cap is from seawater that is diffusing into the surface sedimentary layer.

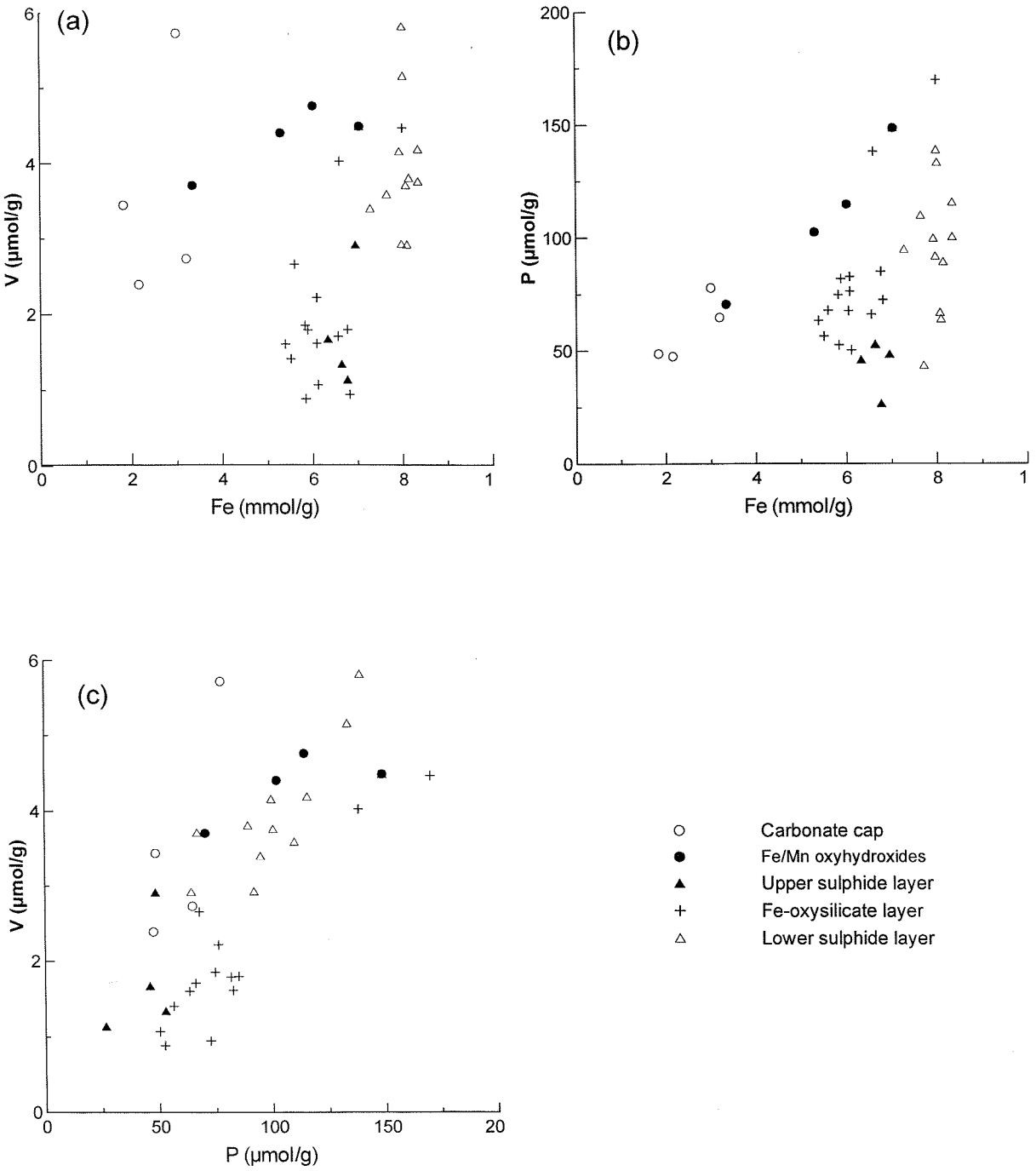

Figure 4.12: Relationship of (a) V with Fe, (b) P with Fe and (d) V with P in core 43.

4.4.4 What is driving the diagenetic metal mobilisation?

The diagenetic alteration of this metalliferous deposit has produced distinctive zones of metal enrichment, and in particular the effective separation of Zn and Cu. The same processes that have been inferred from the solid and porewater data can also be observed on microscopic scale. Zn is released from the sulphide-minerals in the upper sulphide layer, as evident from the marginal corrosion of sphalerite (Figure 4.13). It appears that any chalcopyrite that was present in the original sediment has been almost completely re-mineralised to atacamite and Fe-oxide. Most of the atacamite is now present as fine-grained infill in pore spaces between larger mineral grains and only rarely as distinct mineral grains. A sulphide grain from the lower sulphide layer, in contrast shows how secondary sphalerite has been re-precipitated around pre-existing pyrite minerals (Figure 4.13).

A similar zonation has been observed in the active TAG mound, where the separation of mineral phases into distinct zones has been interpreted as an expression of the chemical and thermal gradients, and hydrothermal reworking (Edmond *et al.*, 1995; Hannington *et al.*, 1995; Tivey *et al.*, 1995). As a result of this zone-refinement high-temperature mineral phases, such as chalcopyrite and anhydrite, are concentrated in the core of the massive sulphide deposit and in the black smoker chimneys, whilst the cooler upper margin hosts primarily Zn-rich mineral phases (Hannington *et al.*, 1995; Fouquet *et al.*, 1998). The deposition of pyrite, anhydrite and chalcopyrite in the mound, which occurs in response to conductive cooling and mixing between hydrothermal fluids and cold seawater, changes the pH of the fluid by producing acid during sulphide precipitation. The lower pH fluid may inhibit the precipitation of sphalerite, or even cause the dissolution of previously precipitated Zn-rich sulphide minerals. The production of acidity by pyrite precipitation is represented by the following reaction:

$$Fe^{2+} + S^0 + H_2S \rightarrow FeS_2 + 2\,H^+. \qquad (4.2)$$

The formation of H^+ ions would cause a drop in pH and could therefore promote dissolution of metal-sulphides. This reaction does, however, require the presence of H_2S, whereas the relatively high porewater sulphate concentrations indicate that conditions in the sediments are not sufficiently reducing to sustain the presence of H_2S, even though microbial incubation experiments have shown that significant sulphate reduction does take place (see Chapter 6).

Alternatively, acidity is produced during the oxidation of pyrite. This process is well documented in mining and ore processing, where the reaction between oxygenated groundwater and sulphide minerals produces an often extremely acidic run-off (Evangelou and Zhang, 1995). Acidic conditions are generated by a series of sulphide-oxidation reactions, such as (Nordstrom, 1982):

$$FeS_2 + 7/2\ O_2 + H_2O \rightarrow Fe^{2+} + 2\ SO_4^{2-} + 2\ H^+ \quad (4.3)$$

$$FeS_2 + 14\ Fe^{2+} + 8\ H_2O = 15\ Fe^{2+} + 2\ SO_4^{2-} + 16\ H^+ \quad (4.4)$$

$$2\ Fe^{2+} + ½\ O_2 + 5\ H_2O = 2\ Fe(OH)_3 + 4\ H^+ \quad (4.5)$$

Similarly, the reaction of exposed pyrite and chalcopyrite with seawater would produce pore-fluids sufficiently acidic to dissolve sphalerite and become saturated with atacamite (Hannington, 1993). The importance of microbial mediation of pyrite oxidation is becoming increasingly recognised (Nordstrom and Southam, 1997), and this will be discussed in more detail in Chapter 6.

Instead of producing the acidity *in situ*, dissolution of the sulphides may have been driven by horizontally advected, reactive, low-temperature fluids during the later stages of hydrothermal activity in this zone. Diffuse fluids are only poorly characterised, but recent studies have shown how a modified hydrothermal fluid may be produced through the entrainment of seawater into the active mound (James and Elderfield, 1996). Circulation of this fluid through the sediments could have led to extensive alteration of the original mineral assemblage of the active mound (Mills *et al.*, 1996).

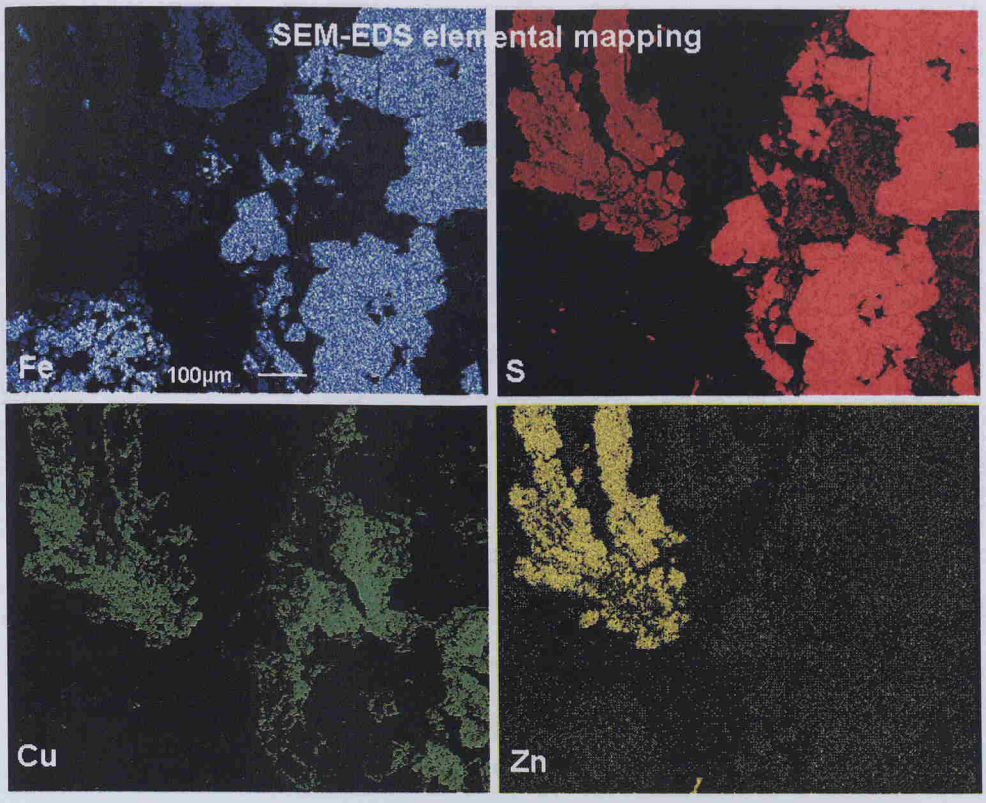

a) Upper sulphide layer

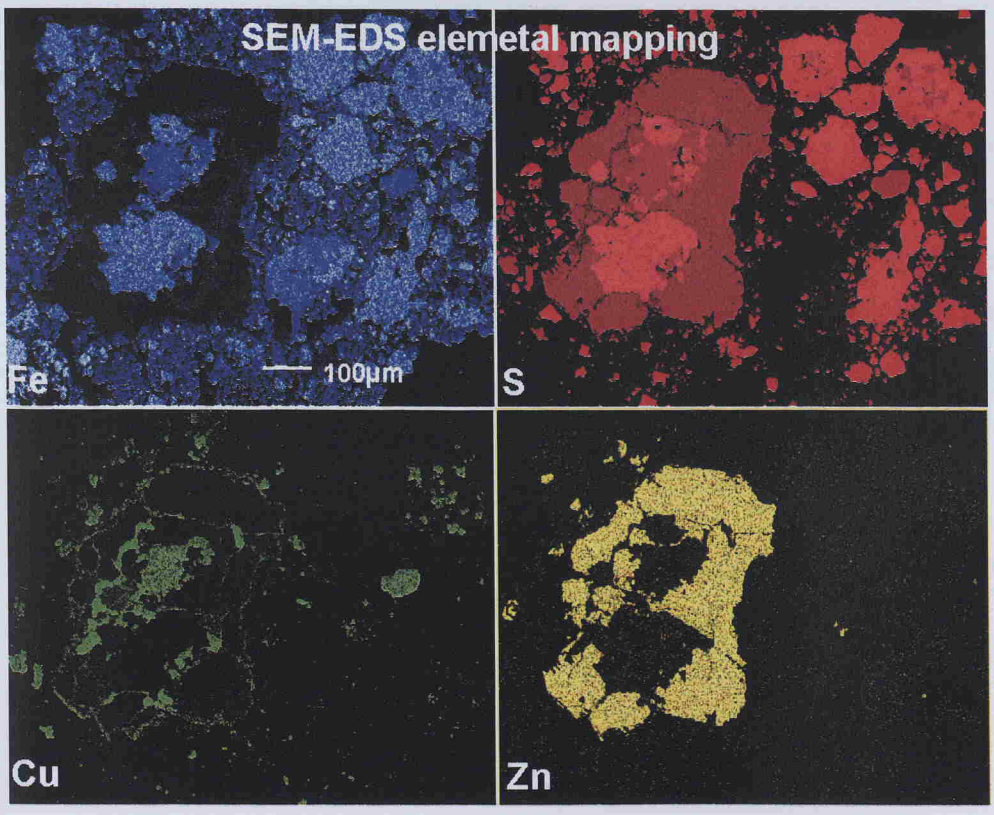

b) Lower sulphide layer

Figure 4.13: EDS elemental mapping of individual sulphide grains. Red areas show total sulphide, and the distribution of Fe-, Cu- and Zn-minerals is shown in blue, green and yellow respectively. The two panels show (a) dissolution of sphalerite in the upper sulphide layer, and (b) precipitation of secondary sphalerite around already existing sulphide grains. In the upper sulphide layer Cu is present as fine grained atacamite in pore spaces between mineral grains, in the lower sulphide layer Cu is present as chalcopyrite and covellite.

4.5 Summary and Conclusions

Significant diagenetic alteration and re-mineralisation of primary sulphide minerals in core 43 is restricted to the upper sulphide layer. It appears that rapid deposition of the intermediate layer and burial of the sulphides below have limited oxidation and dissolution of sulphide minerals at depth. Trace metals are affected by the re-mineralisation process to variable extent, and the distribution of metals in secondary mineral phases reflect their different redox-behaviour.

Most metals entered the sediments during the initial deposition of sulphide debris or plume-fall-out, but some post-depositional uptake from seawater is evident for U and possibly V. Mass balance calculations indicate that the diagenetic porewater flux of Mn from below the carbonate cap is insufficient to explain the observed peak in Mn-oxide. Low temperature fluids might have acted as an additional source of Mn in the surface sedimentary layer.

The types of alteration processes involved are similar to those that are observed in the active TAG mound today, and that would have occurred in the now extinct mounds of the *Alvin* zone. Amongst the metals that are evidently most affected by the post-depositional alteration are Cu and Zn. Dissolution of their primary sulphides and re-precipitation as secondary atacamite and sphalerite respectively has led to their effective separation. This is analogous to the zone-refining that has been described for the active mound.

Table 4.7 summarises the observed alteration processes for all the elements examined in this study.

Element	Source	Associated primary mineral phase	Diagenetic re-mobilisation	Dominant seconday mineral phase
Fe	mound sulphides, low-temperature fluids, plume fall-out	pyrite (FeS_2) goethite (FeOOH) nontronite	pyrite oxidation	Fe-oxides
Mn	plume fall-out, low-temperature fluids	birnessite (MnO_2)	Mn-reduction	Mn-oxide
Zn	mound sulphides	sphalerite (ZnS)	sphalerite dissolution	sphalerite
Cu	mound sulphides	chalcopyrite ($CuFeS_2$)	chalcopyrite re-mineralisation	atacamite ($Cu_2Cl(OH)_3$)
U	plume fall-out, seawater scavenging	U-oxide	U-oxidation	U-oxide
Mo	plume fall-out, seawater scavenging (?), mound sulphides (?)	Mo-sulphide	dissolution of sulphide phase	Mo-sulphide
V	plume fall-out, seawater scavenging (?)	vanadate ($H_2VO_4^-$) adsorbed onto Fe-oxyhydroxides	no evidence	
P	plume fall-out, seawater scavenging	phosphate (HPO_4^{2-}) adsorbed onto Fe-oxyhydroxides	no evidence	
Au	mound sulphides	native Au inclusions in chalcopyrite and pyrite	dissolutions of host mineral	native Au with atacamite
Ag	mound sulphides	Ag-sulphide	no evidence	
Cd	mound sulphides	Cd-sulphide	dissolution of sulphide phase	Cd-sulphide
Pb	mound sulphides	PbS-sulphide	dissolution of sulphide phase	Pb-sulphide
Co	mound sulphides	Co-sulphide	no evidence	

Table 4.7: Summary of trace metal mineralogy and diagenetic alteration. Trace metals are usually present as mixed solid solution of sulphides or as inclusions.

Chapter 5

Low Temperature Alteration of an Inactive Hydrothermal Deposit: Evidence from REE Geochemistry and Clay Mineralogy

5.1 Introduction

5.1.1 The geochemistry of rare earth elements

5.1.1.1 General characteristics of rare earth elements

The rare earth elements (REEs) are amongst the most frequently applied geochemical proxies in the study of modern and ancient hydrothermal systems (Ruhlin and Owen, 1986; Olivarez and Owen, 1989; Herzig *et al.*, 1991; Klinkhammer *et al.*, 1994; Mills and Elderfield, 1995a; James and Elderfield, 1996; Goulding, 1998; Wells, 1998). The elements in this group, which are also known as lanthanides, are characterised by their chemical coherence that controls their concentration and mass fractionation. Their predictable range in solubility and complexation chemistry is a function of their steady decrease in ionic radius with increasing atomic number ("lanthanide contraction"; Henderson, 1984).

REEs are less affected by fractionation than other elements. The fractionation of REEs is typically visualised in the form of REE patterns, where their concentrations are normalised to one component of the system under study to eliminate their regular odd-even variation in atomic mass abundance. In this

study data are normalised to chondrite concentrations after Evensen *et al.* (1978). Figure 5.1 shows typical REE patterns for seawater (Mitra *et al.*, 1994), Mid-Atlantic Ridge basalt (N-MORB; Sun and McDonough, 1989) and TAG hydrothermal endmember fluids (Douville *et al.*, 1999). The preferential oxidation state for most REEs is as trivalent ions. Exceptions are Ce and Eu, which are often fractionated from the other REEs due to their distinct redox-chemistry. The following two parameters are commonly used to quantify the fractionation of Eu and Ce from the remaining REEs:

$$\text{Eu}-\text{anomaly} = \frac{\text{Eu}}{\text{Eu}^*} = \frac{2\text{Eu}_n}{\text{Sm}_n + \text{Gd}_n} \qquad (5.1)$$

$$\text{Ce}-\text{anomaly} = \frac{\text{Ce}}{\text{Ce}^*} = \frac{3\text{Eu}_n}{2\text{La}_n + \text{Nd}_n} \qquad (5.2)$$

where the subscript 'n' refers to chondrite normalised values and the superscript refers to the value obtained by linear interpolation between adjacent elements. In order to be able to compare data from this study with previously reported data that do not give concentrations for Pr, Ce* is interpolated by using Nd instead.

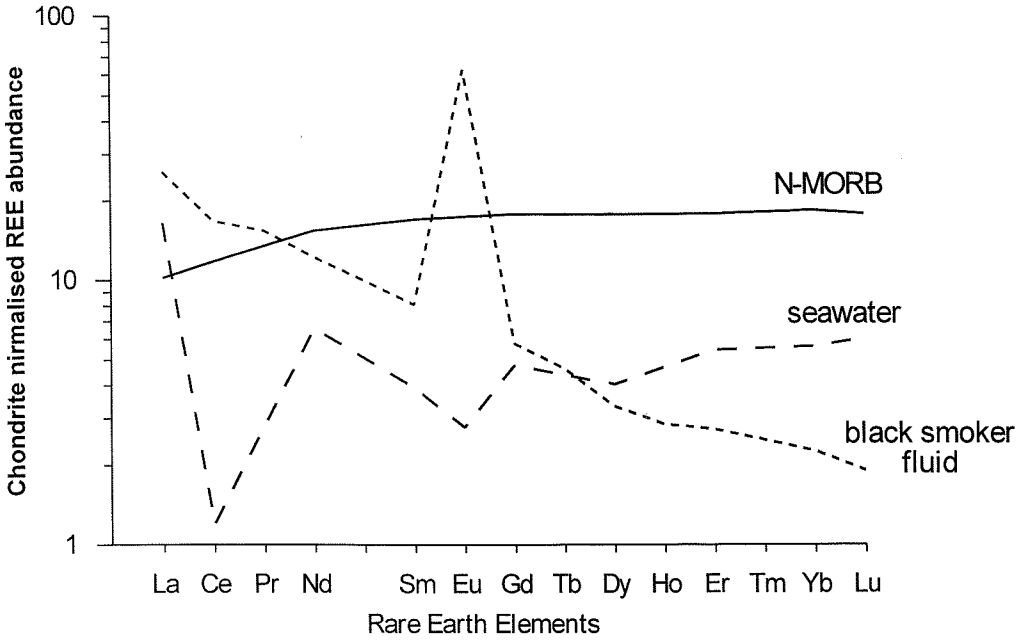

Figure 5.1: Chondrite normalised REE patterns for North Atlantic Deep Water (x 10^6) (Douville *et al.*, 1999), end-member black smoker high temperature hydrothermal fluid from TAG (x 10^4) (Mitra *et al.*, 1994) and N-type Mid-Ocean Ridge Basalt (Sun and McDonough, 1989).

Under oxic conditions Ce exists in its higher oxidation state as Ce^{4+}. Oxidative removal of the highly insoluble CeO_2 is responsible for the markedly decreased Ce concentration in seawater compared to the remaining REEs. This is reflected in a distinct negative Ce anomaly in the seawater REE pattern (Figure 5.1)(Elderfield, 1988). Conversely, the dominance of the more stable Eu^{2+} over Eu^{3+} causes discrimination against Eu during mineral formation from the rising melt and producing plagioclase enriched in Eu (Klinkhammer *et al.*, 1995). Enhanced stability of Eu^{2+} during hydrothermal alteration of the 'normal' MORB (N-MORB, i.e. the most abundant type of ocean ridge basalt) has also been invoked to explain the marked Eu enrichment as the hydrothermal fluid extracts Eu^{2+} from the basalt (Sverjensky, 1984; Wood, 1990b; Klinkhammer *et al.*, 1994). The Eu^{2+}/Eu^{3+} redox-boundary, however, shows very strong temperature dependency and redox-controlled Eu fractionation is restricted to high temperature and low pH such as encountered in submarine hydrothermal fluids (Sverjensky, 1984). The resultant large positive Eu anomaly is common to all known high

temperature fluids from unsedimented ridges (Klinkhammer *et al.*, 1994; Mitra *et al.*, 1994).

The fractionation of light REEs (LREEs: La to Eu) from the heavy REEs (HREEs: Gd to Lu) is a function of their complexation chemistry as well as crystallographic control of mineral phases with, or precipitation from, fluids containing REEs (Cantrell and Byrne, 1987; Wood, 1990b; Koeppenkastrop and De Carlo, 1992). The most important complexant for REEs under near neutral to basic conditions is carbonate (Cantrell and Byrne, 1987). Increasing stability of carbonate complexes with decreasing ionic radius, i.e. increasing atomic number, is responsible for the relative HREE enrichment in seawater, whereas LREEs are more readily removed by reactive particles (Elderfield, 1988). Other complexants such as SO_4^{2-}, Cl^-, OH^- do also occur but are usually less important because of their much lower concentration (e.g. F^-), they relatively weak complexes (e.g. Cl^-) or because they do not produce any discernible fractionation that could be recorded in the sedimentary record (e.g. SO_4^{2-}) (Wood, 1990a; Wood, 1990b). Only little information is available on the complexation chemistry of REEs under varying conditions, but experimental data suggest that changes in T, pH and $f(O_2)$ may greatly affect the types of complexes formed as well as the degree of fractionation (Bau and Dulski, 1999).

5.1.1.2 Rare earth elements in hydrothermal systems

The chemical modification of seawater during reaction with N-MORB at 2 to 3 km depth within the ocean crust produces high-temperature hydrothermal fluids that are 100 to 10,000 fold enriched in REEs over seawater concentrations. Chondrite normalised REE values of these fluids show a positive Eu-anomaly, LREE enrichment, HREE depletion and no Ce anomaly (Klinkhammer *et al.*, 1994; Mitra *et al.*, 1994). The composition of these fluids is believed to be buffered by greenschist mineral assemblages in a reaction zone above or adjacent to a magma chamber (Bowers *et al.*, 1988), and the REE composition is inherited from plagioclase in N-MORB (Klinkhammer *et al.*, 1994).

When these fluids are expelled from hydrothermal vents, they mix with oxygenated seawater and form minerals with distinct hydrothermal REE signature (Bence, 1983; Detrick *et al.*, 1988; Gillis *et al.*, 1990; Mills and Elderfield, 1995a). Sulphide samples from the active TAG mound have a distinct Eu anomaly, no Ce anomaly, thus closely resembling those of hydrothermal fluids (Mills and Elderfield, 1995a). The REE patterns for sulphide from the Snake Pit vent field, in contrast, have been shown to lack any anomalous Eu enrichment and they are more HREE enriched than the venting solution (Gillis *et al.*, 1990). This discrepancy between primary sulphide minerals and black smoker fluids is believed to indicate precipitation of hydrothermal minerals in the shallow subsurface or in the chimneys. The concentrations of REEs in pristine sulphides are extremely low (1 to 10 ppb Nd), but oxidation of the sulphides after cessation of hydrothermal activity causes an increase in concentrations by two orders of magnitude and more seawater like patterns (Mills and Elderfield, 1995a).

Much higher concentrations of REEs have been measured in anhydrite samples from the active TAG mound (0.6 to 6 ppm Nd), and considering the abundance of anhydrite in the mound interior ($2x10^5$ t; Humphris *et al.*, 1995), this appears to be the major phase that removes REEs from solution subsurface at TAG (Humphris, 1998). Considerable fractionation of the REEs during anhydrite formation is evident in the anhydrite itself as well as in the fluid from which it precipitates. The uptake of trivalent REEs into anhydrite is controlled by their complexation in solution, where the enhanced stability of LREE chloride complexes leads to a preferential uptake of HREEs into the mineral. Crystallographic effects control the incorporation of the larger Eu^{2+}, which is discriminated against in the anhydrite (Mills and Elderfield, 1995a; Humphris, 1998). These processes are evident not only in the REE pattern of the anhydrite, but they are also reflected in the fluid from which it precipitated. The continuous evolution of the fluid leads to an increasing LREE enrichment and Eu content, which is eventually imprinted in the REE pattern of the anhydrite itself. Hence, despite the discrimination against LREE and Eu, TAG

anhydrites display positive Eu anomalies and varying degrees of LREE enrichment (Humphris, 1998).

Close to the source of high temperature venting minerals and sediments have distinct hydrothermal signatures that may be used to infer mixing ratios and elucidate mineralisation processed within the mound (Mills and Elderfield, 1995a; James and Elderfield, 1996; Humphris, 1998). With increasing distance from the vent site the hydrothermal signal is rapidly overprinted by continuous scavenging from seawater. Near-vent oxyhydroxide particles from the TAG neutrally buoyant plume have REE patterns that reflect both uptake from vent fluids and seawater source (German *et al.*, 1990; Mitra *et al.*, 1994). Because of their great particle-reactivity, REEs are rapidly removed by adsorption and co-precipitation with hydrothermal precipitates (Klinkhammer *et al.*, 1983; German *et al.*, 1990; Rudnicki and Elderfield, 1993). The deep-sea hydrothermal system therefore acts as a net sink, despite the high concentrations of REEs in the vent fluids compared to seawater (Klinkhammer *et al.*, 1983). With increasing distance from the source particles generated in the advecting plume increasingly reflect REE patterns akin to seawater patterns with negligible chemical signature of the original vent fluid. The continuous adsorption produces particles with increasing REE/Fe ratios as the neutrally buoyant plume is dispersed away from the source (German *et al.*, 1990). This is further reflected in a depletion of dissolved REE in the water column at plume height (Klinkhammer *et al.*, 1983) and an increasing accumulation rate of REEs in sediments underlying plume trajectories (Ruhlin and Owen, 1986; Barrett and Jarvis, 1988; Olivarez and Owen, 1989).

5.1.2 Clay minerals in hydrothermal settings

Owing to their small grain size and their complex mineralogy, clay minerals in hydrothermal systems have received less attention than the more prominent sulphides. The reaction of seawater with volcanigenic material at spreading centres and hydrothermal vents produces a variety of clay minerals. Their mineralogy and chemical composition can provide insight into the fluid chemistry and thermal history of hydrothermal fluids, basalt alteration and

fluid-sediment interaction. Clay minerals are generated on the seafloor associated with spreading centres at temperatures ranging from 0°C-500°C.They can be formed during hydrothermal alteration of oceanic crust by seawater (Humphris *et al.*, 1980; Alt and Honnorez, 1984; Haymon and Kastner, 1986; Alt, 1993; Schöps *et al.*, 1993), or as direct precipitate from hydrothermal fluids (De Carlo *et al.*, 1983; McMurtry *et al.*, 1983; Alt and Jiang, 1991; Percival and Ames, 1993; Gwynn, 1998). Table 5.1 gives chemical compositions for clay minerals that have been formed by either of these two processes and at a wide range of temperatures.

5.1.2.1 Clays as alteration products of oceanic crust

Cold oxidising seawater that is drawn into the upper ~300m of the relatively young volcanic section, causes low-temperature alteration at high water/rock ratios (Alt and Honnorez, 1984; Böhlke *et al.*, 1984; Alt *et al.*, 1986; Teagle *et al.*, 1996). The first mineral phases to be formed during low-temperature alteration of ridge-flank circulation systems relatively near the spreading axis include Fe-oxyhydroxide, celadonite and nontronite (Humphris *et al.*, 1980; Alt and Honnorez, 1984; Alt, 1993). The thin sediment cover allows direct access of large volumes of seawater into the permeable upper crust, resulting in open circulation with temperatures <25°C (Mottl and Wheat, 1994; Wheat and Mottl, 1994). The main alteration processes operating are oxidation and alkali fixation, producing alteration halos and mineral coatings along fractures and exposed surfaces with minimal change to the basement fluid (Alt and Honnorez, 1984; Alt *et al.*, 1993; Teagle *et al.*, 1996).

The marked increased Fe content of celadonite-nontronite bearing alteration halos compared with the unaltered host rock suggests that these minerals form when reduced Fe-rich vent fluids percolate upwards through lava talus and mix with oxidising seawater to produce clay-rich coatings on fresh pillow lavas (Humphris *et al.*, 1980; De Carlo *et al.*, 1983; Alt, 1993). Schöps *et al.* (1993) describe nontronitic smectites from Central Pacific seamounts which differ from other reported nontronites by their much higher Al content (~14% Al_2O_3) and high Ti content (~3.5% TiO_2) (see Table 5.1). Formation

temperatures are between 32°C and 48°C, which is comparable to other hydrothermal nontronites (25°C-50°C; e.g. McMurtry *et al.*, 1983; De Carlo *et al.*, 1983). However, because of the relatively high concentration of immobile elements such as Al, Schöps *et al.* (1993) concluded that the nontronitic smectites formed by authigenic weathering of the associated alkaline volcanics rather than by mixing of hydrothermal fluids with seawater. This was further confirmed by their REE patterns, which closely resemble those of alkaline volcanics, but with a negative Ce anomaly.

With increasing depth in the volcanics (300-500 m) and burial of the crust by sediments farther off-axis, circulation of seawater through the crust becomes increasingly restricted, producing more reduced conditions at lower water/rock ratios and increasing temperatures (Alt and Honnorez, 1984; Alt *et al.*, 1986; Alt, 1993; Mottl and Wheat, 1994). This is further enhanced by clogging of fractures with secondary minerals. Most of the Mg from seawater is fixed as saponite, which is the dominant mineral phase to form during the restricted type of circulation. Mottl (1983) explained the increasing Mg content in these minerals compared to the more Fe-rich smectites with much more rapid $Mg^{2=}$-removal rates at elevated temperatures of 70°C-500°C. Oxygen isotope analysis of saponites revealed formation temperatures of 15°C-170°C (Böhlke *et al.*, 1984). Comparison of REE patterns for secondary mineral phases with their respective host rocks from the upper few hundred metres of the oceanic crust suggest that the REE contents is unaffected by low-temperature alteration processes (Teagle *et al.*, 1996).

	Crustal alteration products			Direct hydrothermal precipitates		
	celadonite[1]	nontronitic smectite[2]	saponite[1]	nontronite[3]	mixed illite/ smectite[4]	saponite[5]
Major elements (wt %)						
SiO_2	45.25	47.02	46.97	46.7	50.42	47.12
TiO_2	0.03	3.41	0.05	0.02	0.03	/
Al_2O_3	4.69	14.38	5.1	0.32	32.82	3.26
Fe_2O_3	28.05	12.06	8.39	33.3	1.9	4.24
FeO	/	/	/	0.4	1.9	1.51
MnO	0.09	0.01	0.13	0.4	0.23	0.18
MgO	7.23	3.71	23.87	2.8	0.31	22.95
CaO	1.17	0.61	1.38	0.4	1.14	0.25
Na_2O	0.15	1.87	0.09	1	3.24	0.36
K_2O	4.49	1.62	0.12	3.4	3.24	0.07
total	91.14	84.69	86.09	88.74	90	79.94
formation temperature*	<40°C	32-48°C	15-170°C	57°C	220-270°C	184-276°C

*from oxygen isotope thermometry

[1] Data from Teagle *et al.*, 1996; ODP Hole 896A, eastern equatorial Pacific (5.9 Ma old crust)
[2] Data from Schöps *et al.*, 1993; Central Pacific seamounts
[3] Data from Murnane and Clagues, 1983; Juan de Fuca Ridge, low temperature deposit
[4] Data from Alt and Jiang, 1991; EPR at 21°N, massive sulphides on Green Seamount
[5] Data from Percival and Ames, 1993; Middle valley, JdFR, moderately hot active chimneys

Table 5.1: Comparative major element geochemistry of hydrothermal clay minerals from basalt alteration and direct precipitation at a range of temperatures.

5.1.2.2 Clays in metalliferous sediments and hydrothermal deposits

Fe-oxyhydroxide precipitates intermixed with clay minerals are amongst the most common deposits observed in hydrothermal settings. These are formed during seafloor weathering of massive sulphides or by direct precipitation from low temperature hydrothermal exhalations (Bischoff, 1972; Corliss *et al.*, 1978; McMurtry and Yeh, 1981; Malahoff *et al.*, 1982; Singer *et al.*, 1984; Thompson *et al.*, 1985; Cole, 1988; Alt, 1988b; Hékinian *et al.*, 1993; Gwynn, 1998). The most commonly observed clay mineral phase in these deposits is nontronite, an Al-poor hydrous Fe-silicate with dioctahedral clay-mineral structure.

Harder (1976) demonstrated that reducing conditions and the presence of Fe^{2+} and Si in solution are prerequisites for the synthesis of nontronites. Poorly crystalline Fe-hydroxides have been proposed as precursor minerals for nontronite, and under more oxidising conditions the Fe-rich minerals will be re-crystallised to goethite (Singer and Stoffers, 1987).

A sequence of nontronite – Fe-oxide – Mn-oxides has commonly been observed on hydrothermal sediment-mounds (Corliss *et al.*, 1978; Dymond *et al.*, 1980). This sequence is interpreted to represent a steady-state oxidation gradient where Mn-oxides are precipitated at the surface of the deposit and the nontronite or amorphous phases are precipitated underneath. Hydrothermal fluids cool slowly as they percolate through the reducing sediments and precipitate nontronite. Closer to the surface, where conditions are more oxidising, nontronite is gradually replaced by Fe-oxides or amorphous silica, until the fluids reach the interface with oxic bottom water and Mn-oxide is precipitated.

De Carlo *et al.* (1983) suggested that with increasing vent temperatures more amorphous Fe-oxide is precipitated relative to smectite. Higher temperatures enhance Fe-oxide precipitation, thus inhibiting crystallisation and increase trace element scavenging. Oxygen isotope geothermometry has shown that most nontronites in metalliferous deposits form at temperatures between 20° and 60°C (McMurtry and Yeh, 1981; De Carlo *et al.*, 1983; McMurtry *et al.*, 1983; Murnane and Clague, 1983; Singer *et al.*, 1984; Alt, 1988b).

Only limited data are available on REE chemistry of hydrothermal Fe-oxysilicates (Corliss *et al.*, 1978; Murnane and Clague, 1983; Alt, 1988b; Puteanus *et al.*, 1991; Hékinian *et al.*, 1993; Gwynn, 1998). In general, the concentrations of REEs in clay minerals and clay rich sediments are higher than sulphides but lower than basalts, with Nd concentrations typically in the order of 1 – 10 ppm (Alt, 1988b; Hékinian *et al.*, 1993). The REE patterns are generally consistent with a seawater source that has been mixed with low temperature hydrothermal fluids (Murnane and Clague, 1983; Alt, 1988b; Gwynn, 1998). The negative Ce-anomaly is typically slightly reduced

compared with seawater. The negative sign of the Ce-anomaly, however, is good evidence that the clays are not of hydrogenous origin, since these would produce a positive Ce-anomaly due to preferential incorporation of Ce via oxidative scavenging from seawater (Piper, 1974). Local variations in the variations in the REE patterns are generally ascribed to variable compositions of the host rocks.

Illite and mixed-layer illite smectite (I/S) are commonly interpreted as alteration products of volcanic rock fragments or as products of burial metamorphism and diagenesis (Kisch, 1983; Weaver, 1989). Alt and Jiang (1991), however, demonstrated that the I/S assemblages that occur in massive sulphide deposits on Green Seamount near the East Pacific Rise were produced by direct precipitation from hydrothermal fluids rather than through alteration of pre-existing material. The formation temperatures of these I/S were between 220°C and 270°C.

Clay minerals observed in chimney samples from active hydrothermal chimneys at Middle Valley, Juan de Fuca Ridge, are dominated by saponite, Mg-rich smectite and chlorite (Percival and Ames, 1993). These were precipitated directly by reaction of Mg-rich seawater with hydrothermal fluids with low $f(O_2)$ and Si activity. The preferential formation of Mg-rich smectite over Fe-rich smectite indicates high temperature and low $f(O_2)$. The occurrence of chlorite requires significant amounts of Al in the hydrothermal fluids and suggests reaction of the hot fluids with proximal sediments.

5.1.3 Chapter outline

The REE geochemistry of bulk sediments from core 43 is discussed with respect of the origin of the different sedimentary units in this core and their relationship to similar deposits from elsewhere in the TAG hydrothermal field. The nature of clay minerals from the intermediate layer and carbonate cap of core 43 is determined. The major-elemental composition as well as the REE chemistry is used to investigate the origin of the Fe-oxysilicate deposits in this core and to infer the low temperature alteration history of the system.

5.2 Material and methods

5.2.1 Purification and separation of clay fraction

A total of six samples were selected from core 43 for geochemical and mineralogical analysis of the clay faction, here operationally defined as the <2μm fraction. Of these six samples two were chosen from the carbonate cap (sections #5 and #8) and four from the intermediate layer (sections #15, #21 #25 and #32). Clay fractions were purified from bulk sediments by size separation of chemically treated samples according to the method of Jackson (1969). Prior to chemical treatment all samples were dried at 105°C and ground using an agate pestle and mortar. All sediments were treated with the following sequential digestion and physical separation unless otherwise stated.

5.2.1.1 Removal of carbonate phase

the carbonate phase was removed by treatment of 5-7g of the bulk sediments with 1N sodium-acetate acetic acid buffer (SAAB). The reagent was prepared by adding 82g sodium-acetate (NaO Ac) and 27ml of glacial acetic acid to double distilled water to make 1 litre. The pH of the solution was buffered at 5. 50ml of the reagent were added to the sample in a 250ml Pyrex glass conical flask and digested in a near-boiling water bath for 30 min with intermittent stirring. Following the treatment, the sample-mixture was centrifuged at 3000 rpm for 5 min and the supernatant discarded. Because of the markedly elevated carbonate content in the carbonate cap, the treatment was repeated for samples #5 and #8 from the carbonate cap. The sediment was washed with ~100 ml double distilled water to which ~10 ml of a saturated NaCl solution was added to aid flocculation.

5.2.1.2 Removal of Fe-oxide phases

Amorphous Fe-oxide phases were removed by treating the samples with sodium citrate-bicarbonate dithionite buffer solution (CBD) following the method described by Mehra and Jackson (1960). This procedure is reported

to be the least destructive of methods for Fe-oxide removal. The reagent was prepared by mixing eight parts of a 0.3 M sodium citrate solution (tribasic sodium citrate – $Na_3C_6H_5O_7.1H_2O$) with one part of 1 M bicarbonate solution ($NaHCO_3$). Following the carbonate removal, 180ml of the mixed reagent was added to the wetted sediments and incubated in a water bath at 75°C-80°C for 15 min. During incubation three aliquots of 4g of sodium-dithionate ($Na_2S_2O_4$) were added and stirred for 4 min between each addition. Following treatment ~10 ml of saturated NaCl solution were added, the mixture was centrifuged at 3000 rpm for 3 min and the supernatant was discarded. To ensure complete removal of all amorphous Fe-oxide, the treatment was repeated for all samples with 90 ml mixed reagent and 3 times 2 g of sodium-dithionate. The sediment was washed with ~100 ml double distilled water to which ~5 ml of a saturated NaCl solution was added.

5.2.1.3 Removal of amorphous silica

Following the removal of amorphous Fe-oxides, the centrifuged samples were re-suspended in 200 ml of a 2% Na_2CO_3 solution. The sediments were dispersed thoroughly, brought to the boil in a sand-bath and left to boil for 5 min. The sediment-mixture was centrifuged at 3000 rpm for 3 min, the supernatant discarded and the sediments washed with ~100 ml double distilled water to which ~5 ml saturated NaCl was added.

5.2.1.4 Separation of <2μm fraction

After washing of the chemically treated samples, the sediments were re-suspended in 75-100 ml of a 0.1% sodium hexametaphosphate solution (Calgon). To aid dispersion the mixture was ultrasonically agitated for 30 min. Dispersed sediments were then centrifuged at 750 rpm for 3 min, the supernatant carefully removed and re-centrifuged, with the addition of ~5 ml of 6% $MgCl_2$ solution, at 3000 rpm for a further 3 min. The treatment was repeated for the residual sediments up to 10 times to ensure near-complete recovery of the clay fraction. Separated clays were then washed with a dilute $MgCl_2$ solution (~1%). At this stage it is important to keep the concentration of

the washing solution to a minimum to reduce contamination. The clays were dried in an oven at 60°C and ground with a pestle and mortar.

5.2.2 Mineralogical and chemical analysis

5.2.2.1 X-ray diffraction

The mineralogy of bulk sediments and clay separates was determined by X-ray diffraction analysis with a Philips EW 1730 automated powder diffractometer using Co-K_α radiation. Dry powder mounts were scanned between 0° and 60° at 1.2° 2θ/min.

5.2.2.2 Major elemental composition

Major elements (Si, Ti, Al, Mg, Ca, Na, K, Fe, Mn, P, Cu, and Zn) were determined on a Philips PW 1400 X-ray Fluorescence Spectrometer. The preparation of fused beads is described for the bulk sediments in Chapter 3 Section 3.1.2.1. The same method was applied for clay separates, and samples were prepared at a dilution of 1:20 for sample #15, #21, #25, and #32, and a dilution of 1:40 for samples #5 and #8.

5.2.2.3 REE content

Rare earth elements were determined in HF digests of bulk sediments and clay fractions by Inductively Coupled Plasma Mass Spectrometry (VG Elemental PlasmaQuad PQ2+). The procedure for the sample dissolution and analysis are described in Chapter 4 Sections 4.2.2.2 and 4.2.2.3 respectively. The external precision for REE measurements was within 5% (2σ) the accuracy was within 4% (2 σ). Counts for sample blanks and reagent blanks were ~10^4 to 10^5 fold less than for counts for sediment samples. Ce and Eu-anomalies were calculated as described in Section 5.1.

5.2.2.4 SEM imaging

The preparation and scanning electron microscope (SEM) image analysis of sediment samples is described in detail in Chapter 4 Section 4.2.3. Polished

thin sections of bulk samples were analysed on a JSM 6400 SEM fitted with an EDS (Energy Dispersive Spectrometry) X-ray detector. All imaging and X-ray microanalysis was done in the backscattered electron imagery (BSEI) mode.

5.3 Results

5.3.1 REE chemistry of bulk sediments

The mineralogy and geochemistry of core 43 was discussed in detail in Chapter 3. REE concentrations were obtained for bulk samples throughout the core. The data are shown together with Ce and Eu-anomalies (Eu/Eu* and Ce/Ce* respectively) in Table 5.2. In addition, REE concentrations and ratios are listed for a number of reference samples, including North Atlantic seawater from the TAG area (Mitra *et al.*, 1994), hydrothermal fluids (Douville *et al.*, 1999), a range of hydrothermal minerals and sediments (Mills *et al.*, 1993; Mills and Elderfield, 1995a; Goulding, 1998), and a representative sample from the background core 10.

Concentrations for Nd range from 1.1 to 15.6 ppm, which compares well with previously observed REE concentrations for metalliferous sediments from this area (1.7 to 12.6 ppm Nd; Mills *et al.*, 1993). The highest REE concentrations were measured in the carbonate cap at ~ 30 cm depth, and correspond with an increased concentration of Mn-oxide in this layer. The lowest concentrations were found in the two sulphide layers. Concentrations in the carbonate cap were similar to those measured in the background core.

Ce-anomalies (Ce/Ce*) are negative throughout core 43 with only little variation. All samples fall within a narrow range (Ce/Ce* = 0.56 - 0.72, and the mean value of 0.64 is identical to that measured in the background core. The almost exclusively positive Eu-anomalies (Eu/Eu*) in core 43 range between 0.9 to 10.4. Values were highest in the upper sulphide layer and in some samples from the upper portion of the intermediate layer. The maximum Eu-anomalies measured here were comparable to, or slightly exceed, values previously reported for black smoker fluids at TAG (Eu/Eu* = 8.3 to 9.4; Mitra *et al.* 1994, Douville *et al.* 1999). In the background core Eu-anomalies were small and consistently negative (mean Eu/Eu* = 0.7). The lowest values in the carbonate cap were close to values in the background core.

Sample ID	Depth (cm)	La	Ce	Pr	Nd	Sm	Eu	Gd	Tb	Dy	Ho	Er	Tm	Yb	Lu	Ce/Ce* chondrite normalised	Eu/Eu* chondrite normalised
		all values ppm															
1	2.5	9.8	13.9	2.21	8.7	1.85	0.61	1.90	0.27	1.68	0.36	0.99	0.14	0.93	0.15	0.7	1.0
3	12.5	13.2	18.7	3.10	11.9	2.45	0.74	2.44	0.33	2.07	0.43	1.17	0.16	1.03	0.17	0.7	0.9
5	22.5	13.8	19.3	3.32	12.8	2.63	0.82	2.57	0.35	2.13	0.43	1.16	0.16	1.03	0.17	0.6	0.9
7	32.5	16.5	24.3	4.02	15.6	3.28	1.05	3.24	0.44	2.77	0.57	1.52	0.22	1.40	0.23	0.7	1.0
8	37.5	12.2	18.1	2.96	12.3	2.65	1.26	2.98	0.42	2.46	0.51	1.33	0.19	1.24	0.19	0.7	1.4
9	42.5	15.9	23.6	3.89	14.8	3.13	1.36	3.03	0.41	2.54	0.52	1.40	0.20	1.30	0.21	0.7	1.3
10	47.5	6.8	9.3	1.56	6.2	1.32	1.08	1.29	0.17	1.07	0.22	0.61	0.08	0.56	0.09	0.6	2.5
11	52.5	0.6	1.0	0.22	1.1	0.31	0.88	0.32	0.04	0.25	0.05	0.14	0.02	0.13	0.02	0.7	8.5
12	57.5	1.5	2.0	0.44	2.2	0.56	1.44	0.47	0.06	0.29	0.06	0.16	0.02	0.15	0.03	0.6	8.4
13	62.5	0.9	1.2	0.27	1.4	0.38	1.10	0.32	0.04	0.22	0.04	0.11	0.02	0.11	0.02	0.6	9.4
14	67.5	2.3	3.1	0.61	2.6	0.61	1.02	0.59	0.07	0.47	0.09	0.26	0.03	0.24	0.04	0.6	5.2
15	72.5	7.7	11.4	1.94	7.8	1.76	1.24	1.67	0.22	1.37	0.27	0.72	0.10	0.67	0.11	0.7	2.2
16	77.5	3.9	5.4	0.94	3.9	0.89	1.30	0.81	0.10	0.63	0.13	0.36	0.05	0.33	0.06	0.6	4.6
17	82.5	3.4	4.4	0.80	3.4	0.74	0.95	0.73	0.10	0.61	0.13	0.35	0.05	0.32	0.06	0.6	3.9
19	92.5	1.1	1.4	0.30	1.4	0.36	1.15	0.30	0.04	0.21	0.04	0.12	0.02	0.11	0.02	0.6	10.4
21	102.5	2.5	3.5	0.69	3.1	0.70	1.12	0.68	0.09	0.55	0.11	0.30	0.04	0.28	0.05	0.6	4.9
22	107.5	3.8	5.3	0.96	4.0	0.91	1.05	0.89	0.12	0.76	0.16	0.43	0.06	0.40	0.07	0.6	3.5
24	117.5	1.1	1.5	0.32	1.5	0.41	0.95	0.34	0.04	0.24	0.05	0.12	0.02	0.12	0.02	0.6	7.6
25	122.5	1.1	1.6	0.36	1.8	0.48	1.42	0.41	0.04	0.25	0.04	0.12	0.02	0.12	0.02	0.6	9.6
26	127.5	1.5	2.4	0.49	2.4	0.64	1.47	0.59	0.07	0.41	0.07	0.20	0.03	0.18	0.03	0.6	7.2
27	132.5	3.6	5.6	1.04	4.8	1.19	1.84	1.07	0.13	0.75	0.14	0.37	0.05	0.33	0.06	0.7	4.9
29	142.5	1.8	2.6	0.50	2.6	0.70	1.21	0.68	0.08	0.44	0.08	0.20	0.03	0.17	0.03	0.6	5.3
30	147.5	3.3	4.3	0.86	4.0	0.96	1.15	0.97	0.13	0.73	0.15	0.40	0.06	0.35	0.06	0.6	3.6
31	152.5	5.8	8.8	1.57	6.8	1.54	1.35	1.58	0.21	1.28	0.25	0.65	0.09	0.57	0.09	0.7	2.6
32	157.5	5.0	6.5	1.24	5.5	1.24	0.94	1.23	0.16	0.99	0.19	0.52	0.07	0.45	0.07	0.6	2.3
33	162.5	6.8	10.0	1.70	7.1	1.64	0.93	1.70	0.23	1.43	0.29	0.76	0.10	0.68	0.11	0.7	1.7

Table 5.2: REE data for bulk samples from core 43 and selected reference data from the literature.

Sample ID	Depth (cm)	La	Ce	Pr	Nd	Sm	Eu	Gd	Tb	Dy	Ho	Er	Tm	Yb	Lu	Ce/Ce*	Eu/Eu*
		all values ppm														chondrite normalised	
35	172.5	2.1	2.9	0.58	2.5	0.63	0.62	0.70	0.10	0.65	0.13	0.36	0.05	0.31	0.05	0.6	2.8
37	182.5	1.7	3.0	0.59	2.8	0.75	1.19	0.75	0.12	0.74	0.14	0.36	0.05	0.33	0.05	0.7	4.8
38	187.5	1.3	2.3	0.47	2.2	0.58	1.01	0.61	0.09	0.56	0.11	0.30	0.04	0.27	0.04	0.7	5.2
39	192.5	1.0	1.7	0.34	1.7	0.47	0.94	0.50	0.07	0.49	0.09	0.24	0.03	0.21	0.03	0.7	5.9
40	197.5	1.4	2.1	0.45	2.1	0.57	0.82	0.60	0.09	0.58	0.12	0.31	0.04	0.27	0.05	0.6	4.2
41	202.5	1.0	1.8	0.38	1.8	0.51	0.66	0.49	0.07	0.45	0.09	0.22	0.03	0.20	0.03	0.7	4.0
42	207.5	1.3	2.3	0.48	2.2	0.61	0.79	0.64	0.10	0.62	0.12	0.31	0.04	0.28	0.05	0.7	3.8
43	212.5	2.5	3.7	0.75	3.4	0.87	0.71	0.92	0.15	0.90	0.18	0.48	0.07	0.41	0.07	0.6	2.4
44	217.5	2.1	3.6	0.71	3.3	0.88	0.63	0.94	0.14	0.88	0.17	0.45	0.06	0.38	0.06	0.7	2.1
45	222.5	2.8	4.0	0.83	3.9	0.97	0.77	1.06	0.15	0.95	0.19	0.51	0.07	0.45	0.07	0.6	2.3
46	227	2.6	3.4	0.68	3.0	0.68	0.57	0.77	0.11	0.74	0.16	0.45	0.06	0.42	0.07	0.6	2.4
(1) N Atlantic seawater *10^6		4.03	0.76	-	3.12	0.61	0.16	0.98	-	1.03	-	0.91	-	0.93	0.15	0.1	0.6
(2) Black smoker fluid *10^4		6.29	10.7	1.5	5.79	1.25	3.68	1.19	0.17	0.85	0.16	0.45	-	0.37	0.05	0.8	9.1
(1) White smoker fluid *10^4		3.57	4.84	-	1.97	0.35	14.50	0.25	-	0.16	-	0.07	-	0.06	0.01	0.7	142.4
(3) Black smoker chalcop. *10^2		1.20	1.40	-	0.85	0.19	0.15	-	-	-	-	0.17	-	0.04	-	0.6	-
(3) Oxidised sulphide		2.96	3.09	-	3.48	0.71	1.68	0.67	-	0.60	-	0.41	-	0.37	0.06	0.5	7.4
(4) Mn-rich umber		10.7	18.4	2.7	12.4	2.60	2.41	2.54	0.35	2.02	0.45	1.24	0.17	1.02	0.17	0.8	2.8
(5) Plume derived sed.		11.6	17.9	-	11.9	2.54	0.85	-	-	2.21	-	1.33	-	1.15	-	0.7	
(5) Hydrothermal sed.		1.64	1.75	-	1.73	0.45	0.75	0.90	-	0.34	-	0.26	-	0.24	-	0.5	3.5
(6) core 10 (core-top)		9.33	13.8	2.2	9.15	1.93	0.45	2.01	0.3	1.77	0.37	0.96	0.13	0.79	0.12	0.7	0.7

dashes indicate element not reported

(1) Data from Mitra *et al.*, (1994); seawater from TAG (3300 m) and white smoker fluid recalculated to Mg = 0

(2) Data from Douville *et al.*, (1999); TAG black smoker fluid, recalculated to Mg = 0

(3) Data from Mills and Elderfield, (1995b); chalcopyrite from active black smoker chimney at TAG and oxidised rim of mound-sulphide from TAG

(4) Data from Goulding *et al.*, (1998); Mn-rich (Mn = 15%) umber from southeastern flank of active TAG mound

(5) Data from Mills *et al.*, (1993); plume derived sediments and hydrothermal sediments from a metalliferous sediment core from southern periphery of *Alvin* zone

(6) This study, core-top sample from background core 10, composed of foraminiferal carbonate ooze

Table 5.2: continued

Chondrite normalised REE patterns are plotted individually for each of the four sedimentary layers as they were identified in the previous chapter (Figure 5.2). The patterns show considerable coherence within each sedimentary layer with the most notable variation occurring in the size of the Eu-anomaly. Variation between the three hydrothermally dominated layers is small, with all samples below 50 cm displaying a marked positive Eu-anomaly and a slight negative Ce-anomaly. Also shown are selected minerals phases from the active mound that display similar REE patterns.

All samples show some degree of HREE enrichment (Nd_n/Yb_n = 2.5-5.5) compared with black smoker fluids (Nd_n/Yb_n = 7.9) or pristine chalcopyrite from an active black smoker chimney (Nd_n/Yb_n = 8.0). The lowest Nd_n/Yb_n values were found in the lower sulphide layer with a relatively narrow range between 2.5 and 3.2. The Nd_n/Yb_n values for the background core range between 3.9 and 4.9.

5.3.2 Geochemistry of separated clay phases

5.3.2.1 Major elemental composition and mineralogy

The position of the six clay samples in relation to the stratigraphy is shown in Figure 5.3. Results for the separation are summarised in Table 5.3. The relative proportion of the <2 µm fraction was markedly higher in the intermediate layer compared to the carbonate cap and suggest that clays comprise a substantial proportion (between 38 and 64 %) of the bulk sediments in the intermediate layer. These figures should be considered as minimum estimates, since it is anticipated that the physical recovery of clays was incomplete. The yellowish-green colour of the clay-separates suggests that the dominant mineral phase is nontronite, which is a frequently observed component of Fe-Si rich, low-temperature hydrothermal deposits (Corliss *et al.*, 1978; Dymond *et al.*, 1980; De Carlo *et al.*, 1983; McMurtry *et al.*, 1983; Alt, 1988b; Hékinian *et al.*, 1993).

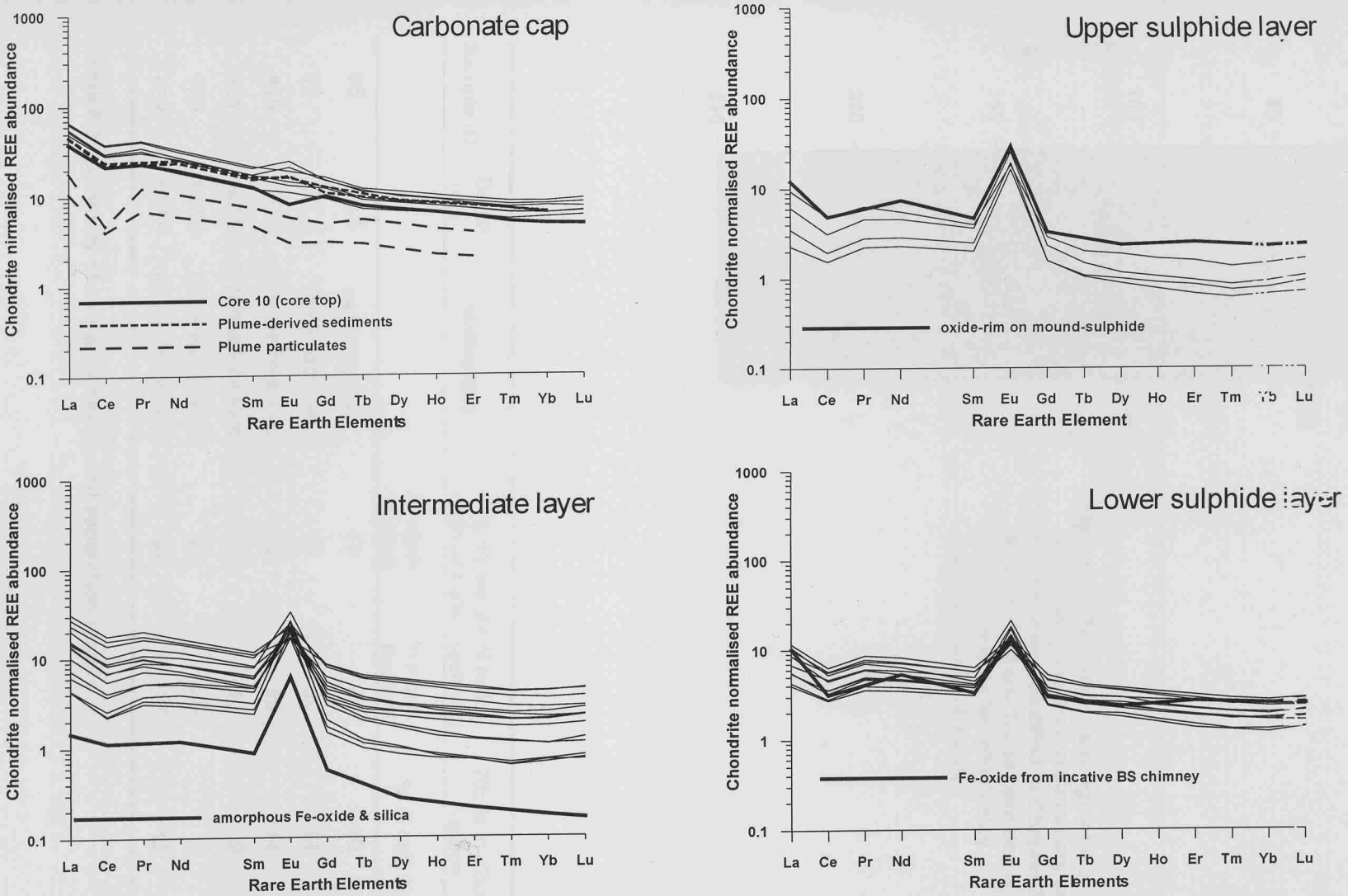

Figure 5.2: REE patterns of bulk sediments for each of the sedimentary units of core 43. Also shown are REE patterns for the carbonate-rich background core 10, local metalliferous sediments and oxidised sulphides from the active mound with similar REE fractionation. Data for plume derived sediments are from Mills *et al.* (1993) and for Plume particles from German *et al.* (1990).

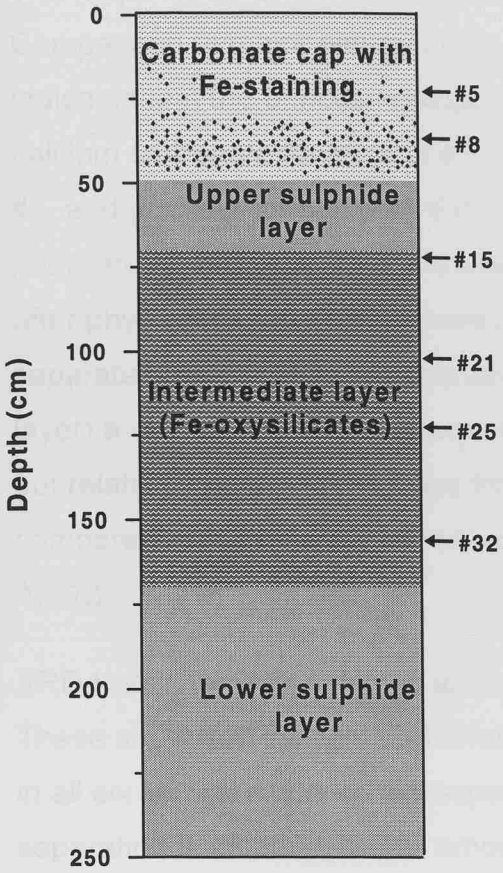

Figure 5.3: Schematic stratigraphy of core 43 showing the four sedimentary layers as they were identified in Chapter 3. Also marked are the sample depth for the six samples for which clay separates were obtained

Sample ID	Depth (cm)	Stratigraphy	% dry weight of bulk sediment after treatment		REEs in <2µm fraction
			In <2µm fraction	In >2µm fraction	% of bulk Nd
#5	22.5	carbonate cap	14	23	40
#8	37.5	carbonate cap	11	38	14
#15	72.5	intermediate layer	39	29	14
#21	102.5	intermediate layer	52	18	9
#25	122.5	intermediate layer	38	39	3
#32	157.5	intermediate layer	64	17	12

Table 5.3: Summary of clay purification and separation results.

The major element data for the clay fractions are shown in Table 5.4. Comparison of major element data for bulk samples and the clay phases indicates that the principal component lost during chemical digestion was calcium carbonate for sample #5, calcium carbonate and goethite for sample #8, and goethite for samples #15, #21, #25 and #32. No further analysis was performed on the chemically leached fraction or the solid phase that remained after physical separation. Marked compositional differences between clay separates from the two sedimentary layers (carbonate cap and intermediate layer) are evident for most elements. The Al concentration is generally low, but relatively higher in the clays from the carbonate cap (~8.2 % Al_2O_3) compared with extremely low values in the intermediate layer (0 – 1.7 % Al_2O_3).

XRD traces for bulk samples and clay separates are plotted in Figure 5.4. These show that calcium carbonate and goethite were successfully removed in all six samples during clay separation, and the principal mineral phase after separation is smectite. Small amounts of kaolinite and quartz were detected in samples #5 and #8 from the carbonate cap. Minor quartz contamination was also present in sample #15. The relatively good definition of the peaks indicates that the smectites from the carbonate cap are moderately to well crystallised, and those from the intermediate layer are well crystallised. Smectites in metalliferous sediments are often associated with amorphous phases, particularly amorphous Si, which is identified by a broad hump in the central region of the XRD traces. None of the XRD data from core 43 show any evidence for the presence of amorphous phases, suggesting that it was successfully removed during the chemical separation. The identification of amorphous phases is important, since it will affect the calculation of the structural formula.

Structural formula were calculated for all six clay separates on the assumption that dioctahedral smectite was the only mineral phase present. The dominantly monomineralic character is generally supported by the X-ray results, although the small amounts of kaolinite and quartz in samples #5, #8

and #15 will introduce minor errors into the calculated formula. The Al content in the smectite should therefore be considered as a maximum estimate for samples #5 and #8. The formulae were calculated on the basis of 20 oxygens and 4 hydroxyls per formula unit [$O_{20}(OH)_4$], and assuming that all Fe is present as Fe^{3+}. The results are listed in Table 5.5.

For an ideal dioctahedral structure the sum of octahedral cations is 4, whereas for trioctahedral structures the sum is closer to 6. The formula for all six clay-separates confirms that the smectites are of dioctahedral character. The interlayer charges are indistinguishable from excess layer charges for all samples.

The chemical compositions as well as the structural formula indicate that the four samples from the intermediate layer are extremely Al-poor nontronites. Because of the very low concentration of Al, the remaining tetrahedral sites have been filled arbitrarily with Fe. Previous Mössbauer studies of Al-poor nontronites have demonstrated that this is justified (Weaver and Pollard, 1973). Fe also occupies most octahedral sites, which is consistent with the dioctahedral character of pure nontronites. The high number of octahedral cations suggests that some of the Mg is present in the interlayer position.

For the two clay separates from the carbonate cap (samples #5 and #8), Al has been assigned to the tetrahedral as well as the octahedral sites. Dioctahedral smectites with high Al are often referred to as Fe-montmorillonites (McMurtry and Yeh, 1981). By definition, if the Fe in the octahedral layer comprises <50% the clays are referred to as Fe-montmorillonites (Weaver, 1989). McMurtry and Yeh (1981) described pelagic-ooze Fe-montmorillonites from the East Pacific Rise with similar composition. The pelagic-ooze smectites from core 43, however, have >50% in the octahedral layer and should therefore be classified as nontronites.

	#5		#8		#15		#21		#25		#32	
	bulk	<2 µm	bulk	<2 µm	bulk	<2 µm	bulk	<2 µm	bulk	<2 µm	bulk	<2 µm
SiO_2	10.3	37.9	18.2	37.7	29.8	44.3	33.8	46.6	29.5	45.0	35.4	46.5
TiO_2	0.1	0.5	0.1	0.5	0.1	0.1	0.0	0.0	0.0	0.0	0.0	0.1
Al_2O_3	1.5	8.2	2.0	8.2	1.2	1.7	0.0	0.3	0.0	0.0	0.6	0.5
Fe_2O_3	17.2	19.3	42.4	19.4	44.8	28.2	44.0	33.6	54.5	34.2	43.1	31.7
MnO	0.5	0.1	0.5	0.1	0.0	0.0	0.0	0.0	0.1	0.0	0.1	0.0
MgO	1.1	3.4	1.5	3.5	2.0	5.3	1.9	4.7	1.6	5.0	2.4	5.2
CaO	35.3	7.9	10.5	7.9	0.5	0.1	0.4	0.0	0.4	0.0	0.4	0.1
Na_2O	0.3	0.5	0.5	1.9	5.5	2.5	2.6	1.6	2.3	0.7	3.1	2.8
K_2O	0.1	1.7	0.7	1.7	1.4	0.7	1.3	0.4	1.0	0.2	1.8	0.7
P_2O_5	0.3	3.4	0.7	3.4	0.5	1.3	0.4	1.1	0.5	1.0	0.5	1.2
CuO	0.2	0.7	0.7	0.7	0.1	0.2	0.2	0.3	0.1	0.2	0.2	0.1
ZnO	0.0	0.1	0.3	0.1	0.9	1.0	0.3	0.4	0.2	0.2	0.0	0.0
total	70.0	83.6	78.1	85.2	86.67	85.21	84.93	89.10	90.10	86.44	87.62	88.73

Concentrations are in wt% and corrected for loss on ignition.

Table 5.4: Major elemental composition for clay phases and associated bulk sediments for selected samples from core 43.

	#5	#8	#15	#21	#25	#32
	22.5cm	37.5cm	72.5cm	102.5cm	122.5cm	157.5cm
	Carbonate cap		Intermediate layer			
Tetrahedral layer						
Si^{4+}	6.56	6.46	7.26	7.30	7.23	7.28
Al^{3+}	1.44	1.54	0.32	0.05	0	0.08
Fe^{3+}	0	0	0.42	0.65	0.77	0.64
Total	8	8	8	8	8	8
Octahedral layer						
Fe^{3+}	2.52	2.50	3.06	3.31	3.37	3.10
Al^{3+}	0.22	0.12	0	0	0	0
Mg^{2+}	0.87	0.89	1.30	1.11	1.20	1.21
Total	3.61	3.50	4.37	4.41	4.57	4.31
Interlayer						
Ca^{2+}	1.47	1.45	0.01	0	0	0
Na^{+}	0.16	0.64	0.78	0.48	0.21	0.85
K^{+}	0.37	0.38	0.14	0.09	0.04	0.14
Total	2.00	2.47	0.93	0.56	0.25	0.98
Interlayer charge	3.47	3.92	0.95	0.56	0.25	0.98
Layer charge	3.47	3.92	0.95	0.57	0.26	1.00

Table 5.5: Atomic proportions and site occupancy of smectites in core 43.

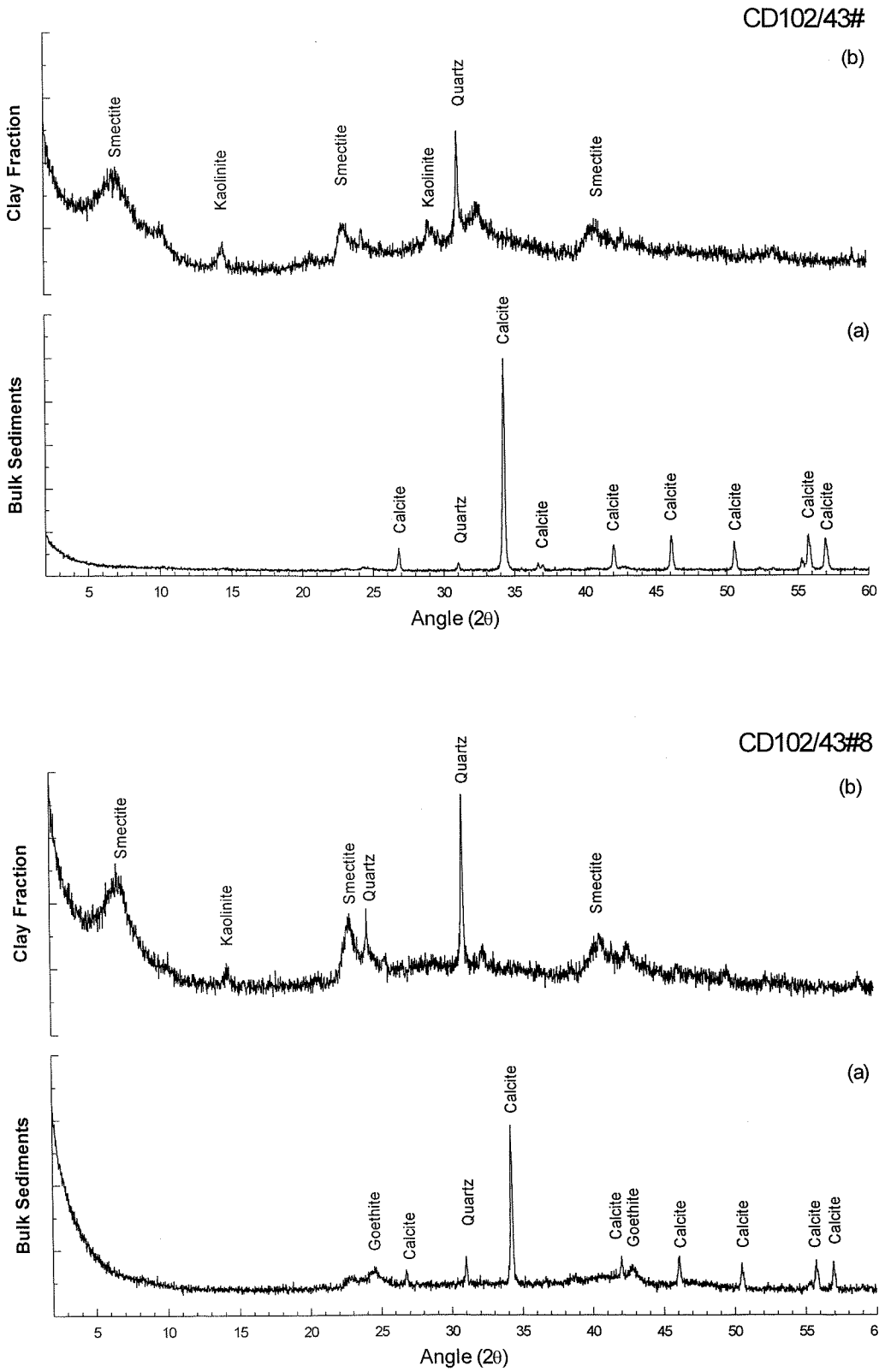

Figure 5.4: Powder diffractograms of (a) bulk sediment and (b) <2μm fractions following chemical digestions, showing known major mineral phases.

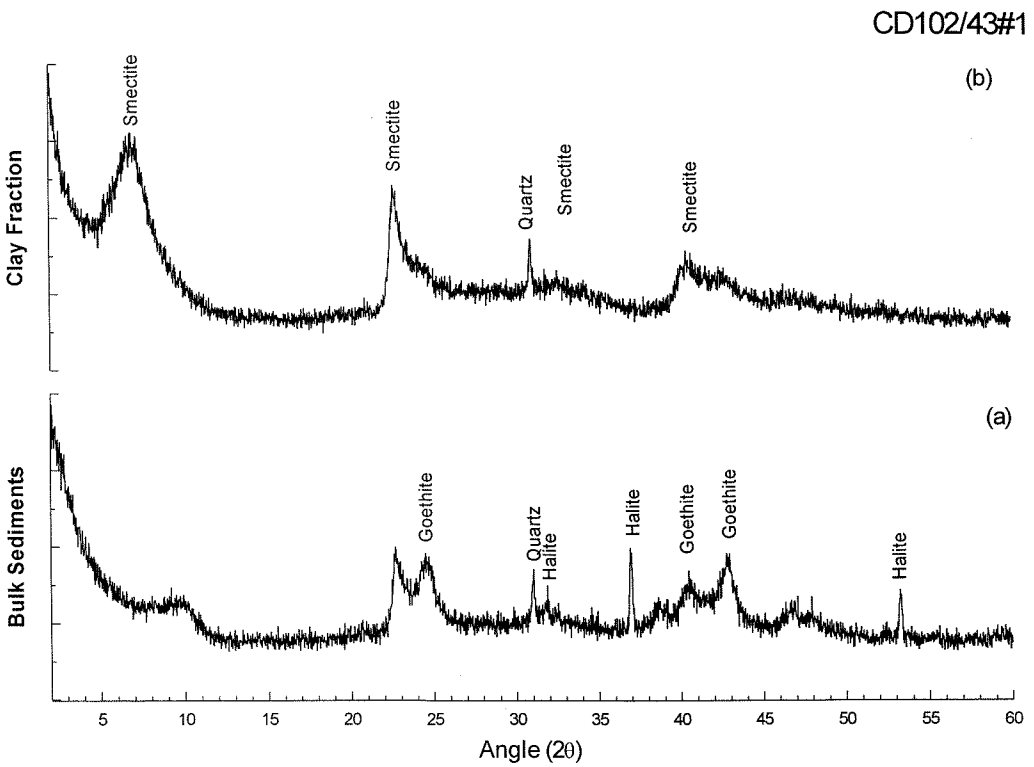

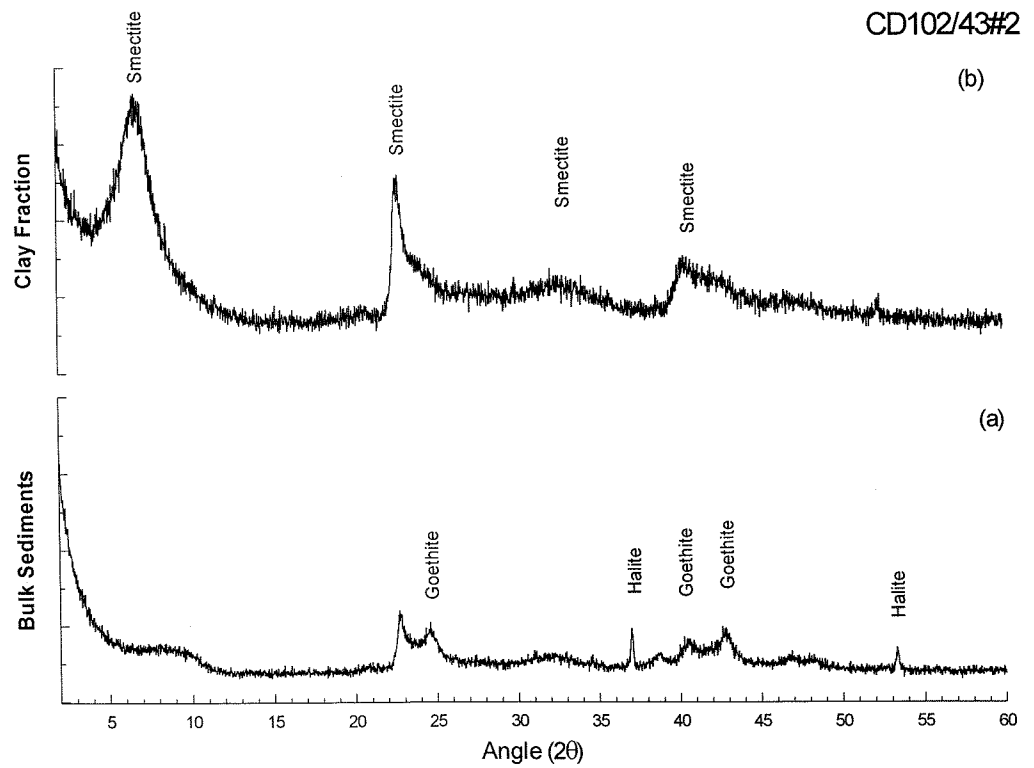

Figure 5.4: continued

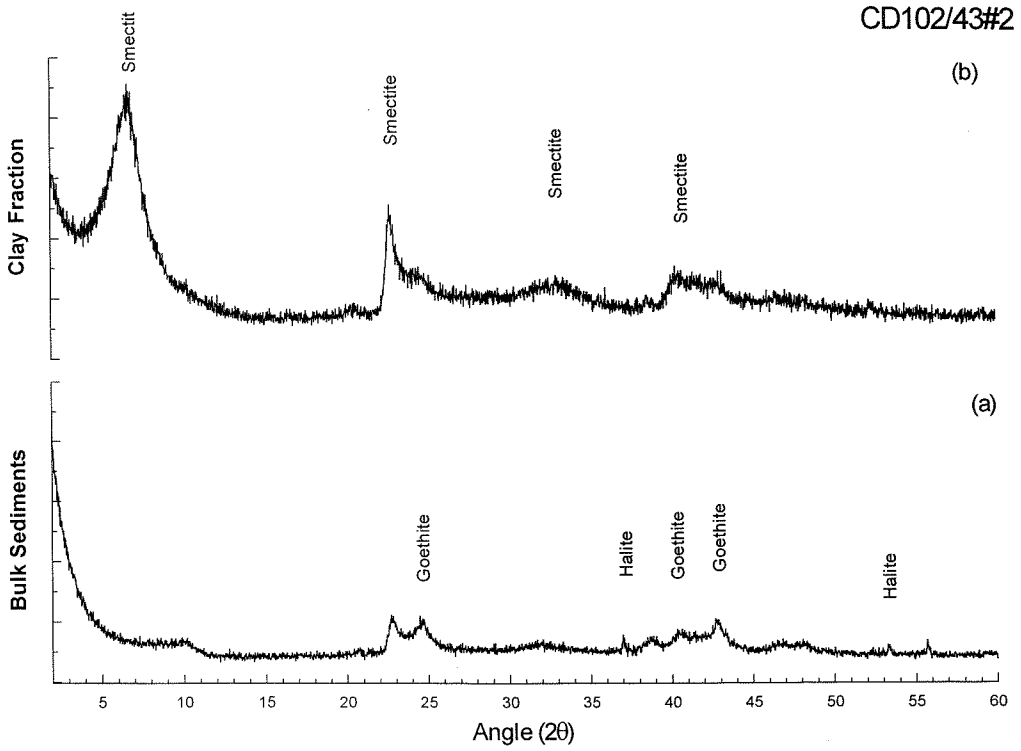

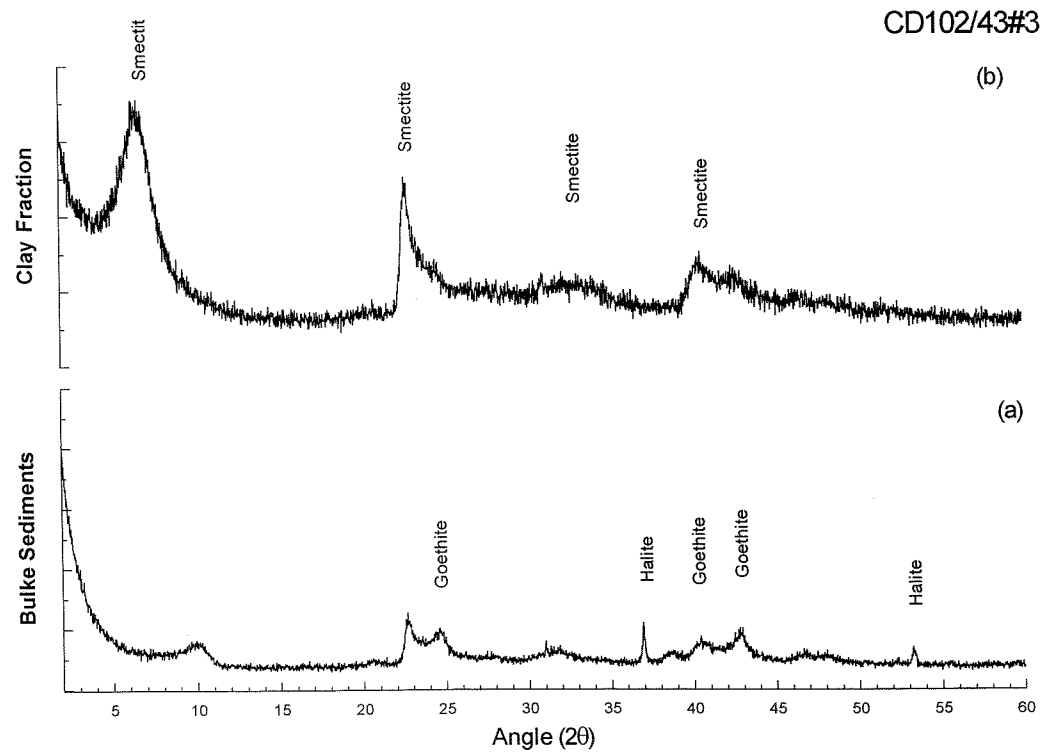

Figure 5.4: continued

5.3.2.2 REE composition

Previous studies have shown that the chemical treatment of the bulk sediments has no discernible leaching effect on the REE content within the <2μm fraction (Gwynn, 1998). REE data for clay separates from core 43 are listed in Table 5.6 and chondrite-normalised values, normalised to chondrite after Evensen *et al.* (1978), are plotted in Figure 5.5 for bulk and clay samples. Also included in Table 5.6 are REE data for clay separates for surface-sediments from the active TAG mound (Gwynn, 1998) and porewater data for TAG mound sediments (Rudnicki and Mills, 1997).

In samples #5 and #8 from the carbonate cap REE concentrations in the clay phase are markedly higher (38 and 15 ppm Nd respectively), exceeding those in the bulk sediments (~12.5 ppm Nd), whereas for the remaining samples the REE concentrations are markedly lower in the clays by a factor of 2 to 10. The REE concentrations in the clays phases from the intermediate layer range between 0.2 and 3 ppm for Nd, which is similar to reported values (Murnane and Clague, 1983; Alt, 1988b; Gwynn, 1998). Table 5.3 also lists the fraction of total REE content that is held in the clay phase. This shows that for samples from the intermediate layer the clays contain only a small proportion of the total REEs (<15%) although the clay phases constitute between 38 and 64 % of the bulk sediments.

The REE patterns of the clay phases generally resemble those of their respective bulk sediments. However, all clay samples have a Ce-anomaly close to unity (Ce/Ce* = 0.9 to 1.1), which is significantly increased compared with the bulk sediments (Ce/Ce* = 0.6 to 0.7). The Eu-anomaly (Eu/Eu*) is reduced in the clay phases, with the most prominent decrease from 9.6 to 5.9 for sample #25 and only small changes in the carbonate cap. All samples except sample #5 show some degree of HREE enrichment (Nd_n/Yb_n = 0.6 to 3.0) compared with the bulk sediments (Nd_n/Yb_n = 3.5 to 5.5). This is most pronounced in sample #25, where the Nd_n/Yb_n decreases from 5.5 to 0.6. The La_n/Nd_n, which is a measure of the LREE enrichment, does not vary significantly between bulk sediments and clay separates.

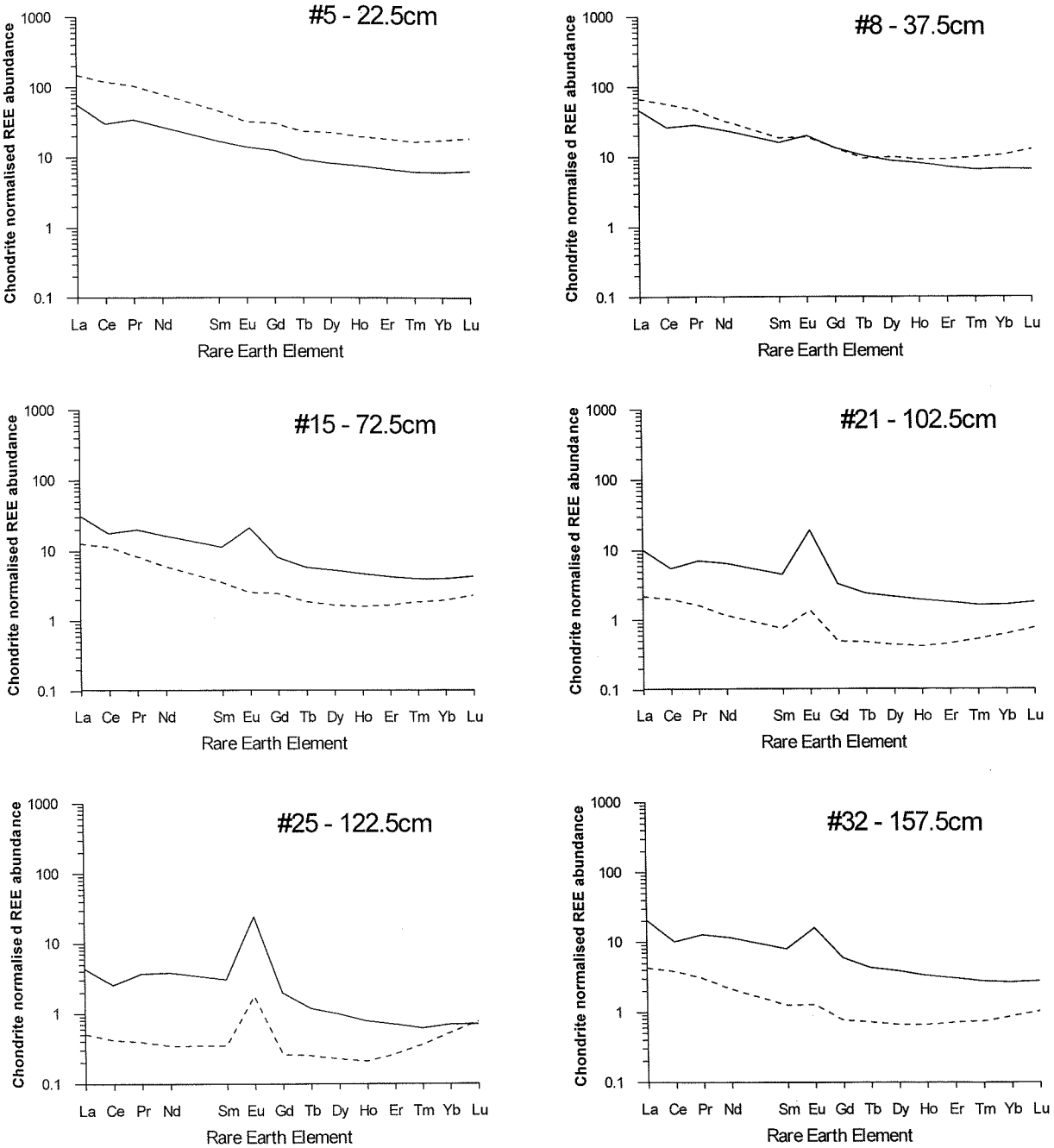

Figure 5.5: REE patterns for bulk sediments (solid line) and separated clay phases (dashed line) for six samples from core 43. Samples in the top two panels are from the carbonate cap, and the remaining samples are from the intermediate layer.

Sample ID	Depth (cm)	La	Ce	Pr	Nd	Sm	Eu	Gd	Tb	Dy	Ho	Er	Tm	Yb	Lu	Ce/Ce*	Eu/Eu*
		all values ppm														chondrite normalised	
Clay separates core 43																	
C#5	22.5	36.4	76.7	10.1	37.7	7.1	1.9	6.3	0.9	5.8	1.1	3.1	0.4	2.9	0.5	1.02	1.20
C#8	37.5	16.4	36.0	4.5	15.4	2.8	1.1	2.7	0.4	2.6	0.5	1.6	0.3	1.8	0.3	1.09	0.84
C#15	72.5	3.1	7.3	0.8	2.9	0.6	0.1	0.5	0.1	0.4	0.1	0.3	0.0	0.3	0.1	1.07	2.20
C#21	102.5	0.5	1.3	0.2	0.6	0.1	0.1	0.1	0.0	0.1	0.0	0.1	0.0	0.1	0.0	0.92	5.89
C#25	122.5	0.1	0.3	0.0	0.2	0.1	0.1	0.1	0.0	0.1	0.0	0.0	0.0	0.1	0.0	1.07	1.26
C#32	157.5	1.0	2.4	0.3	1.0	0.2	0.1	0.2	0.0	0.2	0.0	0.1	0.0	0.1	0.0		
Corresponding bulk samples core 43																	
B#5	22.5	13.8	19.3	3.3	12.8	2.6	0.8	2.6	0.3	2.1	0.4	1.2	0.2	1.0	0.2	0.65	0.95
B#8	37.5	12.2	18.1	3.0	12.3	2.6	1.3	3.0	0.4	2.5	0.5	1.3	0.2	1.2	0.2	0.68	1.36
B#15	72.5	7.7	11.4	1.9	7.8	1.8	1.2	1.7	0.2	1.4	0.3	0.7	0.1	0.7	0.1	0.67	2.19
B#21	102.5	2.5	3.5	0.7	3.1	0.7	1.1	0.7	0.1	0.5	0.1	0.3	0.0	0.3	0.0	0.61	4.89
B#25	122.5	1.1	1.6	0.4	1.8	0.5	1.4	0.4	0.0	0.3	0.0	0.1	0.0	0.1	0.0	0.61	9.61
B#25	157.5	5.0	6.5	1.2	5.5	1.2	0.9	1.2	0.2	1.0	0.2	0.5	0.1	0.5	0.1	0.58	2.31
*TAG pore fluid 2900-5		-	2.1	-	1.0	0.20	0.18	0.36	-	0.47	-	0.47	-	0.76	0.16	5.0	2.0
*TAG pore fluid 2900-8		-	10.2	-	4.6	0.93	0.61	1.62	-	1.72	-	1.39	-	1.11	0.21	4.9	1.5
**Mn-crust 1244 (top)		0.85	0.8	0.16	0.67	0.12	0.04	0.21	0.04	0.32	0.09	0.32	0.04	0.26	0.05	0.47	0.68
**Mn-crust 1244 (base)		1.26	1.9	0.35	1.50	0.35	0.11	0.45	0.09	0.63	0.17	0.56	0.10	0.64	0.12	0.66	0.83

dashes indicate element not reported

* Data from Rudnicki and Mills, (1997); pore fluid from a core from the active TAG mound, recovered near a site of diffuse venting

** Data from Wells, (1999); Mn-crust samples from the low-temperature zone

Table 5.6: REE data for clay phases and corresponding bulk samples from core 43 and selected reference data from the literature.

5.4 Discussion

5.4.1 REE composition of the bulk sediments

Hydrothermal precipitates acquire their initial REE pattern during the precipitation of primary mineral phases from hydrothermal fluids. The concentration of REEs in pristine sulphides from the active TAG mound is typically in the range of 1 to 10 ppb Nd (Mills and Elderfield, 1995a). All samples analysed here have REE concentrations that exceed published values for pristine sulphide phases by three to four orders of magnitude. This indicates that the REE composition of these sediments, including the sulphide layers, is strongly influenced by scavenging from seawater and diagenesis (Ruhlin and Owen, 1986; Mills and Elderfield, 1995a).

The concentrations of REEs in the carbonate cap are similar to concentrations previously measured in plume-derived sediments from TAG (German *et al.*, 1993; Mills *et al.*, 1993). A further indicator for the origin of the Fe-oxyhydroxides from plume fall out is their characteristic REE/Fe ratio. This is demonstrated in Figure 5.6, which shows the down-core relationship for a selection of REE/Fe ratios. Also plotted is the range in values for plume-derived TAG metalliferous sediments from the southern end of the *Alvin* zone (Mills *et al.*, 1993) ('Metz core', see Chapter 3, Figure 3.1) and plume particulates (German *et al.*, 1990). As this plot shows, ratios in the carbonate cap are in good agreement with plume-derived sediments, thus implying a common origin. In both cores, REE/Fe ratios for most REEs are at the lower end of those measured in TAG plume particulates, as is expect for metalliferous sediments from the near-vent field (German *et al.*, 1990). An exception is Ce/Fe, which shows markedly higher range in the sediments compared to the plume particulates. This is believed to reflect the redox-sensitivity of this element, which acts to enhance removal of Ce into the sediments and depletion in seawater relative to the trivalent REEs (Elderfield, 1988). Ratios in the other three layers are markedly lower and more similar to previously observed ratios for mass-flow events (Mills *et al.*, 1993), with ratios in the sulphide layers being the lowest.

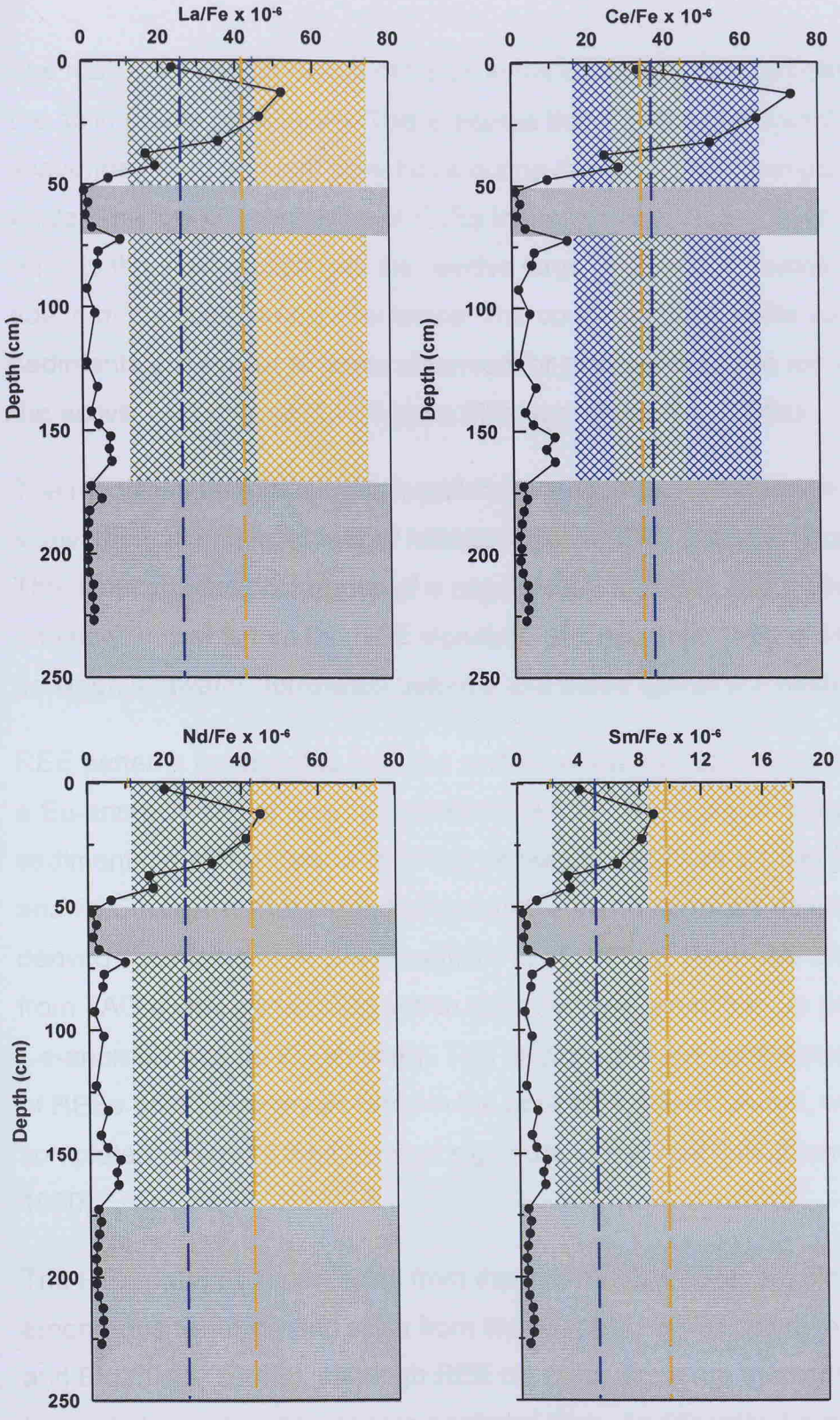

Figure 5.6:Down-core variation in (a) La/Fe, (b) Ce/Fe, (c) Na/Fe and (d) Sm/Fe. Ratios are calculated as molar ratios x10^{-6}. Dashed yellow lines are average plume particulate ratios (German *et al*, 1990), yellow shaded areas indicate range of values. Dashed blue lines are average ratios for plume-derived sediments (Mills *et al*, 1993), blue shaded areas indicate range of values. Shaded green areas indicate where plume particulates and sediments overlap, grey shaded areas mark the sulphide layers.

The maximum concentration of REEs in the carbonate cap correlates well with the solid-phase peak in Mn. This indicates that REEs are efficiently scavenged from ambient pore-fluids during the diagenetic precipitation of Mn-oxide. The low concentration of REEs in the sulphide layers, in contrast, reflects the incompatibility of the relative large REE with the small lattice space of the sulphide-mineral lattice. The concentrations in the sulphide sediments are similar to those observed for oxidised sulphide minerals from the active TAG mound (1 to 4 ppm; Mills and Elderfield, 1995a).

The modification and overprinting of the original REE composition by seawater scavenging is further reflected in their REE patterns (Figure 5.5). The simultaneous occurrence of a negative Ce-anomaly and a positive Eu-anomaly indicates that the REE signature of these sediments is intermediate between seawater-dominated patterns and those typical of massive sulphides.

REE patterns for samples from the surface of the carbonate cap do not show a Eu-anomaly and closely resemble those from the background core. The sediments from the lower part of the carbonate cap have a small Eu-anomaly, and REE patterns that are indistinguishable from previously described plume-derived sediments from this area (Mills *et al.*, 1993). These are distinguished from TAG plume particulates which typically have a much more pronounced Ce-anomaly and no Eu-anomaly. This emphasises the continuous scavenging of REEs onto Fe-oxyhydroxides in the neutrally buoyant plume, which acts to completely overprint the chemical signature of the vent fluid (German *et al.*, 1990).

The REE patterns for samples from the intermediate layer are similar to amorphous Fe-oxide and silica from the periphery of the active mound (Mills and Elderfield, 1995a), although REE concentrations are markedly higher in the metalliferous sediment core analysed here. Additionally, Fe-oxysilicates from core 43 all have a negative Ce anomaly, which is absent in the mound samples and indicates increased seawater influence.

TAG mound sulphides typically have patterns that resemble vents fluids though with a reduced Eu anomaly and a relative HREE enrichment (Mills and Elderfield, 1995a). The variety in patterns that is observed reflects fluid evolution during circulation within the mound. The most notable difference between sulphides from black and white smokers is the elevated Eu-anomaly, which is markedly increased in samples from white smoker chimneys (Mills and Elderfield, 1995a). This pattern mirrors the continual increase in the Eu anomaly of hydrothermal fluids as it precipitates anhydrite in the mound interior (Humphris, 1998). The REE patterns for both sulphide layers match those for the oxidised sulphide samples from inactive black smoker chimneys and chimney debris from the active mound (Mills and Elderfield, 1995a). This suggests that the sulphide minerals in the metalliferous sediment core originate from slumped sulphide chimney debris.

5.4.1.1 Cerium fractionation – the hydrogenous signature

The relatively narrow range in Ce/Ce* as it is shown in Figure 5.7, indicates that the various REE bearing phases were precipitated from a fluid with constant proportions of seawater and high temperature hydrothermal fluid. Similar values have been reported for plume-derived metalliferous sediments from the *Alvin* zone (Ce/Ce* = 0.4-0.7; Mills *et al.*, 1993). Slightly higher values of 0.8 –1.0 were found in a Mn-rich sediment core from the southeast flank of the active TAG mound (Goulding *et al.*, 1998), which is indicative of precipitation of mineral phases mostly from low temperature fluids with only little plume input.

Kuhn *et al.* (1998) introduced the concept of Ce-excess as a new parameter to quantify the degree of de-coupling of Ce from the trivalent REEs during growth of hydrogenous Fe-Mn crusts and sediments. It is a measure of the relative size of the Ce-anomaly compared with that in seawater, and it is defined as:

$$Ce_{xs} = Ce_{SED} - \left[\frac{Ce_{SW} * Nd_{SED}}{Nd_{SW}}\right], \qquad (5.3)$$

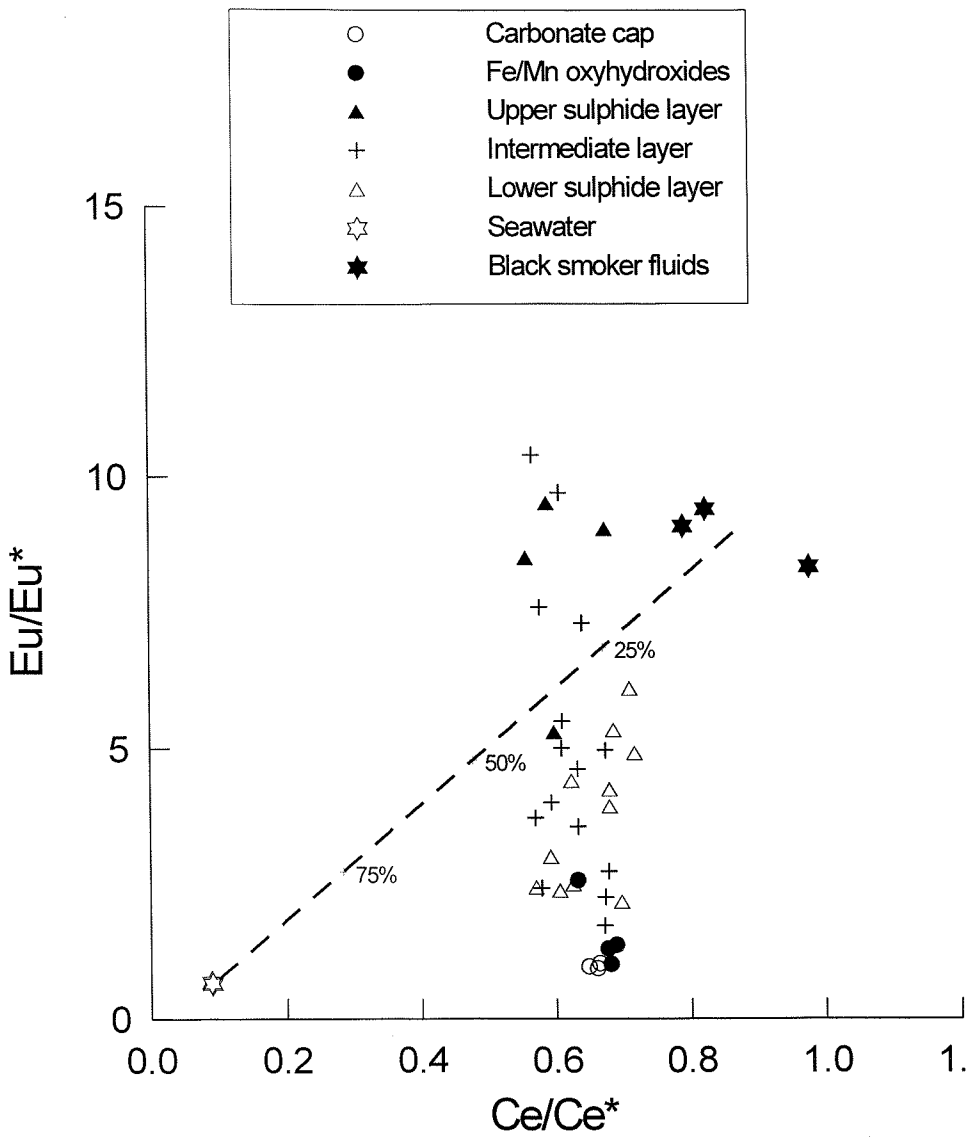

Figure 5.7: Relationship between Eu-anomaly and Ce-anomaly for core 43. The dashed line represents incremental mixing of TAG black smoker fluids with seawater, and numbers indicate proportion of seawater (data from Mitra *et al.,* 1994 and Douville *et al.*, 1999).

where Ce_{SW} and Nd_{SW} are the concentration of the respective REE in local seawater, and Ce_{SED} and Nd_{SED} are the concentration of the same REE in the solid phase. Kuhn *et al.* (1998) used Pr concentrations in their calculations, but Nd is used instead in this study. Although the values will be slightly different, this should not affect the general conclusion from these data because there is no significant fractionation between Pr and Nd. The advantage of using of Nd, however, is that Ce_{xs} may be calculated from published seawater-data where Pr concentrations are not available.

The results are shown in Figure 5.8, were Ce-excess, expressed as Ce_{xs}/Ce_{bulk}, is plotted against Ce_{bulk} (which is the total Ce content, Ce_{SED} above). Minimum values for Ce_{xs}/Ce_{bulk} indicate little or no oxidative uptake of Ce^{4+}. With continuous exposure of the sediments to seawater, Ce^{4+} would eventually become the dominant Ce-species in the mineral phase with maximum Ce_{xs}/Ce_{bulk}-values close to unity. The Ce_{xs} in minerals and sediments thus provides a time-integrated record of their exposure to seawater.

As expected, core 43 shows the highest Ce_{xs}/Ce_{bulk}-values in the carbonate cap, reflecting the significant proportion of hydrogenous precipitates. Values of 0.84 are very similar to those measured for the background core, which contains of about 80% carbonate ooze. All other samples down-core show an increasing hydrothermal signature. If all three hydrothermally derived layers have experienced the same extent of seawater-exposure, it might be expected that they show a similar signature with respect to post-depositional Ce^{4+}-uptake. The absence of significant carbonate or detrital material above the lower sulphide layer suggests that this layer was buried relatively rapidly before any pelagically derived material could accumulate. Higher Ce_{XS} values may be expected in the upper sulphide layer because of its relative proximity to the sediment-water interface compared with the buried, lower sulphide layer.

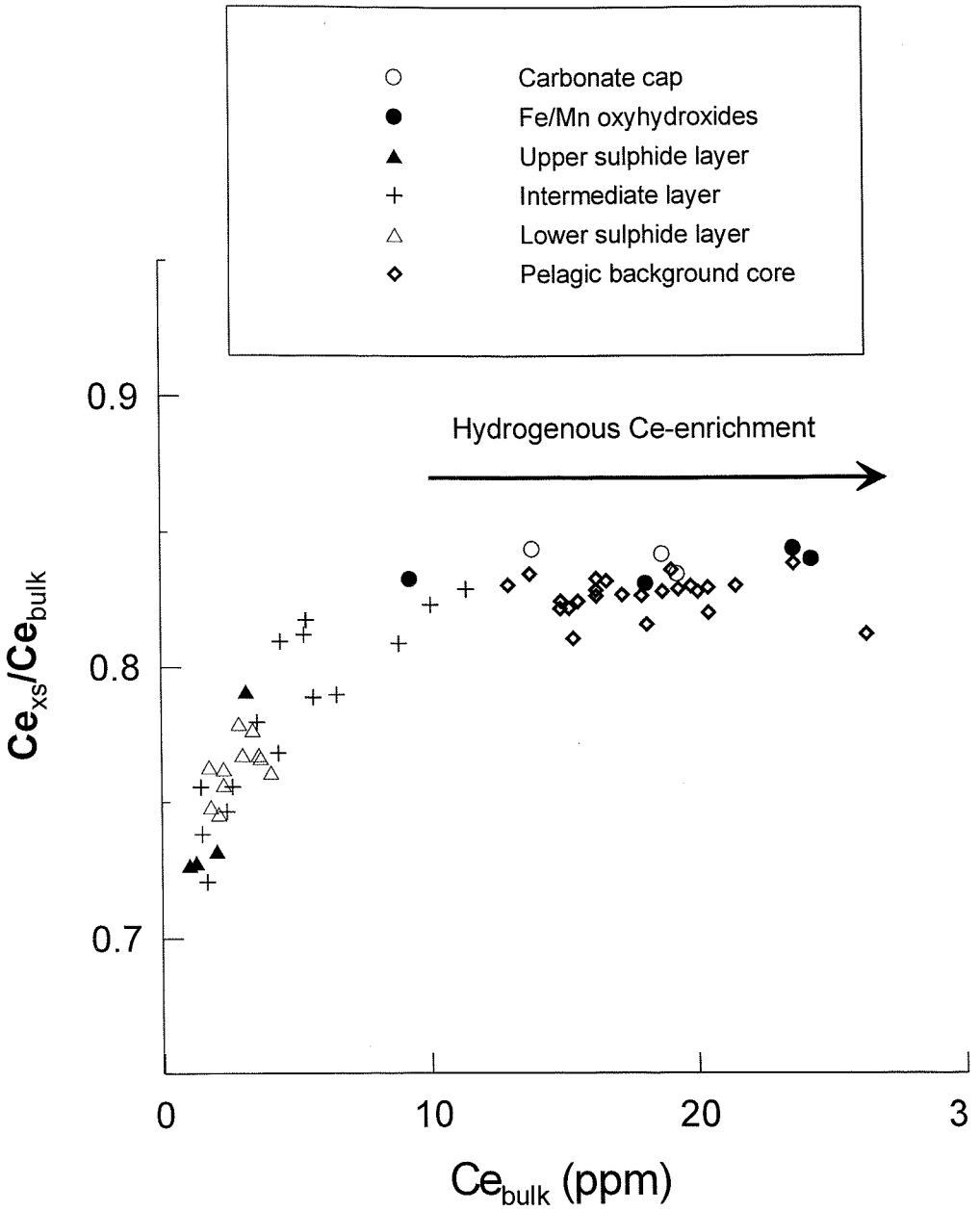

Figure 5.8: Plot of seawater scavenged Ce-excess, expresses as Ce_{xs}/Ce_{bulk}, versus bulk Ce concentration for cores 43 and the pelagic background core 10. For calculations of Ce_{xs} see text. The arrow indicates enrichment in sedimentary Ce due to oxidative scavenging from seawater.

As it can be seen in Figure 5.8, this is not the case. Values of Ce_{xs}/Ce_{bulk} for the two sulphide layers and the intermediate layer cover a relatively broad range from 0.72 to 0.83 with the lowest values in the upper sulphide layer. This may be indication that the upper sulphide layer contains less excess Ce because of its shorter exposure to seawater, possible related to its younger age. More likely, the apparently lower uptake of Ce^{4+} is believed to reflect the diagenetic alteration of the sediments at this depth, as indicated by the re-mobilisation of various trace-metals such as Zn, Cu, Co, Au and Ag. The redox-transition from Ce^{4+} to Ce^{3+} occurs at a similar E_h to the transition from Mn^{4+} to Mn^{2+} (Turner and Whitfield, 1979). A reduction in pH and E_h could cause a change in the proportion of Ce^{4+} to Ce^{3+} in the pore-fluids in favour of the trivalent form. This would reduce the degree of preferential Ce scavenging compared with the trivalent REEs and explain the markedly lower values for Ce_{xs} in the upper sulphide layer

5.4.1.2 Europium fractionation and LREE enrichment – evidence for low-temperature alteration

The occurrence of a positive Eu-anomaly in almost all of the samples from core 43 is a clear testament to a large hydrothermal component in these sediments. Metalliferous sediments acquire their REE signature initially during the precipitation of primary mineral phases from the hydrothermal fluids, as well as from plume-fallout from the neutrally buoyant plume (German *et al.*, 1993; Mills *et al.*, 1993). Exposure of the precipitates on the seafloor and continuous scavenging of REEs from seawater will lead to a gradual reduction of the Eu-anomaly. The persistence of the Eu-anomaly, despite exposure of the sediments to bottom water over several thousands of years, reflects the much higher concentration of REEs in the hydrothermal fluids compared with seawater. The lowest Eu-anomalies were found in the carbonate cap, which is composed of up to 66% of biogenic $CaCO_3$, but even here Eu/Eu* values are still significantly higher than those measured in the background core.

The Eu-anomaly for a number of samples from the upper sulphide layer and the intermediate layer plot markedly above the mixing line defined for

conservative mixing of end-member hydrothermal fluids with seawater. Two of the samples even exceed that of the black smoker fluid endmember (Eu/Eu* = 9.4; Douville *et al.*, 1999). As it was pointed out above, the fractionation of Eu from the remaining REEs is governed by its redox-chemistry. Unlike Ce, however, the redox-controlled fractionation of Eu is very much temperature dependant and is restricted to temperatures above ~230°C (Sverjensky, 1984). It is therefore inconceivable that seawater scavenging or diagenetic alteration at seafloor temperatures could have produced the observed Eu enrichment.

Considerable Eu fractionation, with Eu enrichment significantly exceeding black smoker fluids, is frequently observed in minerals and hydrothermal fluids of the active TAG mound (Gillis *et al.*, 1990; Mills and Elderfield, 1995a; James and Elderfield, 1996a). The modification of REE patterns in these phases is associated with the precipitation of large volumes of anhydrite within the mound (Mills and Elderfield, 1995a; Humphris, 1998). Subsequent dissolution of the anhydrite phases at temperatures <150°C imparts the trapped REEs into solution thus modifying the REE pattern of the ore-forming fluids (James and Elderfield, 1996a). The observed Eu enrichment in samples from core 43 suggests that these minerals were precipitated from or have been altered by an evolved fluid that has been affected by anhydrite precipitation. The fact that samples from both the intermediate layer and the sulphide layer show a similar degree of Eu enrichment might suggest that this pattern was acquired *in situ* from evolved fluids percolating through the sediment pile.

In addition to a markedly increased Eu-anomaly, evolved fluids from the mound interior are also enriched in Zn, which is released during the dissolution of primary sphalerite (Edmond *et al.*, 1995; Tivey *et al.*, 1995). It may therefore be assumed that any mineral-phase that has been in contact with the evolved fluid, as indicated by the increased Eu-anomaly, would also display an increased Zn content. As it can be seen in Figure 5.9, where the two parameters are plotted against each other, no such straight-forward relationship has been observed in this core. This lack of correlation is believed

to reflect the diagenetic mobilisation of Zn, which has been released from primary sulphide phases in the upper sulphide layer to be re-precipitated in the intermediate layer.

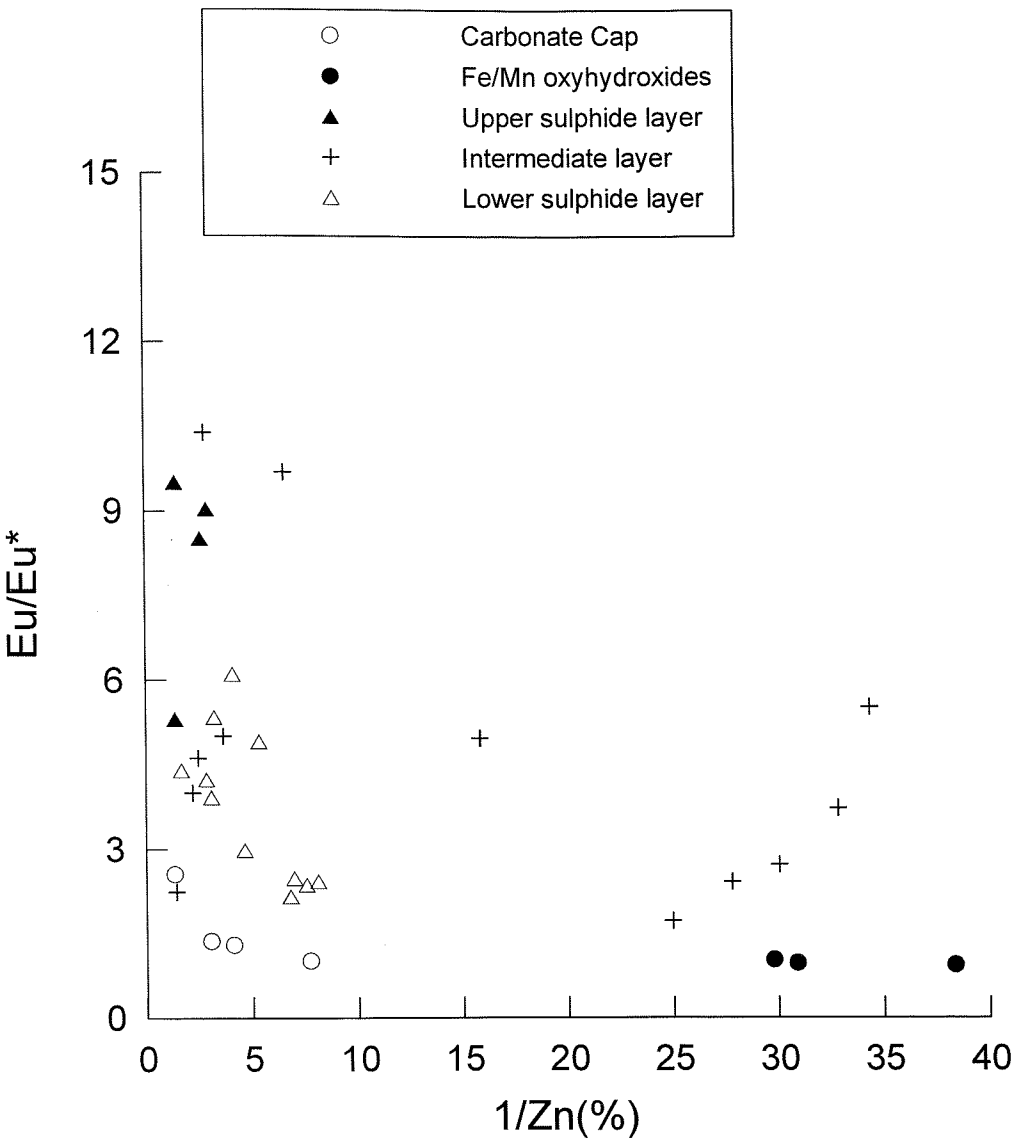

Figure 5.9: Relationship between Eu anomaly and Zn content in core 43. The lack of correlation reflects the diagenetic mobilisation of Zn during post-depositional re-mineralisation.

The extent of fluid evolution is further reflected in the fractionation of LREE from HREE. Humphris (1998b) demonstrated that during the precipitation of anhydrite the LREE are being excluded relative to the HREE. Consequently, LREE are enriched in the evolved fluid. Figure 5.10 illustrates the extent of LREE enrichment, expressed here as Yb_n/La_n, and the alteration of the sediments in core 43 by diffuse fluids. Two groups of samples can be clearly distinguished in samples from core 43. The first group includes all samples from the lower sulphide layer plus one sample from the top of the upper sulphide layer, which have relatively low Si concentration and no LREE enrichment. The second group includes all remaining samples from the upper sulphide layer, the intermediate layer and Fe/Mn-oxyhydroxides from the carbonate cap. These samples are relatively LREE enriched when compared to the lower sulphide layer, which coincides with markedly elevated Si concentrations. The three uppermost samples from the carbonate cap with relatively low Si concentrations are excluded from this group since the LREE enrichment is more likely to reflect of hydrogenous mineral formation.

It has been demonstrated that diffuse fluids from the active TAG mound are depleted in Si relative to black smoker fluids (James and Elderfield, 1996a). This is due to the precipitation of silica, together with anhydrite, in the mound interior. In order to precipitate silica from a hydrothermal fluid, some degree of conductive cooling is required (Janecky and Seyfried, 1984). At the moment no low temperature fluid has been sampled that could explain a simultaneous LREE enrichment and silica precipitation. The observed pattern suggests, however, that the samples from the intermediate layer and most samples from the upper sulphide layer have been overprinted by scavenging from a low-temperature fluid with an evolved REE signature. The lower sulphide layer in contrast is relatively un-altered, as it is also reflected in lack of diagenetic re-mineralisation (see Chapter 4).

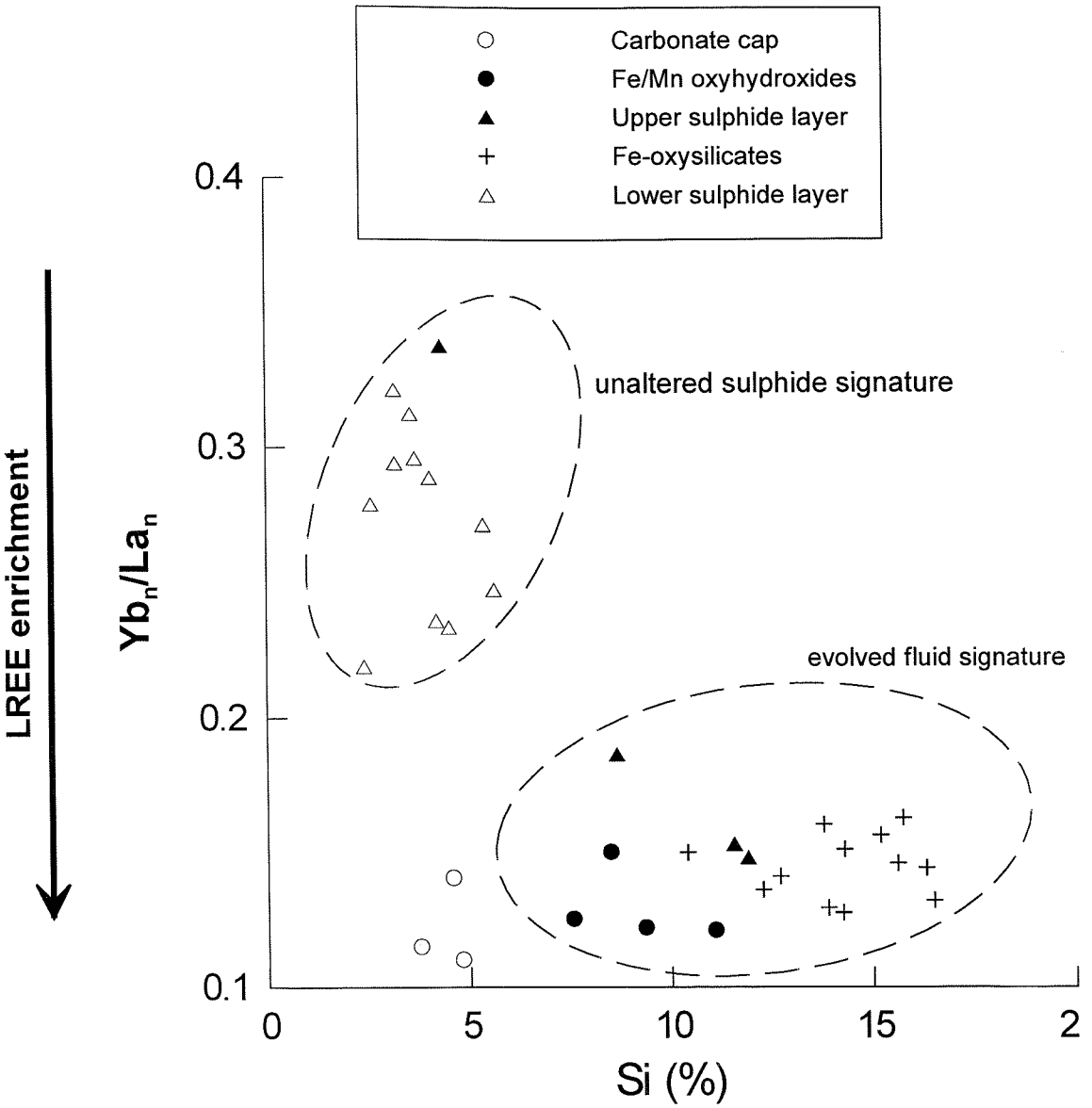

Figure 5.10: Relationship of Si concentration and LREE/HREE fractionation in core 43. The two distinct group represent samples from the upper sulphide layer (except one) and intermediate layer that have undergone low-temperature alteration, and samples from the lower sulphide layer that have not been affected by low-temperature fluid alteration.

5.4.2 *The origin of the intermediate layer – clues from hydrothermal clays*

Chemical and physical separation of the <2 μm fraction from bulk sediments of the intermediate layer have shown that nontronites form a significant proportion of these deposits, thus confirming that they constitute an important component of ridge-crest metalliferous deposits (Thompson *et al.*, 1985). The composition of the nontronites described here is similar to other seafloor nontronites (Table 5.7). Previous studies have also identified the presence of clay minerals other than smectite in metalliferous deposits (Alt and Jiang, 1991). In a core from the southern periphery of the active TAG mound Goulding *et al.* (1998) found a significant clay-rich layer that contained abundant kaolinite and illite. XRD analysis for clay separates from core 43 has shown that only trace amounts of detrital kaolinite are present in the carbonate cap.

Table 5.7 presents comparative chemistry and structural formula for authigenic nontronites and Fe-montmorillonites. The overall agreement with previously reported data is good. The complete absence of Al from the tetrahedral layer, as seen in sample #25, is unusual. Similar Al-free nontronites have, however, been described in sediments from the active TAG mound (Gwynn, 1998).

Fe_2O_3/SiO_2 ratios for the nontronites from the intermediate layer show a narrow range between 0.64 and 0.77, which compares well with other nontronites (0.57 – 0.86; Alt, 1988b; Corliss *et al.*, 1978; Malahoff *et al.*, 1982; McMurtry *et al.*, 1983; Murnane and Clague, 1983; Alt, 1988b; Gwynn, 1998). Interlayers in these samples are occupied by Na^+ (0.21 to 0.85) with only minor K^+ (0.04 to 0.14). These values are within the range of reported values for hydrothermal nontronites (Na^+: 0.05-0.97, K^+: 0.01-0.68; Table 5.7). The relatively low K^+ content indicates the absence of significant illite layers (Weaver, 1989). The interlayer Ca^{2+} content of 1.5 for samples the two carbonate cap samples #5 and #8 is markedly higher than other reported data for pelagic-ooze smectite (0.07–0.23; McMurtry and Yeh, 1981). The excess layer and interlayer charges of 3.5-3.9 for these two samples is also

significantly higher than previously reported values (<1.64; McMurtry and Yeh, 1981).

	TAG *Alvin* zone (1)	TAG mound (2)	Galapago mounds (3)	Galapago mounds (4)	Red Seamount (5)	JdFR (6)	Loihi Seamount (7)	Atlantis I Deep (8)	Bauer Basin (9)	EPR 6°S (9)	Galapago mounds (3)	NE Equat. Pacific (10)
	nontronite								Fe-montmorillonite			
wt%												
SiO_2	44.25	54.41	52.80	47.06	47.60	46.70	50.20	36.60	56.47	69.95	60.00	51.29
TiO_2	0.11	0.01	0.10	-	0.02	0.02	0.30	-	-	-	0.39	1.00
Al_2O_3	1.68	-	1.06	0.18	0.24	0.32	2.40	2.45	6.80	1.57	11.43	7.45
Fe_2O_3	28.24	40.20	27.36	36.36	32.30	33.30	31.90	31.62	10.48	8.02	7.39	14.65
MnO	0.02	0.02	0.32	0.31	0.02	0.40	0.02	0.45	-	-	0.26	0.08
MgO	5.34	2.38	3.13	2.44	2.27	2.80	2.30	1.26	2.42	1.97	2.73	4.21
CaO	0.06	2.16	0.78	0.74	0.10	0.40	0.70	0.43	0.90	0.31	2.55	0.47
Na_2O	2.47	-	0.16	1.54	2.66	1.00	0.20	2.71	1.56	1.23	0.41	1.27
K_2O	0.66	0.06	2.43	1.78	2.89	3.40	0.60	0.78	0.72	0.17	0.93	0.65
P_2O_5	1.25	0.88	-	-	0.06	0.04	-	-	-	-	-	-
FeO					3.5	0.4						
formation temperature		58-92	25-47	-	30	57	31	-	30-50	30-50	27-39	-
Tetrahedral layer												
Si^{4+}	7.26	7.48	7.96	7.33	7.33	7.33	7.58	6.76	7.39	7.92	7.99	7.93
Al^{3+}	0.32	0.00	0.04	0.03	0.04	0.06	0.42	0.53	0.61	0.08	0.01	0.07
Fe^{3+}	0.42	0.52		0.64	0.63	0.62	0	0.71	0	0	0	0
Total	8.00	8.00	8.00	8.00	8.00	8.00	8.00	8.00	8.00	8.00	8.00	8.00
Octahedral layer												
Fe^{3+}	3.06	3.63	3.10	3.57	3.56	3.31	3.62	3.69	1.88	2.27	0.90	1.71
Fe^{2+}	0	0	0	0	0	0.05	0	0	0	0	0	0
Al^{3+}	1.30	0	0.15	0	0	0.00	0.00	0	1.29	0.62	2.17	1.29
Mg^{2+}	0	0.49	0.70	0.43	0.52	0.66	0.35	0.31	0.86	1.11	0.66	0.97
Mn^{2+}	0	0	0	0	0	0	0	0	0	0	0	0
Ti^{4+}	0	0	0.01	0	0	0	0.03	0	0	0	0.05	0.12
Total	4.37	4.12	3.96	4.00	4.08	4.03	4.00	4.00	4.03	4.00	3.78	4.09
Interlayer												
Ca^{2+}	0.01	0.32	0.13	0.12	0.02	0.26	0.11	0.09	0.23	0.11	0.44	0.08
Na^{+}	0.78		0.05	0.14	0.79	0.30	0.04	0.97	0.72	0.91	0.13	0.38
K^{+}	0.14	0.01	0.47	0.35	0.57	0.68	0.12	0.18	0.22	0.09	0.19	0.13
Mg^{2+}	0	0	0	0.13	0	0	0.17	0.04	0	0	0	0
Mn^{2+}	0	0	0.04	0.04	0	0	0	0.07	0	0	0.04	0.01
Total	0.93	0.33	0.69	0.78	1.38	1.24	0.44	1.35	1.17	1.11	0.80	0.60
Interlayer charge	0.95	0.65	0.86	1.10	1.39	1.12	0.72	1.55	1.38	1.19	1.28	0.65
Layer charge	0.95	0.65	0.85	1.07	0.96	1.30	0.74	1.55	1.40	1 22	1.28	0.69

(1) Data from this study, <2µm sample #15
(2) Data from Gwynn, 1998 (formation temperature from R.A. Mills, pers. comm. 1999); <2µm CBD treated
(3) Data from McMurtry *et al.*, 1983; average of six samples
(4) Data from Corliss *et al.*, 1978; average of three samples
(5) Data from Alt, 1988; <2µm CBD treated
(6) Data from Murnane and Clague 1983
(7) Data from Malahoff *et al.* 1982
(8) Data from Bischoff. 1972; average of four samples
(9) Data from McMurtry and Yeh, 1981; <2µm CBD treated
(10) Data from Aoki *et al.* 1974; <2µm chemically treated to remove carbonate and Fe-oxide

Table 5.7: Comparative chemistry and structural formula for hydrothermal nontonites and Fe-montmorillonites from the literature.

No oxygen isotope measurements were obtained for nontronites in this study. However, the striking similarity in mineralogy and chemical composition with previously reported data (Table 5.7), namely their purity and monomineralic character, implies a similar mode of formation. Poorly crystalline Fe-oxyhydroxides have been suggested as precursors of nontronites. Sorption of silica from low temperature hydrothermal fluids onto the Fe-oxyhydroxides under reducing conditions could lead to the formation of nontronites below the sediment-water interface (Dymond *et al.*, 1980; Singer and Stoffers, 1987).

Nontronite deposits are often associated with Mn-oxides, where the Mn layer overlies the nontronite and is often in contact with seawater (Dymond *et al.*, 1980; Murnane and Clague, 1983; Singer *et al.*, 1984). Dymond *et al.* (1980) suggested that the Mn phases precipitate along an advancing oxidation-reduction gradient, and nontronite or amorphous phases precipitate below this redox-boundary. In core 43, a sharp peak of solid phase Mn is observed at 30 cm depth. Similar Mn-peaks are common to all metalliferous sediment cores studied from the TAG area (Shearme *et al.*, 1983; Metz and Trefry, 1988; Goulding *et al.*, 1998). The source of the Mn-peak in core 43, which marks the current locus of the redox-boundary, is Mn-oxide that has been mobilised by reducing hydrothermal fluids at depth, thus producing a vertical segregation of Fe and Mn. In addition to Mn-oxides in the sediments, the hydrothermal fluid itself may have contained appreciable amounts of dissolved Mn which precipitated at the redox-boundary in the carbonate cap.

5.4.2.1 Replacement of pre-existing sediments

Alternatively to the formation of nontronite from precursor Fe-oxide, the clays in the intermediate layer of core 43 could have formed as low-temperature diagenetic products of massive sulphides, as suggested by Malahoff *et al.* (1982), or as replacement of pelagic ooze as suggested by Honnorez *et al.* (1981). Rare sulphide fragments and foraminiferal remains have been found in this layer. The replacement of sulphides would require their initial complete oxidation before the Fe-oxides are converted to nontronite. Because of the substantial thickness of the intermediate layer of 100 cm this seems unlikely.

The sharp contact between the Fe-oxysilicates of the intermediate layer and both sulphide layers is in conflict with the gradual alteration of pre-existing massive sulphides by a reactive fluid. The low concentration of chalcophile metals (Cu, Zn) in the clays (Table 5.4) further argues against a replacement of sulphides. Similarly, the replacement of pelagic ooze would require complete removal of all carbonate. The low concentration of Ca and Al in the clays from the intermediate layer indicates that carbonate and detrital clay concentrations in the intermediate layer were low.

The distinctly different chemistry of the clays from the carbonate cap, namely the higher Al and Ca content and the lower content of Si, suggests that they were formed through intimate interaction between sediments with a significant pelagic component and low temperature fluids. The source of Al may be detrital clay, as indicated by the residual kaolinite, or Al-rich volcanic detritus. The relatively higher proportion of amorphous phases and lower clay content compared with the intermediate layer may reflect a higher proportion of relatively oxidising seawater in the low temperature fluid from which the clays precipitated (De Carlo *et al.*, 1983).

Increased silica concentrations were also observed in the upper sulphide layers (mean: 9.1 %), compared with the lower sulphide layer (mean: 3.9%). This suggests that the circulation of low temperature hydrothermal fluids did continue after deposition of the upper sulphide layer on top of the Fe-oxysilicates through mass wasting. It was shown in Chapter 4 that diagenetic alteration has caused substantial re-mineralisation in the upper sulphide layer, whereas the lower sulphide layer is relatively unaffected. One possible mechanism for the metal-mobilisation is the oxidation of pyrite by oxygenated seawater. Alternatively it may be speculated that the low temperature hydrothermal fluids, which impose reducing conditions and hence lead to the precipitation of nontronites in the intermediate layer, also contributed to the leaching of the sulphide minerals in the upper sulphide layer. The relatively high concentration of 0.8 % Zn in the clay phase for sample #15 from just below the upper sulphide layer corresponds well with the diagenetic enrichment at this depth. It appears that Zn, which has been released from

primary sphalerite, has been incorporated into the clay lattice. This implies that mobilisation of Zn from the upper sulphide layer and precipitation of nontronite directly below this layer occurred simultaneously.

5.4.2.2 Timing and location of clay mineral formation

Hydrothermal clays have frequently been found at considerable distance from known sites of high temperature venting. It has therefore been argued that because circulation of hydrothermal fluids would be restricted to the immediate vicinity of the vent sites, distal Fe-oxide and nontronite deposits were transported by bottom currents rather than formed in situ (Aoki *et al.*, 1974; Heath and Dymond, 1977; Dymond and Eklund, 1978; McMurtry *et al.*, 1983). Most authors agree that nontronites form as precipitates from hydrothermal fluids, and this conclusion is based primarily on formation temperatures for most hydrothermal nontronites between 20 and 60°C, as derived from oxygen-isotope geothermometry (see Table 5.7) (McMurtry and Yeh, 1981; De Carlo *et al.*, 1983; McMurtry *et al.*, 1983; Murnane and Clague, 1983; Singer *et al.*, 1984; Alt, 1988b). These temperatures are appreciably higher than the normal bottom water temperatures in the deep-sea of 0-2°C, and therefore rule out seafloor diagenetic alteration. McMurtry and Yeh (1981) examined Fe-rich smectite samples from the East Pacific Rise and the adjacent Bauer Basin, and the formation temperature of 30°C-50°C clearly demonstrates that clay minerals from both sites were formed by hydrothermal processes. Because of the long distance between the smectites in the Bauer Basin and the ridge as their potential source it was concluded that it was the nontronite and not the Fe hydroxide precursor that was transported.

Fine-grained material from the intermediate layer of core 43 produced a marked change in colour from green to dark red within minutes of exposure of the sediments to air. This strongly suggests that nontronites, which demonstrably form under reducing conditions (Harder, 1976), are rather unstable and easily convert to Fe-oxides when exposed to oxygen. Mass wasting and slumping of hydrothermal material, however, would cause especially the fine-grained material to come into contact with large volumes of

oxygenated bottom water and hence cause the nontronites to become oxidised. It may therefore be assumed that the nontronites in core 43 were formed *in situ* rather then transported after formation on the once active *Alvin* mound.

The observed formation temperatures of nontronites from the active TAG mound of 58-92°C are similar to those measured for diffuse low temperature fluids, which are ubiquitous in areas of hydrothermal activity (Schultz *et al.*, 1992). A survey of massive sulphide deposits in the TAG hydrothermal field has revealed that warm fluids with temperatures of 22.5°C are currently being issued from a sulphide-mound in the apparently inactive *Alvin* zone (Rona *et al.*, 1998). The recent discovery of warm springs on 3.5 Ma old crust near the Juan de Fuca Ridge (Mottl *et al.*, 1998), venting chemically altered seawater at 25°C, further emphasises the ubiquitous nature of low temperature hydrothermal fluids even at great distance from sites of high temperature venting.

5.4.2.3 The case for a biogenic origin of the nontronites

Filamentous microstructures have frequently been observed in association with Fe-oxide deposits (Ghiorse, 1984; Juniper and Fouquet, 1988). Alt (1988b) suggested that bacterial activity may have been associated with nontronite formation through microbial catalysation of Fe-oxidation. Similarly, Juniper and Fouquet (1988) proposed that Fe-oxysilicate deposits from various modern and ancient hydrothermal sites formed around filamentous microbial mats through which hydrothermal fluids diffuse. Köhler *et al.* (1994) suggest that chemolithotrophic Fe-oxidising bacteria had been involved in formation of white smoker nontronites from the Galapagos Rift by locally stabilising the redox-conditions. Filamentous structures have also been identified in sediments from the intermediate layer of core 43 (Figures 5.11 (a) to (d)), and similar structures have previously been interpreted to be of microbial origin (Juniper and Tebo, 1995, Fortin *et al.*, 1998). Additionally, incubation experiments on sediments from a core that was recovered in the immediate vicinity of core 43 have demonstrated the presence of Fe-oxidising

bacteria (a more detailed discussion of the microbiology of these deposits is provided in Chapter 6).

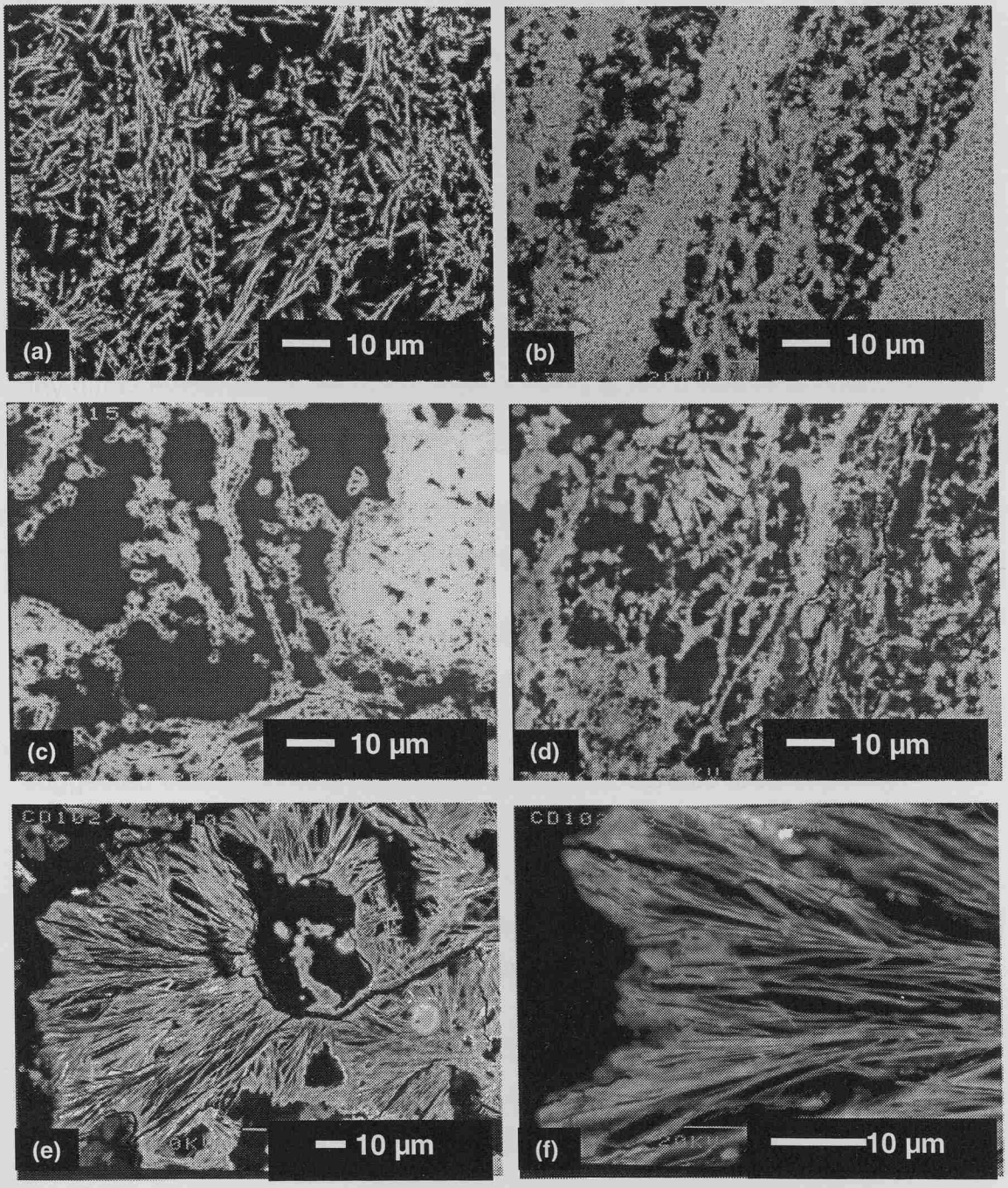

Figure 5.11: SEM images of filamentous structure in sediments from the intermediate layer of core 43, that might be interpreted to be of bacterial origin (a to d), and an example of iron-oxysilicate dendrites that have been formed through self-organisation from an amorphous silica gel (e and f).

However, Jannasch and Wirsen (1981) cautioned against indiscriminately attributing metal accumulation on apparently bacterial filaments to direct or indirect microbial intervention. Non-specific metal deposition is extremely common in hydrothermal deposit and the recognition of bacterial structures purely based on their morphology is questionable. Hopkinson *et al.* (1998) have demonstrated how patterns of iron-oxysilicates that resemble biogenic structures but have no biogenic origin can be produced from an amorphous silica gel through the process of inorganic self-organisation. Figure 5.11 (e) and (f) shows an example of dendritic Fe-oxysilicate from the intermediate layer that are interpreted here to be the result of competitive particle growth as they occur in supersaturation-nucleation-depletion cycles (Ostwald Liesegang cycles; Ortoleva *et al.*, 1987). In view of these findings and in the absence of any direct evidence for microbial intervention it is not possible to unequivocally confirm a biogenic origin of these deposits.

5.4.2.4 The origin and chemistry of low temperature hydrothermal fluids – evidence from REE composition of nontronites

The markedly higher concentration of REEs in samples #5 and #8 from the carbonate cap compared with the clay phases from the intermediate layer (Table 5.6) may be a function of their degree of crystallisation. Alt (1988b) suggested that the smaller grain size and higher surface area of poorly crystallised mineral phases could account for their higher concentration of REEs as well as P. XRD traces for clay phases indicate that sample #5 from the carbonate cap is less well crystallised compared to the remaining samples, thus explaining its markedly higher REE concentration.

Most previous studies of REEs in authigenic nontronites have concluded that the REEs are consistent with a seawater source, as indicated by their negative Ce-anomaly (Murnane and Clague, 1983; Alt, 1988b). In this study, however, no noticeable negative Ce-anomaly was observed in the clay phases. Moreover, Ce/Ce* values in the clays were close to unity, whilst all bulk samples displayed negative Ce-anomalies with Ce/Ce* values of around 0.8 (Table 5.6, Figure 5.12). This implies that Ce/Ce* values in the Fe-oxide

phase were lower than 0.8. Assuming that the clays formed through low temperature alteration of a precursor Fe-oxide, the inference is that the clays gained Ce, possibly through scavenging of Ce^{4+}. Increase in Ce concentration during mineral formation is commonly observed in hydrogenous mineral phases such as Mn-oxide crusts (Piper, 1974; Kuhn *et al.*, 1998). This, however, also requires some increase in total REE concentration, whereas in core 43 REE concentration is markedly less in the clay separates compared with the bulk sediments. Additionally, the reducing conditions that are required for the precipitation of nontronite (Harder, 1976) would mean that Ce occurs predominantly in the trivalent state, thus ruling out preferential scavenging. Consequently, if the nontronites formed by low temperature hydrothermal alteration of Fe-oxides, as it was concluded from the major elemental composition, this implies that the fluid from which they precipitated had only a small seawater component and the existing Fe-oxide phase is not the precursor.

This inference is further supported by the distinct HREE enrichment of the clays compared to the bulk REE data. This is demonstrated in Figure 5.13, where Nd_n/Yb_n is plotted versus Eu/Eu* for both bulk and clay separates, showing the systematic HREE enrichment in all clay samples relative to bulk sediments except sample #5 from the carbonate cap. Because of the relative stability of HREE complexes in seawater, scavenging uptake of REEs from seawater produces a HREE depletion in the solid phase (De Carlo *et al.*, 1983; Cantrell and Byrne, 1987; Elderfield, 1988; Wood, 1990a; Koeppenkastrop and De Carlo, 1992). This has shown to be the case for hydrogenous and plume-derived crusts, which display a marked LREE enrichment (Rudnicki and Elderfield, 1993; Bau and Dulski, 1999). The HREE enrichment in the clay separates from core 43 is therefore incompatible with a seawater source.

In addition to the absence of a Ce-anomaly and the HREE enrichment, the nontronites display a small and systematically decreased positive Eu-anomaly (Figure 5.12). Investigation of diffuse fluids from the active mound has shown

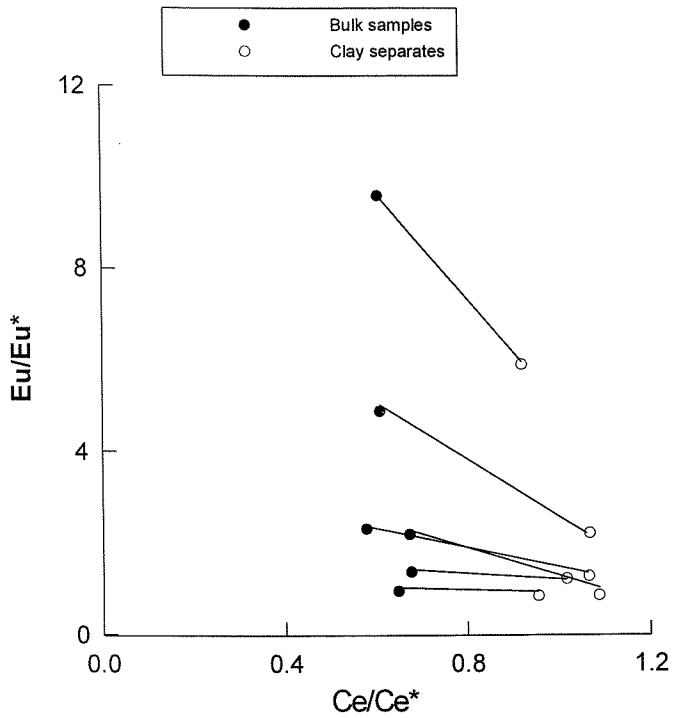

Figure 5.12 : The relationship between Eu/Eu* and Ce/Ce* for bulk sediments and clay phases from core 43, showing the systematically decreased Eu-anomaly and absence of significant Ce-anomalies in the clay phases.

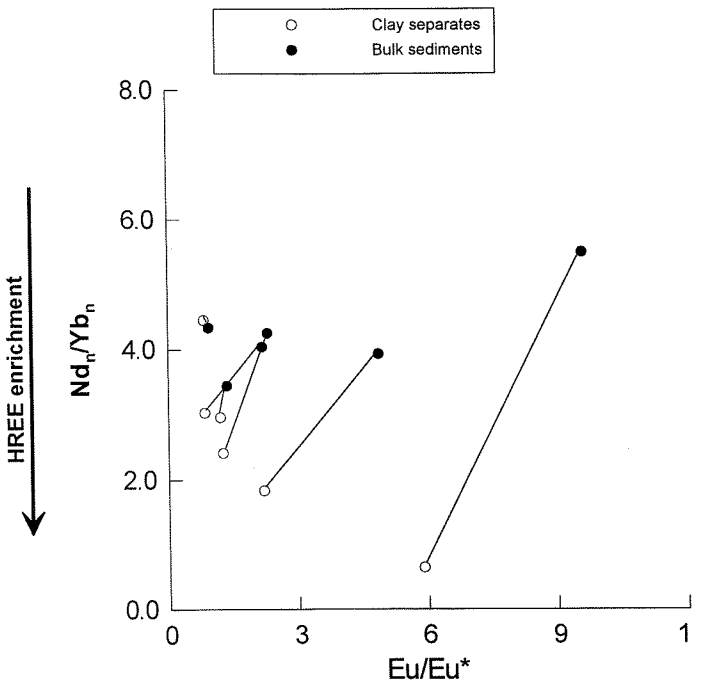

Figure 5.13 : The relationship between Eu-anomaly and Nd_n/Yb_n, showing the systematic HREE enrichment in all clay samples relative to bulk compositions.

that the magnitude of the Eu-anomaly is not simply a function of the degree of mixing between hydrothermal fluids and seawater. Rather it appears that the REE composition of these low-temperature fluids also reflect a range of subsurface mineralisation and dissolution reactions (Mills and Elderfield, 1995a). James and Elderfield (1996a) for example demonstrated how the dissolution of Eu-enriched anhydrite and mixture with seawater and hydrothermal fluid can produce the observed large Eu-anomaly and LREE enrichment. Pore fluids that were collected from a core from the surface of the active mound, in contrast, show a much smaller positive Eu-anomaly together with HREE enrichment (Rudnicki and Mills, 1997). The REE pattern of these pore fluids bears striking resemblance to the REE pattern of the nontronites from the intermediate layer from core 43 (Figure 5.14). Furthermore, similar REE patterns were found in metalliferous oxide crusts from the currently active zone of low temperature venting high on the median valley wall (Wells, 1998). Earlier studies of these Mn-deposits have shown that in addition to birnessite and Fe-oxides, they contain abundant nontronite (Thompson *et al.*, 1985). It is currently not known what mineralisation or alteration process produces the observed REE patterns, but the similarity in patterns of minerals from a number of locations in the TAG hydrothermal field imply that the low temperature deposits precipitate from evolved fluids of similar chemistry.

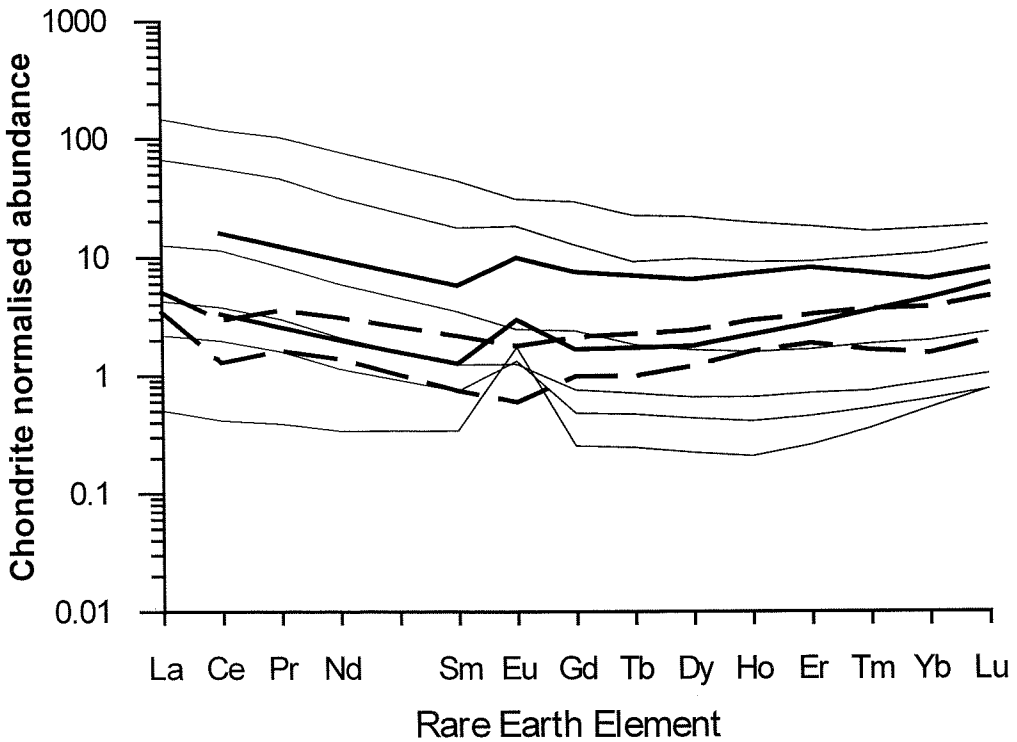

Figure 5.14: Comparison of REE patterns for clay phases from core 43 (thin solid lines) with those for pore fluids from a sediment core from the active TAG mound (dashed lines; Rudnicki and Mills, 1997) and Mn-crusts from the low-temperature zone (thick solid line, Wells, 1998). The core from the TAG mound was recovered in an area were abundant diffuse venting occurred.

5.5 Summary and Conclusions

The REE geochemistry and mineralogy of core 43 from the southern periphery of the *Alvin* zone has been used to elucidate the origin of metalliferous sediments in this area, and the extent and nature of post-depositional alteration. Different modes of deposition are distinguished by their characteristic REE/Fe ratios. The Fe-oxide rich carbonate cap has a relatively high REE/Fe ratio, which closely resembles that of plume-derived deposits. The markedly lower REE/Fe throughout both sulphide layers and the intermediate layer, in contrast, is indicative of much faster deposition as it occurs during slumping of sulphide debris from the mound surface. The lack of admixed detrital and biogenic material in the nontronite-rich intermediate layer can only be explained by rapid deposition of the Fe-oxysilicates.

The excess Ce is used here to differentiate between REE of dominantly hydrogenous origin in the carbonate cap and REEs that are derived from hydrothermal sources in the remainder of the core. The Ce excess provides a time-integrated record of seawater exposure, although some effect of diagenetic overprinting is evident in the upper sulphide layer.

The anomalously high Eu enrichment in samples from the upper sulphide layer and some samples from the intermediate layer is consistent with alteration by an evolved fluid that has been affected by anhydrite dissolution. Scavenging of REEs from Si-rich diffuse fluids with an evolved signature is further demonstrated by the marked LREE enrichment in the intermediate layer and the upper sulphide layer, which correlates with elevated solid phase Si concentrations.

The intermediate layer contains abundant nontronite that is comparable in composition with previously reported data for authigenic, hydrothermal nontronite. This is believed to have formed *in situ* as precipitated from diffuse low temperature fluids. This is confirmed by the distinct REE signature of the clays, with Ce/Ce* values close to unity, relative HREE enrichment and systematically decreased positive Eu anomaly compared to bulk data. These

observations are incompatible with a seawater source for the nontronite formation.

The hypothesis that emerges from this work for the formation and alteration of metalliferous sediments from the southern *Alvin* zone involves rapid deposition of the bulk sediments by slumping from the mound, and over time these were covered by pelagic sediments intermixed with plume-derived precipitates. Post-depositional alteration of the sediments by low-temperature, evolved fluid resulted in precipitation of nontronites in the intermediate layer. Increased Si content in the upper sulphide layer suggests that the observed diagenetic alteration and re-mineralisation, as it was described in Chapter 4, was driven by low-temperature fluids rather than surface seawater.

The nature of diffuse hydrothermal fluids is only poorly characterised, but multiple stages of low-temperature alteration are indicated by LREE of bulk sediments in the upper sulphide layer and intermediate layer in contrast to HREE enrichment of clay phases in the intermediate layer. The lower sulphide layer appears to be unaffected by the inferred low-temperature alteration, as indicated by the relatively low Si content and the absence of HREE enrichment.

Chapter 6

The Geomicrobiology of a Relict Sulphide Deposit: Extending the Boundaries of the Submarine Hydrothermal Ecosystem

6.1 Introduction

It is well established that microbial metabolic activity modifies the chemical and isotopic characteristics of the environment (Ehrlich (1996) and references therein). Similarly, the nature of microbial communities is controlled by a range of physical and chemical parameters such as temperature, pressure, fluid circulation and chemical composition of substrate (Burdige *et al.*, 1992; Parkes *et al.*, 1994; Lovley and Chapelle, 1995; Postma and Jakobsen, 1996; Blochl *et al.*, 1997; Wellsbury *et al.*, 1997). Geomicrobiology is seeking to understand the interaction between biosphere and geosphere on a microbial level. The ubiquitous occurrence of bacteria even under the most extreme conditions (Tuttle *et al.*, 1983; Cragg *et al.*, 1990; Thorseth *et al.*, 1995; Blochl *et al.*, 1997; Grant *et al.*, 1998; Nealson and Conrad, 1999) makes them potentially important catalysts in the geochemical cycling of metals and other metabolites.

The interaction between microbes and metals can be divided into several processes:

1. *Supply of essential trace metals:*

A range of selective trace-metals, including Fe, Zn, Cu, Ni Cr, V, Co, and Mo, are essential for the functioning of the cell, as they are required in basic enzyme activity. Compounds such as siderophores facilitate the concentration and transport of trace metals to the cell if ambient concentrations are low (Jardim and Pearson, 1984; Hausinger, 1987; Reid *et al.*, 1993).

2. *Metabolic suppression:*

At high concentrations most metals, including the above-mentioned essential trace elements, are considered as toxic (Ford and Mitchell, 1992). The inhibition of specific metabolic activities by trace metals is used in experimental controls of bacterial activity. An example is the inhibition of sulphate-reducing bacteria by molybdenum (Oremland and Capone, 1988).

3. *Detoxification:*

A number of microorganism have evolved a whole range of mechanism in order to control transport of metals across the cell wall and aid detoxification (Robinson and Tuovinen, 1984; Wood and Wang, 1985). Some bacteria can enzymatically alter the metals to a less toxic form which can then be accumulated as a means of internal detoxification (Ford and Mitchell, 1992).

4. *Metabolic metal redox-reaction as energy source*

Some microbes are capable of utilising metals directly as an energy source. The coupling of metal reduction to cellular respiration has been discovered only fairly recently (Lovley and Phillips, 1988; Myers and Nealson, 1988), and the study of these processes is still in its infancy (Kostka and Nealson, 1998). Until today, most studies have focussed on the dissimilatory reduction of Fe and Mn, but the metabolic versatility of these microbes is just beginning to be realised (Lovley *et al.*, 1991; Lovley *et al.*, 1993; Lee and Tebo, 1994).

5. *Metal reactions as by-product of other reactions*

Bacterial activity will have an indirect effect on phase-transitions of metals and mineralisation processes by actively driving the chemical conditions of a system. The organism can for example modify its local microenvironment creating conditions suitable for the chemical precipitation of extracellular mineral phases (Lovley, 1990; Bazylinski and Frankel, 1992). Conversely, a large proportion of the reduction and hence dissolution of metal-oxides in shelf sediments is believed to be the result of physiochemical reduction by sulphide, which is the metabolic end product of bacterial sulphate reduction (Pyzik and Sommer, 1981).

6. *Inorganic templating of the bacterial structure*

Another form of biomineralisation is the growth of inorganic particles within or on some organic matrix produced by the organism. Bacteria that produce mineral phases by this process exert strict control over size, morphology, composition, position, and crystallographic orientation of the particles (Mann *et al.*, 1990). The archetypical example of microorganisms using this processes to produce Fe biominerals are magnetotactic bacteria, which synthesize intracellular, membrane-bounded magnetic minerals (Balkwill *et al.*, 1980; Blakemore *et al.*, 1985).

The recognition of microorganisms as important catalysts in many reactions and environments has over the last decade lead to a wide range of studies in the field of Geomicrobiology (Jørgensen, 1982; Bak and Cypionka, 1987; Lovley and Phillips, 1988; Cragg *et al.*, 1990; Jørgensen *et al.*, 1992; Canfield, 1993; Lovley *et al.*, 1993; Thamdrup *et al.*, 1993; Lovley, 1995; Karl, 1995a; Blochl *et al.*, 1997; Vargas *et al.*, 1998). Some examples of metal transformation and mineral formation are discussed in the following sections.

6.1.1 Microbial reactions and sedimentary diagenesis

The zonation of redox-sensitive metals in pelagic sediments is commonly described in terms of energy potential of the relevant metabolic pathways and

E_h gradients (Claypool and Kaplan, 1974; Froelich *et al.*, 1979; Berner, 1980). Under steady state conditions this will lead to a well-defined biogeochemical zonation of each remineralisation process, where the oxidation of organic matter and the cycling of nitrogen and sulphur drive the reduction and oxidation of metals. Whilst these processes are similar in different sedimentary environments, the depth scale of remineralisation varies depending on bottom water oxygen, organic carbon content, bioturbation, and sedimentation rate (Emerson, 1985; Shaw *et al.*, 1990; Canfield, 1993). Recent studies, however, have demonstrated that the concept of redox-zonation in terms of free energy yield is rather simplistic, and that more comprehensive models, including the reactivity of the substrate (Burdige *et al.*, 1992; Postma and Jakobsen, 1996) and physiological controls (Lovley and Phillips, 1987; Lovley and Chapelle, 1995), are required.

Rates of dissimilatory metal transformation are largely unknown, but it has been speculated that microbial Fe and Mn reduction may account for up to 50% of carbon oxidation in coastal marine environments (Aller, 1990; Canfield *et al.*, 1993). The simultaneous occurrence of microbial reduction of secondary oxides (nitrate, sulphate, metal-oxides) together with physiochemical oxidation of Fe, however, makes it difficult to assess the relative contribution of the organic and inorganic reactions. Hence, rates of metal oxide reduction may be significantly underestimated if based purely on chemical gradients. Instead, porewater data, solid phase data and incubation results need to be considered together in order to obtain a more complete picture (Canfield *et al.*, 1993).

Stable isotopes are used in incubation experiments, where radiogenic tracers are injected into the sediments to measure rates of specific activity. Iversen and Jørgensen (1985) used this radiotracer-method to measure the rates of sulphate reduction and methane production in organic-rich coastal marine sediments. Thermodynamic calculations suggest that these two processes are mutually exclusive, but direct measurements revealed a concomitant peak of sulphate reduction and methane oxidation at the sulphate-methane transition. The conclusion from these results and from later stable isotope analysis of

pyrites in similar environmental settings (Jørgensen pers. comm. 1999) is that anaerobic oxidation of upwards diffusing methane is fuelling sulphate reduction in the transition zone. So far it has not been possible to isolate or culture the organism responsible for this process, but mounting geochemical evidence (Hansen *et al.*, 1998; Niewöhner *et al.*, 1998) strongly suggests that anaerobic methane oxidation does indeed take place.

6.1.2 Microbial-metal interactions

A further aspect of microbe-metal interaction is the accumulation of metals in the sedimentary column as a result of scavenging from ground- and surface water by microorganism. Examples of natural metal-enrichments of such kind are manifold. A well-documented mechanism is the bacterial production of magnetite, either intracellularly, as in magnetotactic bacteria (Balkwill *et al.*, 1980; Blakemore *et al.*, 1985), or extracellularly, as in dissimilatory Fe-reducing bacteria (Lovley *et al.*, 1987). The contribution of microbes to mineralisation has important implications for our understanding of the natural remnant magnetisation of sediments (Peterson *et al.*, 1986; Stolz *et al.*, 1986).

Mills *et al.* (1994) have attributed the marked U-enrichment on individual sulphide grains in metalliferous sediments to the activity of bacteria. Microbial U reduction has been demonstrated in the laboratory, where Fe-reducing bacteria utilise U as an alternative energy source to reduce U at rates considerably faster than abiotic U-reduction (Lovley *et al.*, 1991). Most recent experiments have shown that microbial U reduction can also occur at temperatures of 100°C, suggesting that the formation of U-rich hydrothermal deposits could be catalysed by bacteria even at extremely high temperatures (Kashefi and Lovley, 2000).

Direct microbial mediation of sulphide precipitations has been suggested by Zierenberg and Schiffman (1990), who found bacterial filaments in fossilised bacterial mats to be selectivey replaced by Ag- and Cu-bearing sulphides. Eberhard *et al.* (1995) demonstrated substantial fixation of CO_2 by microbial populations that were grown on a variety of polymetal sulphide substrate, including chalcopyrite, sphalerite, galena, and chalcocite. The experiments

were conducted *in situ* at hydrothermal vent sites of the MAR and in laboratory cultures. Silltoe *et al.* (1996) propose microbial fixation of Cu at active replacement fronts as a critical factor in supergene enrichments of copper deposits, and Watterson (1991) present morphological evidence for precipitation of gold on cell walls of hyphal budding bacteria in Alaskan placer deposits.

Acid drainage, often enriched in heavy metals, is an unwelcome side effect of mining and ore processing that has become a significant economic and environmental burden. Exposure of pyritiferous rocks and sulphide ore deposits to air and oxygenated groundwater promotes increased weathering of pyrite, producing often extremely acidic run-off with pH as low as 2 and high concentrations of heavy metals (Barton, 1978; Kelly, 1988). A wide range of abiotic and biotic mechanism of pyrite oxidation have been identified (Evangelou and Zhang, 1995) and the role of microbes in this process is now well established (Nordstrom and Southam, 1997). Similarly, Wirsen *et al.* (1993) experimentally demonstrated the degradation of hydrothermal sulphides by obligate chemoautotrophic bacteria. The importance of microbial intervention during the formation of gossans and aging of seafloor sulphide deposits remains to be quantified.

The ability of microbes to accumulate metals has been exploited by both mining industry and in pollution control. Ore piles and tailing are inoculated with bacteria to aid the recovery of commercially valuable metals such as Au, Zn and Cu. For a review of microbial leaching of economically valuable metals from ores it is referred to Kelly *et al.* (1979) and Ehrlich and Brierley (1990).

The utilisation of microorganism in the recovery of potentially harmful metals is collectively termed as 'bio-remediation'. This term does not, however, give justice to the wide range of mechanism of microbe-metal interaction that finds application in pollution control. These include sorption of metals to the exterior of cell walls (Beveridge and Murray, 1976; Gadd and White, 1993), intra- or extracellular precipitation of metal-rich mineral phases (Strandberg *et al.*,

1981; Lovley, 1995) extracellular complexation and polymerisation (Lester *et al.*, 1984; Chen *et al.*, 1995) and methylisation (Thayer, 1989).

6.1.3 The Deep Biosphere

Recent findings from the Ocean Drilling Program (ODP) have demonstrated the existence of extensive microbial populations beneath the deep ocean floor at much greater depth than was previously thought. Viable bacterial cells have been found as deep as 842 m into the sediment pile and are believed to be present even deeper than that. The increase in pressure and temperature with sediment-depth and the lack of degradable organic carbon requires that the bacteria are well adapted in order to succeed under these extreme conditions (Cragg *et al.*, 1990; Cragg *et al.*, 1992).

Efforts to study the deep biosphere are complicated by a number of factors. The limited accessibility of the study area often makes *in situ* experiments impossible. Many of the common sampling procedures, on the other hand, carry the risk of contamination. Only a very small proportion of the organism can be grown under laboratory conditions, and even if great care is taken to keep disruption of the microbial communities to a minimum, activity measurements are extremely sensitive to sampling and experimental artefacts (Jørgensen, 1978; White, 1983).

Recent developments in microbiology have produced a whole new range of tools, such as DNA probes and molecular analysis, to overcome some of these problems (Burlage *et al.*, 1998). Alternatively, geochemical techniques often provide indirect evidence for microbial activity, and in particular stable isotope signatures are an extremely valuable proxy for past bacterial processes.

An example is the fractionation of stable sulphur isotopes, where the microbial reduction of sulphate produces an enrichment of the lighter ^{32}S over the heavier ^{34}S isotope in the product sulphide (commonly expressed as $\delta^{34}S$). Reaction of H_2S with Fe will form pyrite, thus preserving the isotopic signal in the sedimentary record (Price and Shieh, 1979, Goldhaber and Kaplan, 1980)

In a study of deep sediment cores from the Cascadia Margin (ODP Leg 146), Bottrell *et al.* (submitted) used stable sulphur and oxygen isotopes to examine the cycling of sulphur in these deposits. The usual diagenetic sequence was observed in the upper section of the sediments, with sulphate reduction as the dominant terminal electron accepting process, as indicated by the decreasing sulphate concentrations with depth and corresponding increase in sulphate $\delta^{34}S$. At two sites, however, sulphate concentrations increased again below ~50m, stimulating bacterial sulphate reduction at depths of 70-250m. A concomitant decrease of porewater sulphate $\delta^{34}S$ suggests that the source of sulphur in the sulphate-molecule is isotopically lighter diagenetic pyrite. Despite the lack of any direct microbial evidence Bottrell *et al.* (submitted) believe that these data can only be explained by anaerobic oxidation of pyrite, with Fe^{2+} from the sediments being the most likely oxidising agent.

Investigation of microbial activity in hydrothermal systems until today has focused on the utilisation of geothermal energy emanating from hot vents, and the role of microbes as primary producers in the absence of light (Jannasch and Mottl, 1985; Karl, 1995a). These bacteria utilise the chemical energy that is available from reduced sulphur compounds in the hydrothermal fluids, where they can sustain temperatures of up to 113°C (Blochl *et al.*, 1997). Extensive microbial mats have been observed at established hydrothermal systems where diffuse venting occurs (Jannasch and Wirsen, 1981; Jannasch *et al.*, 1989).

Several studies of hydrothermal systems in the Pacific have examined the regeneration of hydrothermal vent ecosystems following volcanic seafloor eruptions (Haymon *et al.*, 1993; Juniper *et al.*, 1995). After the initial rapid release of large volumes of hydrothermal fluids in form of a megaplume, widespread diffuse flow from fractures and fissures in the fresh lava has been observed (Butterfield and Massoth, 1994). These sites of diffusive venting are often associated with large plumes of bacterial floc and extensive accumulation of microbial mats covering the seafloor (Haymon *et al.*, 1993; Juniper *et al.*, 1995). The detection of thermophilic, anaerobic bacteria in the event plume of the 1996 Gorda Ridge event only shortly after the eruption

strongly points towards a subsurface origin of the bacteria (Summit and Baross, 1998). Juniper *et al.* (1995) examined the newly developing microbial mats near the CoAxial eruption site, Juan de Fuca Ridge. The significant discrepancy between observed carbon accumulation and potential accumulation from CO_2 fixation, with the former markedly exceeding the latter, is further indication that at least some of the observed bacterial population originate below the seafloor.

Based on re-examination of the literature and observations of a positive correlation between DNA abundance and vent fluid temperature, Baross and Deming (1993) formulated a hypothesis stating that the extremely heat-tolerant microbial communities exist in sedimentary layers below high-temperature vent fields. In the absence of direct observations from deep-sea drilling, Baross and Deming (1993) suggested that the more accessible hot smoker vents might be used as "windows" to the deep. Drilling of the active TAG mound on the unsedimented Mid-Atlantic Ridge in 1994 offered the opportunity to test Baross and Deming's hypothesis of a subsurface biosphere along seafloor spreading zones. Reysenbach *et al.* (1998) examined samples from all major lithologies, but did not find any DNA or direct microbial evidence for the presence of significant microbial biomass at this site. On the sedimented ridges at the Middle Valley, NE Pacific, in contrast, Cragg and Parkes (1993) were able to demonstrate that microbial populations exist in hydrothermal sediments in the immediate vicinity of active black smoker vents. More recent results from the same area suggest that they can sustain temperatures of up to about 115°C (Parkes *et al.*, submitted), i.e. close to the currently accepted upper limit for bacterial growth (Blochl *et al.*, 1997).

Similarly, Jørgensen *et al.* (1990; 1992) observed extremely thermophilic sulphate reducers in the deep layers of the organic-rich sediments near black smokers in the Guaymas Basin. Laboratory experiments showed that the optimum temperature for these organisms was as high as 83°C, and rates of sulphate reduction were comparable to those of eutrophic coastal regions.

All these studies have demonstrated that bacteria are ubiquitous and appear to be well adapted to this seemingly hostile environment. However, only few studies of the microbiology of hydrothermal systems have gone beyond the spectacular black and white smokers to examine the subsurface.

6.1.4 Chapter outline

The aim of this study is to investigate the existence of microbial communities in metalliferous sediments from an inactive hydrothermal vent site. Although hydrothermal activity in the *Alvin* zone is believed to have ceased several thousand to tens of thousands of years ago (Metz and Trefry, 1988; Lalou *et al.*, 1995), reduced hydrothermal minerals will potentially provide a continuous inorganic energy source for chemolithotrophic bacteria. The size of the microbial population is quantified, and the effect of the naturally high metal content of the environment is evaluated. The role of microbes in the early diagenesis and mineralisation processes in these deposits is investigated by comparing key microbiological indices for bacterial abundance and activity with geochemical data.

6.2 Methods and materials

Detailed microbial and geochemical analysis was performed on core 43 from the southern tip of the *Alvin* relict hydrothermal zone (Chapter 3, Figure 3.1) as well as on a background core from 50 km west of the Broken Spur vent field (core 10). Further analysis was performed on a total of 14 cores from the *Alvin* zone and the *Mir* mound, but only core 43 will be discussed here in detail.

A complete list of all the microbiological and geochemical analysis that was performed on samples from cores 43 and the background core 10 is given in Table 6.1. A description of the geochemical analysis that was performed in Southampton is given below. All microbiological analysis was performed by members of the Geomicrobiology Group of the Department of Earth Sciences, University of Bristol, namely Barry Cragg and Jon Telling. Detailed descriptions of all the microbiological analysis performed in Bristol are given in Appendix A. Porewater sulphate and hydrogen sulphide was analysed by Jo Rhodes, and the method is described in Chapter 4 Section 4.2.1.2.

Analysis	Laboratory
Bacterial enumeration	
Total viable bacteria	Bristol
Dividing and divided cells	Bristol
Viable heterotrophs (Mn/Fe reducers and oxidisers)	Bristol
Microbial activity measurements	
Thymidine incorporation	Bristol
Potential sulphate reduction rate	Bristol
Potential sulphide oxidation rate (SOR)	Bristol
Porewater acetate and acetate utilisation	Bristol
Geochemical analysis	
Organic carbon	Southampton
Total sulphur	Southampton
Solid phase Fe and Mn	Southampton
Porewater Fe and Mn	Southampton
Porewater sulphide	On board
Porewater sulphate	Bristol
XRD analysis	Southampton

Table 6.1: Summary of microbiological and geochemical analysis

6.2.1 Geochemical analysis

6.2.1.1 Organic carbon and total sulphur

For organic carbon analysis, the inorganic carbon fraction was removed by acidification with hydrochloric acid. Splits of ~100 mg of sample were weighed into clean glass vial and 100 µl of 25 % HCl carefully added. After completion of the reaction, a further 30 µl of acid was added, and if any effervescence was noted on the second addition, the procedure was repeated until complete removal of $CaCO_3$. The acid was evaporated at ~120°C on a hot plate in a fume cupboard. In order to ensure complete evaporation of the acid, which will otherwise accumulate in the elemental analyser combustion tube, ~1 ml of de-ionised water was added to the dry sediments. After repeated drying, the loss of weight was recorded. The sediments were analysed for carbon and total sulphur using a Carlo Erba EA 1108 elemental analyser, as described in Chapter 3, Section 3.1.2.3.

6.2.1.2 Solid phase Fe and Mn

Solid phase Fe and Mn were determined together with all other major elements X-ray fluorescence spectrometry. Details of the analysis, including the sample preparation, are described in Chapter 3 Section 3.1.2.1.

6.2.1.3 Porewater Fe and Mn

Porewater analysis was done using a graphite furnace atomic absorption spectrometer (GF-AAS; Perkin Elmer 1100B, and Varian Spectra AA 300 Zeeman). Both metals were analysed on acidified samples at dilutions of 1:10 to 1:180. A platinum matrix modifier (Sachsenberg *et al.*, 1993) and standard addition were used to minimise any matrix effect.

6.2.1.4 X-ray diffraction

An overview of the mineralogy was obtained from X-ray diffraction (XRD) patterns for selected samples for each sedimentary layer. Details of the analysis are described in Chapter 3 Section 3.1.2.2.

6.3 Results

6.3.1 Microbial abundance and activity

The total counts of viable bacteria where measured throughout core 43 at 10 cm resolution or higher (Table 6.2). These data are compared with a general depth distribution of viable bacteria in non-hydrothermal deep-sea sediments as obtained from 25 ODP cores throughout the Atlantic, Pacific and Mediterranean (Parkes *et al.*, 1994) (Figure 6.2). Counts were also included for two archived sections (130-160 cm and 180-210 cm). These samples were not processed immediately after sampling on board the ship, but kept in storage for several months before samples for total viable counts were taken. The first samples from these archived sediments were taken after eight months, where each section was subdivided into 5 cm subsections similar to processing on board the ship. To monitor any storage effect on these archived sediments, the subsections were re-sampled after 14 and 26 months, and counts were compared with those obtained for the 8 months old samples. In between each sampling interval the subsections were stored at 4°C and under anoxic conditions to keep storage effects to a minimum. Comparison of data for identical subsections over the time of observation did not show any significant difference between time zero samples and archived samples, and no correction was applied.

Microbes were present at levels markedly above the significance limit of ca. 70,000 cells/cm^3 throughout this core. Counts for the carbonate cap and the two sulphide layers followed roughly the general trend for deep-sea sediments with slightly elevated counts in the two sulphide layers. Significant deviation from the expected distribution, however, was found in the lower half of the intermediate Fe-oxysilicate layer, where counts were reduced by a factor of up to 6.

Most bacteria incorporate exogenous thymidine into newly synthesised DNA, the production of which is tightly coupled to cell division and hence carbon production and growth. Some bacteria, however, are not capable of using

exogenous thymidine but will synthesise their own. These include most notably many chemolithoautotrophic bacteria and sulphate-reducing bacteria (Moriarty, 1986; Johnstone and Jones, 1989). Consequently, the thymidine incorporation method (Appendix A 2.1) will underestimate total bacterial production, particularly in anaerobic sediments (Austin and Findlay, 1989). In core 43, thymidine incorporation decreased from the surface to the base of the upper sulphide layer, where no significant growth was detected. The highest growth rates, however, were measured in the intermediate layer, where they reached a maximum of 13 fmol/cm^3/d (Table 6.2). These rates are markedly higher than those in core 10, the carbonate-rich background core (see Chapter 3 for description), where the maximum uptake of thymidine was only 3 fmol/cm^3/d, with an average of 1 fmol/cm^3/d as opposed to an average of 5 fmol/cm^3/d in the metalliferous core.

A second but cruder and less robust measure of growth is the number of dividing and divided cells (Table 6.2). No decrease was observed in the surface layer of core 43, but similar to the thymidine incorporation, the proportion of dividing cells was found to be highest in the intermediate layer, where it reached up to 15%. The average proportion of dividing cells in the background core was indistinguishable (8%) from that in the metalliferous sediments, but with markedly less variation with the highest number not exceeding 10.6%.

Levels of organic carbon were low throughout this core with only little variation (Table 6.2). The mean concentration was 0.2%, which is comparable to the levels commonly observed in deep-sea sediments (Heath *et al.*, 1977a). Dissolved acetate is an intermediate in the anaerobic degradation of organic matter. Porewater concentrations are generally low (mean = 2.3 µmol/l), but a marked peak of 7.3 µmol/l was observed in the carbonate cap. This porewater acetate peak coincides with the maximum rate of acetate utilisation, which is also highest in the carbonate cap (51 pmol/cm^3/d).

6.3.2 Sulphur-species

The different sulphur species are operationally defined as acid-volatile sulphur (AVS: H_2S and FeS), elemental sulphur and chromium-reducible sulphur (CRS: pyrite and other more crystalline sulphides). Analysis of pool sulphides in the solid phase shows that pyrite is the principal sulphur species in the upper sulphide layer (Table 6.3 and Figure 6.1), thus confirming the results from the XRD analysis (see Chapter 3). Elemental sulphur is dominant in the intermediate layer, and FeS is insignificant throughout. The total amount of sulphur as derived from this method however (I% in the upper sulphide layer, assuming an *in situ* bulk density of 0.6g/cm^3) is one order of magnitude lower than the results obtained from the elemental analyser, where total sulphur concentrations were as high as 26%. Further, this method fails to reproduce the clearly much higher sulphur concentrations in the sulphide layers compared to the intermediate layer. A possible explanation for this discrepancy is the heterogeneous nature of the sediments. However, because of the consistently large difference in concentration as derived from both methods, this appears to be unlikely. The accuracy of the sulphur-analysis on the elemental analyser was continuously monitored by repeat measurements of a standard reference material, and values where usually within 2% of the certified value. The thus derived total S concentrations are therefore believed to be more accurate. Errors in the sequential distillation may have derived from incomplete degradation of the pyrite in the chromous chloride solution. Despite this discrepancy measurements for pool sulphides by sequential distillation are used to calculate the specific S-reduction and S–oxidation activity. Consequently it should be kept in mind that, the estimated potential rates might be significantly higher. It is believed, however, that this will affect primarily the CRS, which is less important in the microbial cycling of sulphur in this core. As it will be shown below the effect of an underestimation of the CRS fraction should be minimal, since AVS is the dominant substrate for microbial S-metabolism in this core.

Porewater sulphate concentrations vary only slightly with depth with a mean concentration of 29 mmol/l (Table 6.3). For most samples they are within error

of the average open-ocean seawater concentration of 28 mmol/l. Sulphate concentrations significantly exceeding that of seawater were observed in the carbonate cap at 28 cm (33 mmol/l), and near the surface of the lower sulphide layer between 168 and 178 cm depth (31 to 32 mmol/l). Hydrogen sulphide concentrations were below the detection limit of 1 µmol/l throughout the core.

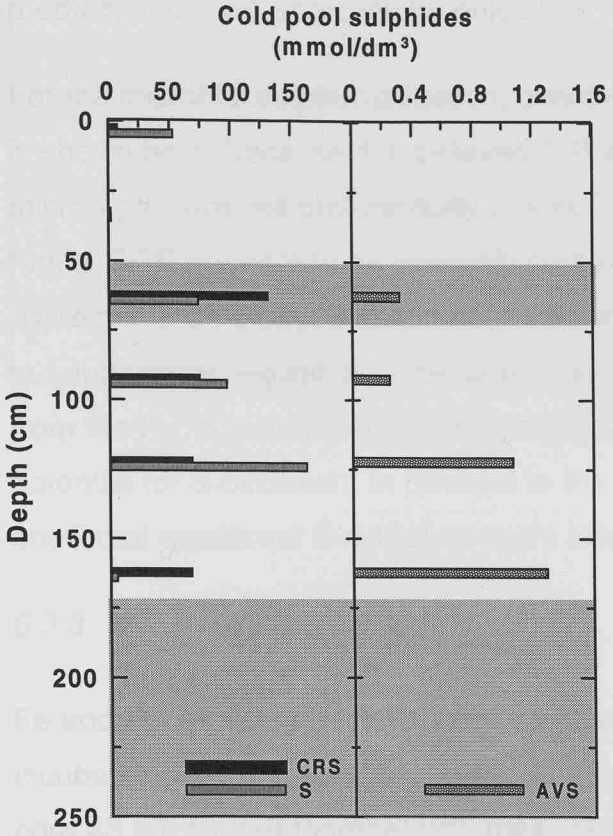

Figure 6.1: Cold pool sulphides for core 43, on which calculations of potential sulphate reduction and sulphur oxidation were based. AVS includes H_2S and FeS, and CRS includes pyrite and other sulphides.

Results from the ^{35}S radiotracer incubation experiment indicate that potential SRR in core 43 were highest directly above the upper sulphide layer and possibly coincide with the Mn^{2+}/Mn^{4+} transition, which is marked by a peak in solid phase Mn. A second but smaller peak was observed in the intermediate layer. The maximum rates of 67 nmol/cm^3/d are similar to those observed in coastal shelf sediments (Jørgensen, 1982; Thamdrup *et al.*, 1994) and in the organic-rich, hydrothermally altered sediments of the Guaymas Basin

(Jørgensen *et al.*, 1990; 1992). For the remainder of the core the potential SRR are low. Where sulphate reduction occurs at an appreciable rate, it is clearly dominated by the production of FeS, which makes up 95 % of the total reduced sulphur production based on the results from the sequential distillation. Production of FeS_2 and S_0 are low throughout the core. Potential SRR in the background core is low with a small peak of 12 nmol/cm^3/d, and production of FeS accounts for only 25 % of total sulphate reduction.

For the microbial sulphur-oxidation, only the potential rate for the AVS fraction is shown here, because it is believed that in the absence of sufficient H_2S the microorganisms will preferentially use FeS rather than the more crystalline forms. SOR appears to be inversely correlated to the SRR, and rates are highest in the Fe-oxysilicate zone, relatively low in the upper sulphide layer but apparently negligible in the carbonate cap (Table 6.3). The net counts from the $H_2{}^{35}S$ incubation experiment give an indication of the relative potential for S-oxidation. In contrast to the actually measured rates, these show that significant S-oxidation might also occur near the surface.

6.3.3 Metal-reducing bacteria

Fe and Mn reducing bacteria were successfully enriched from all cores where incubations were attempted (cores 10, 18, 25, 37, 43, 53, 56 and 66). Data for core 43 are plotted together with their respective porewater metal concentrations. Both Fe and Mn reducers were detected in the intermediate layer. This is matched by the markedly elevated Fe- and Mn- porewater concentrations below 50 and 60 cm depth respectively (Table 6.2). Significant numbers of Fe-reducers were also enriched from the carbonate cap, whilst Mn-reducers were absent in this zone. Metal-reducers in the background core were insignificant or absent.

No incubations for Fe and Mn-oxidisers were attempted for core 43. However, MPN results from core 53, which was recovered in the immediate vicinity of core 43 (see Chapter 3 Figure 3.1), suggest that metal-oxidising bacteria are present in these types of sediments.

Depth	Total counts	Dividing cells	Thymidine incorp.			Mn reducers			porewater Mn	Fe reducers (cells/cm3)			porewater Fe	C_{org}	Acetate utilization	Porewater acetate
cm	log 10 cells/cm^3	%	fmol/cm^3/d mean	min.	max	cells/cm^3 mean	min.	max	µmol/l	cells/cm^3 mean	min.	max	µmol/l	%	pmol/cm_3/d	µmol/l
2.5	7.9	5.87	-	-	-	-	-	-	-	-	-	-	-	0.27	-	-
7.5	-	-	-	-	-	-	-	-	0.0	-	-	-	0.8	-	-	1.28
12.5	8.0	5.78	6.8	3.1	10.1	0	0	0	-	5.8	2.1	16.6	-	0.24	42.6	-
17.2	-	-	-	-	-	-	-	-	0.0	-	-	-	1.3	-	-	-
22.5	6.9	7.31	-	-	-	-	-	-	-	-	-	-	-	0.19	-	-
27.5	-	-	-	-	-	-	-	-	0.0	-	-	-	1.4	0.20	-	7.31
32.5	6.8	4.42	-	-	-	-	-	-	-	-	-	-	-	0.18	-	-
37.5	-	-	-	-	-	-	-	-	-	-	-	-	-	0.20	-	-
42.5	6.5	9.36	3.5	0	10.6	0	0	0	-	125	43.9	354	-	0.20	50.5	-
47.5	-	-	-	-	-	-	-	-	0.2	-	-	-	0.6	0.20	-	-
52.5	7.1	9.65	-	-	-	-	-	-	-	-	-	-	-	0.24	-	-
57.5	-	-	-	-	-	-	-	-	3.4				7.8	0.14	-	1.91
62.5	6.9	9.61	-	-	-	-	-	-	-	-	-	-	-	0.14	-	-
67.5	-	-	-	-	-	-	-	-	3.6	-	-	-	33.3	-	-	2.03
72.5	6.7	11.4	0	0	0	13.1	6.1	28.1	-	12.9	5.0	33.5	-	0.45	21.2	-
77.5	-	-	-	-	-	-	-	-	2.3	-	-	-	*32.3	-	-	1.51
82.5	6.5	12.04	-	-	-	-	-	-	-	-	-	-	-	0.15	-	-
87.5	-	-	-	-	-	-	-	-	3.8	-	-	-	29.0	-	-	2.02
92.5	6.6	15.76	-	-	-	-	-	-	-	-	-	-	-	0.16	-	-
97.5	-	-	-	-	-	-	-	-	3.7	-	-	-	24.7	-	-	1.17
102.5	6.6	10.85	13.3	0	27.0	34.2	15.4	75.8	-	9.7	3.7	26.3	-	0.28	3.0	-
107.5	-	-	-	-	-	-	-	-	2.9	-	-	-	18.9	-	-	1.71
112.5	6.1	4.84	-	-	-	-	-	-	-	-	-	-	-	-	-	-
117.5	-	-	-	-	-	-	-	-	2.7	-	-	-	41.4	-	-	1.89
122.5	6.1	11.6	-	-	-	-	-	-	-	-	-	-	-	0.15	-	-
127.5	-	-	-	-	-	-	-	-	3.5	-	-	-	39.9	-	-	2.02

dashes indicate no measurements were obtained

Table 6.2: Microbial enumeration, general activity and specific activity for metal-reducing bacteria for core 43.

Depth	Total counts	Dividing cells	Thymidine incorp.			Mn reducers			porewater Mn	Fe reducers (cells/cm3)			porewater Fe	C_{org}	Acetate utilization	Porewater acetate
cm	log 10 cells/cm^3	%	fmol/cm^3/d			cells/cm^3			µmol/l	cells/cm^3			µmol/l	%	pmol/cm_3/d	µmol/l
			mean	min.	max	mean	min.	max		mean	min.	max				
132.5	6.3	11.35	-	-	-	-	-	-	-	-	-	-	-	0.17	-	-
137.5	6.0	1.95	-	-	-	-	-	-	-	-	-	-	-	0.14	-	-
142.5	6.2	7.92	-	-	-	-	-	-	-	-	-	-	-	-	-	-
147.5	5.8	6.45	-	-	-	-	-	-	-	-	-	-	-	-	-	-
152.5	5.9	6.22	-	-	-	-	-	-	-	-	-	-	-	-	-	-
157.5	6.1	6.45	-	-	-	-	-	-	-	-	-	-	-	0.21	-	-
162.5	6.5	7.45	-	-	-	42.2	18.9	94.0	-	98.8	36.4	268	-	0.22	-	-
167.5	-	-	-	-	-	-	-	-	3.7	-	-	-	84.3	0.29	-	1.81
172.5	6.1	7.4	1.1	0	3.4	-	-	-	-	-	-	-	-	0.24	21.5	-
177.5	-	-	-	-	-	-	-	-	3.3	-	-	-	93.3	0.24	-	2.25
182.5	6.5	7.68	-	-	-	-	-	-	-	-	-	-	-	-	-	-
187.5	6.6	7.48	-	-	-	-	-	-	-	-	-	-	-	-	-	-
192.5	6.4	7.39	-	-	-	-	-	-	-	-	-	-	-	-	-	-
197.5	6.7	9.68	-	-	-	-	-	-	-	-	-	-	-	0.27	-	-
202.5	6.6	6.59	-	-	-	-	-	-	-	-	-	-	-	-	-	-
207.5	-	-	-	-	-	-	-	-	-	-	-	-	-	0.15	-	-
212.5	6.9	9.85	-	-	-	-	-	-	-	-	-	-	-	0.23	-	-
217.5	6.4	10.67	-	-	-	-	-	-	2.0	-	-	-	82.6	0.25	-	2.77
222.5	7.1	5.97	-	-	-	-	-	-	-	-	-	-	-	-	-	-

dashes indicate no measurements were obtained

Table 6.2 continued.

Depth	Cold pool sulphides from S-reduction (mmol/dm^3)				Porewater SO_4^{2-}	Sulphate reduction activity (nmol/cm^3/d)						S oxidation act. (mmol/cm^3/d)					
									Total			AVS			net DPM		
cm	AVS	PVS	S	Total	mmol/l	AVS	PVS	S									
	mean	mean	mean			mean	mean	mean	mean	min	max	mean	min	max	mean	min	max
2.5	0	7.0	52.4	59.4	-	1.1	1.7	0.6	4.2	0.3	11.8	0	0	0	227804	38622	358826
7.5	-	-	-	-	27.6	-	-	-	-	-	-	-	-	-	-	-	-
27.5	-	-	-	-	33.3	-	-	-	-	-	-	-	-	-	-	-	-
32.5	0	1.3	1.4	2.7	-	65.1	1.2	0.6	66.8	0.0	198.3	0	0	0	143327	807	219973
57.5	-	-	-	-	27.6	-	-	-	-	-	-	-	-	-	-	-	-
62.5	0.32	131.0	72.8	204.2	-	0.9	0	0.6	1.4	0.2	2.6	0.2	0.0	0.4	57006	0	101303
67.5	-	-	-	-	26.9	-	-	-	-	-	-	-	-	-	-	-	-
77.5	-	-	-	-	27.8	-	-	-	-	-	-	-	-	-	-	-	-
87.5	-	-	-	-	27.2	-	-	-	-	-	-	-	-	-	-	-	-
92.5	0.25	73.8	96.5	209.9	-	14.8	0.2	0.5	15.5	0.0	44.8	0.3	0.0	0.9	96300	0	284752
97.5	-	-	-	-	26.9	-	-	-	-	-	-	-	-	-	-	-	-
107.5	-	-	-	-	29.2	-	-	-	-	-	-	-	-	-	-	-	-
117.5	-	-	-	-	28.8	-	-	-	-	-	-	-	-	-	-	-	-
122.5	1.07	67.2	162.8	231.1	-	4.7	0.7	0.3	5.8	0.2	16.6	1.2	1.0	1.5	99138	78798	112711
127.5	-	-	-	-	29.3	-	-	-	-	-	-	-	-	-	-	-	-
162.5	1.30	66.5	4.9	72.6	-	0.7	0.3	0.4	1.3	0.1	2.1	0	0	0	0	0	0
167.5	-	-	-	-	31.1	-	-	-	-	-	-	-	-	-	-	-	-
177.5	-	-	-	-	32.1	-	-	-	-	-	-	-	-	-	-	-	-

dashes indicate no measurements were obtained

Table 6.3: Cold pool sulphides, microbial sulphate reduction and sulphur oxidation activities from incubation experiments with radiotracers.

6.4 Discussion

6.4.1 General microbial abundance and activity

Significant microbial populations were found throughout the core (Figure 6.2). This implies that the detrimental effect of the potentially toxic metals in this environment is limited (Burggraf *et al.*, 1998). More importantly, a number of the experiments carried out on board and in the laboratory clearly demonstrate the occurrence of active microbial processes. The most general indicator of microbial activity is the number of dividing and divided cells. This is a measure of the number of cells involved in cell division and thus an index of the healthiness of the population. A linear correlation between the total number of viable cells and dividing cell counts has previously been observed in non-hydrothermal sediments (Cragg *et al.*, 1990; Cragg *et al.*, 1992). No such simple relationship was found in core 43 (Figure 6.3). In contrast, the numbers of dividing cells were highest in the intermediate layer, whilst total counts showed a marked negative deviation from the general trend. Similarly, the maximum rate of thymidine incorporation was observed in the intermediate layer, thus correlating well with number of dividing cells. This strongly suggests that, although bacterial populations are relatively small, they are healthy and well adapted to this potentially toxic environment.

The evidently active microbial communities in metalliferous deposits of currently inactive hydrothermal systems may play an important role in the revival of the hydrothermal ecosystem, should hydrothermal activity be re-established at this site. Observations from newly established hydrothermal systems in the Pacific have shown that substantial bacterial populations are present at the sites of low and high temperature venting at a very early stage (Haymon *et al.*, 1993; Juniper *et al.*, 1995). The nature and size of these microbial communities suggests that they originate below the seafloor (Summit and Baross, 1998).

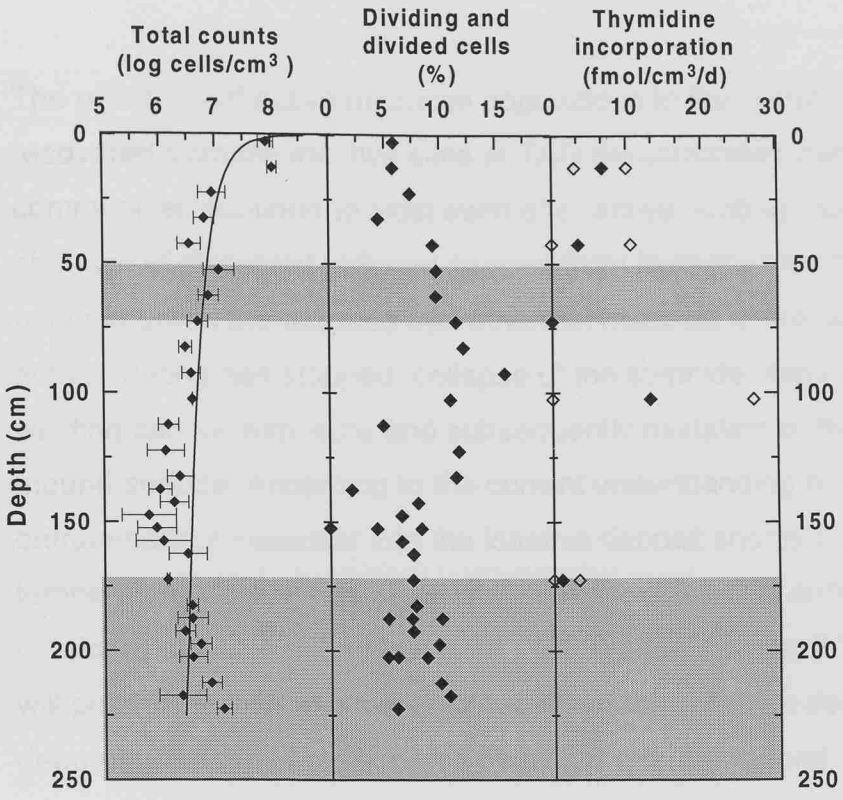

Figure 6.2: Total viable counts, dividing and divided cells, and thymidine incorporation in core 43 as general indicators for microbial abundance and activity. Solid line indicates general depth distribution for typical deep-sea sediments, from Parkes *et al.* (1994). Hollow symbols indicate minimum and maximum rates of Thymidine incorporations from triplicate incubations.

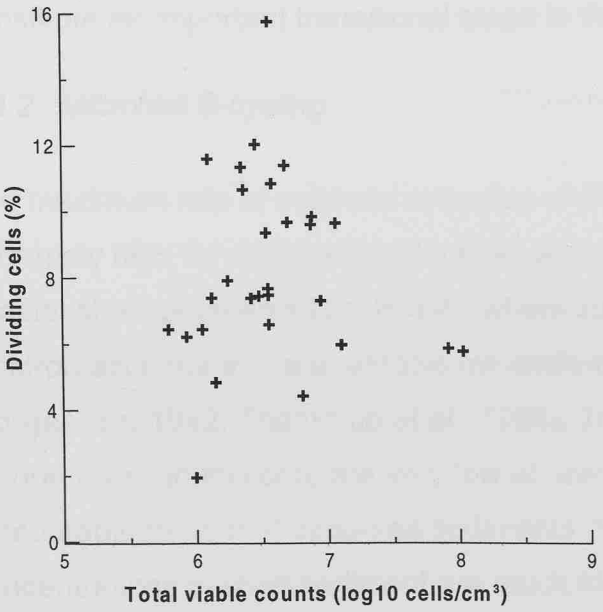

Figure 6.3: Relationship between total viable counts and dividing and divided cells.

The presence of active microbial populations in the metalliferous sediments recovered from the inactive sites at TAG demonstrates that microbial communities continue to exist even after active venting has ceased. In the absence of dissolved reduced species from hydrothermal fluids it appears that bacteria utilise the reduced hydrothermal minerals in the sediments. Once active venting has stopped, collapse of the sulphide chimneys and mass-wasting causes exposure and subsequently oxidation of the sulphides at the mound surface. According to the current understanding of mound evolution, entrainment of seawater into the inactive deposit shortly after high-temperature venting has ceased causes the abundant anhydrite in the mound interior to dissolve (Humphris *et al.*, 1995) (see Chapter 2 Section 2.3.2). This will potentially increase the permeability of the sulphide deposit and facilitate deep penetration of oxygenated seawater into the mound. In addition, the dissolving anhydrite will temporarily provide additional metabolites for subsurface microbial communities. The continuous irrigation of hydrothermal precipitates on the seafloor with fresh seawater will produce steep chemical gradients, thus providing a wealth of inorganic energy sources that can be exploited by the bacteria over long periods of time. The consistent presence of bacteria in the subsurface even during inactive periods may therefore constitute an important transitional stage in the hydrothermal ecosystem.

6.4.2 Microbial S-cycling

The maximum rate of sulphate reduction of 67 nmol/cm^3/d in core 43 is extremely high for deep sea-sediments, and similar to rates measured in coastal shelf sediments (Table 6.4), where sulphate is the dominant terminal electron acceptor in the anaerobic mineralisation of organic matter (Jørgensen, 1982; Thamdrup *et al.*, 1994). This is surprising, since organic carbon levels in this core are very low at only ~0.2% (Figure 6.5), which is comparable to normal deep-sea sediments (Heath *et al.*, 1977a), whereas concentrations in shelf sediment are much higher. The high biological productivity at active vents constitutes a considerable source of organic matter

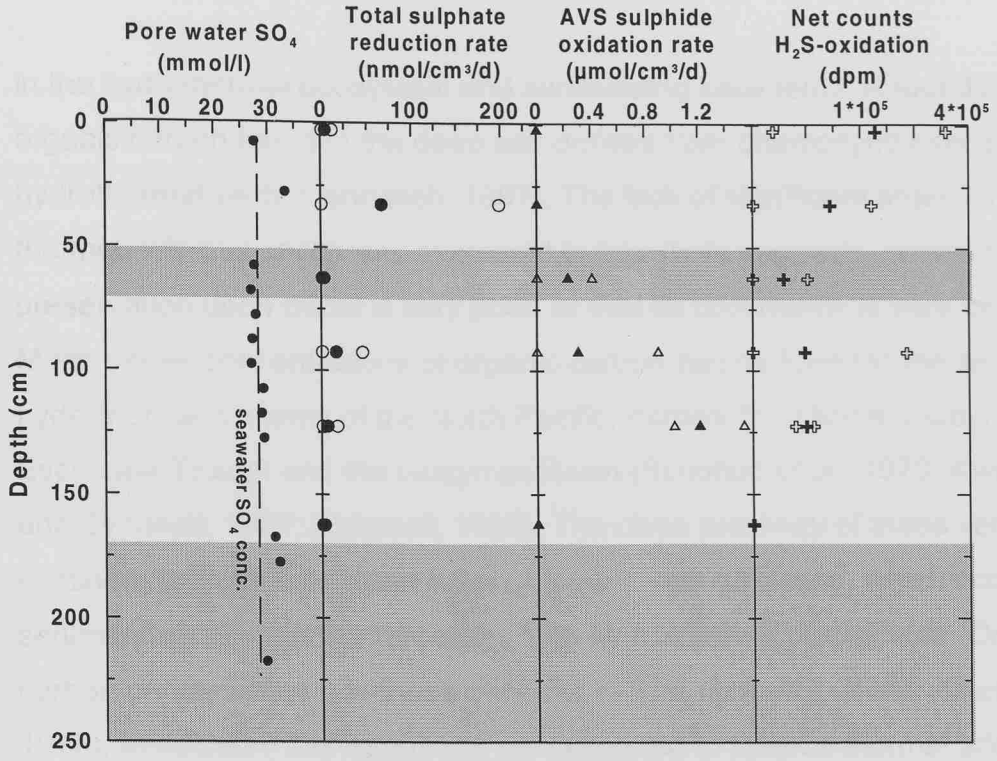

Figure 6.4: Porewater sulphate and microbial sulphur cycling. Hollow symbols indicate minimum and maximum rates from triplicate incubations. Only rates for AVS (FeS and H_sS) are shown for S-oxidation. Net counts give an indication for the potential for S-oxidation.

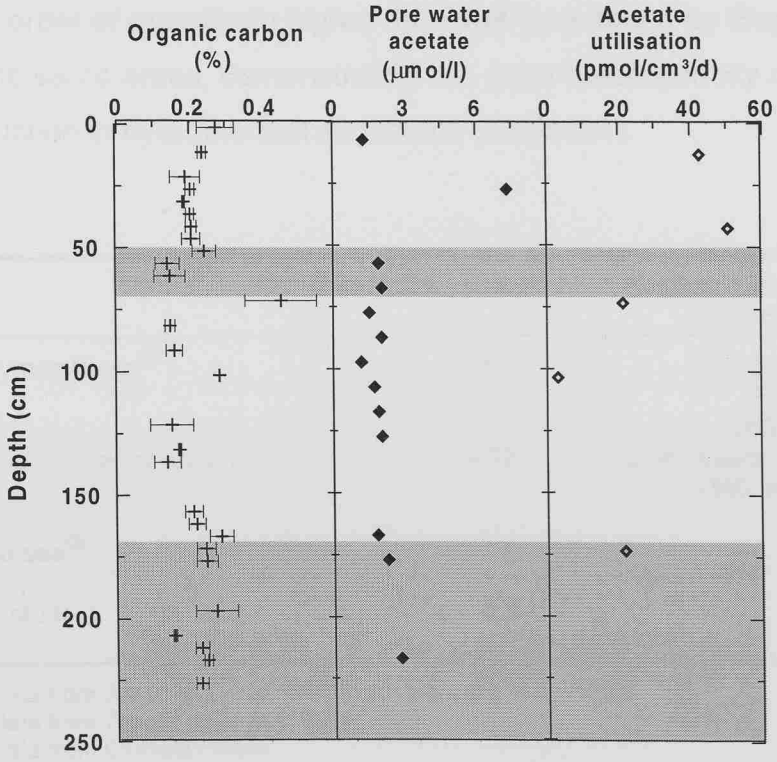

Figure 6.5: Organic carbon, dissolved acetate and microbial acetate utilisation. Acetate is a key intermediate in organic matter break-down.

in the hydrothermal ecosystem and surrounding sediments. About 3% of all organic carbon found in the deep sea derives from chemosynthesis at hydrothermal vents (Jannasch, 1997). The lack of significant organic carbon in the metalliferous sediments examined in this study suggests, however, that preservation upon burial is very poor, or that its occurrence is very localised. Much higher concentrations of organic carbon can be found in the sedimented hydrothermal systems of the North Pacific, namely the Middle Valley, Escanaba Trough and the Guaymas Basin (Simoneit *et al.*, 1979; Kvenvolden and Simoneit, 1987; Simoneit, 1990). The close proximity of these vents to the continent facilitates frequent input of organic-rich turbidites, which occur in the sedimentary sequence intercalated with hydrothermal precipitates. Organic carbon concentrations in these deposits can be up to 4% (Simoneit *et al.*, 1979). In addition, the sediments are subjected to intense thermal alteration with temperatures well above 100°C. In incubation experiments Jørgensen *et al.* (1990; 1992) demonstrated that sulphate-reducing bacteria in sediments from the Guaymas Basin are well adapted to these increased temperatures with maximum sulphate reduction rates of 30 – 140 nmol/cm^3/d. Rates up to one order of magnitude higher than that were found by Elsgaard *et al.* (1994) in the same areas, demonstrating the great heterogeneity of sulphate reduction in hydrothermal sediments (Table 6.4).

	Organic carbon content (%)	Sulphate reduction rate (nmol/cm^3/d)
Guaymas Basin[1]	2-4	30-140 at 50°C 254 at 3°C 1563 at 70°C
Eutrophic coastal region[2]	9-12	25-67 yearly average >150 maximum
Deep sea[3]	0.1-0.2	0.2-2
This study	0.1-0.3	67

(1) Data from Jørgensen *et al.* (1990) and Elsgaard *et al.* (1994)
(2) Data from Thamdrup *et al.* (1994)
(3) Data from Canfield (1991)

Table 6.4: Typical sulphate reduction rates in a variety of sediments and with varying organic carbon content.

The concomitant peak of porewater acetate and sulphate reduction activity in the carbonate cap of core 43 (Figure 6.5) strongly suggests that acetate serves as an electron donor for the sulphate-reducing bacteria. Wellsbury *et al.* (1997) demonstrated that thermal alteration of sediments can significantly stimulate organic matter breakdown and production of acetate. No temperature measurements were obtained during coring, but previous surveys of the relict deposits in the TAG hydrothermal area (Rona *et al.*, 1996; Rona *et al.*, 1998) have failed to identify any heat flow anomalies in the southern area of the *Alvin* zone. Thermally enhanced breakdown of organic matter therefore seems unlikely at this depth.

Acetate is generally considered as a key intermediate in anaerobic organic matter breakdown, and hence it constitutes an important carbon source for sulphate reduction in marine sediments (Lovley and Klug, 1982; Wolin, 1982). Its utilisation will therefore give a first order approximation of the extent of organic carbon oxidation in this core. Reduction of sulphate via oxidation of acetate proceeds through the following two reactions (McCollom and Shock, 1997):

$$H_3COO^- + 4\ H_2O \rightarrow 2\ HCO_3^- + H^+ + 4\ H_2 \qquad (6.1)$$

$$SO_4^{2-} + 2\ H^+ + 4\ H_2 \rightarrow H_2S + 4\ H_2O \qquad (6.2)$$

For each mole of acetate oxidised one mole of sulphate is reduced. Incubation experiments with radiolabelled acetate gave a maximum acetate utilisation rate of 50 pmol/cm^3/d in the surface layer of core 43. Comparison of this rate with the rate of sulphate reduction at this depth (67 nmol/cm^3/d) clearly shows that acetate utilisation alone is insufficient to support the observed rate of sulphate reduction and that an alternative electron donor remains to be identified.

Dissolved hydrogen is present at concentrations of ~ 0.2 to 2 mmol/l in hydrothermal end-member fluids (Von Damm *et al.*, 1985; Von Damm, 1990;

Butterfield and Massoth, 1994), where it originates from degassing of igneous rock and fluid-rock interaction during basalt alteration by seawater. These data are from the East Pacific Rise and include fluids that are affected by phase-separation (Von Damm, 1990). No data are currently available for the active TAG mound, but phase-separation on a slow-spreading ridge is believed to be of limited importance, and H_2 concentrations in the vents fluids would therefore be at the low end of the range cited above. As the hot fluid is expelled from the vent chimneys, it mixes with cold oxygenated seawater and the H_2 will be rapidly oxidised to form water. Hydrogen from water-basalt interaction will therefore only be available for chemoautotrophic metabolism within immediate vicinity of the vents at sufficiently high temperatures (McCollom and Shock, 1997). Despite the inherent instability of molecular hydrogen under most conditions on the seafloor, it commonly serves as an important intermediate in anaerobic metabolism. This can be explained by the tight coupling and high efficiency of interspecies H_2-transfer between hydrogen-producing and -consuming bacterial populations (Novelli *et al.*, 1988). Rapid turnover of molecular hydrogen is further indicated by its commonly very low concentration, typically measured on a nonomolar scale, compared to concentrations of terminal electron acceptors, which are consumed on a millimolar scale (Postma and Jakobsen, 1996).

In order for hydrogen to serve as electron donor for the observed sulphate reduction in core 43, a source in the sediments is required. In addition to fermentation processes, hydrogen may also be produced through inorganic reactions. Drobner *et al.* (1990) demonstrated in laboratory experiments that the formation of pyrite via its precursor Fe-monosulphide could produce H_2 according to the following reaction:

$$FeS + H_2S \rightarrow FeS_2 + H_2 \qquad (6.3)$$

Considering the abundance of polymetallic sulphides in hydrothermal systems, Wächtershäuser (1988) suggested this biogeochemical mechanism as a hypothetical source of energy for the earliest appearance of life on Earth.

In core 43, however, no significant amounts of FeS or FeS_2 where found above the upper sulphide layer, ruling out the possibility of hydrogen formation via oxidation of FeS. The supply of H_2 towards the carbonate cap by diffusion from the sulphide layer is unlikely because of the instability of hydrogen at low temperatures. Further, the production of hydrogen in the sulphide layer would promote increased sulphate reduction or any other general microbial activity in this layer, which has not been observed (Figures 6.4 and 6.2).

The absence of any detectable hydrogen-sulphide in the porewater despite the high sulphate reduction rates observed in the carbonate cap requires that all sulphide is immediately removed. For shelf sediments it has been demonstrated that H_2S is typically removed by reaction with Fe/Mn-oxides via the following reactions-pathway:

$$2\ FeOOH + 3\ H_2S \rightarrow 2\ FeS + S^0 + 4\ H_2O \qquad (6.4)$$

(Pyzik and Sommer, 1981), and

$$H_2S + 2\ H^+ + MnO_2 \rightarrow Mn^{2+} + S^0 + 2\ H_2O \qquad (6.5)$$

(Burdige and Nealson, 1986). Consequently, even at high sulphate reduction activity such as those observed in shelf sediments, sulphide will be low in the presence of reducible Fe(III) or Mn(IV). Solid phase concentrations and XRD analysis have shown that both Fe- and Mn-oxides are readily available above the upper sulphide layer (Figures 6.7 and 6.8). However, neither FeS nor Mn^{2+} were detected in the top 50cm of the sediment core. In fact, the absence of sulphide or reduced metal species in the porewater implies oxic conditions in this section of the core. Sulphate reducing bacteria are, however, considered as obligate anaerobes. In addition to the measured microbial sulphate reduction activity, the simultaneous increase in porewater acetate further suggests that anoxic conditions do prevail at least locally.

The extremely heterogeneous nature of the carbonate cap, as it can be seen in Figure 6.6, was observed in surface sediments from cores throughout this area, including core 43. It appears that fragments of sulphides and iron-oxides from higher up the relict mound are intermixed with carbonate ooze, producing increasing iron-staining towards the sulphide layer. Irrigation of the metalliferous sediments with oxygenated seawater has caused these fragments to become fully oxidised. But in order for anaerobic metabolism such as sulphate reduction to occur, anoxic microenvironments must still be present on this section (Sørensen and Jørgensen, 1987). The lack of H_2S or reduced metal species in the porewater may be explained by diffusion of these species into the oxic portion of the sediments, where they are rapidly oxidised. Similarly, auto-oxidation may have occurred during sampling of the porewater, when oxic and anoxic porewaters were mixed during centrifugation.

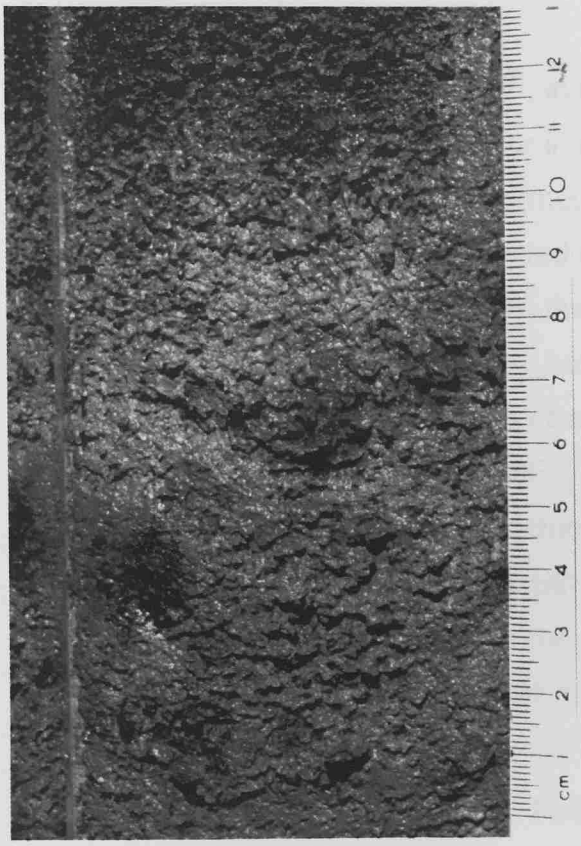

Figure 6.6: Detail from the carbonate cap of a neighbouring core, showing the heterogeneous nature of the surface sedimentary layer.

Another process that could explain the consumption of H_2S from microbial sulphate reduction is the metabolic utilisation of the reduced sulphur species by S-reducing bacteria. Similar to S-reduction, potential rates of S-oxidation were derived by relating raw counts for the radiotracer in the metabolic end-product (i.e. $^{35}SO_4^{2-}$) to the concentration of all available reduced S-species. However, unlike sulphate reduction where the dissolved porewater sulphate is the only oxidised S-species available, a whole range of reduced sulphur compounds can potentially be utilised by sulphur-oxidising bacteria, including H_2S, FeS, FeS_2 and S^0. Bacterial oxidation of AVS (as well as total S, data not shown) was restricted to the intermediate layer, where rates as high as 140 $\mu mol/cm^3/d$ were measured.

Experiments with pyrite minerals of different morphology and surface properties have shown, however, that the available surface area of the sulphide mineral will greatly affect the rate of pyrite oxidation (Evangelou and Zhang, 1995). These rates should therefore be considered as an upper limit of S-oxidation.

Raw counts for radiolabelled $^{35}SO_4^{2-}$, in contrast, indicate that significant microbial S-oxidation may also occur in the carbonate cap, and counts here are markedly higher than in the intermediate layer. This apparent discrepancy between raw counts and the calculated rates reflects the absence of any detectable reduced S-species above the upper sulphide layer. A possible source of reduced S for the bacteria, however, is H_2S that is produced from microbial sulphate reduction. In this case, the lack of detectable H_2S in the porewater combined with the high SRR would indicate rapid microbial cycling of sulphur with microbial sulphate reduction as the rate-determining step. Sulphate reduction activity at this depth might be controlled by the limited availability of reducing microenvironments. The oxidation of H_2S could proceed through the following overall reaction (Jannasch, 1995):

$$H_2S + CO_2 + H_2O + O_2 \rightarrow [CH_2O] + H_2SO_4^{2-} \qquad (6.6)$$

This reaction is anaerobic, and the chemolithotrophic synthesis of organic carbon would provide an energy source for heterotrophic bacterial activity, including S-reduction. Optimum growth of S-oxidising bacteria at hydrothermal vents is believed to occur preferentially at the interface between oxic and anoxic conditions (Karl, 1995b). Close association of S-oxidising and reducing bacteria along the geochemical gradient in the heterogeneous carbonate cap might therefore explain the observed high rates of microbial sulphate reduction in the absence of significant organic carbon. A similar close association of chemosynthetic sulphate reducers and sulphide oxidisers has been proposed to exist in the walls of hydrothermal vent chimneys (McCollom and Shock, 1997) and in the bodies of vestimentiferan tubeworms (Naganuma, 1998). The existence of significant chemolithotrophic organic carbon synthesis in 'cold' hydrothermal systems remains to be confirmed, but in the absence of further data it is the last explanation, which is preferred here.

6.4.3 Metal-reducing bacteria

Both the Fe- and Mn-reducers correlate closely with their corresponding reduced metal concentrations in the intermediate layer (Figures 6.7 and 6.8). This is clear evidence that metal reducing bacteria are actively involved in the mobilisation of metals at this depth. The number of metal reducing bacteria as derived from the MPN statistics, however, constitutes only a small fraction of the total number of bacteria. This may indicate that direct microbial reduction only plays a minor role in metal mobilisation and that most of the Fe and Mn is reduced through physiochemical reactions instead. More likely this is believed to emphasise the inherent uncertainties when using *in vitro* experiments to quantify *in situ* bacterial processes. It is well established that viable or direct counts of bacteria in natural samples only represents a small proportion (0.1 to 10%) of the true size of the microbial community (White, 1983; Kostka and Nealson, 1998).

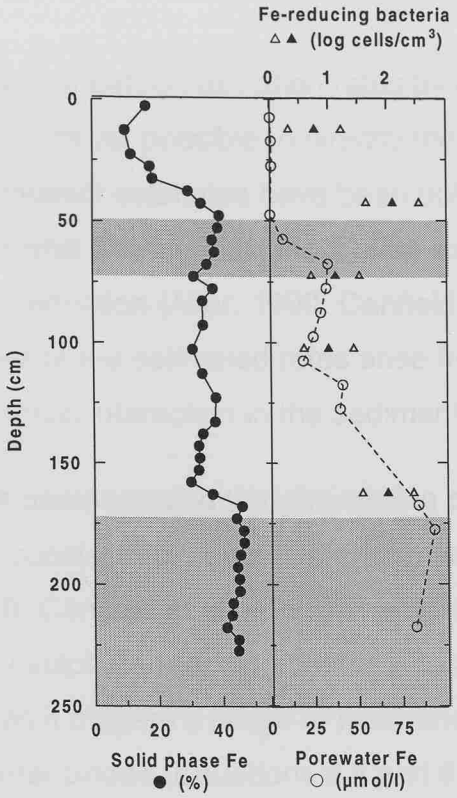

Figure 6.7: Solid phase and porewater Fe concentrations and abundance of Fe reducing bacteria. Hollow symbols indicate minimum and maximum bacterial counts.

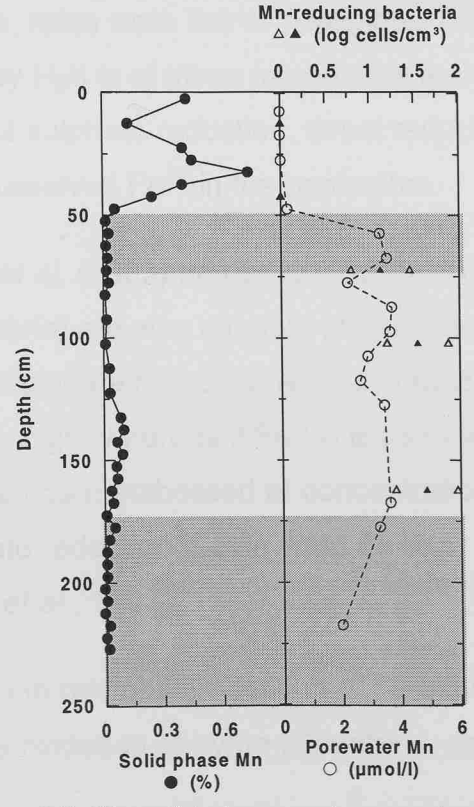

Figure 6.8: Mn solid phase and porewater concentrations and abundance of Mn-reducing bacteria. Hollow symbols indicate minimum and maximum bacterial counts.

Quantification of carbon oxidation rates by metal reducing bacteria is difficult because it is not yet possible to directly measure rates of microbial metal reduction. Indirect estimates have been obtained by combining solid and porewater metal distributions, incubation experiments and rate measurements of sulphate reduction (Aller, 1990; Canfield *et al.*, 1993). The large uncertainties of the estimated rates arise from the complexity of biotic and abiotic chemical interaction in the sedimentary environment.

It has been demonstrated that the cycling of S, Fe and Mn are very closely coupled in coastal sediments (Sørensen and Jørgensen, 1987; Aller and Rude, 1988; Canfield *et al.*, 1993; Thamdrup *et al.*, 1994). The production of sulphide by sulphate reducing bacteria has great effect on the sediment chemistry as it triggers a range of reactions between the dissolved sulphide and the metal-oxides (Equations 6.4 and 6.5). The reduction of Fe(III) by reaction of Fe-oxide with sulphides was shown in reaction (6.4). Results from incubation experiments with radiotracers have revealed that sulphate-reduction activity was highest in the carbonate cap, whereas for the remainder of the core, rates were low or negligible. This suggests that abiotic reduction of Fe(III) by H_2S is of minor importance in the intermediate layer. In the absence of sulphate reduction, direct reduction of Fe(III) by bacteria will produce dissolved Fe^{2+} in the porewater.

Coleman *et al.* (1993) demonstrated that some sulphate reducing bacteria (*Desulfovibrio*) are also capable of reducing Fe(III) to produce siderite ($FeCO_3$). Sulphate reduction will only proceed if H_2 and acetate levels are sufficiently high, whereas if Fe(III) is used as the electron acceptor, H_2 and acetate can be metabolised at concentrations much lower than those required for sulphate reduction (Lovley and Phillips, 1987; Chapelle and Lovley, 1992; Coleman *et al.*, 1993).

In addition to microbial reduction of Fe-oxides, Fe^{2+} will also be released during the oxidation of pyrite (Chapter 4, reactions 4.2 and 4.3).

The distinction of abiotic Mn reduction from microbially mediated reactions is complicated by the fact that Mn (IV) is more easily reduced physiochemically

than Fe(III) (Canfield *et al.*, 1993). In addition to reaction (6.5), which shows the reduction of Mn-oxide by hydrogen-sulphide, abiotic reduction may also occur in the presence of dissolved Fe^{2+} (Postma, 1985)

$$MnO_2 + 2Fe^{2+} + 2H_2O \rightarrow Mn^{2+} + FeOOH + 2H^+. \quad (6.7)$$

A third reductant is FeS via the reaction (Aller and Rude, 1988):

$$FeS + 7\ H^+ + 4.5\ MnO_2 \rightarrow FeOOH + SO_4^{2-} + 4.5\ Mn^{2+} + 3\ H_2O. \quad (6.8)$$

In attempt to model the cycling of Fe, Mn and S in shallow marine sediments, Canfield *et al.* (1993) and Thamdrup *et al.* (1994) concluded that all Mn reduction could be coupled to oxidation of Fe and S. Aller and Rude (1988), however, demonstrated that sulphide-oxidation by Mn was greatly reduced if metabolic inhibiting compounds were added during incubation experiments with coastal sediments.

Microbial Fe- and Mn-reduction is clearly indicated in this core by the presence of Fe-and Mn-reducing bacteria. Because of the multitude of abiotic reactions, however, it is not possible to assess the relative importance of microbial metal reduction.

6.4.4 Redox-zonation: What controls the segregation of TEAPs?

The occurrence of significant porewater Mn at ~55 cm depth above Fe at ~65 cm depth in core 43 suggests that microbial Mn reduction takes place above Fe reduction, thus following the classic model of redox-zonation as a function of relative energy yield for successive terminal electron accepting processes (TEAPs) (Froelich *et al.*, 1979). A simple thermodynamic explanation in terms of the progression of organic matter remineralisation is, however, contradicted by the occurrence of Fe-reducers in the carbonate cap, whilst no Mn-reducing bacteria were found here. Again, this may be explained by the heterogeneous nature of the sediments, and the origin of the respective metal-oxides. Fe-

oxides are concentrated in the dark red areas of the carbonate cap, and these are derived from mound ochres, which are poor in Mn. It is believed that anoxic microenvironments prevail in these Fe-oxide rich zones, i.e. conditions here are suitable for microbial Fe reduction to occur. In addition, since some sulphate-reducing bacteria can also utilise Fe as an alternative electron acceptor (Coleman *et al.*, 1993), the simultaneous occurrence of Fe-reducers and high sulphate reduction rate may therefore indicate that both measurements represent the same bacterial population.

The evidently diagenetic nature of the Mn-oxide in the carbonate cap, in contrast, suggests that the upwards-diffusing Mn^{2+} was mixed with the oxygenated seawater, causing it to precipitate in the oxic portion of the carbonate cap. The source-related and post-depositional segregation of Fe- and Mn-oxides into oxic and anoxic microhabitats may therefore explain why only Fe-reducing bacteria can be found in the surface-sedimentary layer.

A further contradiction to the model of redox-zonation after Froelich *et al.* (1979) is the occurrence of microbial Fe- and Mn-reduction in the intermediate layer, whilst the highest sulphate reduction rates were observed in the surface carbonate cap. According to the relative energy-yield of the two processes, Fe-reduction is thermodynamically favourable and should therefore occur before S-reduction. The Froehlich-model, however, is applicable primarily to one-dimensional steady-state diagenesis with a constant source of organic matter and no significant metals. Its application in these extremely metal-rich but organic carbon poor sediments is therefore very limited, and it is merely discussed here to highlight the complexity of the system. Inhibition of microbial S-reduction by Fe-reducers has been suggested by King *et al.* (1985) and Thamdrup *et al.* (1993). Results for the carbonate-cap, however, show that Fe- and S-reduction do occur simultaneously in the surface, whilst Fe- and Mn-reduction are dominant in the intermediate layer with only little sulphate reduction activity. Postma and Jakobsen (1996) suggested the segregation of Fe(III)- and sulphate-reduction as a function of pH. No direct pH measurements were obtained for this core, but the presence of $CaCO_3$ in the surface layer and its buffering effect on the porewater will potentially

cause an increase in pH, thus making sulphate reduction energetically more favourable in the surface sediments. A decrease in pH at depth, as it is indicated by the enhanced metal-mobility (Chapter 4), may be caused by the oxidation of pyrite or may be due to diffuse fluids.

6.5 Summary and conclusions

The data presented here demonstrate that active microbial communities can be maintained in metalliferous deposits over long periods of time. The extreme conditions that are encountered in the hydrothermal ecosystem, namely the high concentrations of potentially toxic metals and low pH, require a high degree of adaptation. It seems therefore unlikely that the instantaneous colonisation of newly developing vent sites with extensive accumulations of bacterial mats, as observed at several sites in the Pacific (Haymon *et al.*, 1993; Juniper *et al.*, 1995), can originate from ambient seawater. The presence of a significant, well adapted subsurface microbial population could alternative provide a source of bacteria. Hence an active subsurface biosphere, as it was found here in numerous cores from the currently inactive *Alvin* and *Mir* zones, may provide a continuum of bacterial populations between high and low temperature hydrothermal systems.

Because of the high concentration of sulphur species in the vent fluids and in the sediments, sulphur plays a dominant role in the biogeochemistry of the hydrothermal ecosystem. The ability of sulphur to form multi-valent molecular species makes it a very attractive energy source for bacteria. This study has shown that the utilisation of reduced sulphur compounds is not restricted to the hot fluids that emanate from the active vents. Microbially mediated oxidation of pyrite and other reduced sulphur species has been demonstrated from radiotracer experiments, although the calculated rates should only be considered as potential rates. The penetration of oxygenated seawater into the deposit produces steep geochemical gradients that provide a continuous energy source for the bacteria.

Dating of TAG deposits has shown that hydrothermal activity in this area is episodic with quiescent periods lasting several thousand years before active venting of hydrothermal fluids can be re-established (Lalou *et al.*, 1995; You and Bickle, 1998). U-series dating of sulphides dredged from the *Alvin* zone suggests that active venting at this site occurred 50,000 years B.P. (Lalou *et*

al., 1995) and evidence for more recent activity between 8500 and 6000 years B.P. comes from a metalliferous sediment core from the southern part of the *Alvin* zone (Metz and Trefry, 1988). The discovery of low temperature venting from a mound located at the western margin of the *Alvin* zone indicates that remnant hydrothermal circulation does still occur in this deposit (Rona *et al.*, 1998), possible affecting an area much larger than this localised surface expression suggests. Because of the evidently episodic nature of hydrothermalism in the TAG hydrothermal field, it does not seem unreasonable to assume that high temperature venting in the currently inactive sites may eventually be re-established. In this case particularly chemoautotrophic microorganism in the subsurface are likely to play a key-role in the rapid re-colonisation of the site.

Extremely high sulphate reduction rates of 67 nmol/cm^3/d were measured in the carbonate cap, despite the low organic carbon levels. The comparatively low rate of acetate utilisation of only 60 pmol/cm^3/d indicates that organic matter degradation is insufficient to support the observed rates of sulphate-reduction. Chemolithotrophic reduction of sulphate requires the presence of molecular hydrogen, but no suitable sedimentary source has been identified here. An alternative source of electron donors could be the chemolithotrophic oxidation of hydrogen-sulphide at the oxic-anoxic interfaces in the heterogeneous carbonate cap. Such a consortium of S-oxidisers and -reducers is analogous to the microbial communities that have been suggested to exist in the walls of vent chimneys (McCollom and Shock, 1997) and the bodies of tubeworms (Naganuma, 1998). The close association between these two types of microbes would allow the S-oxidisers to benefit from S-reducers during periods of limited supply of hydrogen sulphide from the vent fluids.

The extensive reworking of the hydrothermal deposits and re-mobilisation of metals is outlined in Chapter 4. The presence of Fe- and Mn-reducing bacteria in this core is good evidence that bacteria are actively involved in this process, although it has not been possible here to determine their relative contribution to overall re-mineralisation compared to inorganic reactions.

Chapter 7

Conclusions and Future Work

7.1 Summary and conclusions

Metalliferous sediments from the southern periphery of the *Alvin* zone originate from mass wasting of partially oxidised sulphide debris from the nearby hydrothermal mounds, and from fall-out of plume particulates. The dominant source of trace metals in the sediments is from primary sulphides that were precipitated during earlier periods of high-temperature venting. Variable concentrations on Co and Ag between the two sulphide layers reflect subtle variations in the temperature-regime of mineralisation in the parent sulphide mound. Post-depositional scavenging of metals from seawater is indicated for U, V and P. The effective separation of Zn and Cu into distinct zones in these sediments is analogous to the zone-refining that has been described for the active TAG mound. Remineralisation of the primary sulphide phases occurs through the reaction of the minerals with an acidic pore fluid. The acidity may have been produced *in situ* by pyrite oxidation or it may indicate the diffusion of low-temperature hydrothermal fluids through the sediments.

The depth to which oxygenated seawater has penetrated into the sediments is delineated by the Mn^{2+}/MnO_2 redox boundary at 30 cm depth. Supergene atacamite alteration only occurs at the top of the upper sulphide layer, indicating pervasive seawater alteration of primary sulphide phases. There is evidence for significant enrichment of seawater derived U in the lower sulphide layer, but this is inferred to have occurred prior to emplacement of the sulphidic material.

The current pore water flux of dissolved Mn cannot produce the observed solid phase enrichment in the timescale suggested by the overlying pelagic sediment cap. Low temperature hydrothermal fluids could have served as an additional source of Mn to the surface sedimentary layer. These fluids would also effectively alter the intermediate layer of the sediment core.

Significant alteration of the sediment core is further confirmed by the distinctive REE signature of the sediments, which indicate that minerals have been in contact with an evolved fluid. This REE signature may have been acquired before deposition of the sediments in their current location. The presence of abundant nontronite in the intermediate layer, however, is consistent with *in situ* precipitation from low temperature hydrothermal fluids. A complex picture of REE fractionation in bulk sediments and clay phases, with evidence for both LREE and HREE enrichment suggests multiple stages of low-temperature alteration. The implication is that diffuse fluids play a key role in the alteration of these deposits. The absence of significant post-depositional alteration of the lower sulphide layer indicates that the reactive fluids were advected laterally rather than diffusion through the entire sediment pile from the base.

The significance of low-temperature fluids in the ore forming process and alteration of hydrothermal deposits is increasingly being recognised (Mills *et al.*, 1996), yet only few studies have investigated their chemistry and occurrence (Butterfield and Massoth, 1994; James and Elderfield, 1996; Schultz *et al.*, 1996; Rudnicki and Mills, 1997), particularly in far-field deposits. In principle these fluids form during mixing of high-temperature fluids with seawater, but both the precipitation and dissolution of minerals phases will significantly alter the fluids chemistry (James and Elderfield, 1996). The extent and chemistry of diffuse fluids, and the different mechanism of formation, needs to be resolved in order to quantify their effect on the preservation of hydrothermal deposits and the chemical budget in the TAG hydrothermal field.

The timing of primary sulphide formation and post-depositional U enrichments can be derived from U-series analysis. Preliminary results indicate that the U enrichment in the sample from the top of the upper sulphide layer is extremely recent and cannot be resolved by U-series dating. However, U in the sulphides from the same depth indicates that they were formed ~25 kyr ago, which is in good agreement with estimates derived from carbonate accumulation rates, assuming a sedimentation rate of 0.6g carbonate /cm^2/1000 yr for the carbonate cap. The distinction between primary, sulphide-bound U and later stage U enrichment on the mineral surface is crucial for the application of U-series dating of sulphides and emphasises the importance of adequate sample treatment.

The lack of carbonate or detrital Al between the two sulphide layers indicates that they were deposited in quick succession to each other via mass slumping events. The immediate deposition of Fe-oxysilicates above the lower sulphide layer formed an effective shield and prevented further oxidation of the sulphides by bottom seawater.

The presence of active microbial populations throughout the sediment column confirms their role in seafloor-weathering and gossan formation. Bacteria have been shown to be directly involved in the transformation of metals and sulphur species within this sediment core. The microorganisms are benefiting from the steep geochemical gradients that are produced during the reaction between mineralised reduced sulphur compounds and oxygenated seawater.

An active subsurface biosphere, as found here in numerous cores from the currently inactive *Alvin* and *Mir* zones, may provide the continuum of bacterial populations between high and low temperature hydrothermal systems. If high-temperature hydrothermal venting should become re-established in this zone, well-adapted microorganisms in the subsurface will play an important role in the rapid re-colonisation of the site.

The discovery of high rates of sulphate reduction in the carbonate cap of the core investigated here is surprising and raises questions regarding the energy source, as well as the relative importance of sulphate reduction in the surface

sediments from the TAG field. In the absence of further data it is speculated that a close coupling with chemolithotrophic sulphur oxidation provides the necessary electron donor for the sulphate reduction, but further detailed microbiological investigation is required to confirm this.

7.2 Future Work

Stable isotopes of S and O have in the past proven to be extremely useful tools to reconstruct microbial reactions in the sedimentary record (Goldhaber and Kaplan, 1980; Canfield and Thamdrup, 1990). In addition to bulk and porewater analysis, non-destructive micro-scale techniques for measuring both stable and radiogenic systematics will allow interpretation of this spatially and temporally heterogeneous system.

A new geochemical proxy is currently being developed for stable Fe isotopes, which can be used for the detection of microbial Fe reduction (Beard *et al.*, 1999). This has been made possible by the recent development of a new generation of isotope mass spectrometers, which allows rapid and precise determination of isotopic ratios of transition metals (Maréchal *et al.*, 1999). This is a promising new technique for the further investigation of the interaction between microbes and metals in hydrothermal environments. Other isotopic systematics that have potential use in these metalliferous systems are Cu, Zn and Mo.

The commenced work on U-series isotopes needs to be extended. Only few radiometric dates are currently available for the inactive sulphide deposits of the TAG field. U-series dating of the slumped sulphides and alteration phases from this core will provide further insight into the history of high-temperature venting at this site, and into the timing of alteration processes in the metalliferous deposits.

The Southampton Oceanography Centre has recently been awarded a grant for the acquisition of a remotely operated vehicle (ROV), and it is anticipated that this instrument will be in operation by the year 2004. An ROV could

potentially be used for *in situ* microbiological experimentation and direct sampling of diffuse fluids in this environment.

Appendix A
Microbiological Methods

A.1 Bacterial enumeration

A.1.1 Total viable bacteria

1 cm^3 subsections of sediments, that had previously been extracted with the aid of plastic syringes (see above: on board handling), were extruded into 15 ml serum vials containing 9 ml of filter sterilised (0.2 μm) 4 % formaldehyde. The formaldehyde was made up in 3.5 % NaCl solution. The vials were shaken vigorously to disperse the sediment before taking a fixed sub-sample of 10 to 100 μl. This was diluted with a further 10 ml of filter sterilised 4 % formaldehyde, and 50 μl of acredine orange stain was added to give a final dilution of 5 mg/l. After a reaction time of 3 min, during which the vials were continuously shaken, the solution was filtered through an irgalan black stained membrane filter (25 mm, 0.2 μm pore size). The filter was rinsed with a further 10 ml of 2 % formaldehyde to remove any excess stain. Direct counts were performed using epifluorescence microscopy (Fry, 1988). To correct for bacterial cells obscured by particles, numbers for cells on particles were doubled and added to numbers for cells off particles (Goulder, 1977).

A.1.2 Dividing and divided cells

The frequency of dividing and divided cells (FDDC) was recorded during counts of total viable bacteria. Dividing cells are two cells of identical morphology attached to each other or a large single cell with an observable invagination. Divided cells are two cells of identical morphology side by side

with a gap between them. Dividing bacteria were counted as one cell, whilst divided cells were counted as two cells. Dividing and divided cells are expressed together as a % of the total count. FDDC was calculated as follows (Getliff *et al.*, 1992):

FDDC = [(dividing cells + divided cells) / total counts] x 100. (A.1)

A.1.3 Viable heterotrophs

The most-probable-number (MPN) technique was used to test for the presence of heterotrophic bacteria, including Fe-reducers, Mn-reducers, Fe-oxidisers and Mn-oxidisers. Ten different dilution levels of sample were added to identical growth media. The dilution factor for each step was serially descending by triplicate dilutions of up to 1:6. The number of replicates that were positive for a property indicative of growth was scored for each dilution after incubation. The number of cells in the original sample was estimated by comparison of the results to an MPN table.

All media were made up as salt solutions containing NaCl and $MgCl_2$ at concentrations approximating *in situ* salinities. Reazurin was added as oxygen detector and the pH was adjusted to 7.5 using NaOH or HCl. Media for metal reducing bacteria were made up with the respective metal-oxide as electron acceptor and media for Fe and Mn oxidisers contained the respective reduced form. Further details on media recipes may be obtained from web page 'http://www.geomicro.gly.bris.ac.uk/methods/recipes.html'.

Positive vial where identified from the respective production or consumption of the dissolved reduced metal species, as analysed using ICP-AES.

A.2 Microbial activity measurements

Potential rates of general microbial activity, acetate utilisation, sulphate reduction and sulphide oxidation were obtain by incubation of syringe subcores (5 cm^3) from intact sediment cores with aliquots of sterile radiogenic tracer material (^{3}H-methyl thymidine, (1,2)^{14}C-sodium acetate, $^{35}SO_4^{2-}$ and $H_2{}^{35}S$ respectively). All tracers were diluted to the appropriate activity with

autoclaved distilled water and filter sterilised (0.2 μm) into glass vials. The isotopes were injected separately into the previously prepared syringe cores. One syringe core per section was immediately frozen at –20°C as a control. The remaining incubations were done in triplicate and subcores were incubated at 2°C for 2.5 days for sulphate reduction, 4.6 to 6 hours for sulphide oxidation, 1.1 to 2.7 hours for thymidine incorporation, and 2 to 3 hours for acetate utilisation. Incubations were terminated by freezing of the subcores at –20°C until analysis.

A.2.1 Thymidine incorporation

The incorporation of radiolabelled thymidine into DNA is now widely accepted as a suitable method to assess bacterial growth and activity (Fuhrman and Azam, 1980). The procedure for the extraction of DNA after incubation is fully describes in Cragg *et al.* (1992). Daily activity rates were calculated after subtraction of the time-zero control.

A.2.2 Potential sulphate reduction rate

For the determination of the potential sulphate reduction rate (SRR) a sequential distillation procedure was adapted, which allows separate estimation of production of AVS (acid volatile sulphur: H_2S and FeS), PVS (pyrite-volatile sulphide – may include other sulphides as well as pyrite) and elemental sulphur. The method is described in detail in Parkes & Buckingham (1986). In brief, the AVS fraction was measured by adding the frozen sediments to cold 6N HCl solution and digestion for 2 to 4 hours at 80°C. After completion of the first distillation step, the mixture was allowed to cool down before adding 1M cold chromous chloride solution. For PVS the mixture was cold distilled for several hours, and finally the same mixture was heated to 80°C and distilled for a further 40 minutes for reduction of elemental S. The reaction times varied depending on the nature of the samples, and especially pyrite-rich samples often required longer reaction time to ensure complete recovery. Any H_2S that was produced during each distillation step was carried under a constant flow of nitrogen gas and trapped separately in known volumes of Zn-acetate solution (10 wt.%). Each of these three distillations

provided ^{35}S for counting with liquid scintillation counter (LSC), and using the methylen blue method after Cline (1969) a cold (non-radioactive) pool size for the sulphide was derived. The potential total SRR was calculated from the combined activity measurements for each fraction, the porewater sulphate and the sediment porosity according to the following equation:

$$SRR = \frac{a-b}{A+a}[SO_4^{2-}]\frac{1}{d}\cdot 1.06\,\mathrm{nmol\,cm^{-3}\,d^{-1}} \qquad (A.2)$$

where a is the radioactivity of the reduced sulphur compounds per volume sediment, b is the radioactivity in the ZnAc trap after chromium reduction of the time zero sample of an equivalent volume, A is the radioactivity of the sulphate per volume sediment after incubation, $[SO_4^{2-}]$ is the sulphate concentration in $nmol/cm^3$, d is the incubation time in days, and 1.06 is the isotopic fractionation factor after Jørgensen and Fenchel (1974)

A.2.3 Potential sulphide oxidation rate (SOR)

Following incubation with $H_2{}^{35}S$, frozen samples were treated by a similar distillation procedure as above, only that for sulphur-oxidation all sulphides were removed in a single step (TRIS – total reduced inorganic sulphur) by addition of hot chromous chloride. The production of any $^{35}SO_4^{2-}$, which would have been left behind in the reaction vessel, was counted using an LSC. The potential SOR for each S-bearing fraction was calculated as the product of the experimentally derived activity measurements, the porosity and the sulphide pool size of each fraction.

A.2.4 Porewater acetate and acetate utilisation

Porewater acetate concentration was measured after the method of King (1991), which is based on the reaction of acetate with acetyl coenzyme A (CoA) according to the following reaction:

$$\text{acetate} + \text{ATP} + \text{CoA} \xrightarrow{\text{(via acetyl CoA synthase)}} \text{acetyl CoA} + \text{AMP} + PP_i \qquad (A.3)$$

The AMP produced can be detected at submicromolar concentration by high-pressure liquid chromatography (HPCL). After addition of suitable amounts of ATP and CoA to the untreated porewaters, samples were incubated for 1 h at 37°C. Acetyl CoA synthase was terminated by immersion of the samples in boiling water for 2 min, and assay was done by direct injection into the HPCL system. The detection limit is 0.1 µmol/l with a precision of <3 % (2σ).

Potential rates of acetate utilisation were determined after the method of Wellsbury and Parkes (1995). In brief, post incubation the samples were ejected into pots containing 0.6 M NaOH. Although no methane was expected to be present in the samples, this was checked by removing a fraction of the headspace and injecting it into a methane oxidation apparatus. CO_2 from the incubation, including $^{14}CO_2$ from radiolabelled acetate, was released by acidification of the samples with 2 M $H_2SO_4^{2-}$. In both instances the CO_2 was trapped in gas trap and analysed using an LSC. Potential rates were calculated by relating the raw counts for radiolabelled CO_2 to the acetate pool size.

Appendix B

Glossary of Terms

AVS	Acid volatile sulphur (H_2S and FeS)
BRIDGE	British Mid-Ocean Ridge Initiative
BSC	Black Smoker Complex
CRS	Chromium reducible sulphur
DSDP	Deep sea drilling project
EPR	East Pacific Rise
FeRB	Fe-reducing bacteria
GF-AAS	Graphite furnace atomic adsorption spectrometry
HREE	Heavy rare earth elements
ICP-AES	Inductively coupled plasma atomic emission spectrometer
ICP-MS	Inductively coupled plasma mass spectrometer
JdFR	Juan de Fuca Ridge
LOD	Limit of detection
LREE	Light rare earth elements
MAR	Mid-Atlantic Ridge
mbsf	Metres below seafloor
MnRB	Mn-reducing bacteria
MORB	Mid-ocean ridge basalt
MPN	Most probable number
NADW	North Atlantic deep water
N-MORB	Normal mid-ocean ridge basalt
ODP	Ocean Drilling Program
REE	Rare earth elements
SEM	Scanning electron microscopy
SOR	Sulphur oxidation rate
SRR	Sulphate reduction rate
SRB	Sulphate reducing bacteria
TAG	Trans-Atlantic Geotraverse
TEAPs	Terminal electron accepting process

XRD	X-ray diffraction
XRF	X-ray fluorescence

References

Aller, R. (1990) Bioturbation and manganese cycling in hemipelagic sediments. *Philos. Trans. R. Soc. London A,* 331, 51-68.

Aller, R. and Rude, P.D. (1988) Complete oxidation of solid phase sulfides by manganese and bacteria in anoxic marine sediments. *Geochim. Cosmochim. Acta,* 52, 751-765.

Alt, J.C. (1988a) The chemistry and sulphur isotope composition of massive sulfide and associated deposits on Green Seamount, Eastern Pacific. *Econ. Geol.,* 83, 1026-1033.

Alt, J.C. (1988b) Hydrothermal oxide and nontronite deposits on seamounts in the Eastern Pacific. *Mar. Geol.,* 81, 227-239.

Alt, J.C. (1993) Low-temperature alteration of basalt from the Hawaii Arch, ODP leg 136. In: (eds. Wilkens, R.H., Firth, J., Bender, J. *et al.*) *Proc. ODP, Sci. Results*, Vol. 136, College Station, TX (Ocean Drilling Program), 133-146.

Alt, J.C. (1995) Subseafloor processes in mid-ocean ridge hydrothermal systems. In: (eds. Humphris, S.E., Zierenberg, R.A., Mullineaux, L.S. and Thomson, R.E.) *Seafloor Hydrothermal Systems: Physical, Chemical, Biological and Geological Interactions,* Geophysical Monograph 91, American Geophysical Union, Washington, 85-114.

Alt, J.C. and Honnorez, J. (1984) Alteration of the upper oceanic crust DSDP site 417: Mineralogy and chemistry. *Contrib. Mineral. Petrol.,* 87, 149-169.

Alt, J.C., Honnorez, J. and Laverne, C. (1986) Hydrothermal alteration of a 1 km section through the upper oceanic crust, Deep Sea Drilling Project Hole 504B: Mineralogy, chemistry, and evolution of seawater-basalt interactions. *J. Geophys. Res.,* 91, 10309-10335.

Alt, J.C. and Jiang, W.T. (1991) Hydrothermally precipitated mixed-layer illite-smectite in recent massive sulphide deposits from the seafloor. *Geology,* 19, 570-573.

Alt, J.C., Kinoshita, H., Stokking, L. *et al.* (1993) *Proc. ODP, Init. Reports*, Vol. 148. College Station, TX (Ocean Drilling Program).

Alt, J.C., Lonsdale, P., Haymon, R.M. and Muehlenbachs, K. (1987) Hydrothermal sulfide and oxide deposits on seamounts near 21°N, East Pacific Rise. *Geol. Soc. Am. Bull.,* 98(2), 157-168.

Aoki, S., Kohyama, N. and Sudo, T. (1974) An iron-rich montmorillonite in a sediment core from the northeastern Pacific. *Deep-Sea Res.,* 21, 865-875.

Arrhenius, G. and Bonatti, E. (1965) Neptunism and volcanism in the ocean. In: (ed. Sears, M.) *Progress in Oceanography*, Pergamon Press, London, 7-22.

Austin, H.K. and Findlay, S. (1989) Benthic bacterial biomass and production in the Hudson River Estuary. *Microb. Ecol.,* 18, 105-112.

Bak, F. and Cypionka, H. (1987) A novel type of energy metabolism involving fermentation of inorganic sulphur compounds. *Nature,* 326, 891-892.

Baker, E.T., Chen, Y.J. and Morgan, J.P. (1996) The relationship between near-axis hydrothermal cooling and the spreading rate of mid-ocean ridges. *Earth Planet. Sci. Let.,* 142(1-2), 137-145.

Baker, E.T., Feely, R.A., Mottl, M.J., Sansone, F.T., Wheat, C.G., Resing, J.A. and Lupton, J.E. (1994) Hydrothermal plumes along the East Pacific Rise, 8°40' to 11°50'N - plume distribution and relationship to the apparent magmatic budget. *Earth Planet. Sci. Let.,* 128(1-2), 1-17.

Baker, E.T., Lavelle, J.W. and Massoth, G.J. (1985) Hydrothermal particle plumes over the southern Juan de Fuca Ridge. *Nature,* 316, 342-344.

Baker, E.T., Massoth, G.J. and Feely, R.A. (1987) Cataclysmic hydrothermal venting on the Juan de Fuca Ridge, northeast Pacific ocean. *Nature, 329*, 149-151.

Balkwill, D.L., Maratea, D. and Blakemore, R.P. (1980) Ultrastructure of a magnetotactic spirillum. *J. Bacteriol.,* 141, 1399-1408.

Barrett, T. and Jarvis, I. (1988) Rare earth element geochemistry of metalliferous sediments from DSDP Leg 92: The East Pacific Rise transect. *Chem. Geol.,* 67, 243-259.

Barrett, T., Taylor, P.N. and Lugowski, J. (1987) Metalliferous sediments from DSDP Leg 92: The East Pacific Rise transect. *Geochim. Cosmochim. Acta,* 51, 2241-2253.

Barton, P. (1978) The acid mine drainage. In: (ed. Nriagu, J.O.) *Sulfur in the environment; Part II, Ecological impacts*, Wiley, New York, 313-358.

Bau, M. and Dulski, P. (1999) Comparing yttrium and rare earths in hydrothermal fluids from the Mid-Atlantic Ridge: implications for Y and REE behaviour during near-vent mixing and for the Y/Ho ratio of Proterozoic seawater. *Chem. Geol.,* 155, 77-90.

Bazylinski, D.A. and Frankel, R.B. (1992) Production of iron sulfide minerals by magnetotactic bacteria in sulfidic environments. In: (eds. Skinner, H.C.W. and Fitzpatrick, R.W.) *Biomineralization Processes of Iron and Manganese - Modern and Ancient Environments*, Catena, Cremlingen-Destedt, 147-159.

Beard, B., Johnson, C.M., Cox, L., Sun, H., Nealson, K.H. and Aguilar, C. (1999) Iron Isotope Biosignatures. *Science,* 285, 1889-1896.

Becker, K. and von Herzen, R.P. (1996) Pre-drilling observations of conductive heat flow at the TAG active mound using *Alvin*. In: (eds. Humphris, S.E., Herzig, P.M., Miller, D.J. *et al.*) *Proc. ODP, Sci. Results*, Vol. 158, College station, TX (Ocean Drilling Program), 23-29.

Bence, A.E. (1983) Volcanogenic massive sulfides: rock/water interactions in basaltic systems and their effects on the distribution of rare earth elements and selected first series transition elements. *Proceedings of the 4th International Symposium on water rock interaction*, 48-49.

Bender, M.L., Broecker, W.S., Gornitz, V., Middel, U., Kay, R., Sun, S.-S. and Biscaye, P. (1971) Geochemistry of three cores from the East Pacific Rise. *Earth Planet. Sci. Let.,* 12, 425-433.

Berner, R.A. (1980) *Early diagenesis: a theoretical approach.* Princeton University Press, Princeton.

Beveridge, T.J. and Murray, R.G.E. (1976) Uptake and retention of metals by cell walls of *Bacillus subtilis. J. Bacteriol.,* 127, 1502-1508.

Bischoff, J.L. (1969) Red Sea geothermal brine deposits: Their mineralogy, chemistry, and genesis. In: (eds. Degens, E.T. and Ross, D.A.) *Hot Brines and Recent Heavy Metal Deposits in the Red Sea*, Springer, New York, 369-401.

Bischoff, J.L. (1972) A ferroan nontronite from the Red Sea geothermal system. *Clays & Clay Miner.,* 20, 217-223.

Blakemore, R.P., Short, K.A., Bazylinski, D.A., Rosenblatt, C. and Frankel, R.B. (1985) Microaerobic conditions are required for magnetite formation within *Aquaspirillum magnetotacticum. Geomicrobiol. J.,* 4(1), 53-71.

Blochl, E., Rachel, R., Burggraf, S., Hafenbradl, D., Jannasch, H.W. and Stetter, K.O. (1997) *Pyrolobus fumarii*, gen. and sp. nov., represents a novel group of archaea, extending the upper temperature limit for life to 113°C. *Extremophiles,* 1, 14-21.

Böhlke, J.K., Alt, J.C. and Muehlenbachs, K. (1984) Oxygen isotope - water relations in the altered deep-sea basalts: low temperature mineralogical controls. *Can. J. Earth Sci.,* 21, 67-77.

Bonatti, E. (1975) Metallogenesis at ocean spreading centres. *Ann. Rev. Earth Planet. Sci. Lett.,* 3, 401-431.

Boström, K., Josenuu, O. and Fisher, D.E. (1969) Aluminium-poor ferromanganoan sediments on active oceanic ridges. *J. Geophys. Res.,* 74, 3261-3270.

Boström, K. and Peterson, M.N.A. (1966) Precipitates from the hydrothermal exhalations on the East Pacific Rise. *Econ. Geol.,* 61, 1258-1265.

Boström, K. and Peterson, M.N.A. (1969) The origin of aluminium-poor ferromanganoan sediments in areas of high heat flow on the East Pacific Rise. *Mar. Geol.,* 7, 427-447.

Bottrell, S.H., Parkes, R.J., Cragg, B.A. and Raiswell, R. (submitted) Isotopic evidence for deep anoxic pyrite oxidation and stimulation of bacterial sulfate reduction. *Geology.*

Bowers, T.S., Campbell, A.C., Measures, C.I., Spivak, A.J., Khadem, M. and Edmond, J. (1988) Chemical controls on the composition of vent fluids at 13°-11°N and 21°N, East Pacific Rise. *J. Geophys. Res.,* 93, 4522-4536.

Bowers, T.S., Von Damm, K.L. and Edmond, J.M. (1985) Chemical evolution of mid-ocean ridge hot springs. *Geochim. Cosmochim. Acta,* 49, 2239-1152.

Boyle, J.F. (1987) The composition and origin of oxide metalliferous sediments from the Troodos ophiolite, Cyprus. *Ophiolites - oceanic crustal analogues*, 705-717.

BRAVEX Scientific team. (1994) BRAVEX/94: A joint British-Russian expedition to the TAG and Broken Spur hydrothermal vent sites on the Mid-Atlantic Ridge at 26° and 19° N. *BRIDGE Newsletter,* 7, 6-9.

Broecker, W.S. and Peng, T.-H. (1982) *Tracers in the Sea.* Columbia University & Lamont-Doherty Geological Observatory, Palisades, NY.

Burdige, D.J., Dhakar, S.P. and Nealson, K.H. (1992) The role of manganese oxide mineralogy on microbial and chemical manganese reduction. *Geomicrobiol. J.,* 10, 27-48.

Burdige, D.J. and Nealson, K.H. (1986) Chemical and microbiological studies of sulfide-mediated manganese reduction. *Geomicrobiol. J.,* 4(4), 361-387.

Burggraf, L.W., Hansen, S.D. and Bleckmann, C.A. (1998) Metabolic inhibition by transition metal ions in a slow-growing, toluene-enriched microbial population. *Env. Toxic. Water Qual.,* 13(3), 249-261.

Burlage, R.S., Atlas, R., Stahl, D., Geesey, G. and Sayler, G. (1998) *Techniques in microbial ecology.* Oxford University Press, Oxford.

Butterfield, D.B., Jonasson, I.R., Massoth, G.J., Feely, R.A., Roe, K.K., Embley, R.E., Holden, J.F., McDuff, R.E., Lilley, M.D. and Delaney, J.R. (1997) Seafloor eruptions and evolution of hydrothermal fluid chemistry. *Philos. Trans. R. Soc. London A,* 355(1723), 369-386.

Butterfield, D.B. and Massoth, G.J. (1994) Geochemistry of north Cleft segment vent fluids: temporal changes in chlorinity and their possible relation to recent volcanism. *J. Geophys. Res.,* 99(B3), 4951-4968.

Butterfield, D.B., McDuff, R.E., Mottl, M.J., Lilley, M.D., Lupton, J.E. and Massoth, G.J. (1994) Gradients in the composition of hydrothermal fluids from the Endeavor segment vent field - phase-separation and brine loss. *J. Geophys. Res.,* 99(B5), 9561-9583.

Campbell, A.C. (1991) Mineralogy and chemistry of marine particles by synchotron x-ray spectrometry, Mössbauer spectrometry and plasma-mass spectrometry. In: (eds. Hurd, D.C. and Spencer, D.W.) *Marine particles: analysis and characterization*, Vol. Geophys. Monogr. 63, American Geophysical Union, Washington, 375-390.

Campbell, A.C., Palmer, M.R., Klinkhammer, G.P., Bowers, T.S., Edmond, J.M.L., J.R., Casey, J.F., Thompson, G., Humphris, S.E., Rona, P.A. and Karson, J.A. (1988) Chemistry of hot springs on the Mid-Atlantic Ridge. *Nature,* 335, 514-519.

Canfield, D.E. (1991) Sulfate reduction in deep-sea sediments. *Am. J. Sci.,* 291, 177-188.

Canfield, D.E. (1993) Organic matter oxidation in marine sediments. In: (eds. Wollast, R., Mackenzie, F.T. and Chou, L.) *Interactions of C, N, P and S biogeochemical cycles and global change*, Springer-Verlag, Berlin, 333-363.

Canfield, D.E. and Thamdrup, B. (1990) The production of ^{34}S depleted sulfide during bacterial disproportionation of elemental sulfur. *Science,* 206, 1973-1975.

Canfield, D.E., Thamdrup, B. and Hansen, J.W. (1993) The anaerobic degradation of organic matter in Danish coastal sediments: Iron reduction, manganese reduction, and sulfate reduction. *Geochim. Cosmochim. Acta,* 57, 3867-3883.

Cann, J.R. and Strens, M.R. (1989) Modeling periodic megaplume emission by black smoker systems. *J. Geophys. Res.,* 94(B9), 12,227-12,237.

Cantrell, K.J. and Byrne, R.H. (1987) Rare earth element complexation by carbonate complexation. *J. Sol. Chem.,* 16, 555-566.

Chadwick, W.W., Embley, R.W. and Fox, C.G. (1991) Evidence for volcanic eruption on the southern Juan de Fuca Ridge between 1981 and 1987. *Nature,* 350, 416-418.

Chapelle, F.H. and Lovley, D.R. (1992) Competitive exclusion of sulfate reduction by Fe(III)-reducing bacteria: a mechanism for producing discrete zones of high-iron groundwater. *Ground Water,* 30(1), 29-36.

Chen, J.-H., Lion, L.W., Ghiorse, W.C. and Shuler, M.L. (1995) Mobilization of adsorbed cadmium and lead in aquifer material by bacterial extracellular polymers. *Wat. Res.,* 29, 421-431.

Chiba, H., Uchiyama, N. and Teagle, D.A.H. (1998) Stable isotope study of anhydrite and sulphide minerals at the TAG hydrothermal mound, Mid-Atlantic Ridge, 26°N. In: (eds. Herzig, P.M., Humphris, S.E., Miller, D.J. and Zierenberg, R.A.) *Proc. ODP, Sci. Results*, Vol. 158, College station, TX (Ocean Drilling Program), 85-90.

Claypool, G.E. and Kaplan, I.R. (1974) The origin and distribution of methane in marine sediments. In: (ed. Kaplan, I.R.) *Natural Gases in Marine Sediments*, Plenum Press, New York, 99-139.

Cline, J.D. (1969) Spectrophotometric determination of hydrogen sulfide in natural waters. *Limnol. Oceanogr.,* 14, 454-458.

Cole, T. (1988) The nature and origin of smectite in the Atlantis II Deep, Red Sea. *Can. Min.,* 26, 755-763.

Coleman, M.L., Hedrick, D.B., Lovley, D.R., White, D.C. and Pye, K. (1993) Reduction of Fe(III) in sediments by sulphate-reducing bacteria. *Nature,* 361(6411), 436-438.

Colley, S. and Thomson, J. (1985) Recurrent uranium relocations in distal turbidites emplaced in pelagic conditions. *Geochim. Cosmochim. Acta,* 49(11), 2339-2348.

Colley, S., Thomson, J. and Toole, J. (1989) Uranium relocation and derivation of quasi-isochrons for a turbidite/pelagic sequence in the northeast Atlantic. *Geochim. Cosmochim. Acta,* 53, 1223-1234.

Constantinou, G. and Govett, G.J.S. (1972) Genesis of sulphide deposits, ochre and umber of Cyprus. *Trans. Inst. Min. Metall.,* 81, 34-46.

Converse, D.R., Holland, H.D. and Edmond, J.M. (1984) Flow rates in the axial hot springs of the East Pacific Rise (21°N): implications for the heat budget and the formation of massive sulfides. *Earth Planet. Sci. Let.,* 69, 159-175.

Corliss, J.B. (1971) The origin of metal bearing hydrothermal solutions. *J. Geophys. Res.,* 76, 8128-8138.

Corliss, J.B., Dymond, J., Gordon, L., Edmond, J., von Herzen, R., Ballard, R., Green, K., Williams, D., Bainbridge, A., Crane, K. and van Andel, T. (1979) Submarine thermal springs on the Galapagos rift. *Science,* 203, 1073-1083.

Corliss, J.B., Lyle, M. and Dymond, J. (1978) The chemistry of hydrothermal mounds near the Galapagos Rift. *Earth Planet. Sci. Let.,* 40, 12-24.

Cowen, J.P., Bertram, M.A., Baker, E.T., Feely, R.A., Massoth, G.J. and Summit, M. (1998) Geomicrobial transformation of manganese in Gorda Ridge event plumes. *Deep-Sea Res.,* 45(12), 2713-2737.

Cowen, J.P., Massoth, G.J. and Baker, E.T. (1986) Bacterial scavenging of Mn and Fe in a mid- to far-field hydrothermal particle plume. *Nature,* 322, 169-171.

Cragg, B.A., Harvey, S.M., Fry, J.C., Herbert, R.A. and Parkes, R.J. (1992) Bacterial biomass and activity in the deep sediment layers of the Japanese Sea, Hole 798B. In: (eds. Pisciotte, K.A., Ingle Jr., J.C., Breymann, M.T.v. and Barron, J.) *Proc. ODP, Sci. Results*, Vol. 127/128, Pt.1, College station, TX (Ocean Drilling Program), 761-776.

Cragg, B.A. and Parkes, R.J. (1993) Bacterial profiles in hydrothermally active deep sediment layers from the Middle Valley (N.E. Pacific) Sites 857 and 858. In: (eds. Mottl, M.J., Davis, E.E. and Fisher, A.T.) *Proc. ODP, Sci. Results*, Vol. 139, College Station, TX (Ocean Drilling Program), 509-516.

Cragg, B.A., Parkes, R.J., Fry, J.C., Herbert, R.A., Wimpenny, J.W.T. and J.M.Getliff. (1990) Bacterial biomass and activity profiles within deep sediment layers. In: (eds. Suess, E. and von Huene, R..) *Proc. ODP, Sci. Results*, Vol. 112, College station, TX (Ocean Drilling Program), 607-619.

Cronan, D.S., van Andel, T.H., Heath, G., R., Dinkelmann, M.G., Bennet, R.H., Bukry, D., Charleston, S., Kaneps, A., Rodolfo, K.S. and Yeats, R.S. (1972) Iron-rich basal sediments from the eastern equatorial Pacific: Leg 16, Deep Sea Drilling Project. *Science,* 175, 61-63.

De Carlo, E.H., McMurtry, G.M. and Yeh, H.-W. (1983) Geochemistry of hydrothermal deposits from Loihi submarine volcano, Hawaii. *Earth Planet. Sci. Let.,* 66, 438-449.

Delaney, J.R., Robigou, V., McDuff, R.E. and Tivey, M.K. (1992) Geology of a vigorous hydrothermal system on the Endeavour segment, Juan de Fuca Ridge. *J. Geophys. Res.,* 97, 19,663-19,682.

Deming, J.W. and Baross, J.A. (1993) Deep-sea smokers: Windows to a subsurface biosphere? *Geochim. Cosmochim. Acta,* 57, 3219-3230.

Detrick, R.S., Buhl, P., Vera, J., Mutter, J.C., Orcutt, J., Madsen, J. and Brocher, T. (1987) Multi-channel seismic imaging of a crustal magma chamber along the East Pacific Rise. *Nature,* 326, 35-41.

Detrick, R.S., Honnorez, J., Adamson, A.C., Brass, G., Gillis, K.M., Humphris, S.E., Mevel, C., Meyer, P., Peterson, N., Rautenschlein, M., Shibata, T., Staudigel, H., Yamamoto, K. and Woolridge, A.L. (1988) Drilling the Snake Pit hydrothermal sulfide deposit on the Mid-Atlantic Ridge, latitude 23°22'N. *Geology,* 14, 1004-1007.

Douville, E., Bienvenu, P., Charlou, J.L., Donval, J.P., Fouquet, Y., Appriou, P. and Gamo, T. (1999) Yttrium and rare earth elements in fluids from various deep-sea hydrothermal systems. *Geochim. Cosmochim. Acta,* 63(5), 627-643.

Drobner, E., Huber, H., Wächtershäuser, G., Rose, D. and Stetter, K.O. (1990) Pyrite formation linked with hydrogen evolution under anaerobic conditions. *Nature,* 346, 742-744.

Dymond, J., Corliss, J.B., Cobler, R., Muratli, C.M., Chou, C. and Conard, R. (1980) Composition and origin of sediments recovered by deep drilling of sediment mounds, Galapagos Spreading Centre. In: (eds. Rosenthal, B.R., Hékinian, R. *et al.*) *Init. Repts DSDP*, Vol. 54, U.S. Government Printing Office, Washington, 377-385.

Dymond, J., Corliss, J.B., Heath, G.R., Field, C.W., Dasch, E.J. and Veeh, H.H. (1973) Origin of metalliferous sediments from the Pacific ocean. *Geol. Soc. Am. Bull.,* 84, 3355-3371.

Dymond, J. and Eklund, W. (1978) A microprobe study of metalliferous sediment components. *Earth Planet. Sci. Let.,* 40(2), 243-251.

Eberhard, C., Wirsen, C.O. and Jannasch, H.W. (1995) Oxidation of polymetal sulfides by chemolithoautotrophic bacteria from deep-sea hydrothermal vents. *Geomicrobiol. J.,* 13(3), 145-164.

Eberhart, G.L., Rona, P.A. and Honnorez, J. (1989) Geologic controls of hydrothermal activity in the mid-atlantic ridge rift-valley - tectonics and volcanics. *Mar. Geophys. Res.,* 10(3-4), 233-259.

Edmond, J.M., Campbell, G.A., Palmer, M.R., Klinkhammer, G.P., German, C.R., Edmonds, H.N., Elderfield, H., Thompson, G. and Rona, P.A. (1995) Time series study of vent fluids from the TAG and MARK sites (1986, 1990) Mid-Atlantic Ridge: a new solution chemistry model and a mechanism for Cu/Zn zonation in massive sulphide orebodies. In: (eds. Parson, L.M., Walker, C.L. and Dixon, D.R.) *Hydrothermal Vents and Processes,* Special Publication 87, Geological Society, London, 77-86.

Edmond, J.M., Measures, C., McDudd, R., Chan, L.H., Collier, R., Grant, B., Gordon, L.I. and Corliss, J.B. (1979a) Ridge crest hydrothermal activity and the balances of major and minor elements in the ocean: the Galapagos data. *Earth Planet. Sci. Let.,* 46, 1-18.

Edmond, J.M., Measures, C., Mangum, B., Grant, B., Sclater, F.R., Collier, R., Hudson, A., Gordon, L.I. and Corliss, J.B. (1979b) On the formation of metal-rich deposits at ridge crests. *Earth Planet. Sci. Let.,* 46, 19-30.

Edmonds, H.N., German, C.R., D.R.H., G., Huh, Y., Gamo, T. and Edmond, J.M. (1996) Continuation of the hydrothermal fluid chemistry time series at TAG, and the effects of ODP drilling. *Geophys. Res. Lett.,* 23(23), 3487-3490.

Ehrlich, H.L. (1996) *Geomicrobiology*. Marcel Dekker, New York.

Ehrlich, H.L. and Brierley, C.L. (1990) *Microbial mineral recovery*. McGraw-Hill, New York.

Elderfield, H. (1988) The oceanic chemistry of the rare-earth elements. *Philos. Trans. R. Soc. London A,* 325, 105-126.

Elderfield, H. and Schultz, A. (1996) Mid-ocean ridge hydrothermal fluxes and the chemical composition of the ocean. *Ann. Rev. Earth Planet. Sci. Lett.,* 24, 191-224.

Elsgaard, L., Isaksen, M.F., Jørgensen, B.B., Alayse, A.-M. and Jannasch, H.W. (1994) Microbial sulfate reduction at the Guaymas Basin hydrothermal vent area: Influence of temperature and substrate. *Geochim. Cosmochim. Acta,* 58, 3335-3343.

Embley, R.W., Chadwick, W.W., Jonasson, I.R., Butterfield, D.B. and Baker, E.T. (1995) Initial results of the rapid response to the 1993 Coaxial event - relationships between hydrothermal and volcanic processes. *Geophys. Res. Lett.,* 22(2), 143-146.

Embley, R.W., Jonasson, I.R., Perfit, M.R., Franklin, J.M., Tivey, M.K., Malahoff, A., Smith, M.F. and Francis, T.J.G. (1988) Submersible investigation of an extinct hydrothermal system on the Galapagos Ridge: sulfide mounds, stockwork zone, and differentiated lavas. *Can. Min.,* 26, 517-539.

Emerson, S. (1985) Organic carbon preservation in marine sediments. In: (eds. Sundquist, E.T. and Broecker, W.S.) *The carbon cycle and atmospheric CO2: natural variations Archean to Present,* AGU Geophysical Monograph, Vol. 32, American Geophysical Union, Washington.

Evangelou, V.P. and Zhang, Y.L. (1995) A review: Pyrite oxidation mechanisms and acid mine drainage prevention. *Crit. Rev. Env. Sci. Technol.,* 25(2), 141-199.

Evensen, N.H., Hamilton, P.J. and O'Nions, R.K. (1978) Rare earth abundances in chondritic meteorites. *Geochim. Cosmochim. Acta,* 42, 1199-1212.

Feely, R.A., Geiselman, T.L., Baker, E.T. and Massoth, G.J. (1990) Distribution and composition of hydrothermal plume particles from the ASHES vent field at the Axial Volcano, Juan de Fuca Ridge. *J. Geophys. Res.,* 95(B8), 12,855-12,873.

Feely, R.A., Massoth, G.J., Baker, E.T., Lebon, G.T. and Geiselman, T. (1992) Tracking the dispersal of hydrothermal plumes from the Juan de Fuca Ridge using suspended matter composition. *J. Geophys. Res.,* 94(B3), 3457-3468.

Feely, R.A., Massoth, G.J., Trefry, J.H., Baker, E.T., Paulson, A.J. and Lebon, G.T. (1994) Composition and sedimentation of hydrothermal plume particles from north Cleft segment, Juan de Fuca Ridge. *J. Geophys. Res.,* 99(B3), 4985-5006.

Feely, R.A., Trefry, J.H., Massoth, G.J. and Metz, S. (1991) A comparison of the scavenging of phosphorus and arsenic from seawater by hydrothermal iron oxyhydroxides in the Atlantic and Pacific Oceans. *Deep-Sea Res.,* 38, 617-623.

Ford, T. and Mitchell, R. (1992) Microbial transport of toxic metals. In: (ed. Mitchell, R.) *Environmental Microbiology*, Wiley-Liss, Chichester, 83-101.

Fortin, D., Ferris, F.G. and Scott, S.T. (1998) Formation of Fe-silicates and Fe-oxides on bacterial surfaces in samples collected near hydrothermal vents on the Southern Explorer Ridge in the northeast Pacific Ocean. *Am. Mineral.,* 83, 1399-1408

Fouquet, Y. (1997) Where are the large hydrothermal sulphide deposits in the oceans? *Philos. Trans. R. Soc. London A,* 355(1723), 427-440.

Fouquet, Y., Auclair, G., Cambon, P. and Etoubleau, P.J. (1988) Geological setting, mineralogical, and geochemical investigations on sulfide deposits near 13°N on the East Pacific Rise. *Mar. Geol.,* 84, 145-178.

Fouquet, Y., Henry, K., Knott, R. and Cambon, P. (1998) Geochemical section of the TAG hydrothermal mound. In: (eds. Herzig, P.M., Humphris, S.E., Miller, D.J. and Zierenberg, R.A.) *Proc. ODP, Sci. Results*, Vol. 158, College station, TX (Ocean Drilling Program), 363-387.

Fouquet, Y., von Stackelberg, J.-L., Charlou, J., Erzinger, P.M., Herzig, P.M., Mühe, R. and Wiedicke, M. (1993) Metallogenesis in back-arc environments: The Lau Basin example. *Econ. Geol.,* 88, 2154-2181.

Froelich, P.N., Klinkhammer, G.P., Bender, M.L., Luedtke, N.A., Health, G.R., Cullen, D., Dauphin, P., Hammond, D., Hartman, B. and Maynard, V. (1979) Early organic matter in pelagic sediments of the eastern equatorial Atlantic: suboxic diagenesis. *Geochim. Cosmochim. Acta,* 43, 1075-1090.

Fry, J.C. (1988) Determination of biomass. In: (ed. Austin, B.) *Methods in aquatic bacteriology*, Wiley, Chichester, 27-72.

Fuhrman, J.A. and Azam, F. (1980) Bacterioplankton secondary production estimates for coastal water of British Columbia, Antarctica and California. *Appl. Environ. Microbiol.,* 39, 1085-1095.

Gadd, G.M. and White, C. (1993) Microbial treatment of metal pollution - a working biotechnology? *Trends Biotechnol.,* 11, 353-359.

Gamo, T., Chiba, H., Masuda, H., Edmonds, H.N., Fujioka, K., Kodama, Y., Nanba, H. and Sano, Y. (1996) Chemical characteristics of hydrothermal fluids from the TAG mound of the Mid-Atlantic Ridge in August 1994: Implications for spatial and temporal variability of hydrothermal activity. *Geophys. Res. Lett.,* 23(23), 3483-3486.

Gemmell, J.B. and Sharpe, R. (1998) Detailed sulphur-isotope investigation of the TAG hydrothermal mound and stockwork zone, 26°N, Mid-Atlantic Ridge. In: (eds. Herzig, P.M., Humphris, S.E., Miller, D.J. and Zierenberg, R.A.) *Proc. ODP, Sci. Results*, Vol. 158, College station, TX (Ocean Drilling Program), 71-84.

German, C.R., Baker, E.T. and Klinkhammer, G.P. (1995) Regional settings of hydrothermal activity. In: (eds. Parson, L.M., Walker, C.L. and Dixon, D.R.) *Hydrothermal Vents and Processes,* Special Publication 87, Geological Society, London, 3-15.

German, C.R., Baker, E.T., Mevel, C., Tamaki, K. and the FUJI Science Team. (1998) Hydrothermal activity along the southwest Indian ridge. *Nature,* 395, 490-493.

German, C.R., Campbell, A.C. and Edmond, J.M. (1991a) Hydrothermal scavenging at the Mid-Atlantic Ridge: Modification of trace element dissolved fluxes. *Earth Planet. Sci. Let.,* 107, 101-114.

German, C.R., Fleer, A.P., Bacon, M.P. and Edmond, J.M. (1991b) Hydrothermal scavenging at the Mid-Atlantic Ridge: Radionuclide distribution. *Earth Planet. Sci. Let.,* 105, 170.

German, C.R., Higgs, N.C., Thomson, J., Mills, R.A., Elderfield, H., Blusztajn, J., Fleer, A.P. and Bacon, M.P. (1993) A geochemical study of metalliferous sediment from TAG hydrothermal mound, 26°08'N, Mid-Atlantic Ridge. *J. Geophys. Res.,* 98, 9683-9692.

German, C.R., Klinkhammer, G.P., Edmond, J.M., Mitra, A. and Elderfield, H. (1990) Hydrothermal scavenging of rare earth elements in the ocean. *Nature,* 345, 516-518.

Getliff, J.M., Fry, J.C., Cragg, B.A. and Parkes, R.J. (1992) The potential for bacterial growth in deep sediments layers of the Japan Sea, Hole 789B - Leg 128. In: (eds. Pisciotto, K.A., Ingle, J.C., von Breymann, M.T., Barron, J. *et al.*) *Proc. ODP, Sci. Results*, Vol. 127/128, College station, TX (Ocean Drilling Program), 755-759.

Ghiorse, W.C. (1984) Biology of iron- and manganese depositing bacteria. *Annu. Rev. Microbiol.,* 38, 515-550.

Gillis, K.M., Smith, A.D. and Ludden, J.N. (1990) Trace element and Sr isotopic contents of hydrothermal clays and sulfides from the Snakepit hydrothermal field: ODP site 649. In: (eds. Detrick, R., Honnorez, J., Bryan, W.B. and Juteau, T.) *Proc. ODP, Sci. Results*, Vol. 106/109, College Station, TX (Ocean Drilling Program), 315-319.

Goldhaber, M.B. and Kaplna, I.R. (1980) Mechanism of sulfur incorporation and isotopic fractionation during early diagenesis in sediments of the Gulf of California. *Mar. Chem.,* 9, 95-143.

Goulder, R. (1977) Attached and free bacteria in an estuary with abundant suspended solids. *J. Appl. Bacteriol.,* 43, 399-405.

Goulding, H.C. (1998) Genesis and preservation of metalliferous sediments. PhD, University of Southampton.

Goulding, H.C., Mills, R.A. and Nesbitt, R.W. (1998) Precipitation of hydrothermal sediments on the active TAG mound: implications for ochre formation. In: (eds. Mills, R.A. and Harrison, K.) *Modern Ocean Floor Processes and the Geological Record,* Special Publication 148, Geological Society, London, 201-216.

Govindaraju, K. (1996) 1996 compilation of working values and sample description for 383 geostandards. *Geostand. Newsletter Spec. Iss.,* 18, 1-158.

Grant, W.D., Gemmell, R.T. and McGenity, T.J. (1998) Halobacteria: the evidence for longevity. *Extremophiles,* 2(3), 279-287.

Gwynn, J.P. (1998) Chemical and isotopic investigation into the origin of clay minerals from the TAG hydrothermal mound, Mid-Atlantic Ridge. unpublished MSc, University of Southampton.

Hammond, S.R. (1990) Relationship between lava types, seafloor morphology, and occurrence of hydrothermal venting in the ASHES vent field of Axial volcano. *J. Geophys. Res.,* 95, 12,875-12,894.

Hannington, M.D. (1993) The formation of atacamite during weathering of sulphides on the modern sea-floor. *Can. Min.,* 31(4), 945-956.

Hannington, M.D., Galley, A.G., Herzig, P.M. and Petersen, S. (1998) Comparison of the TAG mound and the stockwork complex with Cyprus-type massive sulphide deposits. In: (eds. Herzig, P.M., Humphris, S.E., Miller, D.J. and Zierenberg, R.A.) *Proc. ODP, Sci. Results*, Vol. 158, College station, TX (Ocean Drilling Program), 389-415.

Hannington, M.D., Herzig, P.M., Scott, S.D., Thompson, G. and Rona, P.A. (1991) Comparative mineralogy and geochemistry of gold-bearing sulfide deposits on the mid-ocean ridges. *Mar. Geol.,* 101, 217-248.

Hannington, M.D., Jonasson, I.R., Herzig, P.M. and Petersen, S. (1995) Physical and chemical processes of seafloor mineralisation at the Mid-Ocean Ridges. In: (eds. Humphris, S.E., Zierenberg, R.A., Mullineaux, L.S. and Thomson, R.E.) *Seafloor Hydrothermal Systems: Physical, Chemical, Biological and Geological Interactions,* Geophysical Monograph 91, American Geophysical Union, Washington, 115-157.

Hannington, M.D., Thompson, G., Rona, P.A. and Scott, S. (1988) Gold and native copper in supergene sulfides from the Mid-Atlantic Ridge. *Nature,* 333, 64-66.

Hansen, L.B., Finster, K., Fossing, H. and Iversen, N. (1998) Anaerobic methane oxidation in sulfate depleted sediments: Effects of sulfate and molybdate additions. *Aquat. Microbial Ecol.,* 14(2), 195-204.

Harder, H. (1976) Nontronite synthesis at low temperatures. *Chem. Geol.,* 18, 169-180.

Hausinger, R.P. (1987) Nickel utilisation by microorganism. *Microbiol. Rev.,* 51, 22-42.

Haymon, R.M., Fornari, D.J., Von Damm, K.L., Lilley, M.D., Perfit, M.R., Edmond, J.M., Shanks, W.C. III, Lutz, R.A., Grebmeier, J.M., Carbotte, S., Wright, C.D., McLaughlin, E., Smith, M., Beedle, N. and Olson, E. (1993) Volcanic eruption of the mid-ocean ridge along the East Pacific Rise crest at 9°45-52'N: Direct submersible observations of seafloor phenomena associated with an eruption event in April, 1991. *Earth Planet. Sci. Let.,* 119(1-2), 85-101.

Haymon, R.M. and Kastner, M. (1986) The formation of high temperature clay minerals from basalt alteration during hydrothermal discharge on the East Pacific Rise axis at 21°N. *Geochim. Cosmochim. Acta,* 50, 1933-1939.

Heath, G.R. and Dymond, J. (1977) Genesis and transformation of metalliferous sediments from the East Pacific Rise, Bauer Deep, and Central Basin, northwest Nazca plate. *Geol. Soc. Am. Bull.,* 88(5), 723-733.

Heath, G.R., Moore, T.C. and Dauphin, J.P. (1977) Organic carbon in deep-sea sediments. In: (eds. Anderson, N.R. and Malahoff, A.) *The fate of fossil fuel CO_2 in the oceans*, Plenum Press, New York, 605-625.

Hékinian, R., Hoffert, M., Larqué, P., Cheminée, J.L., Stoffers, P. and Bideau, D. (1993) Hydrothermal Fe and Si oxyhydroxide deposits from South Pacific intraplate volcanoes and East Pacific Rise axial and off-axial regions. *Econ. Geol.,* 88, 2099-2121.

Henderson, P. (1984) General geochemical properties and abundances of the rare earth elements. In: (ed. Henderson, P.) *Rare earth element geochemistry*, Elsevier, Amsterdam, 1-29.

Herzig, P.M., Hannington, M.D., Scott, S.D., Maliotis, G., Rona, P.A. and Thompson, G. (1991) Gold-rich seafloor gossans in the Troodos ophiolite and on the Mid-Atlantic Ridge. *Econ. Geol.,* 86, 1747-1755.

Herzig, P.M., Petersen, S. and Hannington, M.D. (1998) Geochemistry and sulfur-isotopic composition of the TAG hydrothermal mound, Mid-Atlantic Ridge, 26°N. In: (eds. Herzig, P.M., Humphris, S.E., Miller, D.J. and Zierenberg, R.A.) *Proc. ODP, Sci. Results*, Vol. 158, College station, TX (Ocean Drilling Program), 47-70.

Hodell, D.A., Mueller, P.A. and Garrido, J.R. (1991) Variations in strontium isotopic of seawater during the Neogene. *Geology,* 19, 24-27.

Honnorez, J., Alt, J.C. and Humphris, S.E. (1998) Vivisection and autopsy of active and fossil hydrothermal alterations of basalt beneath and within the TAG hydrothermal mound. In: (eds. Herzig, P.M., Humphris, S.E., Miller, D.J. and Zierenberg, R.A.) *Proc. ODP, Sci. Results*, Vol. 158, College Station, TX (Ocean Drilling Program), 231-254.

Honnorez, J., Von Herzen, R.P., Barret, T.J., Becker, K., Bender, M.L., Borella, P.E., Hubberton, H.W., Jones, S.C., Karato, S., Laverne, C., Levi, S., Migidisov, A.A., Moorby, S.A. and Schrader, E.L. (1981) Hydrothermal mounds and young ocean crust of the Galapagos: preliminary deep sea drilling results, leg 70. *Geol. Soc. Am. Bull.,* 92, 457-472.

Hopkinson, L., Roberts, S., Herrington, R. and Wilkinson, J. (1998) Self-organization of submarine hydrothermal silicious deposits: Evidence from the TAG hydrothermal mound, 26°N Mid-Atlantic Ridge. *Geology,* 26(4), 347-350.

Humphris, S.E. (1998) Rare earth element composition of anhydrite: Implications for deposition and mobility within the active TAG hydrothermal mound. In: (eds. Herzig, P.M., Humphris, S.E., Miller, D.J. and Zierenberg, R.A.) *Proc. ODP, Sci. Results*, Vol. 158, College station, TX (Ocean Drilling Program), 143-159.

Humphris, S.E., Herzig, P.M., Miller, D.J., Alt, J.C., Becker, K., Brown, D., Brugmann, G., Chiba, H., Fouquet, Y., Gemmell, J.B., Guerin, G., Hannington, M.D., Holm, N.G., Honnorez, J., Iturrino, G.J., Knott, R., Ludwig, R., Nakamura, K., Petersen, S., Reysenbach, A.-L., Rona, P.A.,

Smith, S., Sturz, A.A., Tivey, M.K. and Zhao, X. (1995) The internal structure of an active sea-floor massive sulphide deposit. *Nature,* 377, 713-716.

Humphris, S.E. and Kleinrock, M.C. (1996) Detailed morphology of the TAG active hydrothermal mound: Insights into its formation and growth. *Geophys. Res. Lett.,* 23(23), 3443-3446.

Humphris, S.E., Melson, W.G. and Thompson, R.N. (1980) Basalt weathering on the East Pacific Rise and Galapagos Spreading Centre, DSDP Leg 54. In: (eds. Rosendahl, B.R., Hékinian, R. *et al.*) *Init. Repts DSDP*, Vol. 54, U.S. Government Printing Office, Washington.

Iversen, N. and Jørgensen, B.B. (1985) Anaerobic methane oxidation rates at the sulfate-methane transition in marine sediments from Kattegat and Skagerrak (Denmark). *Limnol. Oceanogr.,* 30(5), 944-955.

Jackson, M.L. (1969) *Soil Chemical Analysis - Advanced Course.* Madison, Wisconsin.

James, R.H. and Elderfield, H. (1996a) The chemistry of ore-forming fluids and mineral formation rates in an active hydrothermal sulfide deposit on the Mid-Atlantic Ridge. *Geology,* 24(12), 1147-1150.

James, R.H. and Elderfield, H. (1996b) Dissolved and particulate trace metals in hydrothermal plumes at the Mid-Atlantic Ridge. *Geophys. Res. Lett.,* 23(23), 3499-3502.

Janecky, D.R., Haymon, R.M., Benjamin, T.M., Rogers, P.S.Z. and Bayhurts, G.K. (1989) Microscopic distribution of trace elements in minerals (chlorites, sulfides, sulfates) in hydrothermal systems. In: (ed. Miles, D.L.) *Proceedings of the 6th International Symposium on Water-Rock Interaction*, Britsh Geological Survey, Wallingford, England, 327-330.

Janecky, D.R. and Seyfried, W.E. (1984) Formation of massive sulfide deposits on oceanic ridges: incremental reaction models for mixing between hydrothermal solutions and seawater. *Geochim. Cosmochim. Acta,* 48, 2723-2738.

Jannasch, H.W. (1985) The chemisynthetic support of life and the microbial diversity at deep-sea hydrothermal vents. *Proc. R. Soc. London B,* 225(1240), 277-297.

Jannasch, H.W. (1995) Microbial interactions with hydrothermal fluids. In: (eds. Humphris, S.E., Zierenberg, R.A., Mullineaux, L.S. and Thomson, R.E.) *Seafloor Hydrothermal Systems: Physical, Chemical, Biological and Geological Interactions,* Geophysical Monograph, Vol. 91, American Geophysical Union, Washington, 273-296.

Jannasch, H.W. (1997) Biocatalytic transformations of hydrothermal fluids. *Philos. Trans. R. Soc. London A,* 355(1723), 475-486.

Jannasch, H.W. and Mottl, M.J. (1985) Geomicrobiology of deep-sea hydrothermal vents. *Science,* 229(4715), 717-725.

Jannasch, H.W., Nelsen, T.A. and Wirsen, C.O. (1989) Massive natural occurrence of unusually large bacteria [Beggiatoa sp.] at a hydrothermal deep-sea vent site. *Nature,* 342, 834-836.

Jannasch, H.W. and Wirsen, C.O. (1979) Chemosynthetic primary production at the East Pacific sea floor spreading centers. *Bioscience,* 29, 592-598.

Jannasch, H.W. and Wirsen, C.O. (1981) Morphological survey of microbial mats near deep-sea thermal vents. *Appl. Environ. Microbiol.,* 42(2), 528-538.

Jardim, W.F. and Pearson, H.W. (1984) A study of the copper-complexing compounds released by some species of cyanobacteria. *Wat. Res.,* 18, 985-989.

Jenkins, W.J., Rona, P.A. and Edmond, J.M. (1980) Excess ^{3}He in the deep water over the Mid-Atlantic Ridge at 26°N: Evidence of hydrothermal activity. *Earth Planet. Sci. Let.,* 49, 39-44.

Johnstone, B.H. and Jones, R.D. (1989) A study on the lack of [methyl-^{3}H] thymidine uptake and incorporation by chemolithotrophic bacteria. *Microb. Ecol.,* 18, 73-79.

Jørgensen, B.B. (1978) A comparison of methods for the quantification of bacterial sulfate reduction in coastal marine sediments, I.Measurements with radiotracer techniques. *Geomicrobiol. J.,* 1(1), 11-27.

Jørgensen, B.B. (1982) Mineralisation of organic matter in the sea bed - the role of sulphate reduction. *Nature,* 296, 643-645.

Jørgensen, B.B. and Fenchel, T. (1974) The sulfur cycle a of marine model system. *Mar. Bio.,* 24, 189-201.

Jørgensen, B.B., Isaksen, M.F. and Jannasch, H.W. (1992) Bacterial sulfate reduction above 100°C in deep-sea hydrothermal vent sediments. *Science,* 258, 1756-1757.

Jørgensen, B.B., Zawacki, L.X. and Jannasch, H.W. (1990) Thermophilic bacterial sulfate reduction in deep-sea sediments at the Guaymas Basin hydrothermal vent site (Gulf of California). *Deep-Sea Res.,* 37(4), 695-710.

Juniper, S.K., Bird, D.F., Summit, M., Vong, M.P. and Baker, E.T. (1998) Bacterial and viral abundances in hydrothermal event plumes over northern Gorda Ridge. *Deep-Sea Res.,* 45(12), 2739-2749.

Juniper, S.K. and Fouquet, Y. (1988) Filamentous iron-silica deposits from modern and ancient hydrothermal sites. *Can. Min.,* 26, 859-869.

Juniper, S.K., Martineu, P., Sarrazin, J. and Gélinas, Y. (1995) Microbial mineral floc associated with nascent hydrothermal activity on CoAxial Segment, Juan de Fuca Ridge. *Geophys. Res. Lett.,* 22(2), 179-182.

Juniper, S.K. and Tebo, B.M. (1995) Microbe –metal interactions and mineral deposition at hydrothermal vents. In: (ed. Karl, D.M.) *The microbiology of deep-sea hydrothermal vents*, CRC Press, Boca Raton, FL, 219-253.

Kadko, D. (1993) An asssessment of the effect of chemical scavenging within submarine hydrothermal plumes upon ocean geochemisty. *Earth Planet. Sci. Let.,* 120, 361-374.

Kadko, D., Baross, J. and Alt, J.C. (1995) The magnitude and global implication of hydrothermal flux. In: (eds. Humphris, S.E., Zierenberg, R.A., Mullineaux, L.S. and Thomson, R.) *Seafloor Hydrothermal Systems: Physical, Chemical, Biological and Geological Interactions,* Geophysical Monograph 91, American Geophysical Union, Washington, 446-466.

Kadko, D., Feely, R.A. and Massoth, G.J. (1994) Scavenging of ^{234}Th and phosphorus removal from the hydrothermal effluent plume over the North Cleft segment of the Juan-de-Fuca Ridge. *J. Geophys. Res.,* 99(B3), 5017-5024.

Karl, D.M. (1995a) *The microbiology of deep-sea hydrothermal vents.* CRC Press, Boca Raton.

Karl, D.M. (1995b) Ecology of free-living, hydrothermal vent microbial communities. In: (ed. Karl, D.M.) *The microbiology of deep-sea hydrothermal vents*, CRC Press, Boca Raton, FL, 35-124.

Karpoff, A.M., Walter, A.-V. and Pflumio, C. (1988) Metalliferous sediments within lava sequences of the Sumail ophiolite (Oman): Mineralogical and geochemical characterization, origin and evolution. *Tectonophys.,* 151, 223-245.

Karson, J.A. and Rona, P.A. (1990) Block-tilting, transfer faults, and structural control of magmatic hydrothermal processes in the TAG area, Mid-Atlantic Ridge. *Geol. Soc. Am. Bull.,* 102, 1635-1345.

Kashefi, K. and Lovley, D.R. (2000) Reduction of Fe(III), Mn(IV), and toxic metals at 100°C by Pyrobaculum islandicum. *Appl. Environ. Microbiol.,* 66(3), 1050-1056.

Kelly, D.P., Norris, P.R. and Brierley, C.L. (1979) Microbial methods for the extraction and recovery of metals. In: (eds. Bull, A.T., Ellwood, D.C. and Ratledge, C.) *Microbial technology: current state, future prospects*, Cambridge University Press, Cambridge, 263-308.

Kelly, M. (1988) *Mining and the freshwater environment.* Elsevier, London.

King, G.M., Howes, B.L. and Dacey, J.W.H. (1985) Short-term endproducts of sulfate reduction in a salt marsh: Formation of acid volatile sulfides, elemental sulphur, and pyrite. *Geochim. Cosmochim. Acta,* 49, 1561-1566.

Kisch, H.J. (1983) Mineralogy and petrology of burial diagenesis (burial metamorphism) and incipient metamorphism in clastic rocks. In: (eds. Larsen, G. and Chilingar, G.V.) *Diagenesis in sediments and sedimentary rocks 2*, Elsevier, Amsterdam, 289-493.

Kleinrock, M. and Humphris, S.E. (1996) Structural control on sea-floor hydrothermal activity at the TAG active mound. *Nature,* 382, 149-153.

Kleinrock, M.C., Humphris, S.E. and the Deep-TAG team. (1996) Detailed structure and morphology of the TAG active hydrothermal mound and its geotectonic environment. In: (eds. Humphris, S.E., Herzig, P.M., Miller, D.J. *et al.*) *Proc. ODP, Sci. Results*, Vol. 158, College station, TX (Ocean Drilling Program), 15-21.

Klinkhammer, G.P. (1980) Early diagenesis in sediments from the eastern equatorial Pacific. II. Pore water metal results. *Earth Planet. Sci. Let.,* 49, 81-101.

Klinkhammer, G.P., Chin, C.S., Wilson, C. and German, C.R. (1995) Venting from the Mid-Atlantic Ridge at 37°17'N: the Lucky Strike hydrothermal site. In: (eds. Parson, L.M., Walker, C.L. and Dixon, D.R.) *Hydrothermal Vents and Processes,* Special Publication 87, Geological Society, London, 87-96.

Klinkhammer, G.P., Elderfield, H., Edmond, J.M. and Mitra, A. (1994) Geochemical implications of rare earth element patterns in hydrothermal fluids from mid-ocean ridges. *Geochim. Cosmochim. Acta,* 58, 5105-5113.

Klinkhammer, G.P., Elderfield, H. and Hudson, A. (1983) Rare earth elements in seawater near hydrothermal vents. *Nature,* 305, 185-188.

Klinkhammer, G.P. and Hudson, A. (1986) Dispersal patterns for hydrothermal plumes in the South Pacific using manganese as a tracer. *Earth Planet. Sci. Let.,* 79, 241-249.

Knott, R., Fouquet, Y., Honnorez, J., Petersen, S. and Bohn, M. (1998) Petrology of hydrothermal mineralization: a vertical section through the TAG mound. In: (eds. Herzig, P.M., Humphris, S.E., Miller, D.J. and Zierenberg, R.A.) *Proc. ODP, Sci. Results*, Vol. 158, College Station, TX (Ocean Drilling Program), 5-26.

Koeppenkastrop, D. and De Carlo, E.H. (1992) Sorption of rare-earth elements from seawater onto synthetic mineral particles: An experimental approach. *Chem. Geol.,* 95, 251-263.

Köhler, B., Singer, A. and Stoffers, P. (1994) Biogenic nontronite from marine white smoker chimneys. *Clays & Clay Miner.,* 42(6), 689-701.

Kong, L.S.L., Solomon, S.C. and Purdy, G.M. (1992) Microearthquake characteristics of a mid-ocean along axis. *J. Geophys. Res.,* 97, 1659-1685.

Koroleff, F. (1983) Determination of silicon. In: (eds. Grasshoff, K., Ehrhardt, M. and Kremling, K.) *Methods of seawater analysis*, Verlag Chemie, Basel, 174-183.

Koski, R.A., Clague, D.A. and Oudin, E. (1984) Mineralogy and chemistry of massive sulfide deposits from the Juan de Fuca Ridge. *Geol. Soc. Am. Bull.,* 95, 930-945.

Koski, R.A., Jonasson, I.R., Kadko, D., Smith, V.K. and Wong, F.L. (1994) Compositions, growth mechanisms, and temporal relations of hydrothermal sulfide-sulfate-silica chimneys at the northern Cleft segment, Juan-de-Fuca ridge. *J. Geophys. Res.,* 99(B3), 4813-4832.

Kostka, J.E. and Nealson, K.H. (1998) Isolation, cultivation and characterisation of iron- and manganese-reducing bacteria. In: (eds. Burlage, R.S., Atlas, R., Stahl, D., Geesey, G. and Sayler, G.) *Techniques in microbial ecology*, Oxford University Press, Oxford, 58-78.

Krauskopf, K.B. (1957) Separation of manganese form iron in sedimentary processes. *Geochim. Cosmochim. Acta,* 12, 61-84.

Ku, T.L., Bischoff, J.L. and Boersma, H. (1972) Age studies of Mid-Atlantic Ridge sediments near 42°N and 20°N. *Deep-Sea Res.,* 19, 233-247.

Kuhn, T., Bau, M., Blum, N. and Halbach, P. (1998) Origin of negative Ce anomalies in mixed hydrothermal-hydrogenetic Fe-Mn crusts from the Central Indian Ridge. *Earth Planet. Sci. Let.,* 163, 207-220.

Kvenvolden, K.A. and Simoneit, B.R.T. (1987) Petroleum from Northeast Pacific Ocean hydrothermal systems in Escanaba Trough and Guaymas Basin. *Bull. Am. Ass. Petrol. Geol.,* 71(5), 580.

Lalou, C. and Brichet, E. (1980) Anomalously high uranium contents in the sediment under Galapagos hydrothermal mounds. *Nature,* 284, 251-253.

Lalou, C., Reyss, J.L. and Brichet, E. (1998) Age of sub-bottom sulfide samples at the TAG active mound. In: (eds. Herzig, P.M., Humphris, S.E., Miller, D.J. and Zierenberg, R.A.) *Proc. ODP, Sci. Results*, Vol. 158, College station, TX (Ocean Drilling Program), 111-117.

Lalou, C., Reyss, J.L., Brichet, E., Arnold, M., Thompson, G. and Fouquet, Y. (1993) New age data for Mid-Atlantic ridge hydrothermal sites: TAG and Snakepit chronology revisited. *J. Geophys. Res.,* 98(B6), 9705-9713.

Lalou, C., Reyss, J.L., Brichet, E., Rona, P.A. and Thompson, G. (1995) Hydrothermal activity on a 10^5 -year scale at a slow-spreading ridge, TAG hydrothermal field, Mid-Atlantic Ridge 26°N. *J. Geophys. Res.,* 100, 17,855-17,862.

Lalou, C., Thompson, G., Rona, P.A., Brichet, E. and Jehanno, C. (1986) Chronology of selected hydrothermal Mn oxide deposits from the transatlantic geotraverse "TAG" area, Mid-Atlantic Ridge 26°N. *Geochim. Cosmochim. Acta,* 50, 1737-1743.

Lee, Y. and Tebo, B.M. (1994) Cobalt(II) oxidation by the marine Mn(II) oxidizing *Bacillus* sp. strain SG-1. *Appl. Environ. Microbiol.,* 60, 2949-2957.

Lester, J.N., Sterritt, R.M., Rudd, T. and Brown, M.J. (1984) Assessment of the role of bacterial extracellular polymers in controlling metal removal in biological waste water treatment. In: (eds. Grainger, J.M. and Lynch, J.M.) *Microbial Methods for Environmental Biotechnology*, Academic Press, London, 197-217.

Lister, C.R.B. (1972) On the thermal balance of a mid-ocean ridge. *Geophys. J. R. Astron. Soc.,* 26, 515-535.

Lovley, D.R. (1990) Magnetite formation during microbial dissimilatory iron reduction. In: (eds. Frankel, R.B. and Blakemore, R.P.) *Iron Biominerals*, Plenum Press, New York, 151-166.

Lovley, D.R. (1995) Bioremediation of organic and metal contaminants with dissimilatory metal reduction. *J. Ind. Microbiol.,* 14, 85-93.

Lovley, D.R. and Chapelle, F.H. (1995) Deep subsurface microbial processes. *Rev. Geophys.,* 33(3), 365-381.

Lovley, D.R. and Klug, M.J. (1982) Intermediary metabolism of organic matter in the sediment of a eutrophic lake. *Appl. Environ. Microbiol.,* 43, 552-560.

Lovley, D.R. and Phillips, E.J.P. (1987) Competitive mechanism for inhibition of sulfate reduction and methane production in the zone of ferric iron reduction in sediments. *Appl. Environ. Microbiol.,* 53, 2636-2641.

Lovley, D.R. and Phillips, E.J.P. (1988) Novel mode of microbial energy metabolism: organic carbon oxidation coupled to dissimilatory reduction of iron and manganese. *Nature,* 51, 683-689.

Lovley, D.R., Phillips, E.J.P., Gorby, Y.A. and Landa, E.R. (1991) Microbial reduction of uranium. *Nature,* 350, 413-416.

Lovley, D.R., Roden, E.E., Phillips, E.J.P. and Woodward, J.C. (1993) Enzymatic iron and uranium reduction by sulfate-reducing bacteria. *Mar. Geol.,* 113, 41-53.

Lovley, D.R., Stolz, J.F., Nord, G.L.J. and Phillips, E.J.P. (1987) Anaerobic production of magnetite by a dissimilatory iron-reducing microorganism. *Nature*(330), 252-254.

Lowell, R.P. and Germanovich, L.N. (1995) Dike injection and the formation of megaplumes at ocean ridges. *Science,* 267, 1804-1807.

Lupton, E. (1995) Hydrothermal plumes: near and far field. In: (eds. Humphris, S.E., Zierenberg, R.A., Mullineaux, L.S. and Thomson, R.E.) *Seafloor Hydrothermal Systems: Physical, Chemical, Biological and Geological Interactions,* Geophysical Monograph 91, American Geophysical Union, Washington, 317-346.

Lupton, E., Baker, E.T. and Massoth, G.J. (1989) Variable ^{3}He/heat ratios in submarine hydrothermal systems: evidence from two plumes over the Juan de Fuca ridge. *Nature,* 337, 161-164.

Lupton, E. and Craig, H.A. (1981) A major ^{3}He source on the East Pacific Rise. *Science,* 214, 13-18.

Lupton, J.E., Baker, E.T. and Massoth, G.J. (1999) Helium, heat, and the generation of hydrothermal event plumes at mid-ocean ridges. *Earth Planet. Sci. Let.,* 171(3), 343-350.

Lutz, R.A., Shaw, T.J., Fornari, D.J., Haymon, R.M., Lilley, M.D., Von Damm, K.L. and Desbruyeres, D. (1994) Rapid growth at deep-sea vents. *Nature,* 371(6499), 663-664.

Lydon, J.W. (1984) Some observations on the mineralogical and chemical zonation patterns of the volcanogenic sulphide deposits of Cyprus. *Geol. Surv. Can.,* 84(1A), 611-616.

Malahoff, A., McMurtry, G.M., Wiltshire, J.C. and Yeh, H.-W. (1982) Geology and chemistry of hydrothermal deposits from active submarine volcano Loihi, Hawaii. *Nature,* 298, 234-239.

Mandernack, K.W. and Tebo, B.M. (1993) Manganese scavenging and oxidation at hydrothermal vents and in vent plumes. *Geochim. Cosmochim. Acta,* 57, 3907-3923.

Mann, S., Sparks, N.H.C., Frankel, R.B., Bazylinski, D.A., Lovley, D.R. and Jannasch, H.W. (1990) Biomineralization of ferrimagnetic greigite (Fe_3S_4) and iron pyrite (FeS_2) in a magnetotactic bacterium. *Nature,* 343, 258-261.

Maréchal, C.N., Télouk, P. and Albarède, F. (1999) Precise analysis of copper and zinc isotopic compositions by plasma-source mass spectromety. *Chem. Geol.,* 156, 251-273.

Massoth, G.J., Baker, E.T., Lupton, J.E., Feely, R.A., Butterfield, D.B., Von Damm, K.L., Roe, K.K. and Lebon, G.T. (1994) Temporal and spatial variability of hydrothermal manganese and iron at cleft segment, Juan-de-Fuca ridge. *J. Geophys. Res.,* 99(B3), 4905-4923.

McCollom, T.M. and Shock, E.L. (1997) Geochemical constraints on chemolithoautotrophic metabolism by microorganisms in seafloor hydrothermal systems. *Geochim. Cosmochim. Acta,* 61(20), 4375-4391.

McGregor, B.A., Harrison, C.G.A., Lavelle, J.W. and Rona, P.A. (1977) Magnetic anomaly patterns on the Mid-Atlantic Ridge crest at 26°N. *J. Geophys. Res.,* 82, 231-238.

McMurtry, G.M., Wang, C.-H. and Yeh, H.-W. (1983) Chemical and isotopic investigations into the origin of clay minerals from the Galapagos hydrothermal mound field. *Geochim. Cosmochim. Acta,* 47, 475-489.

McMurtry, G.M. and Yeh, H.-W. (1981) Hydrothermal clay mineral formation of East Pacific Rise Bauer Basin sediments. *Chem. Geol.,* 32, 189-205.

Mehra, O.P. and Jackson, M.L. (1960) Iron oxide removal from soils and clays by a dithionate-citrate system buffered with sodium bicarbonate. *Clays & Clay Miner.,* 7, 317-327.

Metz, S. and Trefry, J.H. (1988) Geochemistry of metalliferous sediments from the TAG hydrothermal field, Mid-Atlantic Ridge. *EOS Trans. AGU,* 66, 936.

Metz, S. and Trefry, J.H. (1993) Field and laboratory studies of metal uptake and release by hydrothermal precipitates. *J. Geophys. Res.,* 98(B6), 9661-9666.

Michard, A. and Albarède, F. (1985) Hydrothermal uranium uptake at ridge crests. *Nature,* 317, 244-246.

Mills, R.A., Alt, J.C. and Clayton, T. (1996) Low-temperature fluid flow through sulfidic sediments from TAG: modification of fluid chemistry and alteration of mineral deposits. *J. Geophys. Res.,* 98, 3495-3498.

Mills, R.A. and Elderfield, H. (1995a) Rare earth element geochemistry of hydrothermal deposits from the active TAG mound, 26°N mid-Atlantic Ridge. *Geochim. Cosmochim. Acta,* 59, 3511-3524.

Mills, R.A. and Elderfield, H. (1995b) Hydrothermal activity and the geochemistry of metalliferous sediments. In: (eds. Humphris, S.E., Zierenberg, R.A., Mullineaux, L.S. and Thomson, R.E.) *Seafloor Hydrothermal Systems: Physical, Chemical, Biological and Geological Interactions,* Geophysical Monograph, Vol. 91, American Geophysical Union Monograph, Washington, 392-407.

Mills, R.A., Elderfield, H. and Thomson, J. (1993) A dual origin for the hydrothermal component in a metalliferous sediment core from the Mid-Atlantic Ridge. *J. Geophys. Res.,* 98, 9671-9681.

Mills, R.A., Teagle, D.A.H. and Tivey, M.K. (1998) Fluid mixing and anhydrite precipitation within the TAG mound. In: (eds. Herzig, P.M., Humphris, S.E., Miller, D.J. and Zierenberg, R.A.) *Proc. ODP, Sci. Results*, Vol. 158, College Station, TX (Ocean Drilling Program), 119-127.

Mills, R.A., Thomson, J., Elderfield, H., Hinton, R.W. and Hyslop, E. (1994) Uranium enrichment in metalliferous sediments from the Mid-Atlantic Ridge. *Earth Planet. Sci. Let.,* 124, 35-47.

Mitra, A., Elderfield, H. and Greaves, M.J. (1994) Rare earth elements in submarine hydrothermal fluids and plumes from the Mid-Atlantic Ridge. *Mar. Chem.,* 46, 217-235.

Moriarty, D. (1986) Measurement of bacterial growth rates in aquatic ecosystems from rates of nucleic acid synthesis. In: (ed. Marshall, K.C.) *Advances in Microbial Ecology*, Vol. 9, Plenum Publishing, New York, 245-263.

Morton, J.L. and Sleep, N.H. (1985) A mid-ocean ridge model: constraints on the volume of axial hydrothermal flux. *J. Geophys. Res.,* 90, 11,345-11,353.

Mottl, M.J. (1983) Hydrothermal processes at seafloor spreading centres: Application of basalt-seawater experimental results. *NATO Advanced Research Institute Conference: Hydrothermal Processes at Seafloor Spreading Centres*, 199-224.

Mottl, M.J. and McConachy, T.F. (1990) Chemical processes in buoyant hydrothermal plumes on the East Pacific Rise near 21°N. *Geochim. Cosmochim. Acta,* 54, 1911-1927.

Mottl, M.J. and Wheat, G. (1994) Hydrothermal circulation through mid-ocean ridge flanks: fluxes of heat and magnesium. *Geochim. Cosmochim. Acta,* 58, 2225-2238.

Mottl, M.J., Wheat, G., Baker, E., Becker, N., Davis, E., Feely, R., Grehan, A., Kadko, D., Lilley, M., Massoth, G., Moyer, C. and Sansone, F. (1998) Warm springs discovered on 3.5 Ma oceanic crust, eastern flank of the Juan de Fuca Ridge. *Geology,* 26(1), 51-54.

Mottl, M.J., Wheat, G. and Boulègue, J. (1994) Timing of ore deposition and sill intrusion at site 856: evidence from stratigraphy, alteration and sediment pore water composition. In: (eds. Mottl, M.J., Davis, E.E. and Fisher, A.T.) *Proc. ODP, Sci. Results*, Vol. 139, College Station, TX (Ocean Drilling Program), 679-693.

Murnane, R. and Clague, D.A. (1983) Nontronite from a low-temperature hydrothermal system on the Juan de Fuca Ridge. *Earth Planet. Sci. Let.,* 65, 343-352.

Myers, C.R. and Nealson, K.H. (1988) Microbial reduction of manganese oxides: interactions with iron and sulphur. *Geochim. Cosmochim. Acta,* 52, 751-756.

Naganuma, T. (1998) A hypothetical microbial consortium that stabilizes oxygen-gradient in chemosynthetic microenvironments. *Supramol. Sci.,* 5, 439-443.

Nealson, K.H. and Conrad, P.G. (1999) Life: past, present and future. *Philos. Trans. R. Soc. London B,* 354(1392), 1923-1939.

Niewöhner, C., Hensen, C., Kasten, S., Zabel, M. and Schulz, H.D. (1998) Deep sulfate reduction completely mediated by anaerobic methane oxidation in sediments of the upwelling area off Namibia. *Geochim. Cosmochim. Acta,* 62(3), 455-464.

Nordstrom, D.K. (1982) Aqueous pyrite oxidation and the consequent formation of secondary minerals. In: (eds. Kittrick, J.A., Fanning, D.S. and Hossner, I.R.) *Acid Sulphate Weathering: Pedogeochemistry and Relationship to Manipulation of Soil Materials*, Soil. Sci. Soc. Am. Press, Madison, Wisconsin, 37-56.

Nordstrom, D.K. and Southam, G. (1997) Geomicrobiology of sulfide mineral formation. *Rev. Mineral.,* 35, 361-390.

Novelli, P.C., Michelson, A.R., Scranton, M.I., Banta, G.T., Hobbie, J.E. and Howarth, R.W. (1988) Hydrogen and acetate cycling in two sulfate-reducing sediments: Buzzards Bay and Town Cove, Mass. *Geochim. Cosmochim. Acta,* 52(10), 2477-2486.

Olivarez, A.M. and Owen, R.M. (1989) REE/Fe variations in hydrothermal sediments: Implications for the REE content of seawater. *Geochim. Cosmochim. Acta,* 53, 757-762.

Oremland, R.S. and Capone, D.G. (1988) Use of specific inhibitors in biogeochemistry and microbial ecology. *Adv. Microb. Ecol.,* 10, 285-383.

Ortoleva, P., Merine, E., Moore, C. and Chadam, J. (1987) Geochemical self-organisation I: Reaction-transport feedbacks and modelling approach. *Am. J. Sci.,* 287, 979-1007.

Oudin, E. (1983) Hydrothermal sulfide deposits of the East Pacific Rise (21°N). 1. Descrpitive mineralogy. *Min. Mag.,* 4(1), 39-72.

Palmer, M.R. and Ernst, G.G.J. (1989) Generation of hydrothermal megaplumes by cooling of pillow basalts at mid-ocean ridges. *Nature,* 393, 643-647.

Palmer, M.R. and scientific party (1996) *The interaction of microbial activity and diagenesis in hydrothermal sediments at the Mid-Atlantic Ridge at 26°N.* University of Bristol, Department of Geology.

Parkes, R.J. and Buckingham, W.J. (1986) The flow of organic carbon through aerobic respiration and sulphate reduction in inshore marine sediments. *Proceedings of the 4th International Symposium on Microbial Ecology*, 617-624.

Parkes, R.J., Cragg, B.A., Bale, S.J., Getliff, J.M., Goodman, K., Rochelle, P.A., Fry, J.C., Weightman, A.J. and Harvey, S.M. (1994) Deep bacterial biosphere in Pacific Ocean sediments. *Nature,* 371, 410-413.

Parkes, R.J., Cragg, B.A., Telling, J. P., Rhodes, J., Severmann, S., Mills, R.A. and Palmer, M.R. (submitted) Extending the boundaries of the submarine hydrothermal ecosystem.

Percival, J.B. and Ames, D.E. (1993) Clay mineralogy of active hydrothermal chimneys and associated mound, Middle Valley, Northern Juan de Fuca Ridge. *Can. Min.,* 31, 957-971.

Peterson, N., von Dobeneck, T. and Vali, H. (1986) Fossil bacterial magnetite in deep-sea sediments from the South-Atlantic Ocean. *Nature,* 320, 611-615.

Piper, D.Z. (1974) Rare earth elements in the sedimentary cycle: a summary. *Chem. Geol.,* 14, 285-304.

Postma, D. (1985) Concentration of Mn and separation from Fe in sediments - I. Kinetics and stoichiometry of the reaction between birnessite and dissolved Fe(II) at 10°C. *Geochim. Cosmochim. Acta,* 49, 1023-1033.

Postma, D. and Jakobsen, R. (1996) Redox zonation: Equilibrium constraints on the Fe(III)/SO_4-reduction interface. *Geochim. Cosmochim. Acta,* 60(17), 3169-3175.

Price, F.T. and Shieh, Y.N. (1979) Fractionation of sulfur isotopes during laboratoy synthesis of pyrite at low temperatures. *Chem. Geol.,* 27, 245-253.

Purdy, G.M., Semperè, J.-C., Schouten, H., Dubois, D.L. and Goldsmith, R. (1990) Bathymetry of the Mid-Atlantic Ridge, 24°-31°N: A map series. *Mar. Geophys. Res.,* 12, 247-252.

Puteanus, D., Glasby, G.P., Stoffers, P. and Kunzendorf, H. (1991) Hydrothermal iron-rich deposits from the Teahitia-Mehitia and Mcdonald hot spot areas, Soutwest Pacific. *Mar. Geol.,* 98, 389-409.

Pyzik, A.J. and Sommer, S.E. (1981) Sedimentary iron monosulfides - kinetics and mechanism of formation. *Geochim. Cosmochim. Acta,* 45(5), 687-698.

Ravizza, G., Martin, C.E., German, C.R. and Thompson, G. (1996) Os isotopes as tracers in seafloor hydrothermal systems: metalliferous deposits from the TAG hydrothermal area, 26°N Mid-Atlantic Ridge. *Earth Planet. Sci. Let.,* 138, 105-119.

Reid, R.T., Live, D.H., Faulkner, D.J. and Butler, A. (1993) A siderophore from a marine bacterium with an exceptional ferric ion affinity constant. *Nature,* 360, 455-458.

Reysenbach, A.-L., Holm, N.G., Hershberger, K., Prieur, D. and Jeanthon, C. (1998) In search of a subsurface biosphere at a slow-spreading ridge. In: (eds. Herzig, P.M., Humphris, S.E., Miller, D.J. and Zierenberg, R.A.) *Proc. ODP, Sci. Results*, Vol. 158, College station, TX (Ocean Drilling Program), 355-360.

Richards, H.G. and Boyle, J.F. (1986) Origin, alteration and mineralisation of intra-lava metalliferous sediments of the Troodos Ophiolite, Cyprus. In: (eds. Gallaher, M.J., Ixer, R.A., Neary, C.R. and Pritchard, H.M.) *Metallogeny of basic and ultrabasic rocks*, The Institute of Mining and Metallurgy, 21-31, .

Rivera-Duarte, I. and Flegal, A.R. (1996) Microtechniques for the determination of nanomolar concentrations of trace elements in ≤ 10 ml of sediment porewater. *Analyt. Chim. Acta,* 328, 13-17.

Robertson, A.H.F. and Boyle, J.F. (1983) Tectonic setting and origin of metalliferous sediments in the Mesozoic Tethys ocean. In: (eds. Rona, P.A., Boström, K., Laubier, L. and Smith, K.L.) *Hydrothermal Processes at Seafloor Spreading Centres*, Plenum Press, New York, 595-663.

Robertson, A.H.F. and Fleet, A.J. (1986) Geochemistry and palaeoceanography of the metalliferous and pelagic sediments from the Late Cretaceous Oman ophiolite. *Mar. Pet. Geol.,* 3, 315-337.

Robertson, A.H.F. and Hudson, J.D. (1973) Cyprus umbers: chemical precipitates on a Tethyan ocean ridge. *Earth Planet. Sci. Let.,* 18, 93-101.

Robinson, J.B. and Tuovinen, O.H. (1984) Mechanism of microbial resistance and detoxification of mercury and organometallic compounds: physiological, biochemical and genetic analysis. *Microbiol. Rev.,* 48, 95-124.

Rona, P.A., Fujioka, K., Ishihara, T., Chiba, H., Masuda-Nakaya, H., Omori, T., Kleinrock, M.C., Tivey, M.A., Watanabe, M. and Lalou, C. (1998) An active low-temperature hydrothermal mound and a large inactive sulfide mound found in the TAG hydrothermal field, Mid-Atlantic Ridge 26N, 45W. *EOS Trans. AGU,* 79, F920.

Rona, P.A., Hannington, M.D., Raman, C.V., Thompson, G., Tivey, M.K., Humphris, S.E., Lalou, C. and Petersen, S. (1993a) Active and relict sea-floor hydrothermal mineralisation at the TAG hydrothermal field, Mid-Atlantic-Ridge. *Econ. Geol.,* 88, 1989-2017.

Rona, P.A., Bogdanov, Y.A., Gurvich, E.G., Rimski-Korsakov, N.A., Sagalevitch, A.M., Hannington, M.D. and Thompson, G. (1993b) Relict hydrothermal zones in the TAG hydrothermal field, Mid-Atlantic ridge 26°N, 45°W. *J. Geophys. Res.,* 98(B6), 9715-9730.

Rona, P.A., Klinkhammer, G.P., Nelsen, T.A., Trefry, J.H. and Elderfield, H. (1986) Black smokers, massive sulfides, and vent biota at the Mid-Atlantic Ridge. *Nature,* 321, 33-37.

Rona, P.A., McGregor, B.A., Betzer, P.R., Bolger, G.W. and Krause, D.C. (1975) Anomalous water temperatures over Mid-Atlantic Ridge crest at 26°N. *Deep-Sea Res. I,* 22, 611-618.

Rona, P.A., Petersen, S., Becker, K., von Herzen, R.P.H., Mark D., Herzig, P.M., Naka, J., Lalou, C. and Thompson, G. (1996) Heatflow and mineralogy of TAG relict high temperature zones; Mid-Atlantic Ridge 26°N, 45°W. *Geophys. Res. Lett.,* 23(23), 3507-3510.

Rona, P.A., Thompson, G., Mottl, M.J., Karson, J.A., Jenkins, W.J., Graham, M., Malette, M., Von Damm, K. and Edmond, J.M. (1984) Hydrothermal activity at the TAG hydrothermal field, Mid-Atlantic Ridge crest at 26°N. *J. Geophys. Res.,* 89, 11,365-11,377.

Rudnicki, M. and Elderfield, H. (1992) Theory applied to the Mid-Atlantic Ridge hydrothermal plumes: the finite difference approach. *J. Volcanol. Geotherm. Res.,* 50(1-2), 161-172.

Rudnicki, M. and Elderfield, H. (1993) A chemical model of the buoyant and neutrally buoyant plume above the TAG vent field, 26°N, Mid-Atlantic Ridge. *Geochim. Cosmochim. Acta,* 57, 2939-2957.

Rudnicki, M. and Mills, R.A. (1997) Pore-fluid advection and reaction within the TAG hydrothermal mound. *EOS Trans. AGU,* 78(46) Supplement, F841.

Ruhlin, D.E. and Owen, R.M. (1986) The rare earth element geochemistry of hydrothermal sediments from the East Pacific Rise: Examination of seawater scavenging mechanism. *Geochim. Cosmochim. Acta,* 50, 393-400.

Sachsenberg, S., Klenke, T., Krumbein, W.E., Schellhuber, H.J. and Zeeck, E. (1993) Direct graphite furnace atomic absorption spectrometric determination of metals in sea water: application of palladium modifiers and a fractal approach to their analytical support. *Analyt. Chim. Acta,* 279(2), 241-251.

Schöps, D., Herzig, P.M., Halbach, P., Friedrich, G. and Blum, N. (1993) Mineralogy, chemistry and oxygne isotope thermometry of nontronitic smectites from Central Pacific Seamounts. *Chem. Geol.,* 106, 331-343.

Schultz, A., Delaney, J.R. and McDuff, R.E. (1992) On the partitioning of heat flux between diffuse and point source venting. *J. Geophys. Res.,* 97, 12,299-12,314.

Schultz, A., Dickson, P. and Elderfield, H. (1996) Temporal variations in diffuse hydrothermal flow at TAG. *Geophys. Res. Lett.,* 23(23), 3471-3474.

Schultz, A. and Elderfield, H. (1997) Controls on the pysics and chemistry of seafloor hydrothermal circulation. *Philos. Trans. R. Soc. London A,* 355, 387-425.

Scott, M.R., Salter, P. and Barnard, L.A. (1979) Chemistry of ridge-crest sediments from the North Atlantic Ocean. In: (eds. Talwani, M., Harrison, C.G. and Hayes, D.E.) *Deep Drilling Results in the Atlantic Ocean: Ocean Crust,* Maurice Ewing Series, Vol. 2, AGU, Washington, 403-428.

Scott, M.R., Scott, R.B., Morse, J.W., Betzer, P.R., Butler, L.W. and Rona, P.A. (1978) Metal-enriched sediments from the TAG hydrothermal field. *Nature,* 276, 811-813.

Scott, M.R., Scott, R.B., Rona, P.A., Butler, L.W. and Nalwalk, A.J. (1974) Rapidly accumulating manganese deposit form the median valley of the Mid-Atlantic Ridge. *Geophys. Res. Lett.,* 1, 355-358.

Shanks, W.C. III, Böhlke, J.K. and Seal, R.R., II. (1995) Stable isotopes in mid-ocean ridge hydrothermal systems: interaction between fluids, minerals and organism. In: (eds. Humphris, S.E., Zierenberg, R.A., Mullineaux, L.S. and Thomson, R.E.) *Seafloor Hydrothermal Systems: Physical, Chemical, Biological and Geological Interactions,* Geophysical Monograph 91, American Geophysical Union, Washington, 194-221.

Shaw, T.J., Gieskes, J. and Jahnke, R.A. (1990) Early diagenesis in differing depositional environments: The response of transition metals in pore water. *Geochim. Cosmochim. Acta,* 54, 1233-1246.

Shearme, S., Cronan, D.S. and Rona, P.A. (1983) Geochemistry of sediments from the TAG hydrothermal field, MAR at latitude 26°N. *Mar. Geol.,* 51, 269-291.

Shimmield, G.B. and Price, N.B. (1988) The scavenging of U, ^{230}Th and ^{231}Pa during pulsed hydrothermal activity at 20°S, EPR. *Geochim. Cosmochim. Acta,* 52, 669-677.

Sillitoe, R.H. and Clark, A.H. (1969) Copper and copper-iron sulfides as the initial products of supergene oxidation, Copiapo mining district. *Am. Mineral.,* 54(1684-1710), .

Sillitoe, R.H., Folk, R.L. and Saric, N. (1996) Bacteria as mediators of copper sulfide enrichment during weathering. *Science,* 272, 1153-1155.

Simoneit, B.R.T. (1990) Organic matter in hydrothermal systems - maturation, migration and biogeochemistry: selected papers from the symposium held at the 3rd Chemical Congress of North America and the 195th American Chemical Society National Meeting, Toronto, Canada, June 1988. *Appl. Geochem.,* 5(1-2), 1-250.

Simoneit, B.R.T., Mazurek, M.A., Brenner, S., Crisp, P.T. and Kaplan, I.R. (1979) Organic geochemistry of recent sediments from Guaymas Basin, Gulf of California. *Deep-Sea Res.,* 26, 879-891.

Singer, A. and Stoffers, P. (1987) Mineralogy of a hydrothermal sequence in a core from the Atlantis II Deep, Red Sea. *Clay Miner.,* 22, 251-267.

Singer, A., Stoffers, P., Heller-Kallai, L. and Szafranek, D. (1984) Nontronite in a deep-sea core from the South Pacific. *Clays & Clay Miner.,* 32(5), 375-383.

Sinton, J.M. and Detrick, R.S. (1992) Midocean ridge magma chambers. *J. Geophys. Res.,* 97(B1), 197-216.

Smith, D.K. and Cann, J.R. (1990) Hundreds of small volcanos on the median valley floor of the Mid-Atlantic ridge at 24°30'N. *Nature,* 348(6297), 152-155.

Sørensen, J. and Jørgensen, B.B. (1987) Early diagenesis in sediments from Danish coastal waters: Microbial activity and Mn-Fe-S geochemistry. *Geochim. Cosmochim. Acta,* 51, 1583-1590.

Stein, C.A. and Stein, S. (1994) Constraints on hydrothermal heat flux through the oceanic lithosphere from global heat flow. *J. Geophys. Res.,* 99, 3081-3095.

Stein, C.A., Stein, S. and Pelayo, A.M. (1995) Heat flow and hydrothermal circulation. In: (eds. Humphris, S.E., Zierenberg, R.A., Mullineaux, L.S. and Thomson, R.E.) *Seafloor Hydrothermal Systems: Physical, Chemical, Biological and Geological Interactions,* Geophysical Monograph 91, American Geophysical Union, Washington, 425-445.

Stolz, J.F., Chang, S.-B.R. and Kirschvink, J.L. (1986) Magnetotactic bacteria and single-domain magnetite in hemipelagic sediments. *Nature,* 321, 849-851.

Strandberg, G.W., Shumate, S.E. and Parrot, J.R. (1981) Microbial cells as biosorbents for heavy metals: Accumulation of uranium by *Saccharomyces cerevisiae* and *Pseudomonas aeruginosa*. *Appl. Environ. Microbiol.,* 41, 237- 246.

Summit, M. and Baross, J.A. (1998) Thermophilic subseafloor microorganism from the 1996 Gorda Ridge eruption. *Deep-Sea Res. II,* 45, 2751-2766.

Sun, S.S. and McDonough, W.F. (1989) Chemical and isotopic systematics of oceanic basalts: implications for mantle composition and processes. In: (eds. Saunders, A.D. and Norry, M.J.) *Magmatism in the Oceans Basins,* Special Publication 42, Geological Society, London, 313-345.

Sverjensky, D.A. (1984) Europium redox equilibria in aqueous solution. *Earth Planet. Sci. Let.,* 67, 70-78.

Teagle, D.A.H., Alt, J.C., Bach, W., Halliday, A.N. and Erzinger, J. (1996) Alteration of upper ocean crust in a ridge-flank hydrothermal upflow zone: Mineral, chemical and isotopic constraints from Hole 896A. In: (eds. Alt, J.C., Kinoshite, H., Stokking, L.B. and Michael, P.J.) *Proc.*

ODP, Sci. Results, Vol. 148, College Station, TX (Ocean Drilling Program), 119-150.

Teagle, D.A.H., Alt, J.C., Chiba, H. and Halliday, A.N. (1998) Dissecting an active hydrothermal deposit: The strontium and oxygen isotopic anatomy of TAG hydrothermal mound - anhydrite. In: (eds. Herzig, P.M., Humphris, S.E., Miller, D.J. and Zierenberg, R.A.) *Proc. ODP, Sci. Results*, Vol. 158, College station, TX (Ocean Drilling Program), 129-141.

Thamdrup, B., Finster, K., Würgler Hansen, J. and Bak, F. (1993) Bacterial disproportionation of elemental sulphur coupled to chemical reduction of iron and manganese. *Appl. Environ. Microbiol.,* 59(1), 101-108.

Thamdrup, B., Fossing, H. and Jørgensen, B.B. (1994) Manganese, iron, and sulfur cycling in a coastal marine sediment, Aarhus Bay, Denmark. *Geochim. Cosmochim. Acta,* 58(23), 5115-5129.

Thayer, J.S. (1989) Methylation: its role in the environmental mobility of heavy elements. *Appl. Organomet. Chem.,* 3, 123-128.

Thompson, G., Humphris, S.E., Schroeder, B., Sulanowska, M. and Rona, P.A. (1988) Active vents and massive sulfides at 26°N (TAG) and 23°N (Snakepit) on the Mid-Atlantic Ridge. *Can. Mineral.,* 26, 697-711.

Thompson, G., Mottl, M.J. and Rona, P.A. (1985) Morphology, mineralogy and chemistry of hydrothermal deposits from the TAG area, 26° N Mid-Atlantic Ridge. *Chem. Geol.,* 49, 243-257.

Thomson, J., Higgs, N.C., Croudace, I.W., Colley, S. and Hydes, D.J. (1993) Redox zonation of elements at an oxic/post-oxic boundary in deep-sea sediments. *Geochim. Cosmochim. Acta,* 57, 579-595.

Thomson, J., Higgs, N.C., Wilson, T.R.S., Croudace, I.W., de Lange, G.J. and van Santvoort, P.J.M. (1995) Redistribution and geochemical behaviour of redox-sensitive elements around S1, the most recent eastern Mediterranean sapropel. *Geochim. Cosmochim. Acta,* 59, 3487-3501.

Thomson, J., Jarvis, I., Green, D.R.H., Green, D. and Clayton, T. (1998) Mobility and immobility of redox-sensitive elements in deep-sea turbidites during shallow burial. *Geochim. Cosmochim. Acta,* 62(4), 643-656.

Thorseth, I.H., Torsvik, T., Furnes, H. and Muehlenbachs, K. (1995) Microbes play an important role in the alteration of oceanic crust. *Chem. Geol.,* 126(2), 137-146.

Tivey, M.K., Humphris, S.E., Thompson, G., Hannington, M.D. and Rona, P.A. (1995) Deducing patterns of fluid flow and mixing within the TAG active hydrothermal mound using mineralogical and geochemical data. *J. Geophys. Res.,* 100(B7), 12,427-12,555.

Trefry, J.H., Butterfield, D.B., Metz, S., Massoth, G.J., Trocine, R.P. and Feely, R.A. (1994) Trace metals in hydrothermal solutions from Cleft segment on the southern Juan de Fuca Ridge. *J. Geophys. Res.,* 99(B3), 4925-4935.

Trefry, J.H. and Metz, S. (1989) Role of hydrothermal precipitates in the geochemical cycling of vanadium. *Nature,* 342, 531-533.

Trocine, R.P. and Trefry, J. (1988) Distribution and chemistry of suspended particles from an active hydrothermal vent site on the Mid-Atlantic Ridge at 26°N. *Earth Planet. Sci. Let.,* 88, 1-15.

Tunnicliffe, V., Embley, R.W., Holden, J.F., Butterfield, D.B., Massoth, G.J. and Juniper, S.K. (1997) Biological colonization of new hydrothermal vents following an eruption on Juan de Fuca Ridge. *Deep-Sea Res.,* 44, 1627-1644.

Turekian, K.K. and Bertine, K.K. (1971) Deposition of molybdenum and uranium along the major ocean ridge systems. *Nature,* 229, 250-251.

Turner, D.R. and Whitfield, M. (1979) Control of seawater composition. *Nature,* 281, 468-469.

Tuttle, J.H., Wirsen, C.O. and Jannasch, H.W. (1983) Microbial activities in the Emitted hydrothermal waters of the Galapagos Rift Vents. *Mar. Bio.,* 73, 293-299.

Vargas, M., Kashefi, K., Blunt-Harris, E.L. and Lovley, D.R. (1998) Microbiological evidence for Fe(III) reduction on early Earth. *Nature,* 395, 65-67.

Vaughan, D.J. and Craig, J.R. (1978) *Mineral chemistry of metal sulfide.* Cambridge University Press, Cambridge.

Von Damm, K.L. (1990) Seafloor hydrothermal activity: black smoker chemistry and chimneys. *Ann. Rev. Earth Planet. Sci. Lett.,* 18, 173-205.

Von Damm, K.L. (1995) Controls on the chemistry and temporal variability of seafloor hydrothermal fluids. In: (eds. Humphris, S.E., Zierenberg, R.A., Mullineaux, L.S. and Thomson, R.E.) *Seafloor Hydrothermal Systems: Physical, Chemical, Biological and Geological Interactions*, Vol. 91, American Geophysical Union Monograph, Washington, 222-247.

Von Damm, K.L., Edmond, J.M., Measures, C.I. and Grant, B. (1985) Chemistry of submarine hydrothermal solutions at Guaymas Basin, Gulf of California. *Geochim. Cosmochim. Acta,* 49, 2221-2237.

von der Borch, C.C. and Rex, R.W. (1970) Amorphous iron oxide precipitates in sediments cored during Leg 5, Deep Sea Drilling Project. *Init. Repts DSDP,* 5, 541-544.

Wächtershäuser, G. (1988) Pyrite formation, the 1st energy source for life - a hypothesis. *System. Appl. Microbiol.,* 10(3), 207-210.

Watterson, J. (1991) Preliminary evidence for the involvement of budding bacteria in the origin of Alaskan placer gold. *Geology,* 20, 315-318.

Weaver, C.E. (1989) *Clays, muds and shales*, Vol. 44. Elsevier, Amsterdam.

Weaver, C.E. and Pollard, L.D. (1973) *The chemistry of clay minerals.* Elsevier, New York.

Wells, D.M. (1998) Rare earth element systematics in ancient and modern hydrothermal systems. PhD, University of Southampton.

Wellsbury, P., Goodman, K., Barth, T., Cragg, B., Barnes, S. and Parkes, R. (1997) Deep marine biosphere fuelled by increasing organic matter availability during burial and heating. *Nature,* 388(6642), 573-576.

Wheat, G. and Mottl, M.J. (1994) Hydrothermal circulation, Juan de Fuca Ridge eastern flank: factors controlling basement water composition. *J. Geophys. Res.,* 99, 3067-3080.

White, D.C. (1983) Analysis of microorganism in terms of quantity and activity in natural environments. In: (eds. Slater, J.H., Whittenbury, R. and Wimpenny, J.W.T.) *Microbes in their natural environment,* Society for General Microbiology Symposium 34, Cambridge University Press, New York, 37-66.

White, S.N., Humphris, S.E. and Kleinrock, M.C. (1998) New observations on the distribution of past and present hydrothermal activity in the TAG area of the Mid-Atlantic Ridge (26°08' N). *Mar. Geophys. Res.,* 20, 41-56.

Wilcock, W.S.D. (1997) A model for the formation of transient event plumes above mid-ocean ridge hydrothermal systems. *J. Geophys. Res.,* 102(B6), 12,109-12,121.

Wilcock, W.S.D. and Delaney, J.R. (1996) Mid-ocean ridge sulfide deposits: Evidence for heat extraction from magma chambers or cracking fronts? *Earth Planet. Sci. Let.,* 145(1-4), 49-64.

Wirsen, C.O., Jannasch, H.W. and Molineaux, S.J. (1993) Chemosynthetic microbial activity at Mid-Atlantic Ridge hydrothermal vent sites. *J. Geophys. Res.,* 98, 9693-9703.

Wolery, T.J. and Sleep, N.H. (1976) Hydrothermal circulation and geochemical flux at mid-ocean ridges. *J. Geol.,* 84, 249-275.

Wolery, T.J. and Sleep, N.H. (1988) Interactions of geochemical cycles with the mantle. In: (eds. Gregor, C.B., Garrels, R.M., Mckenzie, F.T. and Maynard, J.B.) *Chemical Cycles in the Evolution of the Earth*, Wiley, New York, 77-103.

Wolin, M.J. (1982) Hydrogen transfer in microbial communities. In: (eds. Bull, A.T. and Slater, J.H.) *Microbial interactions and communities*, Academic Press, New Yok, 323-356.

Wood, J.M. and Wang, H.K. (1985) Strategies for microbial resistance to heavy metals. In: (ed. Stumm, W.) *Chemical Processes in Lakes*, Wiley, New York, 81-98.

Wood, S.A. (1990a) The aqueous geochemistry of REE and yttrium, 1. Review of available low-temperature data for inorganic complexes and the inorganic REE speciation of natural waters. *Chem. Geol.,* 82, 159-186.

Wood, S.A. (1990b) The aqueous geochemistry of the rare-earth elements and yttrium, 2. Theoretical predictions of speciation in hydrothermal solutions to 350°C at saturation water-vapor pressure. *Chem. Geol.*, 88, 99-123.

You, C.-F. and Bickle, M.J. (1998) Evolution of an active sea-floor massive sulphide deposit. *Nature,* 394, 668-671.

Zierenberg, R.A. and Schiffman, P. (1990) Microbial control of silver mineralization at the sea-floor hydrothermal site on the northern Gorda Ridge. *Nature,* 348, 155-157.

Zonenshain, L.P., Kuzmin, M.I., Lisitsyn, A.P., Bogdanov, Y.A. and Baranov, B.V. (1989) Tectonics of the Mid-Atlantic rift valley between TAG and MARK areas: evidence for vertical tectonism. *Tectonophys.,* 159, 1-23.

SOUTHAMPTON UNIVERSITY LIBRARY

USER'S DECLARATION

AUTHOR: Severmann, Silke. TITLE: The Geochemistry and Geomicrobiology of relict hydrothermal sulphide deposits

DATE:

I undertake not to reproduce this thesis, or any substantial portion of it, or to quote extensively from it without first obtaining the permission, in writing, of the Librarian of the University of Southampton.

To be signed by each user of this thesis

DATE	SIGNATURE	ADDRESS